# High Mobility in OFDM based Wireless Communication Systems

DISSERTATION

zur Erlangung des Grades

*des Doktors der Ingenieurwissenschaften (Dr.-Ing)*

der Fakultät für Mathematik und Informatik

der Unversität des Saarlandes

vorgelegt von

**KELVIN CHELLI**

Saarbrücken, 2021

Colloquium Date: 15.09.2021
Dean of Faculty: Prof. Dr. Thomas Schuster

Doctoral Committee:
Prof. Dr. Hans-Peter Lenhof
Prof. DR.-Ing Thorsten Herfet
Prof. Dr. Romanus Dyczij-Edlinger
Prof. Dr. David Gomez-Barquero
Dr. Pascal Peter

*When all Thy mercies, O my God, My rising soul surveys,*
*Transported with the view, I'm lost in wonder, love, and praise.*

—Joseph Addison

Dedicated to my wonderful wife *Shreya* and my loving daughter *Hannah*.

## Short Abstract

*Orthogonal Frequency Division Multiplexing* (OFDM) has been adopted as the transmission scheme in most of the wireless systems we use on a daily basis. It brings with it several inherent advantages that make it an ideal waveform candidate in the physical layer. However, OFDM based wireless systems are severely affected in High Mobility scenarios. In this thesis, we investigate the effects of mobility on OFDM based wireless systems and develop novel techniques to estimate the channel and compensate its effects at the receiver. *Compressed Sensing* (CS) based channel estimation techniques like the *Rake Matching Pursuit* (RMP) and the *Gradient Rake Matching Pursuit* (GRMP) are developed to estimate the channel in a precise, robust and computationally efficient manner. In addition to this, a *Cognitive Framework* that can detect the mobility in the channel and configure an optimal estimation scheme is also developed and tested. The *Cognitive Framework* ensures a computationally optimal channel estimation scheme in all channel conditions. We also demonstrate that the proposed schemes can be adapted to other wireless standards easily. Accordingly, evaluation is done for three current broadcast, broadband and cellular standards. The results show the clear benefit of the proposed schemes in enabling high mobility in OFDM based wireless communication systems.

## Kurze Zusammenfassung

*Orthogonal Frequency Division Multiplexing* (OFDM) wurde als Übertragungsschema in die meisten drahtlosen Systemen, die wir täglich verwenden, übernommen. Es bringt mehrere inhärente Vorteile mit sich, die es zu einem idealen Waveform-Kandidaten in der Bitübertragungsschicht (Physical Layer) machen. Allerdings sind OFDM-basierte drahtlose Systeme in Szenarien mit hoher Mobilität stark beeinträchtigt. In dieser Arbeit untersuchen wir die Auswirkungen der Mobilität auf OFDM-basierte drahtlose Systeme und entwickeln neuartige Techniken, um das Verhalten des Kanals abzuschätzen und seine Auswirkungen am Empfänger zu kompensieren. Auf *Compressed Sensing* (CS) basierende Kanalschätzverfahren wie das *Rake Matching Pursuit* (RMP) und das *Gradient Rake Matching Pursuit* (GRMP) werden entwickelt, um den Kanal präzise, robust und rechnerisch effizient abzuschätzen. Darüber hinaus wird ein *Cognitive Framework* entwickelt und getestet, das die Mobilität im Kanal erkennt und ein optimales Schätzungsschema konfiguriert. Das *Cognitive Framework* gewährleistet ein rechnerisch optimales Kanalschätzungsschema für alle möglichen Kanalbedingungen. Wir zeigen außerdem, dass die vorgeschlagenen Schemata

auch leicht an andere Funkstandards angepasst werden können. Dementsprechend wird eine Evaluierung für drei aktuelle Rundfunk-, Breitband- und Mobilfunkstandards durchgeführt. Die Ergebnisse zeigen den klaren Vorteil der vorgeschlagenen Schemata bei der Ermöglichung hoher Mobilität in OFDM-basierten drahtlosen Kommunikationssystemen.

# ABSTRACT

Wireless communication systems have become a ubiquitous part of human life. The extensive use of these systems in various aspects of daily life has not only drastically changed the way we live, but also placed ambitious expectations on the future of wireless systems. Advances in wireless systems during the last decade have brought us to the brink of 5G, a new generation of cellular communication that is envisioned to bring high speed, ultra low latency and a unification of broadband, broadcast and cellular systems in the near future.

A commonality in modern wireless communications systems is the use of Orthogonal Frequency Division Multiplexing (OFDM) as the transmission scheme in the physical layer. Although the use of OFDM has several advantages like computational complexity, robustness against echoes and ease in spectrum shaping, it is sensitive to the effects of high mobility. A relative motion between communicating end devices results in a Doppler shift that distorts the OFDM signal at the receiver. In this thesis, we study the effects of a doubly selective or a time varying multipath channel present in scenarios of high mobility. We propose novel compressed sensing based channel estimation schemes that precisely estimate such a channel and equalize the effects of high mobility at the receiver. The proposed schemes are also optimized in terms of computational complexity. In addition to this, we have also developed a cognitive framework that detects the mobility in the channel and configures an optimal estimation scheme at the receiver.

In order to show the flexibility and robustness of the proposed schemes, evaluation is done for three different wireless standards that are part of our daily life. These include the LTE, LTE-V (Cellular), DVB-T2 (Broadcast) and the IEEE 802.11p (Broadband) standards. The evaluations will highlight the benefits of the proposed schemes in varying channel conditions for these wireless standards. Moreover, the simulation platforms are also made available as open source software. The goal of this thesis is to contribute towards bringing high mobility in OFDM based wireless communication systems.

# ACKNOWLEDGEMENTS

First and foremost my sincere gratitude to Thorsten Herfet for his time, advice and guidance since 2012 when I began my Masters program at the Saarland Informatics Campus. After an oral exam in 2013, he told me to be my own harshest critic and indeed, this advise has help me quite a bit in my research. In addition to being an excellent supervisor, he has also mentored me in several aspects over the past years. Our conference trips together are memories that I will always cherish and the insightful discussions during these journeys have had a positive impact on my way of life. I also want to thank David Gomez-Barquero for agreeing to review my thesis. I truly enjoyed our discussions about my work when we met in Cagliari, València and Oulu. His work as part of the 5GXCast project made me realize the relevance of my research. I am also deeply grateful to Prof. Romanus Dyczij-Edlinger for agreeing to review my thesis. I am always inspired by the way Prof. Edlinger integrates enthusiasm and pragmatism in his research. Working with him on a few projects have been very insightful.

I am also very thankful to work in a great team at the Telecommunications lab. The atmosphere at our lab has been optimal in encouraging creative ideas to solve various research problems. After around five years together, my colleagues are some of my closest friends in Germany. Andreas, Tobias, and Harini have been with me for the entire journey. We struck a good work-life balance and I cherish the many discussions we had at the university as well as the times we spent outside of work. I know Andreas since 2012 when we did TC1 together. I thank him for all the deep discussions that we had on a regular basis. A special thanks to Tobias who has been an invariant in this journey. I truly enjoyed our collaboration on light field research. I would also like to thank Zakaria and Diane for helping out in administrative processes.

I would also like to thank Ashwini, Sarika and Shreya who have been my friends for around 20 years. Although, as life evolves and we find it difficult to keep in touch, we absolutely know that we are available for each other. Some of my fondest memories are the things we did together. I also like to thank my friends at Löschbezirk 20 from the Freiwillige

Feuerwehr in Schafbrücke. These include, Ralf, Bass, Dietmar, Dirk, Karsten, Nico, Christof, Sven and Carmelo. Thank you for making it so easy to be part of the team. I have the best neighbors in Christian, Britta and Ben. I enjoyed cooking together, having an occasional beer in the garden and the time we spend together.

Finally, I would like to thank my wife Shreya for always being there and for loving me unconditionally. I am also thankful for enabling me to become a father. I love you and our daughter Hannah. I thank my brother Melvin for his support in the past years. I also thank my parents for enabling me with a good education in India and providing me with the means to pursue my education in Germany.

# TABLE OF CONTENTS

# LIST OF FIGURES

# LIST OF TABLES

# ABBREVIATIONS

| | |
|---|---|
| 3GPP | 3rd Generation Partnership Project. |
| AMC | Adaptive Modulation and Coding. |
| ATSC | Advanced Television Systems Committee. |
| AWGN | Additive White Gaussian Noise. |
| BBC | British Broadcasting Corporation. |
| BCH | Bose–Chaudhuri–Hocquenghem. |
| BEM | Basis Expansion Model. |
| BER | Bit Error Rate. |
| BICM | Bit Interleaved Coding and Modulation. |
| BMP | Basic Matching Pursuit. |
| BPSK | Binary Phase Shift Keying. |

| | |
|---|---|
| COFDM | Coded Orthogonal Frequency Division Multiplexing. |
| COST | European Cooperation in the Field of Science and Technology Research. |
| CP | Cyclic Prefix. |
| CP-OFDM | Cyclic Prefix Orthogonal Frequency Division Multiplexing. |
| CS | Compressed Sensing. |
| CSP | Common Simulation Platform. |
| CTF | Channel Transfer Function. |
| DFT | Discrete Fourier Transform. |
| DSRC | Dedicated Short Range Communications. |
| DVB | Digital Video Broadcasting. |
| DVB-T | Digital Video Broadcasting - Terrestrial. |
| DVB-T2 | Digital Video Broadcasting - Second Generation Terrestrial. |
| EPA | Extended Pedestrian A mode. |
| ETSI | European Telecommunications Standards Institute. |
| ETU | Extended Typical Urban. |
| EVA | Extended Vehicular A mode. |
| FCC | Federal Communications Commission. |
| FDD | Frequency Division Duplex. |
| FEC | Forward Error Coding. |
| FEF | Future Extension Frame. |
| FFT | Fast Fourier Transform. |
| FPGA | Field-Programmable Gate Array. |
| GRMP | Gradient Rake Matching Pursuit. |
| HARQ | Hybrid Automatic Repeat Request. |
| ICI | Inter Carrier Interference. |
| IDFT | Inverse Discrete Fourier Transform. |
| IFFT | Inverse Fast Fourier Transform. |
| ISDB-T | Integrated Services Digital Broadcasting - Terrestrial. |
| ISI | Inter Symbol Interference. |

| | |
|---|---|
| ITS | Intelligent Transport Systems. |
| ITU | International Telecommunication Union. |
| LDPC | Low-Density Parity-Check. |
| LMMSE | Linear Minimum Mean Square Error. |
| LS | Least Squares. |
| LTE | Long-Term Evolution. |
| LTI | Linear Time-Invariant. |
| MIMO | Multiple-Input Multiple-Output. |
| MMSE | Minimum Mean Square Error. |
| MP | Matching Pursuit. |
| MPEG | Moving Picture Experts Group. |
| OFDM | Orthogonal Frequency Division Multiplexing. |
| OFDMA | Orthogonal Frequency Division Multiple Access. |
| OMP | Orthogonal Matching Pursuit. |
| PAPR | Peak to Average Power Ratio. |
| PC | Personal Computer. |
| PCSI | Perfect Channel State Information. |
| PLCP | Physical layer Convergence Protocol. |
| PLP | Physical Layer Pipes. |
| PN | Pseudo Noise. |
| PPDU | Physical layer Protocol Data Unit. |
| PSDU | Physical layer Service Data Unit. |
| RB | Resource Block. |
| RMP | Rake Matching Pursuit. |
| SC-FDM | Single Carrier Frequency Division Multiplexing. |
| SC-FDMA | Single Carrier Frequency Division Multiple Access. |
| SDR | Software Defined Radio. |
| SIC | Successive Interference Cancellation. |
| SICIR | Successive Interference Cancellation with Interference Reduction. |
| SISO | Single Input Single Output. |

| | |
|---|---|
| SNR | Signal to Noise Ratio. |
| TC | Tanimoto Coefficient. |
| TDD | Time Division Duplex. |
| V2X | Vehicle to Everything. |
| VMR | Variance to Mean Ratio. |
| WAVE | Wireless Access in Vehicular Environments. |
| WLAN | Wireless Local Area Networks. |

# NOTATIONS

| | |
|---|---|
| $\lvert(\cdot)\rvert$ | Absolute value or magnitude of a complex number. |
| $(\cdot)^H$ | Hermitian transpose or conjugate transpose of a matrix/vector. |
| $(\cdot)^{-1}$ | Inverse of a matrix. |
| $\lVert(\cdot)\rVert_p$ | $l_p$ Norm. |
| $\lVert(\cdot)\rVert_2$ | $l_2$ Norm gives the length of a vector in the Euclidean space. |
| $\lVert(\cdot)\rVert_0$ | $l_0$ Norm that gives the number of non-zero elements in a vector/matrix. |
| **card** | Cardinality of a set. |

# Part I

# Building Blocks

The pursuit of truth and beauty is a sphere of activity in which we are permitted to remain children all our lives.

---

*Albert Einstein*

# CHAPTER 1

# PROLOGUE

It was the summer of 1890 and a curious sixteen year old teenager fascinated by electricity and physics, called Guglielmo Marconi began conducting experiments to transmit telegraph messages wirelessly using electromagnetic waves that were then known as Hertzian waves. After numerous attempts, in December 1894, Guglielmo demonstrated a radio system comprising of a transmitter and receiver. This has been one of the most notable breakthroughs that ignited the development of wireless communication systems.

Wireless systems have been constantly developed through the years to include novel usage scenarios in different applications. Wireless radios found several applications in the $19^{th}$ century that included news, entertainment, military and safety applications. The availability of radio equipment aboard the Titanic played a vital role in saving 700 people and demonstrated the effectiveness of Radio when compared to carrier pigeons as a medium for communication [157]. The advent of broadcast television in the early $20^{th}$ century marked another milestone in wireless communication and is one of the few inventions that continues to have a significant impact on the society by enabling news and entertainment to reach a vast number of households. The fascinating television coverage of the Apollo 11 mission landing on the surface of the Moon on 20 July 1969 has been one of the greatest broadcasts in the history of television. The cellular revolution that began in 1990 has continued to positively impact the society by providing a seamless connectivity that is bringing the world closer together. Cellular technology also evolves at a rapid pace and 5G, the current generation envisions ultra reliable low latency, massive machine type and enhanced mobile broadband communication. Moreover, it envisions to incorporate broadcast and multicast capabilities and create a network architecture that can be adapted dynamically as described in [66]. The future of wireless communications systems is promising and has a potential for wider spectrum resources in the $THz$ band, use of artificial intelligence, dynamic spectrum access and

cell-free massive Multiple-Input Multiple-Output (MIMO) networks just to name a few.

Mobility has become an important requirement for present as well as future wireless communication systems. It enables a plethora of safety and non-safety applications in vehicular scenarios. However, the relative motion between communicating end devices results in a Doppler shift that significantly affects the performance of modern wireless systems that use Orthogonal Frequency Division Multiplexing (OFDM) as the transmission technology in the physical layer[1]. In this thesis, we study the effects of mobility on OFDM based systems and develop novel schemes to robustly estimate and equalize the effects of the wireless channel at the receiver. The ultimate goal is to enable *High Mobility in OFDM based Wireless Communication Systems*.

## 1.1 The Problem Statement

The advancements in wireless communication have resulted in an unprecedented variety of different systems from Body- over Local- to Wide-Area Networks; from low energy low data rate sensor networks to multi-Gigabit wireless display interfaces. Despite this variety, there is a commonality with respect to future expectations of telecommunication systems:

**High Frequency:** Frequencies are a scarce resource and communication systems for the future face increasing carrier frequencies of several GHz[2] up to several 10 GHz[3]. Moreover, the $5^{th}$ generation of cellular systems (5G) proposes a spectrum that aggregates frequency bands up to 86 GHz [84].

**Relative Motion:** Mobility requirements are increasing. Scenarios like the use of telecommunication systems in fast moving vehicles like high speed trains or airplanes, where potentially both, sender and receiver are in motion (vehicle-to-X communication[4]) have led to the requirement of coping with high relative speeds. The 5G standard specifies a maximum relative speed of 500 km/h [51].

[1] OFDM is a non-trivial frequency-division multiplexing scheme wherein the frequency band is split into several narrowband sub-carriers that overlap each other and is introduced in Chapter 2

[2] https://standards.ieee.org/standard/802_11p-2010.html

[3] https://standards.ieee.org/findstds/standard/802.11ad-2012.html

[4] https://www.car-2-car.org/

**Subcarrier Spacing:** The evolution of signal processing capabilities has led to a mass market application of multicarrier systems with up to 32k carriers[5] while the channel raster has remained unchanged. This has resulted in a carrier spacing that is continuously decreasing.

We notice a trend in which wireless communication systems are required to work with higher frequencies, in a highly mobile environment and with an ever increasing number of subcarriers [21]. Although the use of OFDM in the physical layer offers many inherent advantages, a Doppler shift resulting from the relative mobility between end devices distorts the OFDM signal by destroying the orthogonality between the narrowband subcarriers. As a result, adjacent subcarriers begin to interfere with each other causing Inter Carrier Interference (ICI). This poses a severe obstacle for the flexible design of future high mobility multicarrier systems and Doppler compensation becomes an obligatory component that must be considered. Moreover, a smaller sub-carrier spacing along with the use of higher frequencies proportionally increases the effects of Doppler shifts at the receiver. Accordingly, the question that lays the foundation to this thesis is,

*How to enable high mobility in modern wireless systems in a robust, transparent and computationally effective manner?*

We approach this problem by surveying the state-of-art, systematically identifying the requirements, proposing novel techniques that overcome the effects of the wireless channel and ensuring robust performance at the OFDM receiver.

## 1.2 Contributions

The notable contributions that stem from this thesis are:

- Robust delay metric for the rake matching pursuit algorithm. This has enabled a robust estimation of the delays when compared to the classical compressed sensing based delay search algorithms.
- Doppler shift estimation: A novel technique to estimate the Doppler shift by tracking tap-coefficients for the OFDM symbols in the physical layer frame is proposed and developed.

[5]https://www.itu.int/dms_pub/itu-r/opb/rep/R-REP-BT.2254-4-2020-PDF-E.pdf

- A novel cognitive framework for channel estimation has also been implemented. It chooses the most efficient channel estimation scheme for a given channel condition.
- The proposed schemes have been implemented and evaluated for current Broadband, Broadcast, and Cellular standards.
- Time domain pilots are also explored in this thesis. A mechanism to generate them without significantly affecting the transmitted structure is proposed. Time domain pilots can be very useful in the estimation of doubly selective channels and help get measurements from the time signal at the receiver.
- The prospects of deep learning in channel estimation is also explored in this thesis and the challenges involved are highlighted.
- Standard compliant simulation platforms have also been developed to evaluate the proposed schemes. The simulation platforms along with the proposed schemes for channel estimation are made available open source.

The work of this thesis has resulted in novel channel estimation and equalization schemes that perform consistently better than conventional schemes in varying channel conditions and also for different wireless standards. It has also led to eight publications at well renowned conferences and are listed below in chronological order.

- **Chelli, Kelvin; Herfet, Thorsten**: "Doppler Shift Compensation in Vehicular Communication Systems", in the *IEEE International Conference on Computer and Communications (ICCC)*, Chengdu, October 2016
- **Chelli, Kelvin; Herfet, Thorsten**: "Time-Domain Pilots in DVB-T2", in the *12th IEEE International Symposium on Broadband Multimedia Systems and Broadcasting 2017*, Cagliari, Italy, June 2017
- **Chelli, Kelvin; Sirsi, Praharsha; Herfet, Thorsten**: "Sparse Doubly-Selective Channels: Estimating Path Parameters Unambiguously" in the *26th European Conference on Networks and Communications*, Oulu, Finland, June 2017
- **Chelli, Kelvin; Sirsi, Praharsha; Herfet, Thorsten**: "Complexity Reduction for Consumer Device Compressed Sensing Channel Estimation" in the *7th IEEE International Conference of Consumer Electronics*, Berlin, Germany, September 2017
- **Chelli, Kelvin; Sirsi, Praharsha; Herfet, Thorsten**: "Cognitive Framework for the Estimation of Doubly Selective Channels" in the *86th IEEE Vehicular Technology Conference*, Toronto, Canada, September 2017

- **Sirsi, Praharsha; Chelli, Kelvin; Herfet, Thorsten**: "Tap Coefficient Based Cognitive Framework for Estimating a Dynamic Channel", in the *2nd International Conference on Circuits, Controls and Communications*, Bangalore, December 2017
- **Chelli, Kelvin; Herfet, Thorsten**: "Estimating Doubly-Selective Channels in DVB-T2", in the *IEEE International Symposium on Broadband Multimedia Systems and Broadcasting 2018*, Valencia, Spain, 2018
- **Chelli, Kelvin; Theodory, Ramzi; Herfet, Thorsten**: "Compressed Sensing Channel Estimation for LTE-V", in the *2nd International Conference on 5G for Ubiquitous Connectivity (5Gu)*, Nanjing, China, 2018

## 1.3 Outline

This thesis is organized to introduce the foundations in Part 1. In Chapter 2, multicarrier systems are introduced with a focus on OFDM. The effects of the wireless channel are systematically described and the resulting channel model is derived in Chapter 3. Moreover, the recommended channel models to simulate the wireless channel are given in Section 3.5. In Chapter 4, the wireless standards (ranging from cellular to broadband to broadcast) used for the evaluation of the proposed channel estimation and equalization schemes are introduced and the difference in physical layer specifications are highlighted.

Once the foundation is laid, the problem of channel estimation is addressed in Chapter 5. The system model is derived in Section 5.1 and the classical approaches for channel estimation are described in Section 5.2. In Section 5.3, the state-of-art techniques are discussed and the strengths and weaknesses of each are highlighted. In Section 5.4, we look into the prospects of deep learning in estimating the wireless channel. The fundamentals are introduced and the results of a few experiments with deep learning are discussed in Section 5.4.2. Compressed sensing based channel estimation methods are discussed in Chapter 6. We begin by introducing the fundamentals of compressed sensing in Section 6.1 followed by a detailed survey of compressed sensing schemes used for channel estimation in Section 6.2. The conventional approach of estimating a doubly selective channel using compressed sensing is described in Section 6.3. In Section 6.4, the proposed rake matching pursuit algorithm is introduced and the differences to the conventional scheme are highlighted. The gradient rake matching pursuit algorithm proposes an intuitive modification that reduces the computational effort and is described in Section 6.5. The dictionary is a vital prerequisite for MP algorithms and is one of the decisive factors that affects the performance of channel estimation. The gen-

eration of the dictionary is also a computationally intensive process. In Section 6.6, we look into the problem of dictionary generation and propose a solution that significantly reduces memory and computational requirements. In Chapter 7, the cognitive framework introduced with a goal to provide the best error performance at an optimal computational complexity in varying transmission scenarios. The cognitive framework is able to sense the degree of mobility in the channel and choose an appropriate estimation scheme.

The proposed compressed sensing based channel estimation schemes are evaluated for three modern wireless telecommunication systems in different domains like cellular, broadcast and broadband. The motivation is to show that the proposed schemes are flexible, robust and able to provide good results for wireless standards with significant differences in physical layer specifications. The simulation platforms used for the evaluations are described in Chapter 9. The results of the evaluations are given in Chapter 10. Finally, the thesis concludes with a few remarks in Chapter 11 on the possible impact of this thesis and its role in bringing high mobility in OFDM based wireless communication systems.

# CHAPTER 2

# MULTICARRIER TRANSMISSION TECHNIQUES

This chapter gives an introduction to OFDM and its variants that are used in modern wireless communication standards.

## 2.1 Orthogonal Frequency Division Multiplexing

OFDM is a form of "non-trivial" frequency-division multiplexing. While classical telecommunications always divides the allocated bandwidth between different applications/channels, OFDM offers a way to split up the bandwidth of a single application. Accordingly, OFDM is a multicarrier transmission technique, where the input stream of bits is split into parallel streams that are used to modulate different carriers. The underlying idea is to divide the allocated spectrum into a number of narrowband subcarriers. Although the spectra of the modulated signals overlap in the frequency domain, they remain to be orthogonal to each other as seen in Figure 2.1.

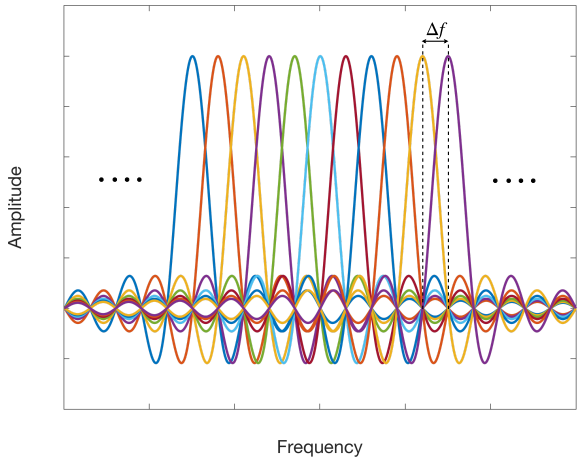


Fig. 2.1: OFDM Subcarriers in the Frequency Domain

The use of harmonic functions with frequencies $f_{sc} = \frac{n}{T}$ for the subcarriers establish an orthonormal basis which can be exploited in a transmission scenario as the communication is free of ICI[1]. Here, $T$ is the OFDM symbol duration and $n \in \mathbb{N}$. The complex baseband of OFDM can be written as shown in Equation (2.1).

$$y_l(i) = \underbrace{\sum_{n=0}^{N-1} \left[ a_n\left(\frac{iT}{N}\right) + jb_n\left(\frac{iT}{N}\right) \right] \cdot \exp\left(j2\pi\frac{ni}{N}\right)}_{\text{N-IDFT}} \cdot \overbrace{\exp\left(-j2\pi\frac{(N-1)i}{2N}\right)}^{\text{Center to Zero}} \tag{2.1}$$

On a closer look, it can be seen that the OFDM signal in Equation (2.1) is related to the Inverse Discrete Fourier Transform (IDFT). Note that, $N$ is the IDFT size. Over the years, OFDM has become the choice for the physical layer in many of the wireless standards we use today. This is mostly due to the optimized hardware implementations using Fast Fourier Transform (FFT) that make it an ideal choice for practical deployment on consumer hardware. OFDM has been adopted for terrestrial broadcasting, cellular and broadband wireless standards. The upcoming 5G cellular communication standard also proposes the use of OFDM in the physical layer. The structure of an OFDM signal is best captured in Figure 2.2. It can be seen that the signal is divided in both the time and the frequency domain. Division along frequency provides an increase in capacity while division in time ensures reduced Inter Symbol Interference (ISI)[2] or simply, less interference to the adjacent symbols. Accordingly, the symbols in time domain have a guard interval between them. In a multipath environment, many copies of the same symbol will be received at the receiver after undergoing different delays resulting in ISI. To compensate for this effect, OFDM systems typically make use of a Cyclic Prefix (CP) , where defined number of samples from the end of the data stream are added to the start of the OFDM symbol in the time domain. In addition to the guard interval/cyclic prefix, a guard band is also realized by setting a few narrowband subcarriers at the beginning and towards the end of the allocated spectrum to zero. The guard band not only simplifies spectrum shaping but it also important to avoid aliasing on the outer subcarriers. Moreover, Figures 2.1 and 2.2 also show that the narrowband subcarriers are free from ICI (i.e no contribution of neighboring subcarriers at sampling points).

[1] ICI is a phenomenon where, the narrowband subcarriers in an OFDM symbol interfere with each other. It is mainly caused due to frequency offsets experienced in doubly selective channels as explained in Section 3.4

[2] ISI is the interference between adjacent OFDM symbols in the time domain. It is caused due to multipath propagation as explained in Section 3.2

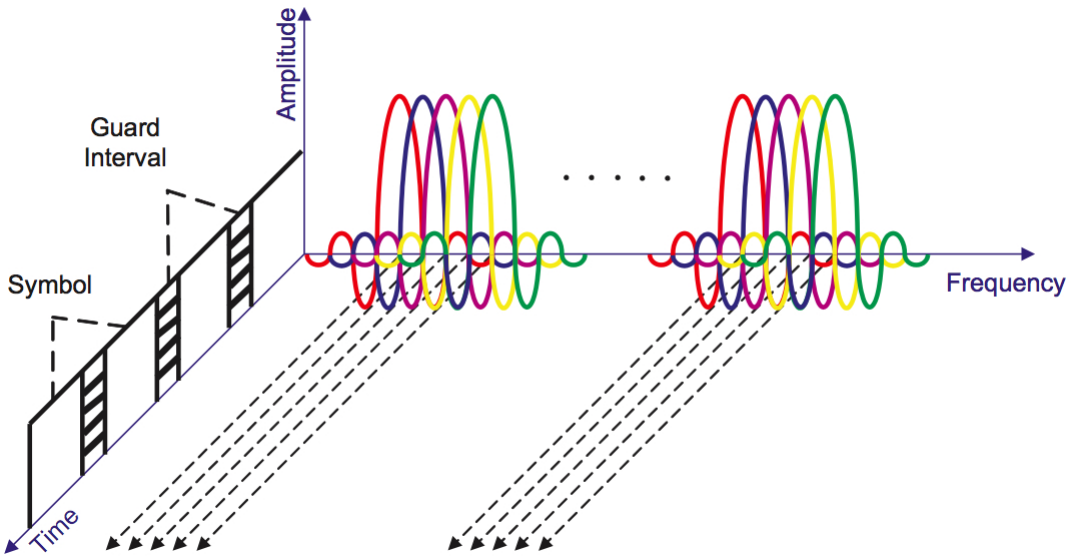


Fig. 2.2: OFDM Signal Structure (Source: [77])

A generic block diagram of an OFDM transmitter is seen in Figure 2.3. The modulated symbols in the frequency domain are transformed to the time domain using an Inverse Fast Fourier Transform (IFFT). A cyclic prefix is then appended to each OFDM symbol to produce the signal to be transmitted.

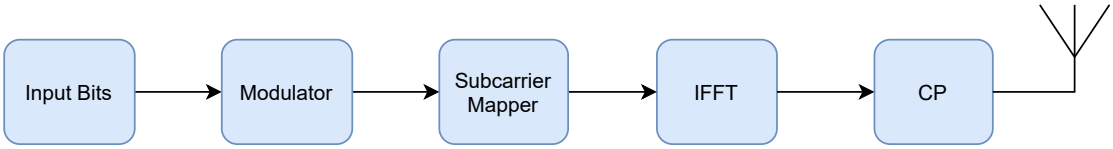


Fig. 2.3: Generic OFDM Block Diagram

**Advantages of OFDM** The technique of splitting up the bandwidth among narrowband subcarriers in OFDM offers several advantages. Some of the benefits of using OFDM are listed below

- Commercial wireless communication systems need to adhere to strict spectral masks. The use of OFDM makes spectral shaping easier and more efficient to implement.
- In OFDM, the input data stream is split into a lower bit rate parallel stream. This increases the symbol duration and makes the system more resilient to the effects of multipath propagation. By using a cyclic prefix, an inherent robustness against ISI is ensured.

- A simplified transmitter and receiver design is aided because, a separate filter is not needed for the subcarriers. Additionally, for every narrowband subcarrier, the wireless channel can be considered as a flat fader that makes the equalization process easier.
- An efficient implementation is also ensured using the FFT algorithm. This makes OFDM an ideal choice for battery power consumer devices.

**Disadvantages of OFDM** Although there are many advantages to OFDM, there are a few drawbacks that have to be taken into account. Some of the disadvantages are listed below.

- An important aspect of OFDM signals is the orthogonality between the narrowband subcarriers. In the presence of Doppler shifts, the subcarriers are no longer orthogonal to each other. This will result in ICI and drastically affect the performance of an OFDM system.
- OFDM signals have a significant amplitude variation due to the linear combination of the subcarriers that have been modulated individually. Thus, in certain instances this could result in the subcarriers being combined either in-phase or out-of-phase, resulting in a high Peak to Average Power Ratio (PAPR). A high PAPR implies that a highly linear amplifier would be required at the transmitter to avoid distortion. This can be a problem especially in battery driven mobile devices since amplifiers with a large (linear) working range consume more power.

## 2.2 Single Carrier Frequency Division Multiplexing

Single Carrier Frequency Division Multiplexing (SC-FDM) is closely related to OFDM and can be regarded as DFT- spread OFDM. It helps alleviate the the problem of high PAPR in an OFDM signal and has been adopted by the Long-Term Evolution (LTE) standard in the uplink transmission in order to increase the power efficiency of battery operated mobile devices. SC-FDM shares the principles of OFDM, thus exhibiting the same benefits in terms of multipath mitigation and low-complexity equalization.

SC-FDM is realized by applying a Discrete Fourier Transform (DFT) to the modulated input symbols. This spreads the symbols over all the subcarriers and produces a virtual single carrier structure. It also reduces the variations in the instantaneous transmit power and helps reduce the PAPR of the transmitted signal. Accordingly, each subcarrier in SC-FDM will contain information about all of the transmitted symbols due to DFT spreading [143]. This is in contrast to OFDM wherein, each subcarrier carries information about only one of the modulated input symbols. Figure 2.4 illustrates the differences between OFDM and SC-FDM signals.

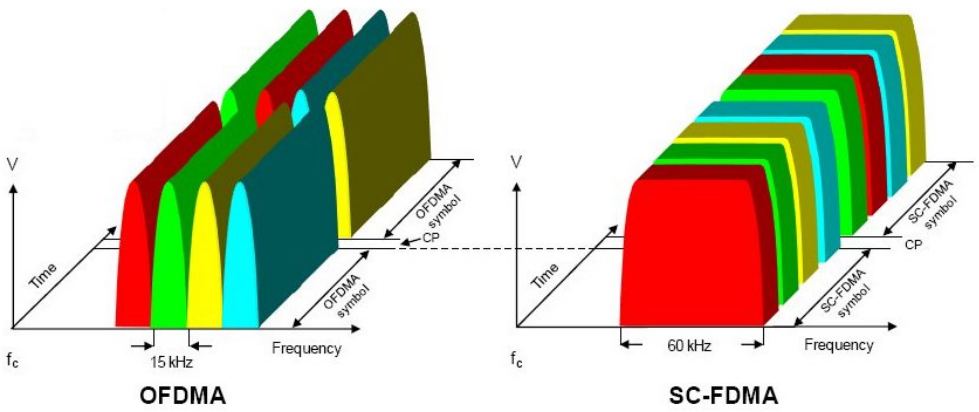


Fig. 2.4: Time-Frequency Representation for OFDM and SC-FDM Signals

A generic block diagram of a SC-FDM transmitter is seen in Figure 2.5. After the modulation process is completed, the DFT block spreads the modulated symbols over all the subcarriers. The remainder of the block diagram is the same as OFDM in Figure 2.3.

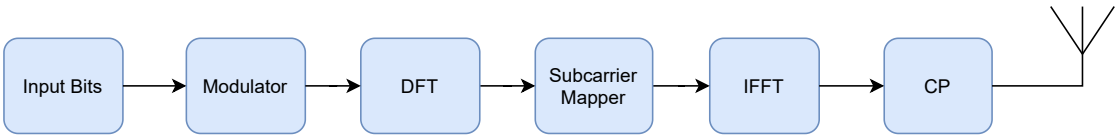


Fig. 2.5: Generic SC-FDM Block Diagram (Source: [64])

The exact structure of the transmitter and the associated parameters for uplink transmission in the LTE standard is comprehensively described in Section 4.1. It is also interesting to note that, since all subcarriers in an SC-FDM symbol contains information about all the input symbols, an increased robustness to deep fading can be achieved and the information can still be recovered from other subcarriers experiencing better channel conditions [122].

Despite of the attractive merits of SC-FDM, it has a significant disadvantage in the form of noise enhancement. At the receiver, the IDFT despreading spreads the noise introduced by the wireless channel onto all the subcarriers [122]. This phenomenon is called noise enhancement and can degrade the performance of the SC-FDM signal.

## 2.3 Coded OFDM

Coded Orthogonal Frequency Division Multiplexing (COFDM) is another important variant of OFDM that is specified for the DVB-T2 standard. Here, the information bits that are to be transmitted are first error protected after which OFDM modulation is done. The DVB-T2 standard even specifies two Forward Error Coding (FEC) schemes to ensure robustness against the effects of the channel. A Low-Density Parity-Check (LDPC) inner code and a Bose–Chaudhuri–Hocquenghem (BCH) outer code is specified to ensure good performance in an environment with high noise levels and interference [131, 153]. The inner LDPC code enables the generation of long codes with a powerful error correction capability while the outer BCH code is intended to reduce the error floor of the LDPC code [126]. The specifications of COFDM and the Forward Error Coding (FEC) schemes are described in Section 4.2 A generic block diagram of COFDM is shown in Figure 2.6. The information bits are first encoded using FEC schemes. The encoded bits are modulated and then transformed to the time domain. Finally, a cyclic prefix is added to every COFDM signal before transmission.

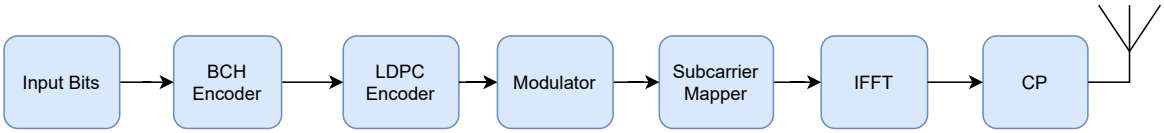


Fig. 2.6: Generic COFDM Block Diagram

## 2.4 Other Variants of OFDM

Most of the wireless technologies that we use on a daily basis specify OFDM in the physical layer due to its indisputable advantages. It is also intensively studied in the research community and has resulted in several improvements that focus on increasing efficiency, flexibility, and robustness of the underlying waveform. Some of the most notable developments are briefly mentioned in this section.

**Generalized Frequency Division Multiplexing (GFDM)** GFDM is a digital multicarrier modulation scheme which incorporates a flexible pulse shaping technique and opportunistically exploit spectrum white spaces for wireless data communications [58]. The architecture in GFDM makes it possible to design a waveform that is optimized to the requirements (latency, power consumption, reliability) of the underlying application [111]. It has been one of the waveform candidates considered for 5G [63].
The underlying idea in GFDM is to independently modulate a subset of carriers and symbols (termed as subcarriers and subsymbols respectively) that makes up a block. Accordingly, each data block can be composed of $K$ subcarriers and $M$ time slots and transmits $KM$ complex modulated data as explained in [58]. The data blocks are then filtered using a prototype filter [3] in the time and frequency domains. At the end of each block, a CP is added to avoid ISI. The result is a non-orthogonal waveform that is shown to reduce emissions outside the spectral mask, allows for usage of a fragmented spectrum and provide dynamic spectrum allocation capabilities [111].
However, the filtering of a carrier subset in each block can introduce both ISI and ICI that would require additional processing at the receiver to eliminate them. This severely increases the computation complexity at the receiver [63].

**Filter Bank Multicarrier (FBMC) Modulation** is one of the most investigated filtered multicarrier systems in literature [8, 54] and has also been considered as an alternate waveform for 5G [80]. Here, the subcarriers are pulse shaped individually in order to reduce the out-of-band emissions significantly compared to an OFDM waveform. However, a major disadvantage in FBMC is that spectral efficiency cannot be ensured when the number of transmitted symbols is small. This makes FBMC suboptimal in low latency applications [63, 111]. In addition to this, the computational complexity involved is significantly higher when compared to OFDM [63].

OFDM and its variants cover most of the wireless communication systems in the cellular, broadband and broadcast domains. It provides the flexibility, reliability, and robustness at a computational cost that has made it an attractive waveform for wireless systems. However, in scenarios of high mobility the performance of OFDM based wireless systems deteriorate. The characteristics of such a wireless channel and its effects on an OFDM signal are discussed in Chapter 3.

[3] the design of appropriate filters is a dedicated research topic

# CHAPTER 3

# THE WIRELESS CHANNEL

The wireless channel is the physical medium that connects communicating end devices. Signals passing through the wireless channel undergo several physical phenomena like noise, reflection, and mobility resulting in a distorted signal at the receiver. In this Chapter, we mathematically describe these physical properties and discuss the effects they have on an OFDM based wireless communication system. Additionally, we also describe the channel models that are commonly used to simulate the wireless channel.

## 3.1 Additive White Gaussian Noise

Additive White Gaussian Noise (AWGN) is a simple time-continuous noise model that is commonly used to emulate the effect of (several) random processes occurring in nature [74]. The AWGN model has the following characteristics: (i) *Additive* where the noise is added to the transmitted signal (example: thermal noise), (ii) *White* refers to a large bandwidth where the power spectral density of the noise is constant. In other words, this means that the noise is not frequency selective over a large bandwidth and, (iii) *Gaussian* refers to a Gaussian probability density function. This is the result of several independent sources with equal power being superimposed (central limit theorem). The amplitude of the noise follows the Gaussian distribution and the corresponding probability density function is given in Equation (3.1) [3].

$$p(z) = \frac{1}{\sqrt{2\pi\sigma^2}} exp\Big(\frac{-z^2}{2\sigma^2}\Big) \tag{3.1}$$

Here, $z$ is a random variable that denotes the amplitude of the noise, $p(z)$ is the probability of $z$ and $\sigma^2$ is the variance. The output of an AWGN channel will be the input signal with noise added to it. Accordingly, if the input signal and noise are denoted as $x(t)$ and $w(t)$

respectively, the output signal can be written as $r(t) = x(t) + w(t)$. The AWGN channel does not take into account any other channel effects such as frequency selectivity or time selectivity, these effects will be described in the following sections.

## 3.2 Time Dispersion and Multipath

In a transmission scenario, multipath occurs when the electromagnetic waves reflect at obstacles and are received at the receiver. Let us consider a Linear Time-Invariant (LTI) single-path scenario where the environment is stationary. The received signal $r(t)$ is computed by delaying the sent signal $x(t)$ by the path delay $\tau_0$ and scaling it by some complex value $\tilde{c}_0$, resulting in a gain and phase shift [62] as shown in Equation (3.2).

$$r(t) = \tilde{c}_0 x(t - \tau_0) \tag{3.2}$$

This models the behavior of an electromagnetic wave propagating through free space. Additionally in many wireless communication applications, the use of non-directional (or omni-directional) antennas radiates the signal in all directions which results in multiple propagation paths, each with a different delay and scaling factor. Consequently, the receiver that also uses a non-directional antenna, will receive a superposition of all incoming signals. For a discrete set of $K$ significant propagation paths, this phenomenon can be expressed as in Equation (3.3).

$$r(t) = \sum_{k=1}^{K} \tilde{c}_k x(t - \tau_k) \tag{3.3}$$

Since a superposition of differently shifted and differently weighted versions of the transmitted signal is received, the channel is called *time dispersive*. Figure 3.1 illustrates the multipath propagation in a transmission scenario.

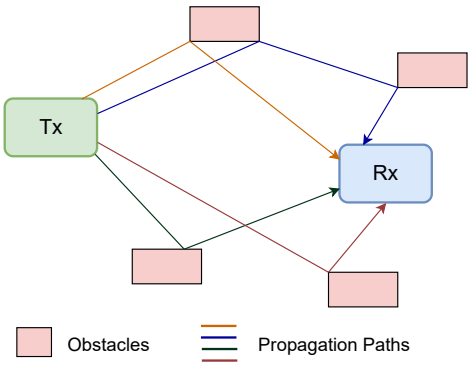


Fig. 3.1: Multipath Propogation

We can also associate each propagation path with its corresponding delay and parameterize the equation on $\tau$. If we consider $\tau$ to be a continuous variable, the transmit-receive relation is expressed as,

$$r(t) = \int_{-\infty}^{\infty} h(\tau)x(t-\tau)d\tau \tag{3.4}$$

here, $h(\tau)$ denotes the channel impulse response and is shown in Equation (3.5). Note that, the complex gains $c_k$ are constant for a given delay [74, 91] and $\tau_k$ denotes the relative delay for the $k^{th}$ path.

$$h(\tau) = \sum_{k=1}^{K} \tilde{c}_k \delta(\tau - \tau_k) \tag{3.5}$$

It is also very interesting to see that Equation (3.4) is equal to the general input-output relation of an LTI system, representing a convolution of the input with its channel impulse response. Using the convolutional property of the Fourier transform, we can express the transmit-receive relation in the frequency domain as $R(f) = H(f) \cdot X(f)$. Let us now consider the frequency domain representation of Equation (3.5). A delay in the time domain corresponds to a frequency dependent phase shift according to the time shift property of the Fourier transform ($\delta(t-\tau) \circ\!\!-\!\!\bullet \exp(-j2\pi f\tau)$). Thus, multipath propagation results in a time dispersive channel that is *frequency selective*. An important characteristic of frequency selective channels is the coherence bandwidth. According to [74], the coherence bandwidth is defined as the frequency separation at which the attenuation of two frequency domain samples of the channel become decorrelated. The coherence bandwidth is inversely proportional to the multipath delay spread $T_{max}$ of the underlying channel and is given in Equation (3.6).

$$B_{coherence} \approx \frac{1}{2 \cdot T_{max}} \tag{3.6}$$

## 3.3 Frequency Dispersion and Doppler

Another important physical phenomenon is the effect of mobility on OFDM based wireless systems. The relative motion between communicating end devices results in a Doppler shift $f_d$ (measured in $Hz$). Accordingly, the frequency $f_0$ of the signal is shifted to $f_0 \pm f_d$. The amount of Doppler shift is dependent on the frequency of the transmitted signal $f_0$ and the relative velocity $v$ (measured in $m/s$). The Doppler shift for moving receivers is calculated

as in Equation (3.7) where, $c$ represents the speed of light and $\phi$ denotes the angle between the transmitter and the receiver.

$$f_d = f_0 \cdot \frac{v}{c} \cos\phi \tag{3.7}$$

It is also important to note that the end devices may move closer to; or away from each other. Thus, the relative velocity $v$ can be positive or negative, resulting in possible Doppler shifts $f \pm |f_d|$. Let us again consider the simple single-path scenario where the transmitted signal experiences a certain Doppler shift $f_{d_0}$ as seen in Equation (3.8).

$$R(f) = X(f \pm f_{d_0}) \tag{3.8}$$

Transforming Equation (3.8) to the time domain we get,

$$r(t) = x(t) \cdot exp(\mp j2\pi f_{d_0} t) \tag{3.9}$$

We observe that the Doppler shift has resulted in a time-dependent phase shift in the time domain (frequency shift property of the Fourier transform). This results in a channel that is selective with time and accordingly, such channels are known as *time varying* or *time selective* channels. The transmit-receive relation considering the effects of Doppler shift is found in Equation (3.10). Note that, the channel impulse response $h(t)$ is now a function of time.

$$r(t) = \int_{-\infty}^{\infty} h(t)x(t)exp(\mp j2\pi f_d t)df_d \tag{3.10}$$

Furthermore, if we consider multipath propagation, each path can have a unique Doppler shift associated with it and the superposition of different frequency shifts make the channel frequency dispersive. Frequency dispersion critically affects an OFDM signal by affecting the orthogonality between subcarriers and introducing ICI.

An important parameter of time selective channels is the coherence time $T_{coherence}$. Coherence time is defined as the period where the channel impulse response is constant [4, 10]. It is inversely proportional to the maximum Doppler frequency encountered in the channel and is given by Equation (3.11) [167].

$$T_{coherence} \approx \frac{1}{2 \cdot f_{d_{max}}} \tag{3.11}$$

## 3.4 Doubly Selective Channels

The wireless channel in a typical vehicular environment exhibits both multipath propagation and Doppler shift. Thus, the channel is selective in both the time and the frequency domain and is termed as a doubly selective or a time-varying multipath channel [62]. An environment with several obstacles (for example an urban setup) results in many propagation paths each with different delays and Doppler shifts. We can therefore express the wireless channel as a two dimensional function to represent the delays and Doppler shift. Combining Equation (3.4) and Equation (3.10), we can write the transmit-receive relation for a doubly selective channel as in Equation (3.12).

$$r(t) = \int_{-\infty}^{\infty}\int_{-\infty}^{\infty} \tilde{c}(\tau, f_d)x(t-\tau)\exp(\mp j2\pi f_d t)d\tau\, df_d \tag{3.12}$$

Here, $\tilde{c}(\tau, f_d)$ is the spreading function. The time-varying channel impulse response $h(t,\tau)$ can be formulated as Equation (3.13) and an equivalent formulation of the transmit-receive relation in terms of the channel impulse response is given in Equation (3.14).

$$h(t,\tau) := \int_{-\infty}^{\infty} \tilde{c}(\tau, f_d)\exp(\mp j2\pi f_d t)df_d \tag{3.13}$$

$$r(t) = \int_{-\infty}^{\infty} h(t,\tau)x(t-\tau)d\tau \tag{3.14}$$

This is the channel that distorts an OFDM signal in a highly mobile or a vehicular environment. Although robust against frequency selectivity (or time dispersion), OFDM signals are sensitive to time selectivity (or frequency dispersion). Moreover, the use of higher frequencies, smaller subcarrier spacing and higher speeds in present as well as future wireless communications systems further amplifies this problem. The goal of this thesis is to improve the robustness of OFDM signals under such doubly selective channels. In the next section, channel models that emulate the characteristics of a doubly selective channel are introduced.

## 3.5 Channel Models

Channel models provide the means to evaluate the effectiveness of the proposed estimation algorithms and can be considered as a mathematical description of the transfer characteristics that emulate the behavior of the underlying channel. In order to enable the evaluation of proposed algorithms with competing methods, it is imperative that channel models that are both extensively tested and widely accepted in the research community must be chosen.

As described in the Section 3.2, a transmitted wireless signal by its nature undergoes multiple reflections, is attenuated, and diffracted around obstacles before reaching the receiver. Since a thorough testing of all the different combinations of channel perturbations is not possible in the practical development of channel estimation algorithms, statistical approaches based on real world simulations are generally employed in research and in this thesis. An example of such an empirical channel model defined by the International Telecommunication Union (ITU) suited for vehicular environments is shown in Table 3.1.

Table 3.1: Channel Model for Vehicular Scenarios proposed by ITU [124]

| Tap | Low *Delay* Spread | | High *Delay* Spread | | Doppler Spectrum |
|---|---|---|---|---|---|
| | $\tau(\mu s)$ | $P_{avg}$(dB) | $\tau(\mu s)$ | $P_{avg}$(dB) | |
| 1 | 0 | 0.0 | 0 | −2.5 | classic |
| 2 | 0.310 | −1.0 | 0.300 | 0 | classic |
| 3 | 0.710 | −9.0 | 8.900 | −12.8 | classic |
| 4 | 1.090 | −10.0 | 12.900 | −10.0 | classic |
| 5 | 1.730 | −15.0 | 17.100 | −25.2 | classic |
| 6 | 2.510 | −20.0 | 20.000 | −16.0 | classic |

The empirical channel model is further categorized based on the extent of the delay spread. The propagation delay $\tau$ (measured in $\mu$s) and the average power $P_{avg}$ (measured in dB) are both relative to the first path. A *classic* Doppler spectrum that denotes the use of Jake's model (also called Clarke's model) is modeled on each delay tap [124]. In this thesis, the delay taps and their respective power profiles are chosen according to the recommendations of the respective standards.

The European Cooperation in the Field of Science and Technology Research (COST)-207 channel model is another widely used model to emulate a time-variant frequency selective or a doubly selective wireless channel. This channel model is the outcome of extensive data collection from different regions in Europe aimed to characterize propagation in various terrains and provide appropriate fading channel models [53]. The channel model defines four profiles based on varying terrains and define the number of delay taps, the corresponding delays, the relative power on each of these taps as well the type of the Doppler spectrum. Table 3.2 shows the different echo profiles.

Table 3.2: Channel Model based on Terrain proposed by COST 207 [77]

| Terrain Type | $\tau_{max}$ ($\mu$s) | $\Delta\tau$ ($\mu$s) | Echo profile |
|---|---|---|---|
| Rural Area | 0.5 | 0.1 | $e^{(-9.2\tau)}$ for $0 \leq \tau \leq 0.7$ |
| Typical Urban | 5.0 | 1.0 | $e^{(-\tau)}$ for $0 \leq \tau \leq 7$ |
| Bad Urban | 10 | 2.5 | $e^{(-\tau)}$ for $0 \leq \tau \leq 5$<br>$0.5 \cdot e^{(5-\tau)}$ for $5 < \tau \leq 10$ |
| Hilly Terrain | 20 | 5.0 | $e^{(-3.5\tau)}$ for $0 \leq \tau \leq 2$<br>$0.1 \cdot e^{(15-\tau)}$ for $15 \leq \tau \leq 20$ |

A 6-Delay Tap Typical Urban fader (often known as TU-6) is another popularly used configuration recommended by COST and is shown in Table 3.3. A Doppler spectrum *classic* indicates the use of the Jake's spectrum, *Gaus1*, and *Gaus2* refers to a Gaussian spectrum.

Table 3.3: TU-6 fader configuration proposed by COST

| Tap Num. | $\tau$ ($\mu$s) | Linear Power | Power (dB) | Doppler Spectrum |
|---|---|---|---|---|
| 1 | 0.0 | 0.5 | $-3$ | classic |
| 2 | 0.2 | 1.0 | 0 | classic |
| 3 | 0.6 | 0.63 | $-2$ | Gaus1 |
| 4 | 1.6 | 0.25 | $-6$ | Gaus1 |
| 5 | 2.4 | 0.16 | $-8$ | Gaus2 |
| 6 | 5.0 | 0.10 | $-10$ | Gaus2 |

In this thesis, the Rayleigh channel in Matlab is used for the evaluation of the various channel estimation and equalization schemes for the IEEE 802.11p and the DVB-T2 standard. This channel model in Matlab constructs a frequency selective or a multi-path fading channel object where, each discrete path is modeled as an independent Rayleigh fading process [91]. It is then configured with a recommended delay profile. Additionally, on each path a random Doppler shift is simulated for isotropic scattering.

With the recent advancements in wireless communication systems and the advent of 5G, the requirements of high mobility along with the need to use higher as well as a wider range of frequencies has led to the need for more challenging and realistic channel models to be developed and standardized. To address these requirements, the European Telecommunica-

tions Standards Institute (ETSI) has initiated the 3rd Generation Partnership Project (3GPP) project to develop channel models for Pan-European digital cellular systems [46]. The proposed channel models are similar to those proposed by COST 207 with modifications to the Doppler spectrum (restricted to only the Jake's model). The recommended channel model for use in battery driven mobile devices is shown in Table 3.4. Moreover, the similarities between Tables 3.3 and 3.4 can also be noticed.

Table 3.4: TU-6 Cellular channel model

| Tap Num. | $\tau$ ($\mu$s) | Relative power (dB) | Doppler Spectrum |
|---|---|---|---|
| 1 | 0.0 | $-3$ | classic |
| 2 | 0.2 | 0 | classic |
| 3 | 0.6 | $-2$ | classic |
| 4 | 1.6 | $-6$ | classic |
| 5 | 2.4 | $-8$ | classic |
| 6 | 5.0 | $-10$ | classic |

Channel modeling is closely coupled with the evolution of wireless systems and as such is constantly being adapted and improved. To cater to the needs of 5G, 3GPP has commissioned the item, "Study on channel models for frequencies from 0.5 to 100 GHz" to understand through systematic channel sounding experiments in a wide variety of scenarios, and develop relevant channel models for 5G [52]. The new channel models have optimized the propagation, Doppler shift, and loss models while introducing elements to address higher frequencies. In the Release 14 of LTE, the Extended Vehicular A mode (EVA) is recommended and is used to test the proposed algorithms for the LTE-V standard. This channel model is available in Matlab as part of the LTE toolbox[1]. The EVA model is shown in Table 3.5 and is used for the evaluation of the schemes discussed in this thesis for the LTE standard.

[1] Available at: https://www.mathworks.com/help/lte/ug/propagation-channel-models.html

Table 3.5: EVA channel model for LTE-V [43]

| Tap Num. | $\tau$ ($\mu$s) | Relative power (dB) |
|---|---|---|
| 1 | 0.0 | 0 |
| 2 | 0.02 | $-1.5$ |
| 3 | 0.15 | $-1.4$ |
| 4 | 0.310 | $-3.6$ |
| 5 | 0.370 | $-0.6$ |
| 6 | 0.710 | $-9.1$ |
| 7 | 1.090 | $-7.0$ |
| 8 | 1.730 | $-12.0$ |
| 9 | 2.510 | $-16.9$ |

In general the channel models introduced here confirm the observations made in Section 3.4 that, although radio transmission in a mobile environment is highly dispersive due to reflectors and scatterers, most of the transmitted energy is concentrated in a handful of propagation paths and thus wireless communication channels exhibit a *sparse multipath environment*.

# CHAPTER 4

# THE WIRELESS STANDARDS

In this chapter, the specifications of three different wireless systems (that are evaluated in this thesis) are described and exhibit the various similarities and differences among them. The specifications of wireless standards also pose different challenges in the design and development of effective channel estimation and equalization techniques.

## 4.1 Cellular

Cellular telecommunication systems have played a significant role in shaping today's society by providing the means for a nearly seamless connectivity that is bringing people, cultures, and more generally our world closer together. The LTE standard for cellular communication is specified by 3GPP. The current LTE or 4G era has made significantly bigger steps in improving the fidelity, response times, data rates, and the overall quality of service compared to previous iterations. Even on the cellular network infrastructure front, LTE has been able to reduce the complexity and power consumption at the base stations while providing the means to utilize new RF bands, which provides the flexibility to application specific use cases [122]. In the recent releases for 4G, new features that would be part of 5G are being tested [44]. In this section, the details regarding the physical layer of the LTE standard including one of the latest release that enables vehicle to vehicle communication are compiled from the 3GPP specifications and presented here.

The commonality in the physical layer for the different framing structures in LTE including the uplink, downlink, and the recently introduced Release 14 (also called LTE-V) is the use of Orthogonal Frequency Division Multiple Access (OFDMA) and one of its variants called Single Carrier Frequency Division Multiple Access (SC-FDMA). These schemes are explained in Section 2.2. Radio frequencies are a scarce and valuable resource and as such,

LTE uses different RF bands globally that range from 450 to 5900 MHz. These are specified by 3GPP in [49]. The LTE standard also offers numerous bandwidth options which in turn decides the number of subcarriers, the sampling frequency, and the number of Resource Block (RB) available. A RB in LTE refers to the smallest unit of available resource that can be assigned to a user. In the LTE terminology, a base station is referred to as an *Evolved Node B* (eNB) and the devices connected to the base station are called *User Equipment* (UE) [48].

A typical physical layer frame in LTE has a duration of 10 ms. These frames consists of ten subframes, each with a duration of 1 ms. Each subframe is further divided into two slots, each having a duration of 0.5 ms. Each of these slots is a RB that consists of 12 OFDM or SC-FDM subcarriers. The illustration in Figure 4.1 shows a generic LTE physical layer frame.

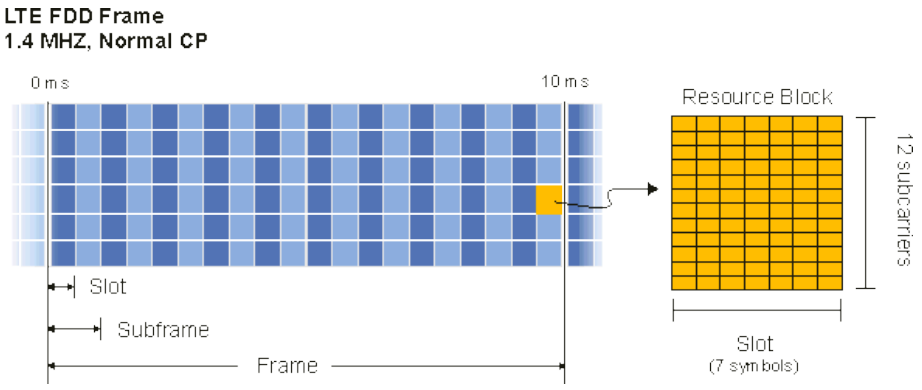


Fig. 4.1: LTE Physical Layer Frame [145]

The OFDM signal in an LTE frame has a subcarrier spacing of 15 kHz. Thus, a resource block consisting of 12 subcarriers has a frequency span of 180 kHz. Depending on the bandwidth, the LTE standard has different configurations for the number of resource blocks, the sampling frequency, and the number of subcarriers as listed in Table 4.1 [122]. It is seen that the number of resource blocks increases with increasing bandwidth. Also note that the subcarrier spacing for all the different configurations is specified to be 15 kHz.

The LTE standard offers different configurations that give it the flexibility to serve various needs and applications. Taking a closer look at the 15.0 MHz mode a 1536 point FFT is required to maintain a subcarrier spacing of 15 kHz. FFT sizes in natural number power of 2 are mostly used in signal processing applications, and are readily available in efficient software and hardware solutions. The 1536 point FFT is computed using three separate 512 point FFT's. Accordingly, the input sequence is split into three parallel vectors each of which

goes through a 512 point FFT. Finally the three sequences are combined to get a 1536 point FFT [31].

Table 4.1: Physical Layer Configurations in LTE

| | Bandwidth (MHz) | | | | | |
|---|---|---|---|---|---|---|
| | 1.4 | 3.0 | 5.0 | 10.0 | 15.0 | 20.0 |
| Resource Blocks | 6 | 15 | 25 | 50 | 75 | 100 |
| Num. Data Subcarriers | 72 | 180 | 300 | 600 | 900 | 1200 |
| Sampling Frequency $f_s$ (MHz) | 1.92 | 3.84 | 7.68 | 15.36 | 23.04 | 30.72 |
| FFT Size (N) | 128 | 256 | 512 | 1024 | 1536 | 2048 |
| Subcarrier Spacing $\Delta f$ | $\Delta f = \frac{f_s}{N} = 15\ kHz$ | | | | | |

LTE also defines different modulation schemes that can be used depending on the quality of the underlying wireless channel. In addition to this, two cyclic prefix options are provided. A short cyclic prefix ($\frac{9}{128}$ of the OFDM symbol duration) is typically intended to be used in urban cells to serve higher data rate applications. A long cyclic prefix ($\frac{1}{4}$ of the OFDM symbol duration) is used where the cells are very large (like in rural areas) or in special cases like multi-cell broadcast as explained in [88]. Consequently, the choice of cyclic prefix influences the number of OFDM symbols in a resource block or an LTE physical layer slot of 0.5 ms. Using a short cyclic prefix allows 7 OFDM symbols to fit in a resource block while, the use of a long cyclic prefix can only fit 6 OFDM symbols in a resource block. The durations of the cyclic prefix for the different modes are part of Table 4.2.

The downlink LTE transmission uses OFDMA as the physical layer waveform while in the uplink, SC-FDMA is specified. These are multiple access schemes based on OFDM and SC-FDM respectively. The use of SC-FDMA in the uplink is justified due to the indubitable advantages in power efficiency that is crucial in battery driven mobile devices as explained in Section 5.3. A summary of the waveform configurations is given in Table 4.2.

Table 4.2: Physical Layer Waveform Specifications in LTE

| Parameter | Value |
|---|---|
| Modulation Schemes | BPSK, QPSK, 16-QAM,<br>64-QAM or 256-QAM |
| Downlink Access Scheme | OFDMA |
| Uplink Access Scheme | SC-FDMA |
| OFDM Symbol Duration | $\frac{1}{\Delta f} = \frac{1}{15000} \approx 66.7\mu s$ |
| Cyclic Prefix Length | Short cyclic prefix:<br>$\frac{9}{128}$ of OFDM symbol duration<br>Note: $5.2\mu$ for the first symbol and<br>$4.7\mu s$ for the remaining symbols in a RB<br>Long cyclic prefix:<br>$\frac{1}{4}$ of OFDM symbol duration<br>Duration: $16.7\mu s$ |
| Num. OFDM Symbols in RB | 7 when a short cyclic prefix is used<br>6 when a long cyclic prefix is used |

Given the inherent flexibility of the LTE physical layer, at any given point in time, the base station and the mobile station should agree on the correct parameters to ensure decodability. Moreover the use of OFDMA and SC-FDMA allows for multiple mobile devices to be in a single physical layer frame. Thus, the base station needs to transmit control information at the beginning of every frame. The frame control information informs the mobile stations if the current frame contains data intended for it. In addition to this, it also contains the information necessary to decode the data payload scheduled by the base station. This information is contained in the control channel and plays a vital role in the ability to correctly decode the data plane. Thus, the control information is shorter in comparison to the size of the data payload and is protected using a convolutional code with a low code rate [98]. To ensure robust data transmission over the wireless channel, LTE specifies a Hybrid Automatic Repeat Request (HARQ) consisting of a FEC technique and a re-transmission scheme. A high throughput

turbo decoder is employed as a FEC scheme for the data channel. The exact format of the control sequences are not directly relevant to this thesis and can be found in [44] and [98].

An illustration of a generic LTE time-frequency grid can be found in Figure 4.2. The fundamentals of an OFDM signal and the relationship between time and frequency domains are clearly depicted. In the frequency domain, multiple subcarriers with harmonic frequencies are independently modulated by data. An IFFT is then performed on the OFDM subcarriers to produce the time domain OFDM signal which are then grouped into a resource block. In this figure, the resource block has 7 OFDM symbols that provides a total of 84 ($7 \times 12$ subcarriers) resource elements. Also the presence of 7 OFDM symbols in the resource block indicates that a short cyclic prefix is employed. An extensive description of OFDM along with its variants can be found in Section 2.1.

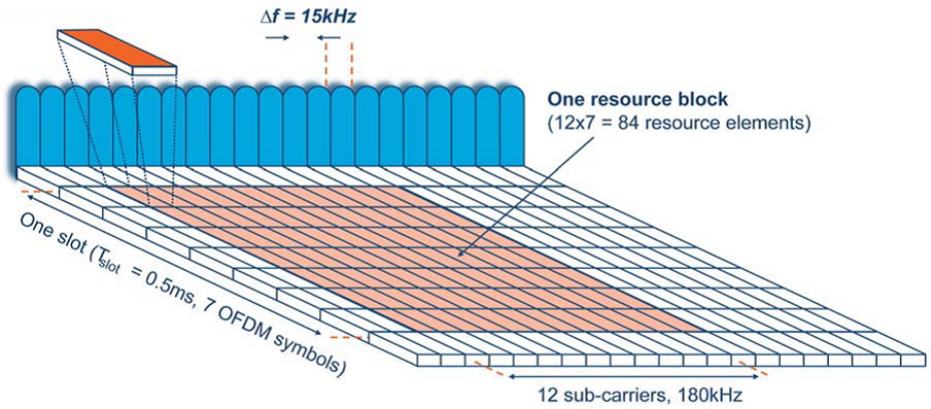


Fig. 4.2: Time-Frequency Resource Grid [122]

A simplified generic transceiver chain for Single Input Single Output (SISO) LTE downlink and LTE uplink is shown in Figure 4.3 and Figure 4.4 respectively. The only differentiating factor between the uplink and the downlink is the use of SC-FDM in the uplink transmission. The use of SC-FDM is justified in the uplink due to a lower PAPR that helps in reducing power consumption in battery operated mobile devices. The application of a DFT to the modulated input symbols as seen in Figure 4.4 produces a virtual single carrier structure known as SC-FDM.

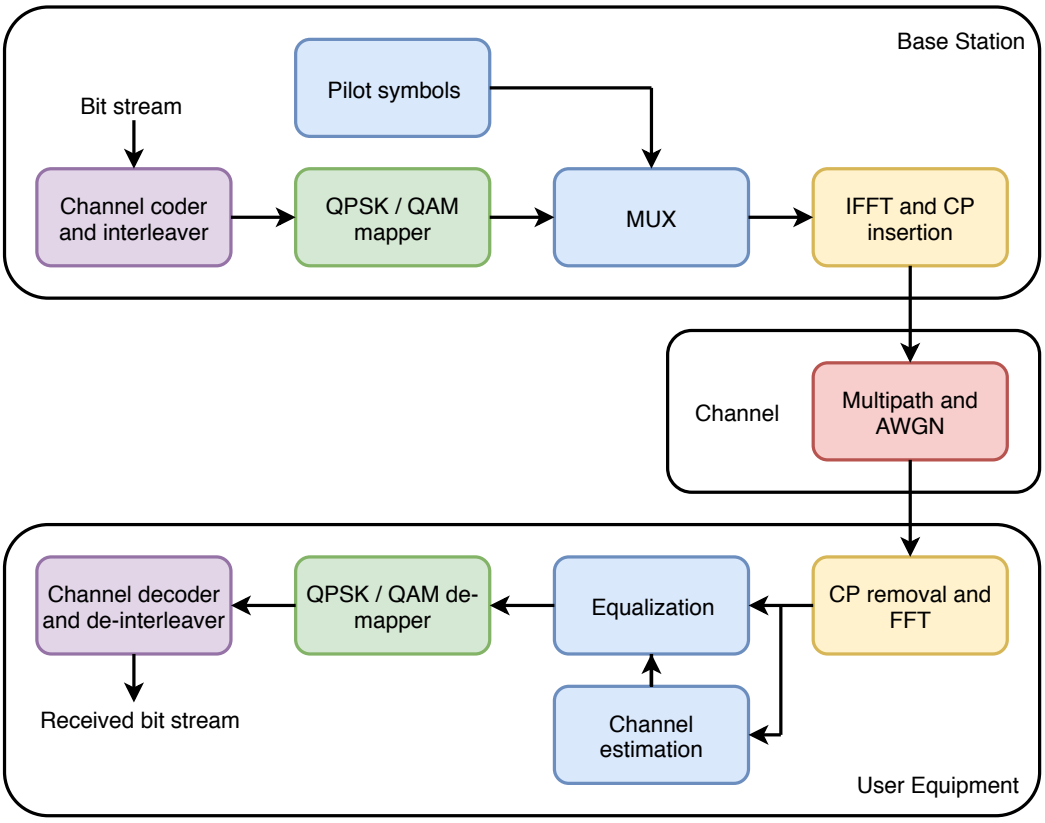


Fig. 4.3: A Generic Downlink OFDM Transceiver

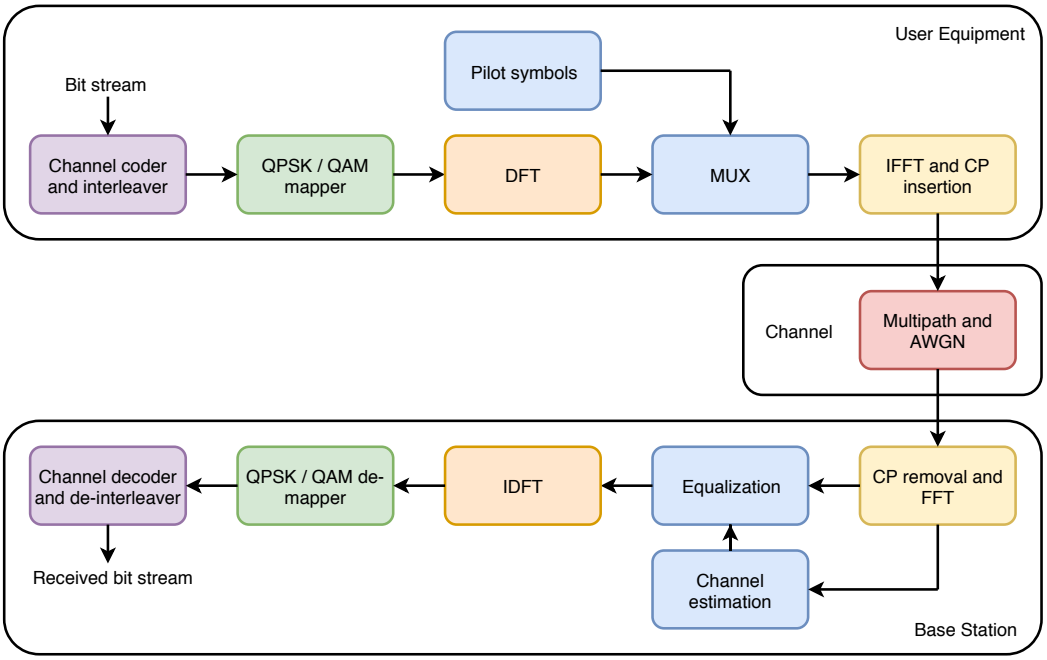


Fig. 4.4: A Generic Uplink OFDM Transceiver

Pilots are reference signals that help estimating the distortions caused by the wireless channel. Pilot-aided channel estimation techniques involve transmitting known reference signals at known locations in a physical layer frame. Since the receiver knows about these pilots, distortions introduced by the channel can be estimated using various channel estimation techniques. The density and structure of the pilots play an important role in alleviating the effects of the channel. However, introducing a large number of pilots that do not carry useful information reduces the net data rate. Thus, wireless standards have to draw a systematic trade-off that on the one hand allows for reliable channel estimation while ensuring that the overheads are kept low.

In LTE, the downlink and uplink transmission modes have a different structure for pilots. For downlink transmission, a sparse pilot arrangement in a resource block is specified in the standard. Figure 4.5 shows the pilot pattern specified for downlink transmission in two adjacent resource blocks with short cyclic prefixes (7 OFDM symbols in each resource block). The pilots are placed in the first and the fifth OFDM symbol in a resource block. In the first OFDM symbol, pilots are specified in the first and the seventh subcarrier while in the fifth OFDM symbol, the pilots are found in the fourth and the tenth subcarriers. Such an offset comb-type pilot pattern is not uncommon and can also be seen in other standards like DVB-T2 as will be seen in Section 4.2. The purpose of such a pilot arrangement enables to acquire information about the channel at different frequencies over time.

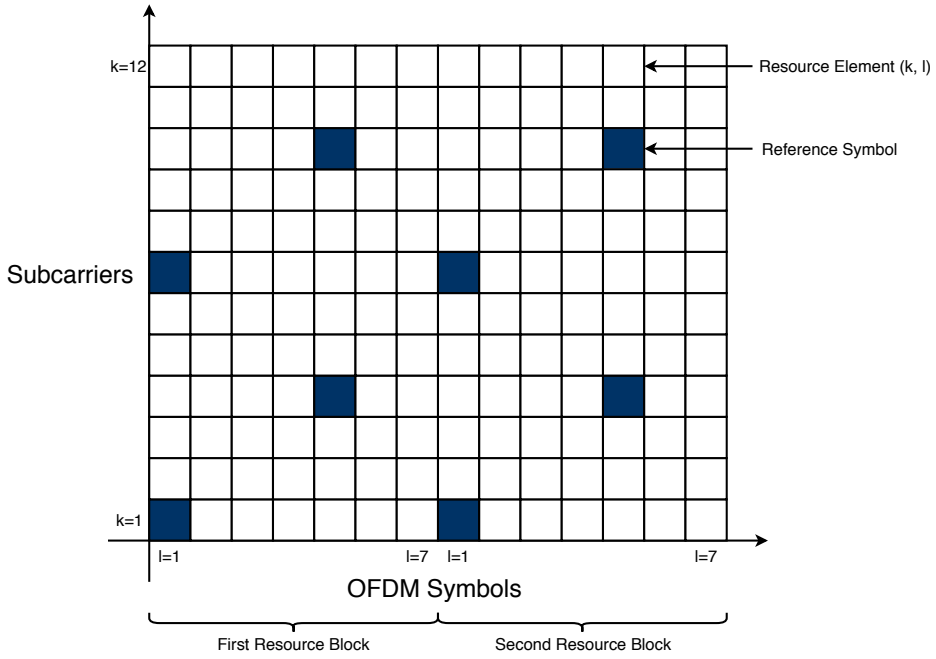


Fig. 4.5: LTE Downlink Pilot Symbols

For uplink transmissions, a block-type pilot pattern occupying an entire OFDM symbol in a resource block is specified. Every uplink resource block contains such a pilot pattern as illustrated in Figure 4.6. Such a block-type pilot pattern is necessary for uplink transmission since the use of SC-FDM (additional spreading by means of an DFT in the uplink) spreads the input symbols over all of the subcarriers in an OFDM symbol. As a result, there are no subcarriers available in an OFDM symbol that can be assigned with pilots. Thus, the standard specifies/reserves a dedicated OFDM symbol in every resource block for the pilots.

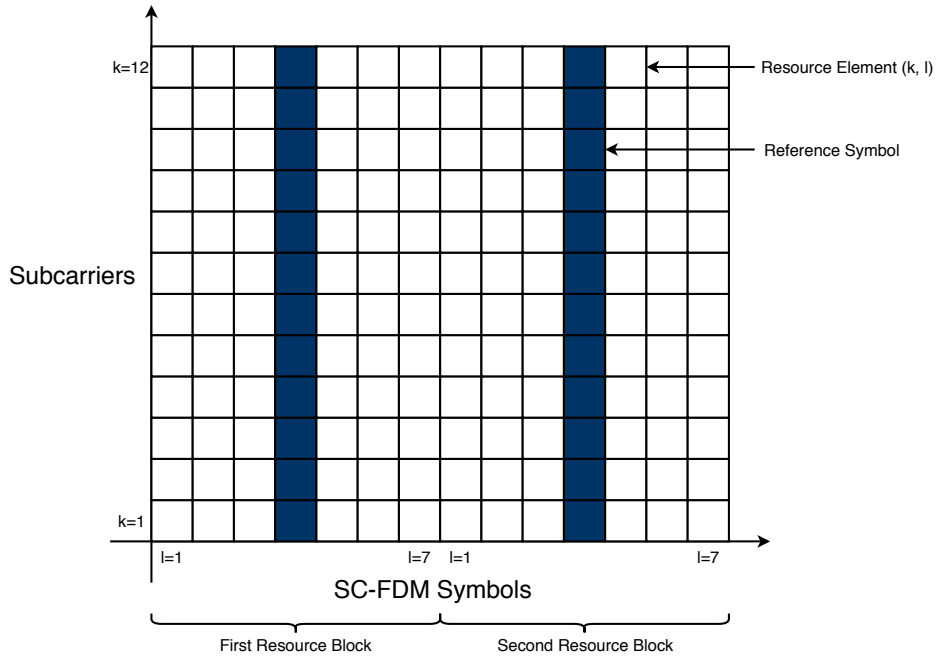


Fig. 4.6: LTE Uplink Pilot Symbols

LTE Release 14 is one of the latest updates that adds new functionality to cellular networks that would also be part of 5G. Release 14 introduces support for Vehicle to Everything (V2X) mode that should enable a robust vehicular communication. The V2X mode also specifies the use of SC-FDMA like the uplink transmission. However, to address the highly dispersive environment along with high mobility conditions, the addition of more pilots is one of the most important modifications compared to the uplink. The presence of more pilots allows for a more precise channel estimate especially in high mobility conditions as shown in [1]. Figure 4.7 shows block-type pilots on two OFDM symbols in a V2X mode resource block with a short cyclic prefix (7 OFDM symbols in each resource block). Block pilots are located at the third and the sixth OFDM symbol in each resource block.

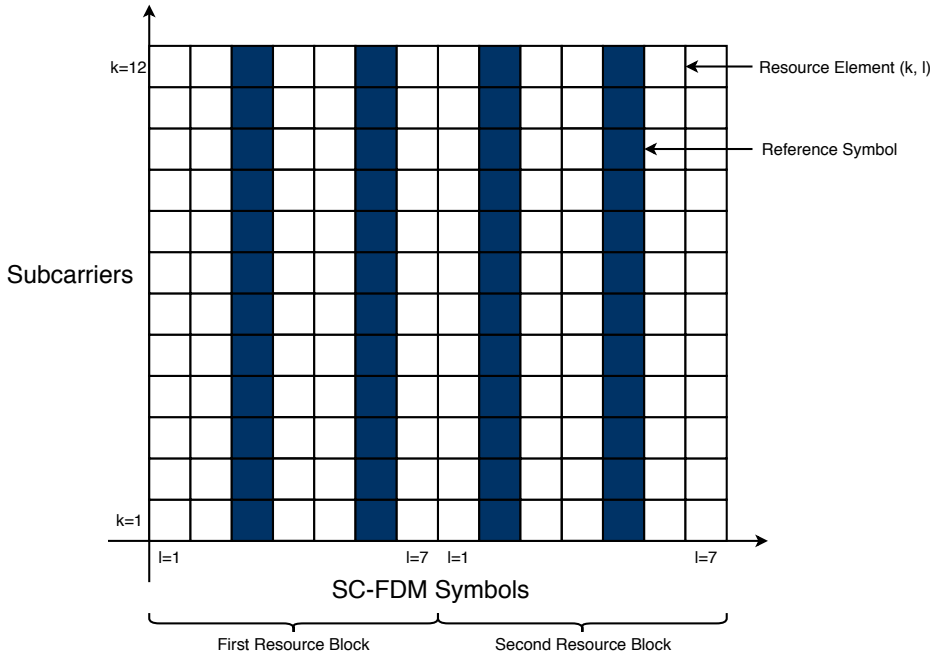


Fig. 4.7: LTE V2X Pilot Symbols

The next aspect of LTE specification is the so called duplex schemes that allows simultaneous transmission and reception of data. In LTE, two forms of duplex schemes are specified, Frequency Division Duplex (FDD) and Time Division Duplex (TDD). In the TDD mode, the uplink and downlink are multiplexed using different time slots while using the same frequency. Consequently, in the FDD mode, the use of different frequency bands for the uplink and downlink allows for a simultaneous transmission and reception of data.

The frame structure is thus dependent on the duplex scheme employed. An LTE FDD frame is shown in Figure 4.8. The FDD duplex mode is simple to understand as the uplink and downlink use different frequencies with synchronous slots [143]. From the figure, 10 ms is the length of the LTE frame, 1 ms is the length of a subframe that consists of two slots with a duration of 0.5 ms each. DL and UL represent downlink and uplink respectively.

The TDD duplex mode has a more complicated framing structure. Figure 4.9 shows all the specified configurations for the TDD framing structure. The location of the uplink, downlink, and a so called *S* subframe is determined by the chosen configuration. A special sub frame S is used to facilitate the switch from the downlink to uplink. Interestingly, this subframe is only required when switching from the downlink to uplink. This can be justified with the following line of thought. The mobile devices or user equipment devices can be at

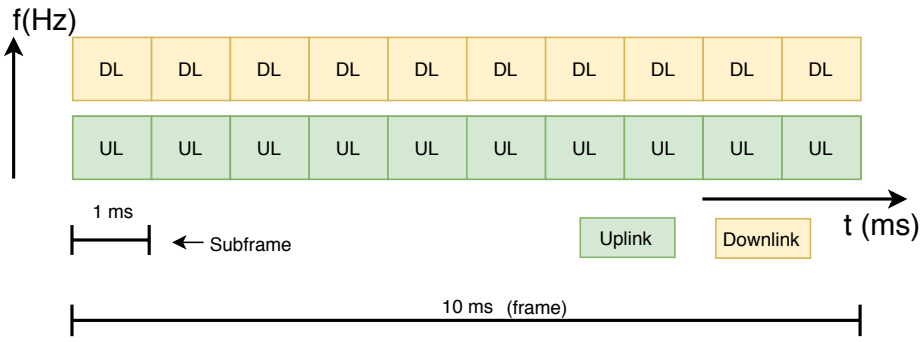


Fig. 4.8: LTE FDD Frame Structure

different distances from the base station they are connected to. The data from the base station in the downlink will logically arrive at different instances to each device (due to different distances from the base station). To compensate for this and ensure that all user devices will switch to the uplink at the same instant, the S subframe is introduced. Moreover, due to the significantly better infrastructure and higher processing capability at the base station, the switch from uplink and downlink is seamless and needs no special subframe.

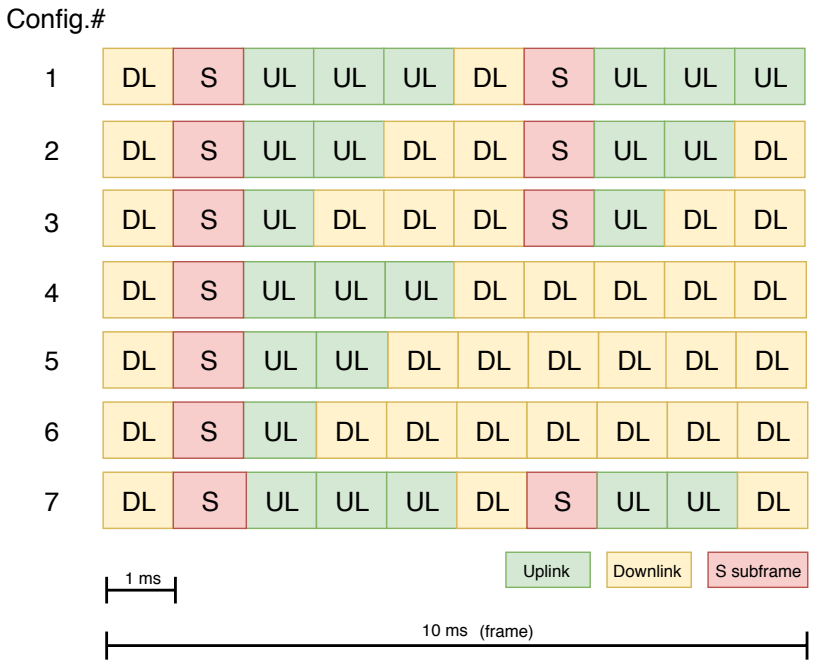


Fig. 4.9: LTE TDD Frame Structure [146]

Each subframe in the two duplex schemes contains resource blocks that carry six or seven OFDM symbols depending on the length of the cyclic prefix. Figures 4.10 and 4.11 shows the downlink and uplink slots with a short and a long cyclic prefix respectively.

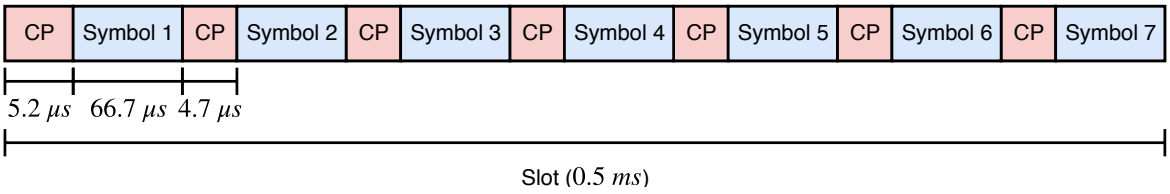


Fig. 4.10: DL/UL Slot Structure with Short CP

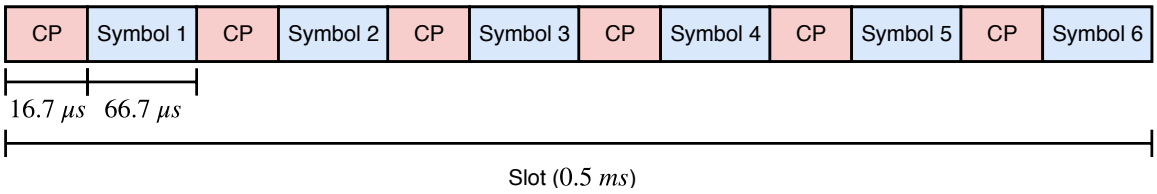


Fig. 4.11: DL/UL Slot Structure with Long CP

All the specifications discussed here are implemented in the LTE simulation platform[1] that is introduced in Section 9.2. The LTE standard has been systematically investigated and developed for nearly a decade and as such is a fairly complicated wireless standard. Nevertheless, this chapter has aspired to provide a detailed overview of the specifications that are relevant for this thesis. The provided simulation platform is ensured to be modular and enable the addition of modules that implement the physical layer with a finer granularity.

[1] Available at: https://git.nt.uni-saarland.de/HiMo/SimTool_LTE. ©Telecommunications Lab, Saarland Informatics Campus. Authors: Kelvin Chelli, Ramzi Theodory, and Thorsten Herfet

## 4.2 Terrestrial Broadcasting

Terrestrial broadcasting technology is concerned with the distribution of television signals (or stations) to households with a television receiver. This technology has been evolving ever since its first experimental broadcast on 30$^{th}$ September 1929 by the British Broadcasting Corporation (BBC). Already in the year 1936, a full television program was started that simultaneously transmitted both audio and pictures[2]. Through the decades, the terrestrial broadcasting technology has stood the test of times and is one of the few inventions that continues to have a significant impact on the society by enabling news and entertainment to reach a vast number of households.

Digital terrestrial television is the transmission of digitized content like video, audio, and auxiliary information such as data signals [125]. The design and development of such digital broadcast systems began in 1990 after more than five decades of analog television. In the USA, the Federal Communications Commission (FCC) adopted the Advanced Television Systems Committee (ATSC) digital television standard and mandated its use for terrestrial television broadcasts in 1996 [81]. Since then, the standard has evolved significantly and its latest version, the ATSC 3.0 standard [27] has been deployed in South Korea in 2017.

In Europe, the Digital Video Broadcasting (DVB) consortium has been the driving force behind the development of digital television in Europe and many other parts of the world. This is an industry-led consortium of regulatory institutes, various broadcasters, hardware manufacturers, software developers, and content owners. The specifications for terrestrial transmission was adopted in 1995 as a European telecommunication standard, *ETSI f300 744* and is known as the Digital Video Broadcasting - Terrestrial (DVB-T) standard. The DVB-T standard was first deployed in England in the year 1998. The success of DVB-T encouraged the DVB consortium to investigate improvements already in 2006. The resulting Digital Video Broadcasting - Second Generation Terrestrial (DVB-T2) standard provides increased capacity, flexibility, and robustness relative to the DVB-T standard. It was adopted as a ETSI standard in 2009. Deployments across Europe have started from 2018.

In Japan, the development of digital television started in the year 1994. The terrestrial digital television standard was designated as Integrated Services Digital Broadcasting - Terrestrial (ISDB-T) and shares several similarities with the DVB-T standard [152]. Digital terrestrial services was launched in Japan in 2003 [152]. The global market penetration of

[2]Appeared in the 'Radio Times' magazine on 01.11.1936. Link: bit.ly/RadioTimes1936

these terrestrial broadcasting technologies is seen in Figure 4.12.

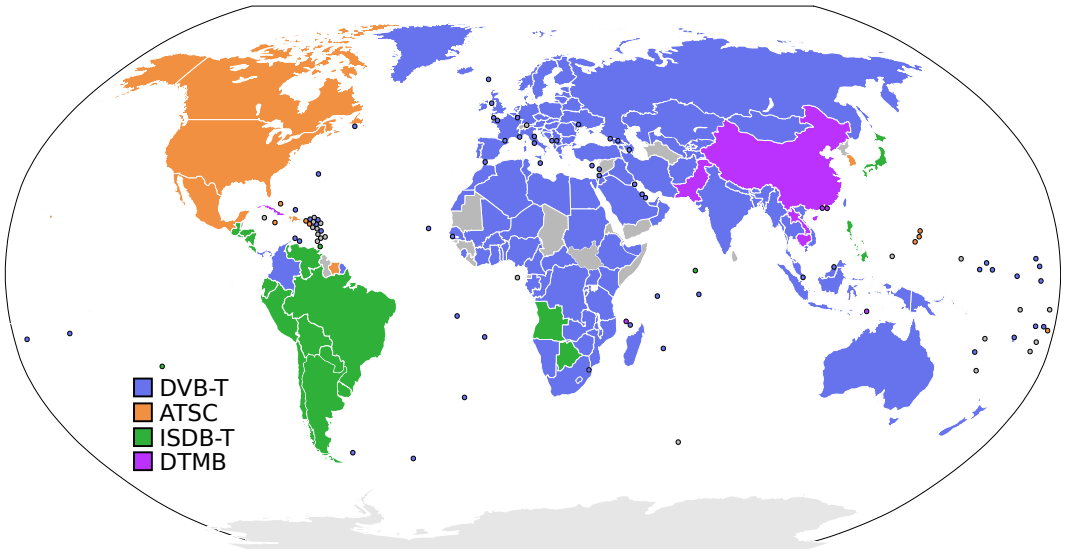


Fig. 4.12: Digital Terrestrial Television Systems Adoption [3]

In this chapter, the specifications of the DVB-T2 standard that are relevant for this thesis are discussed. Like most of the wireless communication system that we use on a daily basis, DVB-T2 also uses a variant of OFDM in the physical layer called COFDM. Here, FEC schemes along with time and frequency interleaving are applied to the signal before the generation of OFDM symbols. This is expected to provide a better robustness against the effects of a wireless channel at the receiver. Correspondingly, this scheme is known as *Coded-OFDM*. The DVB-T2 standard provides significant improvements to the physical layer waveform compared to the older DVB-T standard. Table 4.3 compares the COFDM numerology of the two standards and shows the improvements along with the added flexibility of the DVB-T2 standard. The extended FFT sizes, guard interval lengths, bandwidths, modulation, and FEC schemes provides the flexibility needed to tailor an optimal solution for a given requirement. The configurable scattered and continual pilots help in adapting the capabilities of channel estimation and equalization at the receiver while optimizing the achievable data rate.

[3] Source: https://commons.wikimedia.org/wiki/File:Digital_terrestrial_television_standards.svg

Table 4.3: Comparison of DVB-T and DVB-T2 Standards.

| Parameters | DVB-T | DVB-T2 |
|---|---|---|
| FFT Size | 2K, 8K | 1K, 2K, 4K, 8K, 16K, 32K |
| Guard Interval | $\frac{1}{4}, \frac{1}{8}, \frac{1}{16}, \frac{1}{32}$ | $\frac{1}{4}, \frac{19}{128}, \frac{1}{8}, \frac{19}{256}, \frac{1}{16}, \frac{1}{32}, \frac{1}{128}$ |
| Bandwidth (MHz) | 6, 7, 8 | 1.7, 5, 6, 7, 8, 10 |
| Modulation Mode | QPSK, 16QAM, 64QAM | QPSK, 16QAM, 64QAM, 256QAM |
| FEC Schemes | Convolutional and RS | LDPC and BCH |
| Scattered Pilots | 8% of total | 1%, 2%, 4%, 8% of total |
| Continual Pilots | 2% of total | $0.4\% - 2\%$ of total |
| Typical Data rate (Mbps) | 24 | 40 |
| Max Data rate (Mbps) | 31.7 | 45.5 |
| Required C/N (dB) | 16.7 | 10.8 |

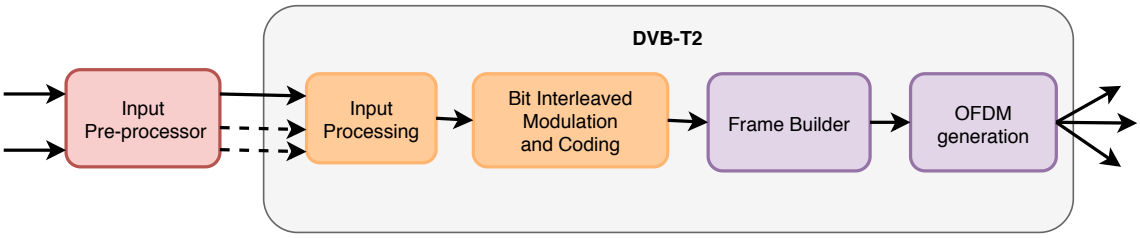


Fig. 4.13: Generic DVB-T2 High Level Architecture

Figure 4.13 shows the the generic system architecture in DVB-T2. The *Input Pre-processor* block is not part of DVB-T2 but enables the system to process multiple Transport (TS) and/or Generic Streams (GS). These are then carried into the individual Physical Layer Pipes (PLP) of the DVB-T2 system. A PLP is basically a logical channel that may carry one or multiple services in a broadcasting scenario. The *Input Processing* block enables mode and stream adaption allowing either a single PLP or multiple PLP's to be processed. The

output of this block are the baseband frames that are passed onto the *Bit Interleaved Modulation and Coding* (BICM) block. The BICM block is concerned with FEC operations to make the transmitted signal robust against channel perturbations. In DVB-T2, LDPC and BCH schemes are specified with different code rates. The LDPC is specified as an inner code and the BCH is specified as the outer code. The BICM block also implements bit interleaving, constellation rotation, cell, and time interleaving. Finer aspects of this block are not relevant for this thesis and can be found in [45].

The *Frame Builder* block assembles the FEC encoded and interleaved cells from the previous block into arrays of active OFDM cells that will correspond to the OFDM symbols which will eventually make up the overall frame structure [47]. The DVB-T2 hierarchical frame structure is shown in Figure 4.14.

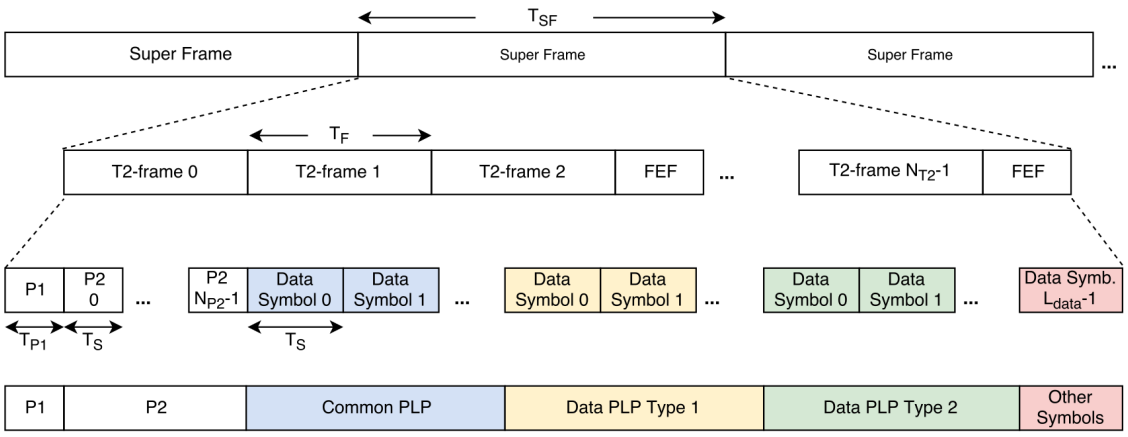


Fig. 4.14: DVB-T2 Frame Structure

The frame structure in DVB-T2 consists of *Super Frames* that are divided into so-called *T2 Frames* and these are further divided into OFDM symbols. The super frame, T2 frame, and the OFDM symbols have a duration of $T_{SF}$, $T_F$, and $T_S$ respectively. Each of the T2 frames contain an additional Future Extension Frame (FEF) as seen from Figure 4.15. The purpose of these FEF frames is to enable the possibility to test frames that would be defined in a future evolution of the underlying standard. The DVB-T2 standard specifies multiple FEF frames in a super frame provided that they are not adjacent to each other [45]. The number of the T2 frames and the FEF parts are configurable parameters that are signaled during a transmission. The maximum duration of a DVB-T2 super frame is specified to be $T_{SF} = 63.75s$ in the absence of FEF's or $T_{SF} = 127.5s$ with the FEF's being used.

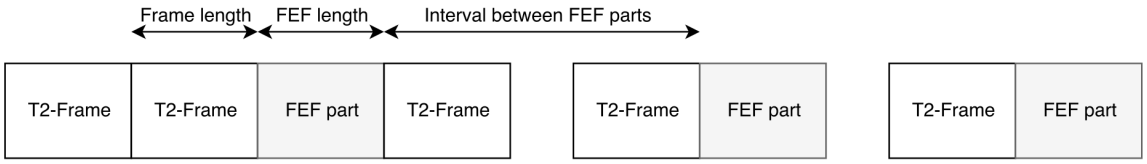


Fig. 4.15: DVB-T2 Super Frame

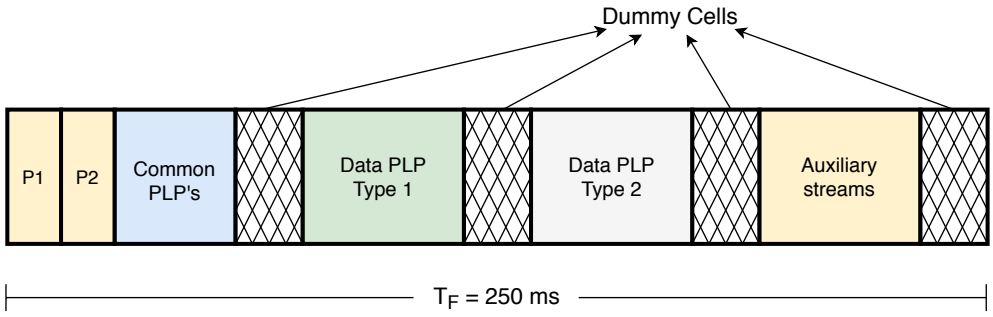


Fig. 4.16: T2-Frame Structure

Figure 4.16 shows the structure of a T2 frame. It begins with the P1 preamble that aids in signal detection, synchronization, and contain basic transmit parameters. It is followed by one or more P2 preambles. The propose of the P2 preamble is to carry the so called L1 signaling information that is required by the receiver in order to access the PLP's in a T2 frame. It contains information like the guard interval used in the current super frame, PAPR mode, constellation type, code rates, pilot pattern types, PLP type, and other system specific parameters as described in [47]. The rest of the T2 frame consists of different types of PLP's namely, common PLP, data PLP type 1, and data PLP type 2 that mainly differ in the way they are sub-sliced in a T2 frame. The elementary resource unit in a T2 frame is an *active OFDM cell*. The T2 frame elements may occupy multiple active OFDM cells in a T2 frame.

In the next step, the cells that are produced by the frame builder are given to the *OFDM Generation* block (seen in Figure 4.13). The OFDM generation block also inserts the pilots that are vital for channel estimation and equalization at the receiver. Pilots contain reference information that are modulated on various OFDM cells. DVB-T2 also specifies the pilot cells to be transmitted at a higher power level to improve its robustness against noise at the receiver. To ensure a rich diversity of reference information at the receiver, the DVB-T2 standard specifies different pilot groups that are summarized in Table 4.4.

Table 4.4: Pilot Patters in DVB-T2

| DVB-T2 Symbol | Pilot Pattern Type | | | | |
|---|---|---|---|---|---|
| | Edge | Frame-closing | P2 | Scattered | Continual |
| P1 | - | - | - | - | - |
| P2 | - | - | Present | - | - |
| Data | Present | - | - | Present | Present |
| Frame-closing | Present | Present | - | - | - |

**Edge Pilots** are present on the edge carriers in all the data OFDM symbols and frame closing symbols in a DVB-T2 frame. The edge pilots are present to ensure frequency interpolation of the channel transfer function up to the edge of the spectrum.

**Frame-closing Pilots:** The frame closing OFDM symbols are present in a few specific transmission modes where due to the underlying numerology a special frame is needed to cleanly close the frame. These frame closing symbols contain the frame-closing pilots.

**P2 Pilots** are present in P2 symbols of the DVB-T2 frame along with the L1 signaling information. The P2 pilots have a dense comb-type pattern with a pilot at every third subcarrier in an OFDM symbol. Thus, these pilots are an ideal choice for channel compensation techniques since the higher density enables a precise estimate of the wireless channel in the beginning of every T2 frame.

**Scattered Pilots** are present in all the data OFDM symbols in a T2 frame. The DVB-T2 standard specifies 8 different scattered pilot patterns. This flexibility in the pilot patterns enables the broadcasters to find an optimal mode for a given transmission scenario. Scattered pilots are parameterized by the frequency separation of pilots denoted by $D_x$, and the number of OFDM symbols $D_y$ that form a complete scattered pilot sequence. The different scattered pilot patterns and the parameters that define them are shown in Table 4.5.

Table 4.5: Scattered Pilot Patterns [47]

| Pilot Pattern | Separation of pilot bearing carriers ($D_X$) | No.of symbols forming one scattered pilot sequence ($D_Y$) |
|---|---|---|
| PP1 | 3 | 4 |
| PP2 | 6 | 2 |
| PP3 | 6 | 4 |
| PP4 | 12 | 2 |
| PP5 | 12 | 4 |
| PP6 | 24 | 2 |
| PP7 | 24 | 4 |
| PP8 | 6 | 16 |

The choice of a given pilot pattern is governed by the payload capacity and the Doppler performance at the receiver. Dense pilot patterns (smaller distance between pilots) occupy more subcarriers in an OFDM symbol and thus, fewer subcarriers are used for data which reduces the payload capacity. In a similar manner, pilot patterns with a faster repeat cycle (like $D_Y = 2$) provide a better performance in Doppler mitigation. The impact of the scattered pilot configuration on the performance of channel estimation is studied in [59].

Figure 4.17 shows the PP1 pilot pattern for DVB-T2. Accordingly, the separation of pilot bearing carriers in the frequency domain $D_X$ is 3 and the number of OFDM symbols that form a complete scattered pilot sequence $D_Y$ is 4.

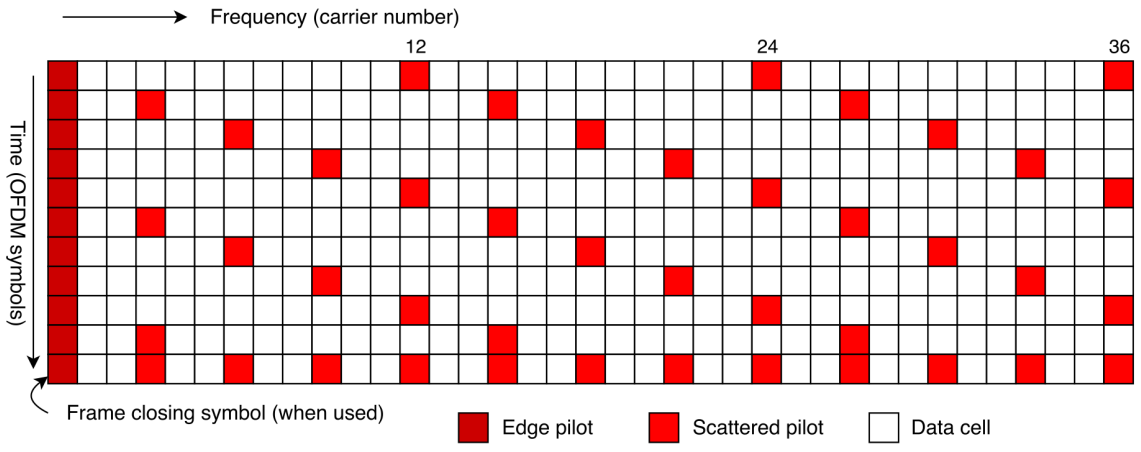


Fig. 4.17: DVB-T2 P1 Pilot Pattern

The availability of a given scattered pilot pattern depends on the FFT size and guard interval of the underlying OFDM configuration. Table 4.6 summarizes the available pilot patterns for different configurations of the SISO transmission mode in DVB-T2. The scattered pilot patterns enable a precise analysis of the frequency and temporal characteristics of the channel at the receiver and is thus used for channel estimation.

Table 4.6: Scatter Pilot Patterns available for Different OFDM Configurations [47]

| FFT Size | Guard Interval Fraction | | | | | | |
|---|---|---|---|---|---|---|---|
| | 1/128 | 1/32 | 1/16 | 19/256 | 1/8 | 19/128 | 1/4 |
| 32K | PP7 | PP4<br>PP6 | PP2<br>PP8<br>PP4 | PP2<br>PP8<br>PP4 | PP2<br>PP8 | PP2<br>PP8 | NA |
| 16K | PP7 | PP7<br>PP4<br>PP6 | PP2<br>PP8<br>PP4<br>PP5 | PP2<br>PP8<br>PP4<br>PP5 | PP2<br>PP3<br>PP8 | PP2<br>PP3<br>PP8 | PP1<br>PP8 |
| 8K | PP7 | PP7<br>PP4 | PP8<br>PP4<br>PP5 | PP8<br>PP4<br>PP5 | PP2<br>PP3<br>PP8 | PP2<br>PP3<br>PP8 | PP1<br>PP8 |
| 4K, 2K | NA | PP7<br>PP4 | PP4<br>PP5 | NA | PP2<br>PP3 | NA | PP1 |
| 1K | NA | NA | PP4<br>PP5 | NA | PP2<br>PP3 | NA | PP1 |

**Continual Pilots** are much sparser compared to the scattered pilots and are present in each of the OFDM data signal at the same carrier positions for a given FFT mode. The distribution of these pilots are chosen such that no repetitions occur within an OFDM symbol. These pilots are intended to be used for coarse frequency offset adjustment and are also suitable for channel estimation and compensation schemes.

The rich diversity of the pilots in DVB-T2 is a significant improvement over the older DVB-T standard. This flexibility enables the network planner to tailor a transmission mode that provides the best payload capacity with the least overhead for a given transmission scenario. It is also expected that the signal processing blocks in the receiver must have a flexible

structure to allow for the different transmission options in order to exhibit an improvement in performance [110].

After the insertion of the pilots, the frame builder organizes the active OFDM cells into the specified frame structure. The *OFDM Generation* block (in Figure 4.13) then performs an IFFT on the active cells. If specified in the L1 signaling, PAPR reduction is performed after which a guard interval is inserted to the OFDM signals to give the complete DVB-T2 signal that can be transmitted. The DVB-T2 standard also specifies different guard intervals for the each of FFT modes that is shown in Table 4.7. The choice of a guard interval depends on the distance between neighboring broadcasting stations and the corresponding receivers to be served.

Table 4.7: Guard Intervals ($\mu$s) in DVB-T2

| FFT Size | $T_u$ (ms) | Guard Intervals | | | | | | |
|---|---|---|---|---|---|---|---|---|
| | | 1/128 | 1/32 | 1/16 | 19/256 | 1/8 | 19/128 | 1/4 |
| 32 K | 3.584 | 28 | 112 | 224 | 266 | 448 | 532 | - |
| 16 K | 1.792 | 14 | 56 | 112 | 133 | 224 | 266 | 448 |
| 8 K | 0.896 | 7 | 28 | 56 | 66.5 | 112 | 133 | 224 |
| 4 K | 0.448 | - | 14 | 28 | - | 56 | - | 112 |
| 2 K | 0.224 | - | 7 | 14 | - | 28 | - | 56 |
| 1 K | 0.112 | - | - | 7 | - | 14 | - | 28 |

The DVB-T2 is a complex and complicated standard that aims to offer an efficient and reliable broadcast transmission for a wide variety of portable, fixed, and mobile receivers. It is accepted as the state-of-art digital terrestrial transmission scheme in Europe and is used in this thesis to evaluate the proposed channel estimation and equalization schemes in Section 10.3.

## 4.3 Broadband

The broadband transmission technology has enabled short range communication and played a significant role in improving the indoor atmosphere by providing a nearly seamless wireless connectivity. It has increased the productivity in offices while at the same time, enhanced comfort at home. Introduced in the year 1997 with a vision to quite literally untether the Per-

sonal Computer (PC) from the Ethernet cable, the IEEE 802.11 has evolved into a ubiquitous standard for indoor wireless communication and specifies Wireless Local Area Networks (WLAN) [60]. Over the years, several capabilities have been added to the original standard and have been named by the various amendments. Each of these provide specifications that dictate the implementation of WLAN's in various frequency bands. As described by the Wi-Fi Alliance, it is indeed one of the most significant success stories in the high tech era that brings connectivity that is affordable and most importantly works reliably around the world. The Wi-Fi alliance has been promoting the technology and ensuring interoperability by certifying Wi-Fi products since 1999. The IEEE802.11 working group[4] is part of the IEEE Standards Association and concerns itself with investigating and standardization of different Wi-Fi standards.

The IEEE 802.11p is a relatively new standard approved in late 2011 for Wireless Access in Vehicular Environments (WAVE) and Dedicated Short Range Communications (DSRC) that provides a wireless communication system for vehicles, paving the way for Intelligent Transport Systems (ITS). The vision of ITS is a vast network of connected vehicles that are able to communicate with each other, sharing data that can be leveraged by various applications to enhance the safety and quality of road travel [149]. Realizing the potential of ITS, various standardization groups and regulatory bodies have allocated a dedicated frequency band for DSRC applications. Table 4.8 gives an overview of the allocated frequency bands in different regions.

Table 4.8: Spectrum Allocation for DSRC Applications [101]

| Country/Region | Frequency Bands (MHz) |
|---|---|
| Europe | 5795 – 5815, 5855 – 5905 |
| North America | 902 – 928, 5850 – 5925 |
| Japan | 715 – 725, 5770 – 5850 |

In Europe, the 70 MHz of spectrum in the 5.9 GHz frequency band is shared among 7 channels that have a bandwidth of 10 MHz each. The upper band of the IEEE 802.11p spectrum is illustrated in Figure 4.18 and shows the different service and control channels.

[4]http://www.ieee802.org/11/

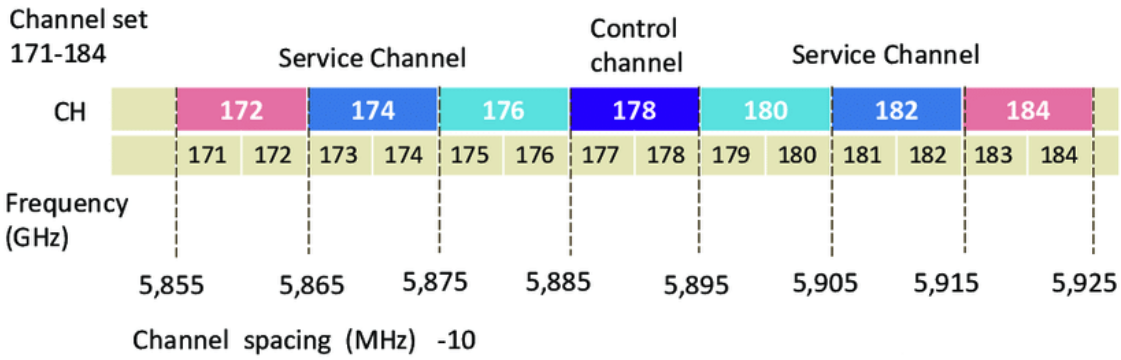


Fig. 4.18: IEEE 802.11p Frequency Allocation [130]

The control channel is often reserved for safety messages, while the service channels are intended for less critical data transmissions [86]. The standard provides a transmission range of roughly 1 km at a transmission rate of 3 Mbps in the most robust mode and can support vehicles with a relative velocity of 250 Kmph, as described in [130]. At first glance, a data rate of 3 Mbps seems to be slow especially when compared to the data rates that can be achieved by competing wireless standards. However, the usage scenarios in DSRC mostly include the exchange of short messages. Moreover, vehicular environments inherently pose a more challenging wireless channel. Thus, more precedence has been given to a robust and reliable communication capabilitiy.

The IEEE 802.11p physical layer is relevant to understand the schemes proposed in this thesis. It is a close adaptation of the IEEE 802.11a standard that is a well known WLAN standard typically used in stationary indoor environments. However, in vehicular usage scenarios the IEEE 802.11p standard must cope with time-variant multipath channels [17]. The modifications introduced in the IEEE 802.11p standard are discussed in this section and their effectiveness in overcoming the effects of mobility are investigated.

The physical layer of the IEEE 802.11p is based on OFDM that is described in Section 2.1 and the frame structure is analogous to the IEEE 802.11a standard [86]. Table 4.9 compares the physical layer parameters of both the standards and helps in understanding the changes made to the IEEE 802.11p standard.

Table 4.9: Comparison of IEEE 802.11a and IEEE 802.11p [129].

| Parameters | IEEE 802.11a | IEEE 802.11p | Changes |
|---|---|---|---|
| Guard Interval | $0.8\mu sec$ | $1.6\mu sec$ | Double |
| Bandwidth | $20MHz$ | $10MHz$ | Half |
| Symbol duration | $4\mu sec$ | $8\mu sec$ | Double |
| Bit Rate(Mbps) | 6, 9,12,18, 24, 36, 48, 54 | 3, 4.5, 6, 9, 12, 18, 24, 27 | Half |
| Modulation Mode | BPSK, QPSK, 16QAM, 64QAM | BPSK, QPSK, 16QAM, 64QAM | No Change |
| Code rate | $1/2$, $2/3$, $3/4$ | $1/2$, $2/3$, $3/4$ | No Change |
| Number of subcarriers | 52 | 52 | No Change |
| FFT period | $3.2\mu sec$ | $6.4\mu sec$ | Double |
| Preamble duration | $16\mu sec$ | $32\mu sec$ | Double |
| Sub-carrier spacing | $0.3125MHz$ | $0.15625MHz$ | Half |

The essential differences are highlighted as follows:

- In typical vehicular environments, in addition to a rich multipath, the path delay difference is also expected to be significantly bigger in comparison to indoor environments. Thus, in order to cope with longer delays, the guard interval has been doubled when compared to IEEE 802.11a.
- The bandwidth of the IEEE 802.11p standard is halved compared to its counterpart, which consequently doubles the symbol duration. Since the 802.11p standard is conceived for vehicle-to-vehicle communication involving the exchange of short safety critical information rather than continuous communication for home or office usage, a bandwidth of 10 MHz is adequate for the purpose. Consequently, the data rate for the same modulation schemes is also halved.
- The subcarrier frequency spacing $f_{sc}$ is the ratio of the channel bandwidth $W$ to the total number of subcarriers $N$ given by $f_{sc} = W/N$. Since the number of subcarriers are the same in both the cases and the bandwidth in halved in the 802.11p standard, the

subcarrier spacing in the 802.11p is halved. Thus, the subcarriers in the IEEE 802.11p standard are relatively more narrowband than its counterparts. This is surprising at the first glance since it makes the IEEE 802.11p standard more susceptible to Doppler shift. However, the carrier spacing is still very large (156.25 KHz) so that the influence of Doppler shift and ICI can be easily managed at the receiver.

The structure of a physical layer OFDM frame is seen in Figure 4.19. Every physical layer frame starts with a specified set of preambles, also known as the Physical layer Convergence Protocol (PLCP) header. The purpose of preambles is to enable the receiver to detect the start of a frame and ensure a reliable estimate of the timing and frequency offsets that is used to establish synchronization. Thus, the preambles play a vital role in aligning the data payload in time and amplitude, as described in [76].

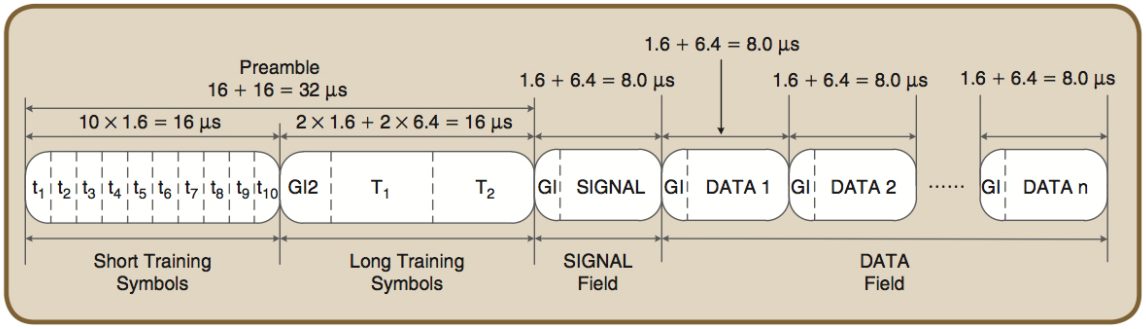


Fig. 4.19: IEEE 802.11p Frame structure [169]

The first part of the PLCP header are the *short preambles* or the *short training symbols*. The short preambles span two OFDM symbols or 16$\mu$s ($2 \times 8\mu s$). These are then divided into 10 short symbols each consisting of 16 samples and spanning 1.6$\mu s$. According to the specifications, the short preamble should enable signal detection, coarse timing synchronization, and coarse frequency offset estimation [144]. Every fourth subcarrier in a short preamble has an equal magnitude and a predefined phase shift. The rest of the subcarriers within a short preamble are all set to zero.

The second part of the PLCP header is the *long preamble* or the *long training symbols*. The long preambles consist of two OFDM symbols spanning 16$\mu$s. The long preambles are used by channel estimation and equalization algorithms along with mechanisms that provide fine frequency offset estimates [133]. The CS based channel estimation techniques proposed in this thesis use the long preambles to get a robust and accurate estimate of the delay profile as described in Chapter 6. Moreover, the long preambles are also used to quantify the channel variations between two physical layer frames. Each of the long preambles consist of 52

predefined subcarriers ( shown in Equation (4.1) ) and 12 null subcarriers that form the guard band.

$$\begin{aligned} \boldsymbol{l}_{-26,26} = &(1,1,-1,-1,1,1,-1,1,-1,1,1,1,1,1,\\ &1,1,-1,-1,1,1,-1,1,-1,1,1,1,1,1,\\ &0,1,-1,-1,1,1,-1,1,-1,1,-1,-1,-1,\\ &-1,-1,1,1,-1,-1,1,-1,1,-1,1,1,1,1) \end{aligned} \tag{4.1}$$

The next part of the physical layer frame is the *signal* field and is shown in Figure 4.20. This field conveys information to the receiver that is required to decode the data [2, 86]. The *rate* field uses four bits to specify the bit rate at which the data in the payload has been transmitted. Bit 4 is reserved for future use and is set to 0 [97]. The *length* field consisting of 12 bits that indicate the number of data octets that are part of the data payload in the current frame. Bit number 17 is the parity bit. The *signal tail* is consisting of 6 bits set to zero [90]. The entire signal field is Binary Phase Shift Keying (BPSK) modulated with a code rate $r = \frac{1}{2}$ that has consequently restricted it to 24 bits, as seen in Figure 4.20.

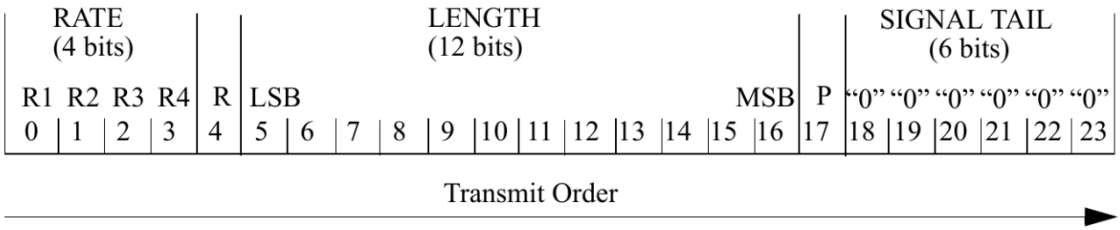


Fig. 4.20: IEEE 802.11p Signal Field Bit Assignment [86]

The last part of the physical layer frame is the *data* field. To get a deeper understanding of this field, the Physical layer Protocol Data Unit (PPDU) is shown in Figure 4.21.

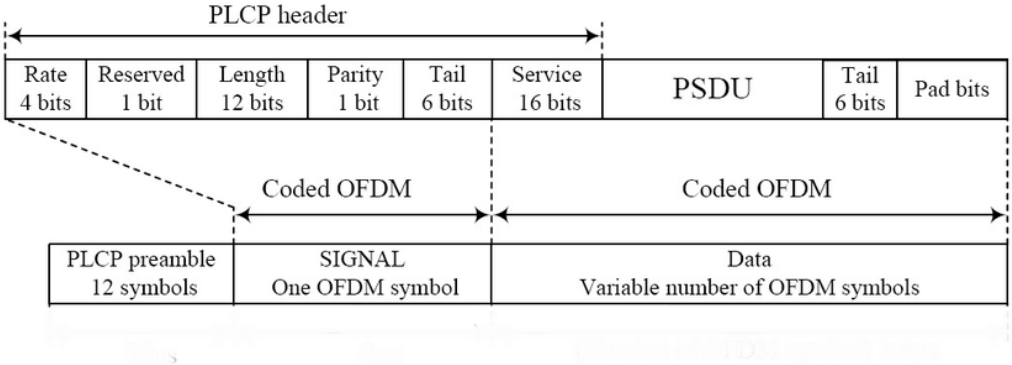


Fig. 4.21: IEEE 802.11p PPDU format [156]

Observe that the data field begins with a *service* field that is 16 bits long and is used by the descrambler in the receiver to initialize itself. Bits 0-6 of the service field are initially set to 0 (before scrambling) and are used to synchronize the descrambler in the receiver. The remaining 9 bits of the service field are reserved for future use and are set to 0 in the specifications [30]. The standard specifies a pseudo random nonzero vector as the initial state of the scrambler. Thus, these seven bits (bits 0-6) of the service field are all set to 0 before scrambling so that the initial state of the scrambler can be estimated at the receiver [30]. The next part of the PPDU consists of the data payload or the data for the MAC layer that is aggregated into a Physical layer Service Data Unit (PSDU). The six *tail* bits in the end are set to 0 and are required to return the convolutional encoder to the zero state [90]. The final part of the PPDU is the *pad* bits. This field ensures that the number of bits in the *data* field is an integer multiple of the number of coded bits in an OFDM symbol by extending the length of the message. The number of *pad* bits $N_{PAD}$ required depends on the length of the message and is computed by a simple equation as seen in Equation (4.2) [30]. Here, $N_{DATA}$ is the number of bits in the *data* field and $LENGTH$ refers to the number of bits in the PSDU.

$$N_{PAD} = N_{DATA} - (16 + LENGTH + 6) \tag{4.2}$$

Now, at the transmitter, the data field of every frame is scrambled using a frame synchronous scrambler with the generator polynomial shown in Equation (4.3).

$$m(x) = x^7 + x^4 + 1 \tag{4.3}$$

After scrambling, the data field is then encoded using a convolution encoder shown in Figure 4.22. The encoder uses the $g_0 = 133_8$ and $g_1 = 171_8$ generator polynomials and has constraint length of 7. This is also the reason for the 6 PPDU *tail* bits. The output of the encoding stage is then combined with specified puncturing matrices that results in different code rates after which interleaving is performed. The purpose of scrambling, encoding, and interleaving data in the transmitter is to make the data robust against the effects of frequency selectivity in the wireless channel. Thus, the above schemes, pseudo randomly distributes data over the entire stream in addition to adding redundancy that help in detecting and correcting errors at the receiver.

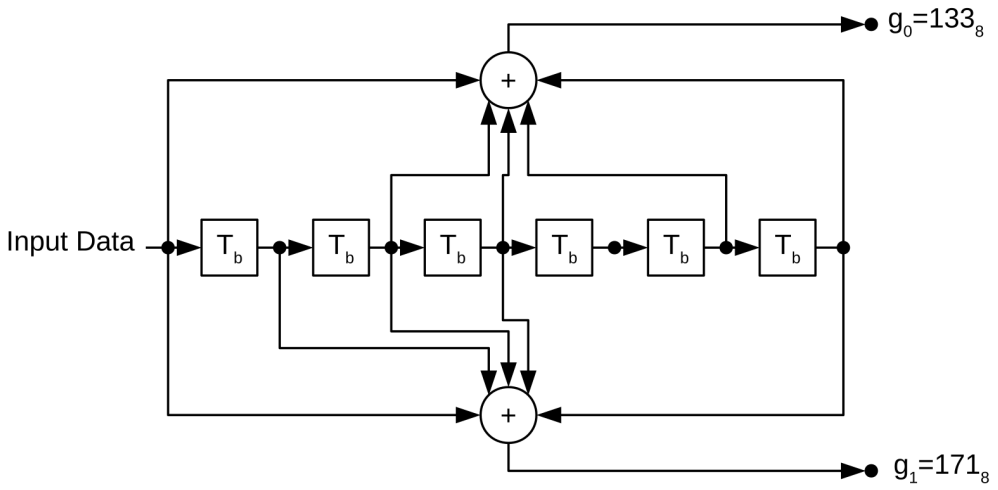


Fig. 4.22: Convolutional Encoder in IEEE 802.11p

Finally, every OFDM symbol in the frame is prepended with a guard interval or a cyclic prefix. The guard interval helps to overcome the multipath effects and makes the OFDM symbol robust against ISI. In IEEE 802.11p, the guard interval is specified to be 25% of the symbol duration. Thus the guard interval spans $1.6\mu s$ and consists of 16 samples.

The guard band is a set of subcarriers that are set to zero (in the frequency domain) and play a vital role in spectral shaping as wireless standards must adhere to the specified spectral masks. Although guard bands reduce the net data rate, it is important to avoid aliasing on the outer subcarriers. In the IEEE 802.11p standard the guard band is composed of 11 subcarriers, 6 of which are at the beginning of the OFDM symbol and 5 are at the end.

The IEEE 802.11p standard in intended to be used in vehicular environments and must be robust against the effects of high mobility. Although the long training symbols in the PLCP header can be used for channel estimation at the beginning of the frame, the time-varying nature of the channel in the presence of high mobility requires the tracking/recomputation of the channel estimate for the data OFDM symbols in the PSDU. To enable this, 4 pilot subcarriers are specified for every OFDM symbol by the standard. Thus, at the beginning of the frame the high density of pilots provided by the long training symbols can be used to compute an accurate estimate of the channel that can be temporally tracked throughout the physical layer frame using the 4 pilots in every OFDM data symbol. Thus in principle, the effects of high mobility can be compensated in IEEE 802.11p. Subcarriers with the indices, $-21$, $-7$, $+7$, $+21$ are defined as pilots with the corresponding initial values $(1 + j0)$,

$(1+j0)$, $(1+j0)$, $(-1+j0)$. The pilots for subsequent OFDM symbols are multiplied by a Pseudo Noise (PN) sequence and the resulting pilots for the first seven OFDM symbols are shown in Table 4.10. All the specifications discussed here have been implemented in the IEEE 802.11p simulation platform [5] that is introduced in Section 9.1.

Table 4.10: Pilots for Data OFDM Symbols [138]

| OFDM Symbol | Pilots | | | |
|---|---|---|---|---|
| | $-21$ | $-7$ | 21 | 7 |
| 0 | $(1+j0)$ | $(1+j0)$ | $(1+j0)$ | $(-1+j0)$ |
| 1 | $(1+j0)$ | $(1+j0)$ | $(1+j0)$ | $(-1+j0)$ |
| 2 | $(1+j0)$ | $(1+j0)$ | $(1+j0)$ | $(-1+j0)$ |
| 3 | $(1+j0)$ | $(1+j0)$ | $(1+j0)$ | $(-1+j0)$ |
| 4 | $(-1+j0)$ | $(-1+j0)$ | $(-1+j0)$ | $(1+j0)$ |
| 5 | $(-1+j0)$ | $(-1+j0)$ | $(-1+j0)$ | $(1+j0)$ |
| 6 | $(-1+j0)$ | $(-1+j0)$ | $(-1+j0)$ | $(1+j0)$ |
| 7 | $(1+j0)$ | $(1+j0)$ | $(1+j0)$ | $(-1+j0)$ |

To conclude, this part of the thesis strives to establish the foundations vital to understand the contributions of this thesis towards enabling high mobility in OFDM based wireless communication systems. Accordingly, a comprehensive description of the various multicarrier schemes relevant for state-of-art wireless standards is provided. A mathematical discourse on the wireless channels has identified the various distortions that have to be overcome by wireless systems. Schemes to overcome the effects of such channels are required to work reliably for wireless standards that share the same or have similar physical layer specifications. Accordingly, commonly used wireless standards are chosen for broadband, broadcast, and cellular domains. The different nuances in the standards and the motivation behind them have been explained. Identifying the problem statement and providing a clear set of contributions further helps the reader to understand the proposed schemes and the results in the remainder of this thesis.

[5] Available at: https://git.nt.uni-saarland.de/HiMo/SimTool_IEEE802.11p. ©Telecommunications Lab, Saarland Informatics Campus. Authors: Kelvin Chelli, Praharsha Sirsi, and Thorsten Herfet

# Part II

# Plot

We know the past but cannot control it.
We control the future but cannot know it.

---

*Claude Elwood Shannon*

# CHAPTER 5

# CHANNEL ESTIMATION

Wireless communication systems have rapidly evolved to become a ubiquitous part of every day life. Depending on the application, modern wireless communication systems are not only expected to provide a reliable connectivity, but also fulfill requirements with respect to latency, bandwidth and energy consumption. However, the physical medium which is the wireless channel poses tough challenges that have been discussed in Chapter 3 of this thesis. A viable technique to overcome these effects is to develop algorithms that estimate the wireless channel at the receiver.

Channel estimation can be considered as the problem of accurately reconstructing the wireless channel. It is a fundamental step towards overcoming the effects of a time-varying multipath channel at the OFDM receiver. In this chapter, the problem of channel estimation is mathematically described and is mostly based on [61, 123]. This will be followed by a comprehensive account of conventional and state-of-art channel estimation schemes.

## 5.1 Formulation

From an implementation point of view, all data and channel models are described in a discrete form in this chapter. Information bit sequences at the transmitter are mapped to a sequence of modulated symbols $(s[i])_{i\in\mathbb{Z}}$ that form a set denoted by $\mathsf{S}$. The set $\mathsf{S}$ is dependent on the underlying modulation scheme and contains the respective constellation points as a subset of the complex plane. Without loss of generality, we consider that a block of $N$ such symbols is transmitted (as one OFDM symbol), undergoes distortion by the wireless channel and is received at the receiver. This enables us to write the subsequence as a $N \times 1$ vector $\mathbf{s}$ and

perform linear operations on it using matrices[1]. This symbol vector **s** is modulated by a linear modulation scheme like Cyclic Prefix Orthogonal Frequency Division Multiplexing (CP-OFDM)[2]. If the modulation matrix is denoted as **T**, the vector of sent symbols can be written as $\mathbf{x} = \mathbf{T} \cdot \mathbf{s}$. The transmitter sends this vector over the wireless channel with a channel transfer function denoted as **H**. The wireless channel also introduces AWGN noise **w**. Thus, a vector of symbols given by $\mathbf{r} = \mathbf{H} \cdot \mathbf{x} + \mathbf{w}$ is received. OFDM demodulation is performed on the received vector **r** using the demodulation matrix **R** to give the vector of demodulated symbols **y** as shown in Equation (5.1). Note that after OFDM demodulation at the receiver, the analysis is done in the frequency domain. On simplifying, the effective channel matrix and the demodulated noise is denoted as $\mathbf{Q} = \mathbf{RHT}$ and $\mathbf{z} = \mathbf{Rw}$ as in Equation (5.1).

$$\begin{aligned} \mathbf{y} &= \mathbf{Rr} && \text{| Substitute for } \mathbf{r} \\ &= \mathbf{R}(\mathbf{Hx} + \mathbf{w}) && \text{| Substitute for } \mathbf{s} \\ &= \mathbf{RHTs} + \mathbf{Rw} \\ &= \mathbf{Qs} + \mathbf{z} \end{aligned} \tag{5.1}$$

To infer the dimensions of the matrices in Equation (5.1) and justify the chosen representation, let us discretize the received signal $r(t) = \int_{-\infty}^{\infty} h(t,\tau) \cdot x(t-\tau) d\tau + w(t)$ (discussed in Section 3.4). The time $t$ and multipath delays $\tau$ are represented by indices $n$ and $m$ respectively. Accordingly, the discretized received signal is given in Equation (5.2).

$$r[n] = \sum_{m=0}^{M-1} h[n,m]x[n-m] + w[n] \tag{5.2}$$

We know that the wireless channel is sparse with a handful of dominant paths that make up most of the signal energy at the receiver [78]. Accordingly, by using $M$ in Equation (5.2), we enforce a finite bound on the number of delay taps in the channel. Thus, if a discrete sample $x[n]$ is sent over the channel, the received sample $r[n]$ consists of the sample $x[n]$ (direct path) and also incorporates the $M-1$ previously transmitted samples with the last one being $x[n-M+1]$. Extending this line of thought, the received sample $r[n+M-1]$ will be the last sample that contains information about $x[n]$. This behavior hints at that property of convolution where the length of the filter is $M$. The channel transfer function **H** that represents this convolutional operation in the matrix form will have the dimension $N_{sym} \times (N_{sym} + M - 1)$ where, $N_{sym} = N + M - 1$ is size of one OFDM symbol including the cyclic prefix. The $M$ non-zero elements in a row are shifted by one position to the right, thereby moving the filter

[1] as the underlying system is linear and the channel distortions are linear or can be linearized

[2] commonly referred to as OFDM in literature and in this thesis

over the transmitted samples.

A visualization of the channel matrix is shown in Figure 5.1. Here, a $N = 64$ subcarrier OFDM system is chosen with a guard interval fraction of $\frac{1}{4}$ that makes $N_{sym} = 80$. The maximum allowed delay is assumed to be $M - 1 = N_{cp} = 16$ samples. This gives the dimension of the channel matrix $\mathbf{H}$ as $80 \times (80 + 16)$ corresponding to $N_{sym} \times N_{sym} + M - 1$ or $N + M - 1 \times N + 2(M - 1)$ when $N_{sym} = N + M - 1$ is substituted.

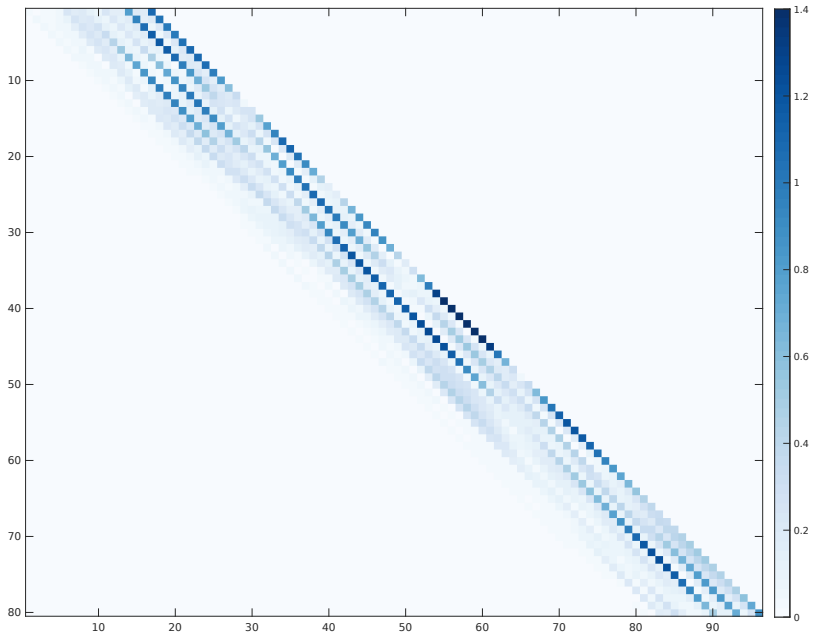


Fig. 5.1: Simulated $80 \times 96$ Channel Matrix in the Time Domain

The CP in an OFDM symbol ensures that all signal energy contributes to the current symbol, thus alleviating the problem of ISI inherently. Note that, in this thesis we only consider OFDM schemes that employ a CP. The length of the prefix is designed based on the application scenario in which the OFDM system would be deployed. In other words, the cyclic prefix considers the maximum delay that a wireless channel will introduce for a given application. For the sake of simplicity, it is a common practice to assume the maximum delay to be equal to the length of the cyclic prefix, so that $N_{cp} = M - 1$.

The wireless channel distorts the OFDM signal with the cyclic prefix whereas, channel estimation takes place at the receiver after stripping out the cyclic prefix. Accordingly, this should be considered in the system model. To begin with, the modulation matrix $\mathbf{T}$ is split into the generic modulation operation denoted by the matrix $\mathbf{T_m}$ and a matrix $\mathbf{T_{cp}}$ that adds

the cyclic prefix by copying the last $M-1$ samples to the beginning of the OFDM symbol. Thus, the modulation matrix can be written as $\mathbf{T} = \mathbf{T_{cp}}\mathbf{T_m}$, where the dimensions of $\mathbf{T_{cp}}$ and $\mathbf{T_m}$ are $N+M-1 \times N$ and $N \times N$ respectively. In a similar manner, the demodulation matrix $\mathbf{R}$ is also split up into a CP removal part $\mathbf{R_{cp}}$ and a generic demodulation part $\mathbf{R_m}$. At the receiver, the CP removal operation takes place first and the additional samples are simply discarded. Thus, the demodulation matrix can be written as $\mathbf{R} = \mathbf{R_m}\mathbf{R_{cp}}$. By virtue of removing the $M-1$ samples in the beginning of the OFDM symbol, no information from the previous block is included in the current block. Accordingly, the first $M-1$ columns of the channel matrix $\mathbf{H}$ can also be dropped. This results in a dimensionality reduction of the channel matrix $\mathbf{H}$ from $N+M-1 \times N+2(M-1)$ to $N+M-1 \times N+M-1$ (or from $N_{sym} \times N_{sym}+M-1$ to $N_{sym} \times N_{sym}$). This also keeps the mathematical formulation to the current block. The simplified channel matrix in the time domain is denoted as $\mathbf{H_t} = \mathbf{R_{cp}}\mathbf{H}\mathbf{T_{cp}}$, has the dimension $N \times N$, and is derived as shown in Equation (5.3).

$$\begin{aligned} \mathbf{Q} &= \mathbf{RHT} && \text{| Substitute for } \mathbf{R} \text{ and } \mathbf{T} \\ &= \mathbf{R_m}\mathbf{R_{cp}}\mathbf{H}\mathbf{T_{cp}}\mathbf{T_m} && \text{| Substitute } \mathbf{H_t} = \mathbf{R_{cp}}\mathbf{H}\mathbf{T_{cp}} \\ &= \mathbf{R_m}\mathbf{H_t}\mathbf{T_m} \end{aligned} \tag{5.3}$$

Thus for cyclic prefix based schemes, Equation (5.1), can be rewritten as,

$$\begin{aligned} \mathbf{y} &= \mathbf{Qs} + \mathbf{z} \\ &= \mathbf{R_m}\mathbf{H_t}\mathbf{T_m}\mathbf{s} + \mathbf{z} \end{aligned} \tag{5.4}$$

In practical systems, it should be noted that the CP is transmitted on the channel and fills the gap between two consecutive blocks. Intuitively, the channel matrix in the time domain $\mathbf{H_t}$ is obtained from $\mathbf{H}$ by dropping the first $M-1$ rows and columns and then adding the next $M-1$ columns to the respective columns at the end as illustrated in Figure 5.2.

To summarize, the vectors $\mathbf{x}$, $\mathbf{w}$ and $\mathbf{r}$ include the CP and have the dimensions, $N+M-1 \times 1$. The matrix $\mathbf{T}$ has the dimension $N+M-1 \times N$. The demodulation matrix $\mathbf{R}$ has the dimension $N \times N+M-1$ and it created the demodulated symbol vector $\mathbf{y}$ with the dimensions $N \times 1$. Thus, the resulting dimension of the channel matrix in the time domain $\mathbf{H_t}$ is simply $N \times N$ and is depicted in Figure 5.2.

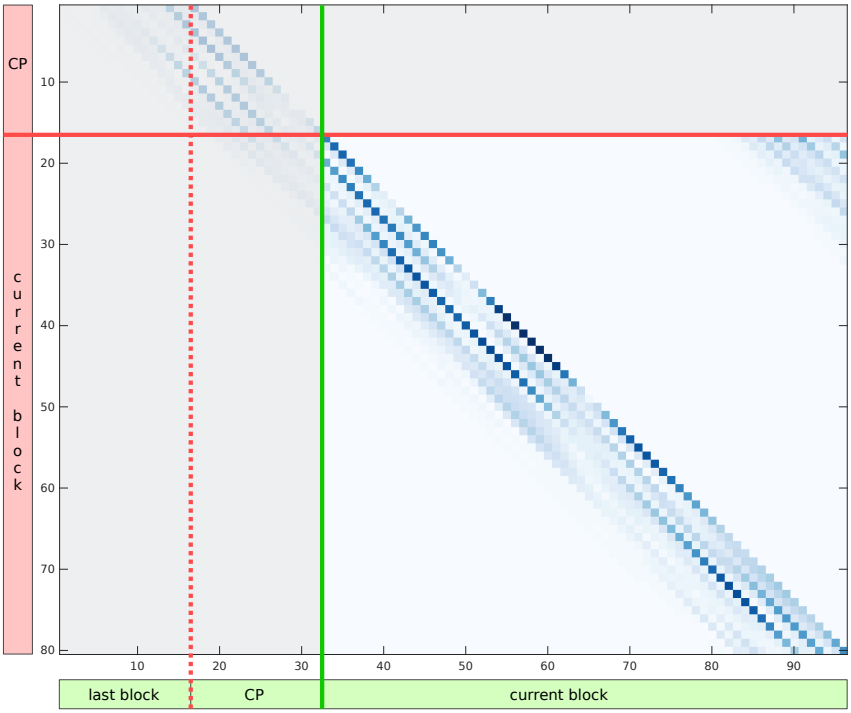


Fig. 5.2: Dissecting the Channel Matrix: Obtaining $\mathbf{H_t}$ from $\mathbf{H}$

The noise vector $\mathbf{z}$ at the receiver has the dimension $N \times 1$. This mathematical formulation considers the complete OFDM signal that is transmitted through the channel, identifies the cyclic prefix component, and derives the effective channel matrix $\mathbf{H_t}$ that should be estimated at the receiver.

Since $\mathbf{H_t}$ is the effective channel matrix to be estimated at the receiver, it is worthwhile to investigate its structure. The channel model has been systematically derived in Chapter 3. We know that, for a time-invariant multipath channel, the channel matrix in the time domain $\mathbf{H_t}$ has a circular structure (due to multipath propagation) wherein, each row is a shifted version of the row above. Performing a DFT on this circular matrix transforms it into the frequency domain and gives the channel matrix in the frequency domain denoted as $\mathbf{H_f}$. The Fourier transform operation turns the circular matrix in the time domain to a diagonal matrix in the frequency domain [55]. This Fourier correspondence property is often used to simplify the estimation of wireless channels since operations on diagonal matrices are more computationally efficient and tractable. In Figure 5.3, multipath delays with a large delay spread along with a low normalized Doppler shift of 1% is simulated and the channel matrix is visualized in both the time and frequency domains. In Figure 5.3a, the circular structure is

seen while in Figure 5.3b, the corresponding channel matrix in the frequency domain has a diagonal structure.

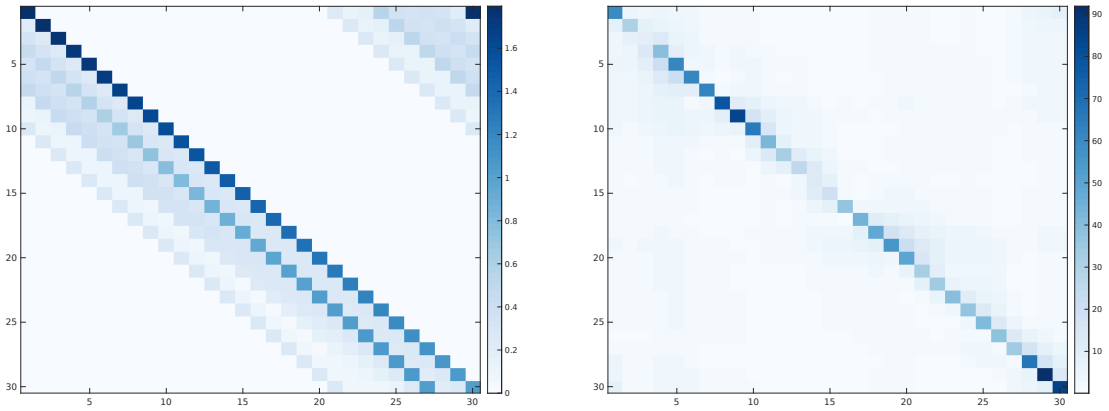

(a) $\mathbf{H_t}$ (Time Domain) (b) $\mathbf{H_f}$ (Frequency Domain)

Fig. 5.3: Channel Matrix for a Large Delay Spread and Negligible Doppler Shift ($N = 30$ for simple visualization)

In the presence of mobility, a Doppler shift is introduced which makes the channel selective in the time domain. The resulting time-varying multipath channel distorts the circular nature of $\mathbf{H_t}$ and cause stronger minor diagonals in $\mathbf{H_f}$. Thus, the channel transfer function $\mathbf{H_f}$ becomes banded due to the effect of mobility and the bandedness is directly proportional to the amount of Doppler spread. This is evident in Figure 5.4 where, weak delays along with a 10% normalized Doppler shift is simulated.

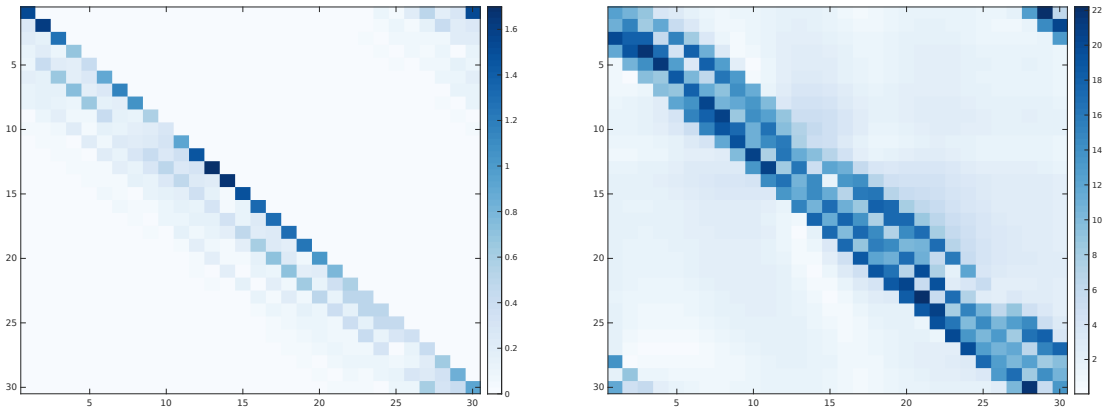

(a) $\mathbf{H_t}$ (Time Domain) (b) $\mathbf{H_f}$ (Frequency Domain)

Fig. 5.4: Channel Matrix for a Small Delay Spread and a Strong Doppler Shift ($N = 30$ for simple visualization)

These properties of the channel matrix can be exploited by channel estimation and equalization algorithms to increase accuracy and reduce the computational effort and will be discussed in the rest of this chapter.

## 5.2 Classical Approaches

Channel estimation schemes can be broadly separated into three categories. The first category includes approximation schemes that use a decision directed technique where the output of the demodulator at the receiver is used to infer statistical characteristics and provide virtual pilots. These schemes improve an existing channel estimate and can be used when the specified pilots are not adequate to provide an accurate estimate of the wireless channel. However, in addition to the added complexity, latency issues must also be addressed since these schemes rely on the output of the demodulator [7, 93, 117]. The second category are semi-blind and blind algorithms for channel estimation that either use spectral fitting or Eigen structure techniques to gather an estimate of the channel [127]. These schemes have not been widely used for SISO-OFDM systems due to the high complexity involved in channel estimation. The third category of channel estimation schemes leverages the specified pilots and preambles of a given wireless standard to estimate channel information at those locations and interpolate it to the rest of the OFDM symbol to yield the complete channel transfer function. Using the pilots and preambles enable an accurate estimate of the channel at an acceptable computational cost as shown in [28]. Thus, pilot based channel estimation is widely used in practice and is also investigated in this thesis. Note that, schemes that leverage an estimate of the channel matrix are also referred to as coherent channel equalizers [71].

A straightforward and simple channel estimation mechanism that provides an adequate estimate of the channel is the Least Squares (LS) scheme. Due to its simplicity and effectiveness, LS based channel estimation techniques are widely used and practically implemented on consumer hardware. The underlying idea is to use the specified pilots and preambles of a given wireless standard to estimate the distortions introduced by the wireless channel. To derive a mathematical formulation of the LS estimator, consider the IEEE 802.11p standard that specifies two long preambles as part of the PLCP header[3]. If the two received preambles in the frequency domain are denoted as $\mathbf{y}_{L1} \in \mathbb{C}^{N\times 1}$ and $\mathbf{y}_{L2} \in \mathbb{C}^{N\times 1}$, the LS channel estimate is obtained by dividing the received preambles by the known preamble $\mathbf{x}_L \in \mathbb{C}^{N\times 1}$ and then averaging them as shown in Equation (5.5). Note that $N$ denotes the FFT size and $\mathbb{C}$ refers to

[3] part of the IEEE 802.11p specifications; used for synchronization, estimation and as a start frame delimiter

the set of complex numbers. The outcome of LS estimation is a vector $\mathbf{h_f}$ in the frequency domain that contain the complex coefficients for each subcarrier of the underlying OFDM symbol.

$$\mathbf{h_f} = \frac{\mathbf{y}_{L1} + \mathbf{y}_{L2}}{2 \cdot \mathbf{x}_L} \qquad \mathbf{h_f} \in \mathbb{C}^{N \times 1} \tag{5.5}$$

In the case of the IEEE 802.11p standard, the averaging of the two preambles as seen in Equation (5.5) makes the channel estimate robust in low Signal to Noise Ratio (SNR) conditions. It must be noted that the formulation in Equation (5.5) must be adapted slightly for different wireless communication standards depending on the respective specifications like the structure, location, and the total number of pilots. If a comb-type pilot is specified in the underlying standard, a suitable interpolation should also be performed to provide the complete channel vector for all the active subcarriers. The most notable advantage of the LS scheme is its low computational complexity and its benefits in stationary channel conditions [169]. It is also straightforward to adapt these schemes to different wireless systems and is thus chosen as a baseline against which the channel estimation schemes proposed in this thesis are evaluated.

## 5.3 State-of-Art Approaches

The problem of channel estimation and equalization has been investigated in the research community for the past couple of decades and has yielded several innovative schemes with a common goal to provide the best equalization results at the receiver. In this section, state-of-art preamble (or pilot) based coherent channel estimation techniques are described along with their respective advantages and disadvantages.

A popular technique to estimate a doubly selective channel is based on Basis Expansion Model (BEM). The idea is to adopt several mutually orthogonal basis functions to approximate the doubly selective channel. Since the basis functions are already defined, the problem boils down to estimating the coefficients for the corresponding base functions [159]. Channel estimation schemes based on BEM assume that the time-varying impulse response of the channel is varying smoothly and thus justify the use of smooth functions for estimation. The

sender receiver relation given in Equation (5.2) is rewritten without the noise component in Equation (5.6). Here, $M$ is the maximum number of delay taps in the channel.

$$r[n] = \sum_{m=0}^{M-1} h[n,m]x[n-m] \tag{5.6}$$

Using BEM, the channel matrix is formulated in Equation (5.7). Here, each delay tap $m$ is independently modeled as a linear combination of basis functions denoted as $u_i$. The $i^{th}$ coefficient of the $m^{th}$ delay tap is denoted as $c_i[m]$ and must be estimated at the receiver.

$$h[n,m] = \sum_{i=0}^{I-1} c_i[m]u_i[n] \tag{5.7}$$

The term *basis expansion* can be intuitively seen in the above equation where, the samples of the impulse response are expanded into an arbitrary parameter space that is in a different basis. To employ BEM for channel estimation, a suitable basis is necessary that can model the channel with an order $I$ that is significantly smaller than the amount of time samples as explained in [62]. The use of complex exponentials as the basis is intuitive because, a Doppler shift $\pm\nu$ corresponds to a time-dependent phase shift $exp(\mp j2\pi\nu\frac{n}{N})$ in the time domain [116]. Thus, for each delay tap a complex exponential can be used to model the time-varying impulse response of the channel as initially proposed in [29, 65, 69, 151]. In order to use a complex exponential basis, a maximum discrete Doppler spread must be assumed in prior. But, due to the limited resolution, the sampled Doppler shifts will significantly vary from the actual values and ultimately result in a large modeling error [83]. This is the so called Gibbs phenomenon wherein, the reconstruction with the truncated Fourier series introduces large distortions at the boundaries of the underlying OFDM symbols and also becomes more severe at larger Doppler spreads [68, 164, 165]. This phenomenon gravely affects the precision of the estimated channel model as pointed out in [164]. A straightforward mechanism to combat the Gibbs phenomenon is to over sample the basis in the frequency domain [99], but this approach significantly increases the computational effort [147]. In [99], a BEM with a non uniform Doppler spacing is proposed in order to get a better modeling accuracy. However, the spacing must be appropriately designed in order to have good results. Other modifications to the complex exponential BEM model include windowing techniques to improve accuracy as shown in [134]. Another example of a modified complex exponential has been been developed for the LTE downlink in [87]. However, this scheme has not been adapted to the LTE uplink. A complex exponential BEM based channel estimation scheme has been applied for LTE-R [4] systems in [36] in which fast time-varying channel estimation

[4] specifies a railway wireless communication system based on LTE

in LTE-R communication systems is investigated. The authors propose a scheme where the channel is modeled as a sum of basis functions that are multiplied by different coefficients.

Another interesting basis is to use polynomials that correspond to a Taylor series as shown in [164]. But, for a arbitrary model order, polynomials exhibit lower temporal variation when compared to complex exponentials. Thus, polynomial based BEM are only useful in scenarios of a low Doppler shift. Another basis that has been proposed to alleviate the problems with complex exponentials are the so called Discrete Prolate Spheroidal (DPS) sequences. The DPS sequences can be used to find a set of orthogonal sequences that are concentrated in time and band limited in the frequency domain. This is in stark contrast to complex exponentials since DPS sequences have a negligible energy outside a specified interval. To use the DPS sequences for channel estimation and equalization, they have to be truncated to some arbitrary time interval like the block length $N$. Truncated DSP sequences are called Slepian sequences. The use of Slepian sequences was first seen in [148] where it is shown to provide an adequate modeling accuracy given that the maximum Doppler shift is known with a sufficient confidence. In [82], a basis expansion model is used to develop a low complexity equalization scheme by computing a regularized solution for a linear system using iterative algorithms like the LSQR algorithm. However, the coefficients of the basis functions are assumed to be known accurately which is not the case in practical systems. An oversampled Legendre basis is proposed in [163] for estimation with minor improvements in error performance. In general, none of these schemes exploit the inherent sparsity of the wireless channel that can provide a significant gain in performance and complexity as explained in [141]. As part of a thesis [95], a simple BEM scheme has been developed to estimate a doubly selective channel using the complex exponential and the Slepian basis. The results indicate that although the BEM based methods do a good job in estimating a slow temporal variation (low Doppler shift) in the channel, the performance in estimating the correct delay taps is relatively poor. Thus we see that, BEM's have been extensively researched in literature for the estimation of doubly selective channels. However, a trade-off between complexity and performance must be drawn that makes it less attractive for practical implementation.

Another interesting scheme is the Constructed Data Pilots (CDP) technique that can work well when the SNR is high and a high correlation between received symbols is assumed [169]. However, this scheme is not able to provide adequate results in scenarios of high mobility [154]. The authors propose this scheme for the IEEE 802.11p standard and use the long preambles to generate an initial estimate of the channel. This is then used to generate additional data pilots for the subsequent OFDM symbol. These data pilots are then

used by a LS estimator to provide a channel estimate for the current data OFDM symbol. In the next step, the estimated channel response is compared to the previous estimate and the best channel response is used to equalize the current OFDM symbol. The effectiveness of this scheme is heavily dependent on the high temporal correlation between OFDM symbols which cannot be guaranteed in highly mobile vehicular environments or for wireless standards that specify a longer OFDM symbol duration. However, the work in [169] has lead to a Time domain Reliable test Frequency domain Interpolation (TRFI) scheme in [162] where the authors classify the subcarriers as reliable and non-reliable subcarriers. The channel estimate at the reliable subcarriers is then used to interpolate the channel at the unreliable subcarriers. However, as pointed out in [154], both these schemes are heavily dependent on the demapping errors in the previous OFDM symbols and also the noise in the channel. In such cases, the error propagates and increases in the subsequent OFDM data symbols of the physical layer frame deteriorating the error performance significantly.

A technique to estimate the doubly selective channel that also mitigates ICI has been proposed for OFDM systems in [115]. In this paper, the authors propose an Minimum Mean Square Error (MMSE) estimator to acquire the channel transfer function. This is followed by a three step ICI mitigation procedure. Similar work can also be found in literature where the ICI is considered as an additional noise component. However, from this paper, the channel model used to generate the results is unclear as the authors generate a custom channel model using Bessel functions. Moreover, the results only consider a maximum normalized Doppler shift of 1.5% in their evaluations.

The Successive Interference Cancellation (SIC) and the Successive Interference Cancellation with Interference Reduction (SICIR) are approaches proposed in [160] that are the outcome of recent research efforts. The main goal of these schemes is to reduce the complexity seen in conventional equalizers like the LMMSE or the zero forcing (ZF) equalizer which is typically $\mathbb{O}(N^3)$ [See [5]]. Many approaches target achieving lower complexity by iteratively equalizing smaller blocks of the channel matrix called windowed MMSE. These approaches are successful in reducing the complexity to at most $\mathbb{O}(N^2)$ as seen in [25, 72]. The SIC and the SICIR target a linear complexity but assume only a small Doppler shift affecting the received signal. This implies that the corresponding effective channel matrix in the frequency domain is tightly banded and can effectively be approximated to be a diagonal matrix as discussed in [55]. Based on this approximation, a single-tap equalizer is constructed using

[5]The Big-O notation ($\mathbb{O}$) is used here to classify algorithms depending on how their run time increases with the size of the input.

the diagonal elements of the channel matrix denoted by the vector $\lambda_{\mathbf{F}}$. This equalizer is the SIC equalizer described in the Equation (5.8),

$$\hat{X}_{SIC} = \frac{Y}{\lambda_{\mathbf{F}}} \tag{5.8}$$

Thus, the SIC equalizer provides a cost effective technique to equalize the data. However, the SIC equalizer assumes Perfect Channel State Information (PCSI) at the receiver [160] which is not available in a practical system. Experiments done in [22] conclude that combining the SIC equalizer with conventional estimation schemes to remove the dependency on the PCSI, heavily depend on the accuracy on the underlying channel estimate.

An extension to the SIC equalizer, the SICIR equalizer performs an interference reduction step after the one-tap equalization described in the SIC equalizer. The non-diagonal elements of the channel matrix $\mathbf{H_F}$ represent the interference from the neighboring subcarriers. Thus, after each detected symbol the following received symbols are updated by removing the interference components from the previously detected symbols as described in Equation (5.9),

$$(\hat{y}_{SICIR})_i = (y)_i - \sum_{q=1}^{Q} (h_f)_{i,i-q} (\hat{x})_{i-q} \tag{5.9}$$

where, $(\hat{x})_{i-q}$ is a previously detected symbol and $Q$ is the number of interference terms to be considered. The complexity of the SICIR equalizer depends on the number of interference terms considered and is $\mathbb{O}(QN)$.The SIC and the SICIR equalizers approach the problem of equalization intuitively by performing a one-tap equalization using the diagonal elements of the channel matrix and then subtracting the interference components from the neighboring subcarriers. However, the number of interference terms considered $Q$ must be fixed in the algorithm and might not be the optimal choice for all channel conditions. We conclude that the problem of channel estimation has been intensively studied in the community and there are several solutions each with their own advantages and drawbacks. In the next section, we briefly explore the advances in deep learning for channel estimation.

## 5.4 Deep Learning for Channel Estimation

In recent years, deep learning has been applied to solve various problems in different research areas with good success. As part of a thesis [95], we have investigated the feasibility of using deep learning for the estimation of a doubly selective channel and describe the results in

Section 5.4.2. The building blocks of deep learning are briefly introduced in the following section and will be mostly based on [67].

### 5.4.1 Fundamentals of Deep Learning

The concept of neural networks has been studied and evolved over the years. A comprehensive account on the development of neural networks and the underlying concepts are described in [67, 132]. The goal has been to observe and emulate the function of actual neurons in nature. A neuron is defined as an elementary unit that performs a simple task. It combines a (potentially very large) number of inputs to a single non linearly computed value. An artificial neural network builds on this concept and exploits the fact that non linearities allow for a higher computational expressivity. In practice, a neuron (known as a 'unit' in artificial neural network terminology) linearly combines its inputs with respective weights and computes its output using a fixed activation function that incorporates the non linear behavior. An important consideration to be able to perform complex computations is the number of connections and their respective weights. In practice, units are stacked as layers, where there are no connections within a layer (all units run in parallel), but potentially many connections between adjacent layers.

To formulate a neural network as a machine learning problem, it can be viewed as a parameterized function $f(\mathbf{x}, \theta)$ that is used to approximate a given target function $f^*(\mathbf{x})$ and the effort lies in finding the best parameter set $\theta$ (which in this case are the weights of the units) that gives the least approximation error. Since only the input data and output result are directly observable, the intermediate layers are termed as hidden layers and the learning strategy can use them to get the best possible result. This way of learning the optimal weights for a deep network with several hidden layers motivated the term deep learning.

#### Deep Neural Network Architecture

A deep neural network is described as having $L > 0$ layers with the $0^{th}$ layer being the input layer and the values of the $L^{th}$ layer represent the output. Neural networks can be categorized based on whether connections are made from the current layer to previous layers (or even to the same layer) or if the connections are strictly leading to the following layers only. The former is categorized as a recurrent network and the latter is categorized as a feed forward neural network. An advantage of the feed-forward network is that the derivatives of its weights can be easily computed by using the back-propagation algorithm. The back-propagation algorithm computes the derivatives only with respect to the next layer after which, these

values are propagated backwards, utilizing the chain rule of derivation [67]. Recurrent neural networks introduce memory that make processing time series input feasible. Research in neural networks have yielded several other network architectures that build on the previously mentioned types and are suited for different applications.

Taking a closer look at a feed forward network, the output of an arbitrary layer $l$ denoted as $\mathbf{x}_l$ can be formulated as a dependency on the output of previous layers $\mathbf{x}_{l-1}$ and the parameter set $\theta_l$ by using the function $f_l(\mathbf{x}, \theta)$ as shown in Equation (5.10).

$$\mathbf{x}_l = f_l(\mathbf{x}_{l-1}, \theta_l) \tag{5.10}$$

Here, we assume that the input of a layer is exactly equal to the output of the previous layer. A practical and widely used layer type builds on the model of a unit formulated in Equation (5.10). Here, each layer is built up of several parallel units each of which computes a weighted sum of inputs and gives a non linearly transformed (also referred to as activated) version of it. Accordingly, an activation function $\sigma$ that performs the component wise activation function that allows us to write,

$$f_l(\mathbf{x}_{l-1}, \theta_l) = \sigma_l(\mathbf{W}_l\mathbf{x}_{l-1}, +\mathbf{b}_l) \tag{5.11}$$

Here, the weight matrix and the bias vector of a layer $l$ are denoted as $\mathbf{W}_l$ and $\mathbf{b}_l$, respectively. The dimensions of the weight matrix and the bias vector is dependent on the layer width. The parameter set that has to be learnt consists of $\mathbf{W}_l$ and $\mathbf{b}_l$. Note that in this layer type, the output value of a unit is computed using every input value and is thus called a *fully connected* layer. By extension, a network consisting of multiple fully connected layers is termed as a *multi-layer perceptron*.

There are also various other types of layers like the convolutional layer which builds on the concept of discrete convolution. It defines a kernel of a fixed size and moves it over the input data which is similar to the concept of filtering. Due to the fact that the same kernel is used over the entire data, the results are spatially invariant. This property provides good results especially in image recognition tasks. It is also interesting to note that the convolutional operation can be alternatively expressed by a fully connected layer with many zeros and equal values (like a time-invariant convolution matrix).

Another important layer type is the pooling stage, that shrinks several values in a small region to a single value by using a simple operation like a maximum or a mean. The pooling

stage reduces the output width and the amount of required parameters in subsequent layers.

Other layer types mainly deal with improving the characteristics of the neural network like overfitting and convergence. For instance, a normalization layer is used to normalize the output of a given layer so that in subsequent layers, the parameters are more likely to be in an optimal range assuming that they are initialized correctly. A dropout layer has the function of randomly masking values of a layer with zeroes during training. This forces the network to avoid assigning too specific functionality to the units.

Finally, the choice of a suitable activation function $\sigma$ for computational layers with linear input combining is vital to ensure optimal results. The activation function is non linear and monotonically rising. Classical choices include the sigmoid $\frac{1}{1+exp(-x)}$ and the hyperbolic tangent $tanh(x)$ functions that are smooth functions without discontinuities and thus differentiable everywhere. The derivative of activation functions is important since it is included in the derivatives of the previous layers due to back-propagation. Other functions include the rectified linear unit (ReLU) that performs $max(0,x)$ and the softmax function that take the other outputs of a layer into consideration. In order to achieve good results with deep learning in a reasonable amount of time, it is vital to optimally constrain free parameters and incorporate the properties of the input data as well as the specific application into the design of the layers.

## Training Deep Neural Networks

Training is the process of finding a set of weights for the layers in the network that would provide a good result on the training data and adequately solve the problem at hand. Due to non-linearities, the problem of training is non-convex and it is difficult to find the global minimum. There are different approaches for training in literature and the most widely used method is based on gradient optimization. In this method, the optimizer of the learning algorithm starts on some initial value (that must chosen carefully for performance and convergence) and iteratively computes the derivative of the loss function for all the parameters and uses the result to update them. The loss function quantifies the performance of the neural network in modeling the given data. Here, the underlying idea is to follow the gradient in the negative direction hoping that it will lead to a global minimum. In order to avoid saddle points, higher order derivatives are also commonly used.

To begin with, the loss function should be chosen systematically because the derivatives that are computed will be based on it. The loss function takes the output of the network

and the respective labels of the training data (assume supervised learning) and quantifies it into a single metric that indicates the performance of the network. The choice of the loss functions also depends on the specific task. A cross entropy based loss function is suitable for classification tasks where the output of the network is typically a probability while, for vector outputs a mean square error metric is more suitable to be used as the loss function.

Another important parameter is the learning rate that regulates the impact of a single learning (or optimization) step on the parameters. Choosing the right learning rate is a non-trivial problem. A low value significantly slows down convergence while a large value of the learning rate might jump over the optimal minimum. Thus, a viable approach would be to dynamically adjust the learning rate by starting with a large value and reducing it when the improvement between steps become smaller. This technique has already been widely adopted and are part of stochastic optimization algorithms like *Adam*, *Adadelta*, and *RMSprop*. Other approaches that address the learning rate dilemma try to achieve more useful updates by incorporating history in order to get a more reliable direction for optimization. A detailed comparison of the optimizer variants is given in [128].

Finally, the problem of overfitting while training neural networks should also be considered. During the process of training, the value of the loss function keeps decreasing. But it must be noted that the loss is computed on the training data only and the actual inputs (testing data) to the network would not be part of the training data. During optimization, it could happen that the network has been optimized specifically on the training data such that training loss keeps decreasing to a very small value but it keeps increasing on the testing data. This characteristic behavior is an indication of overfitting since the parameters that are learnt are too focused on specifics of the training data. A common technique to overcome this problem is ensure a representative split of the training and testing data. It is also important to keep these two sets of data separated and ensure that no sample of the testing data is used for model optimization and in the same way, no training data is used for evaluation. In some cases, a third category of data called the validation data is defined that is used to tune the so called hyperparameters. These hyperparameters consist of non learnable network parameters like the size, architecture type and the learning rate. A simple and effective way to avoid overfitting is to keep the weights small by adding a term dependent on the weights to the loss function. Adding a dropout layer is also a viable means to avoid overfitting. Overfitting causes the network to generalize poorly and techniques that help overcome this problem are called regularization schemes.

The fundamentals of deep learning described in this section paves the way to discuss its application in channel estimation and equalization. A comprehensive survey of research that applies deep learning to the problem of channel estimation along with a basic neural network implementation is discussed in the next chapter.

### 5.4.2 Related Work

The concept of neural networks and their applications have been discussed for several years. In fact, applying a neural network to the problem of channel estimation can be found in a paper [94] published in 1994 and concludes that, the non-linear structure of a neural network can be suitable for the estimation of a wireless channel. However, only the theoretical capabilities of neural networks are considered and a concrete practical implementation has not been done. Over the years, with the evolution of computers that provided significantly more computational resources and a more mature understanding of neural networks, several interesting results can be found in literature.

Developing a neural network model that offers good performance with an acceptable computation burden has been the goal of recent research efforts. An overview of equalization approaches that also include the effect of Rayleigh fading is provided in [13]. The authors state that a multi-layer perceptron was not able to converge and investigate alternatives like shallow approaches that operate on expanded inputs or the use of radial basis function networks that solve a fitting problem using weighted Gaussians. The paper concludes that some neural network based schemes were able to outperform conventional linear equalizers. Unfortunately, most of these approaches are not used in practice as pointed out in [118] either due to the required computational resource or inadequate results that would justify the complexity. The authors of [118] interpret the entire communication chain as an autoencoder that jointly optimizes the transmitter, channel, and the receiver as an end-to-end reconstruction problem. Thus, the autoencoder is tasked with finding an optimal (lowest dimension) representation of the input that allows for the best reconstruction (minimal error) at the output. It is also interesting to note that although most autoencoders are designed to get rid of redundancy in the input data, the autoencoder proposed in [118] added redundancy that is used to learn intermediate representations in order to be robust to the distortions caused by the wireless channel. The authors also present other interesting ideas like the use of radio transformer networks and adversarial networks in communication systems.

A few examples that provide an implementation for channel estimation using deep learning can be found in literature. A deep learning based equalizer for OFDM systems can be

found in [161] and is shown to deliver good results. Here the model is trained using simulated data that include the channel effects like frequency selectivity and additive noise. The resulting model with trained weights is then deployed at the receiver. The authors create a network architecture that takes two 64 carrier OFDM symbols as inputs. The input layer is followed by three hidden layers that are fully connected with ReLU activation functions. The neural network is designed to perform a joint equalization and symbol detection and in essence, the output of the network solves a classification problem that tries to find the best estimate of the transmitted information. A sigmoid activation is used in the final layer. Similar to this work, an equalizer based on ResNet is proposed in [26].

An interesting approach is presented in [168] where both an OFDM receiver trained using a neural network and an independent channel estimator that is prepended to deal with mulipath fading are deployed. However, Doppler shift due to mobility and the offsets due to synchronization inaccuracies are not considered. The neural network based equalizer is sophisticated and is composed of several layers. The first layer in the network mimics the functionality of a conventional LS estimator. In the second layer, residual errors are computed using the specified pilots and in the subsequent layers residuals are computed between the layers. The output of these layers are fed to a three layer neural network after which a complex convolutional layer is employed. Finally, the output of the network is used to perform equalization by dividing the received signal in the frequency domain with the channel estimate.

To summarize, it has been shown in literature that, developing a neural network based solution for the estimation of wireless communication channels is a complex task. However, this is a very interesting research question and has been investigated in this thesis. Although several sophisticated approaches have been proposed in literature, we approach the problem at a fundamental level to gain an understanding of the strengths and weaknesses of neural networks in channel estimation.

### Data Generation

The quality of the data that is used for training and testing plays a vital role in the effectiveness of the learned model. The easiest way to generate training data for the neural network was to use the already implemented IEEE 802.11p transceiver chain that has been implemented in this thesis[6]. However, several components of the data generated by this standard compliant simulation platform are constant (example: signaling fields, preambles, and head-

[6]Available at: https://git.nt.uni-saarland.de/HiMo/SimTool_IEEE802.11p

ers), that would cause a statistical bias in the results. For this reason, a transceiver chain has been implemented in Matlab® to produce random unbiased data that can be used to train and test the neural network. The transceiver chain comprises of a random bit generator, BPSK modulator, and an IFFT transformation block to provide OFDM symbols in the time domain. A cyclic prefix is then added to the symbols after which they are distorted by the channel model. A Rayleigh fading object that models the frequency and time selectivity is used to emulate the doubly selective channel. At the receiver, the cyclic prefix is first removed followed by an FFT transformation that provides OFDM symbols in the frequency domain that are then used by the neural network. It must also be noted that, though some of the specifications of the IEEE 802.11p standard are ignored, the frequency spectrum shape is respected. Accordingly, 48 data subcarriers are used in the OFDM symbol, the pilots are present in their specified locations and the specified guard band is also defined.

A modular approach has been chosen wherein, the channel equalization and the symbol demapping are decoupled. This is unlike some examples in literature which design a network to jointly perform equalization and demapping [161]. Accordingly, the input to the network are FFT transformed OFDM symbols that are distorted by the channel model. Thus, the task of the network is to provide an estimate of the transmitted symbols. The distorted frequency domain symbols at the input of the receiver are denoted as $\mathbf{Y}$ and the outputs of the network are represented as $\hat{\mathbf{X}}$ . The original sent symbols (labels) are denoted as $\mathbf{X}$. The size and shape of these vectors depend on the experiment. Initial experiments already showed that to achieve consistent results, the dataset should be relatively large. Thus, several datasets with a total number of samples ranging from 20000 to 40000 are generated. The dataset was then split into a training set that consisted 80% of the dataset and the rest is used for testing.

#### What We Learnt

A systematic investigation carried out at a fundamental level helped us understand several aspects of neural networks and the challenges involved in deploying a learning based solution for channel estimation. These observations are described in the remainder of this section.

**LOS Propagation:** The initial experiments confirmed that a naively designed network architecture is not adequate to equalize a trivial channel with a single path (0 delay and 0 Doppler shift). Thus, the initial efforts were directed towards systematically designing an architecture that would equalize such a trivial channel. For this purpose, a dataset comprising 20000 samples (each of which is a single OFDM symbol) were generated. The only effect of the channel on the transmitted OFDM symbols is a complex

multiplication (average $0dB$) on each of the subcarrier. Thus, even though BPSK modulation is used at the transmitter, the receiver has to work with complex values. Since complex numbers are not widely supported in neural networks and handling them is not straightforward, the input to the network is split into real and imaginary parts like in [161]. At the output of the network, we considered only the data subcarriers of the OFDM symbols to ensure that the error metric is not distorted by the null and pilot subcarriers. As far as the error metric is concerned, any $l_p$ norm (denoted by $\|(\cdot)\|_p$) between the labels $\mathbf{X}$ and the network prediction $\hat{\mathbf{X}}$ is suitable. However, considering the task of equalization, penalizing deviations unequally depending on their value does not seen intuitive and thus a simple $l_1$ norm (absolute error) is chosen as the error metric. Additionally, to achieve consistent results that are independent of the batch size, the absolute error is averaged over the carriers and the batch size.

As a first approach, fully connected layers (called FC layer in the figures) are chosen for the network structure. The number of layers and the width of each layer must be chosen appropriately. Different combinations with up to two layers with activation functions like ReLU, tanh, sigmoid and linear (no activation function) have been experimented. The results indicated that atleast two layers with a non-linear activation function is necessary to ensure convergence towards an acceptable error. Some results are compiled in Figure 5.5 where an Adam optimizer with TensorFlow default parameters with a learning rate of 0.001 and batch size of 100 is used. In the figures, the space between two vertical gray lines corresponds to 50 epochs.

From Figure 5.5a we made an initial conclusion that a simple linear function is not suitable to compute the desired result. Note that due to the BPSK modulation only a binary output value of $-1$ and 1 are expected from the output of the network. However, in this case, the network provides a constant value of 0 which results in a mean absolute error of 0.5. This indicates that the network in this configuration has not been able to learn anything meaningful. In Figure 5.5b, a tanh activation function is inserted that significantly improves the results but is still mediocre on an absolute scale. A further improvement is observed in Figure 5.5c where a second fully connected layer is introduced.

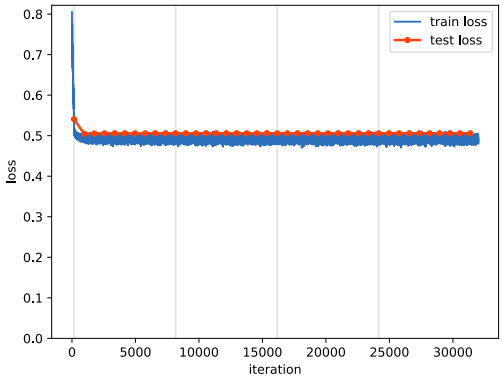


(a) Single FC Layer, Linear

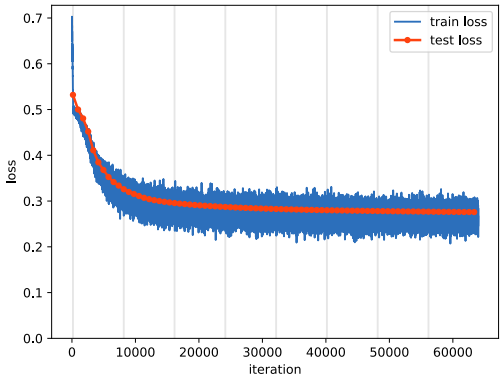


(b) Single FC Layer, tanh

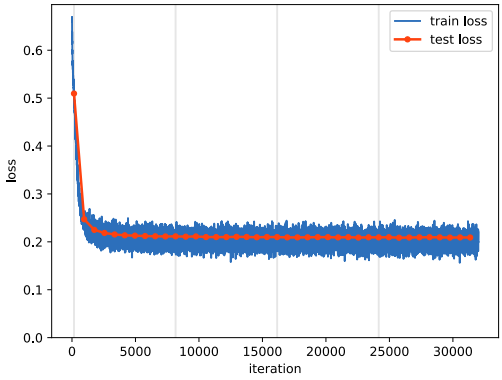


(c) 128 FC Layer, ReLU FC, Linear

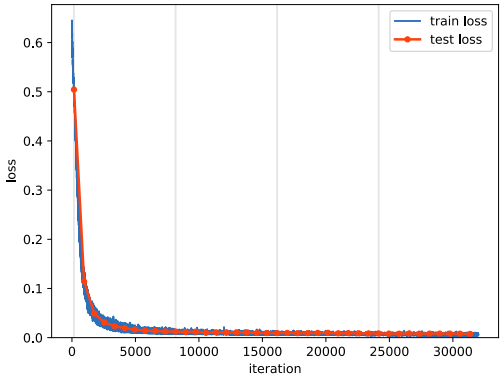


(d) 128 FC Layer, ReLU FC, tanh

Fig. 5.5: Behavior of Network Architectures

In Figure 5.5d, both the activation functions are combined and this resulted in a fast converging process and the error is effectively 0. Such a fast convergence could not be achieved by any other network architecture that was tested. Network architectures with 3 or more layers produced similar results in the best case and increasing the depth and the width of the network more often worsened the results.

**Pilots in Training:** The next interesting question is to find out if the network is able to learn adequately using the data carriers alone. In Figure 5.6a, only the distorted data subcarriers are used while in Figure 5.6b, both the distorted data and the pilot subcarriers are used in the training phase. The results indicated that the network indeed learns to use the fixed pilot values in the OFDM symbols and also provide better results. When only the data subcarriers are used for training the network learns some

statistical properties of the training dataset and causes the divergence between training and testing loss as seen in Figure 5.6a which could stem from overfitting.

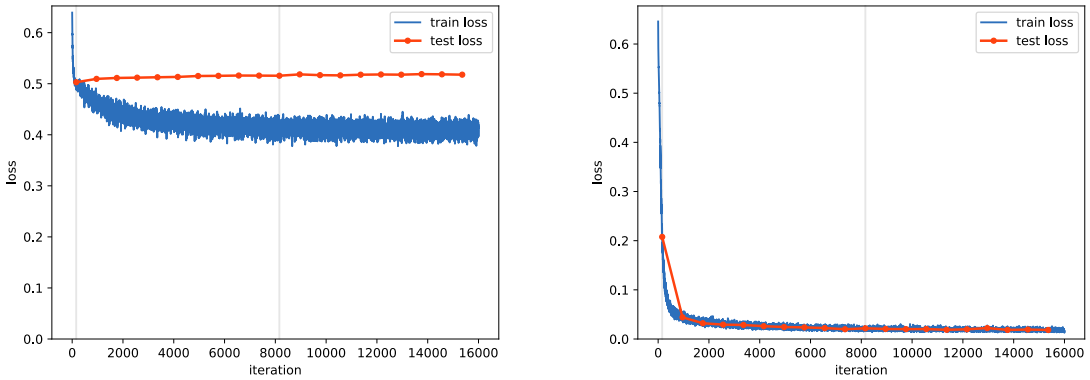


(a) Data Carriers Used

(b) Data and Pilot Carriers Used

Fig. 5.6: Impact of Pilots with Adam, $\lambda = 0.005$ on 128-FC, ReLU FC, tanh architecture

**Learning Rate** is an optimization parameter that can be tuned and plays an important role in finding good results. The learning rate (denoted as $\lambda$) not only influences the convergence speed but also determines the ability of the optimizer in finding the global minimum. We experimented with different optimizers and tuned the learning rates to show the importance of this factor. In Figure 5.7a, the Adam optimizer with a learning rate of 0.001 has not been able to reach a minimum (evident from the fairly high error rate). The same optimizer with a learning rate $\lambda = 0.01$ found the optimal minimum and thereby exhibited good error performance in Figure 5.7b. Thus, for each network setup, it is essential that the optimization parameters are tweaked and tested. Moreover, different optimizers behave differently as seen in Figures 5.7c and 5.7d, where a momentum and an RMSprop optimizer respectively have been tested. The momentum optimizer with $m = 0.5$ is slow and needs a substantially higher learning rate to operate in roughly the same convergence speeds. A similar behavior has been observed with the stochastic gradient descent and the Adadelta optimizers and the results are also comparable to the momentum optimizer in Figure 5.7c. We also observed that for the RMSprop optimizer, a very careful adjustment of the learning rate is required and we speculate that it is very easy to skip over the minimum and consequently produce poor results. Comparing the Adam and the RMSprop optimizers from Figures 5.7b and 5.7d respectively, we can also observe that the RMSprop optimizer is able to find the minimum with a lower learning rate but it also retains a noise floor on the training set and produces a slightly higher error compared to the Adam optimizer. This peculiar

behavior was also observed on several other datasets. Thus, it was concluded that the Adam optimizer is the best choice for our application and has been used for subsequent experiments.

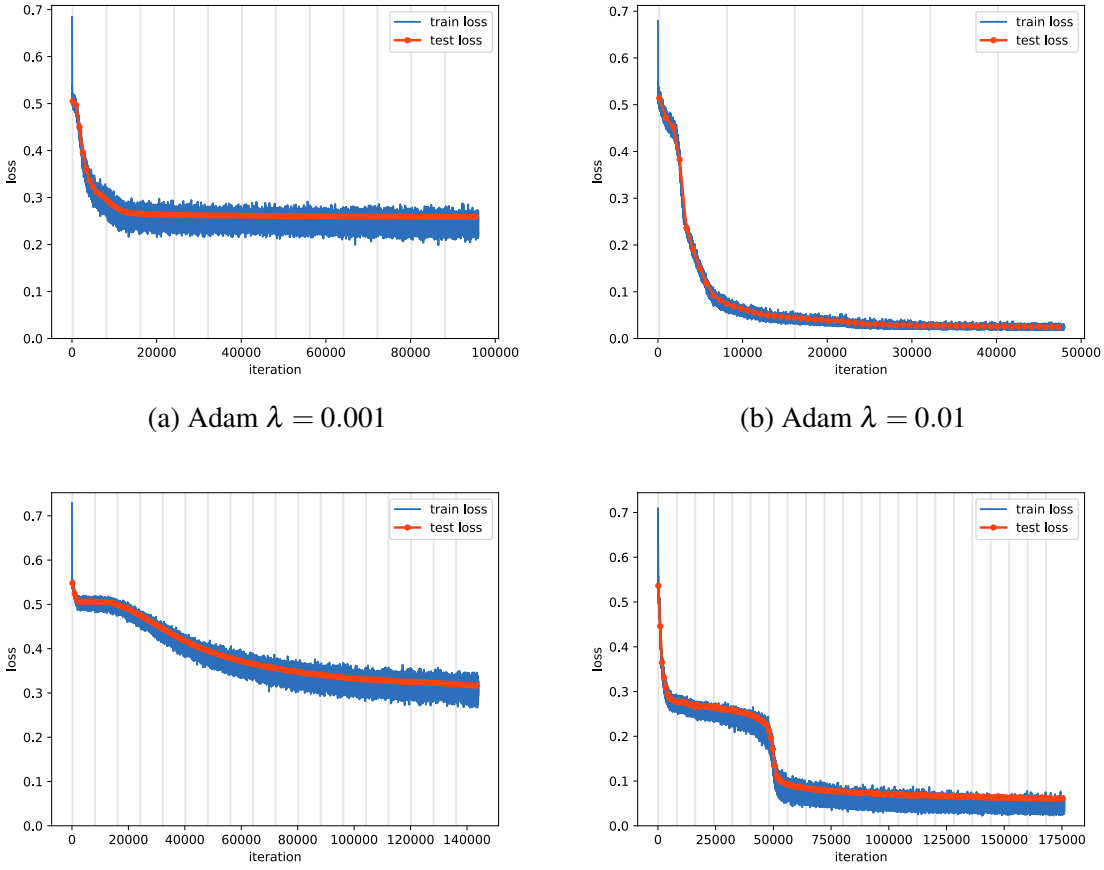


(a) Adam $\lambda = 0.001$

(b) Adam $\lambda = 0.01$

(c) Momentum $\lambda = 0.1, m = 0.5$

(d) RMSprop $\lambda = 0.001, m = 0.5$

Fig. 5.7: Performance of different optimizers on 128-FC, sigmoid — FC, tanh architecture

**Batch Size:** For the given data, a batch size of 100 was found to be appropriate and yielded acceptable results in convergence speed and error performance as seen in Figure 5.8a. We also observed that certain activation functions (like the tanh) introduce more noise than others. Increasing the batch size in Figure 5.8b resulted in a lower noise and also provide a faster convergence but might lead to poor generalization as described in [79].

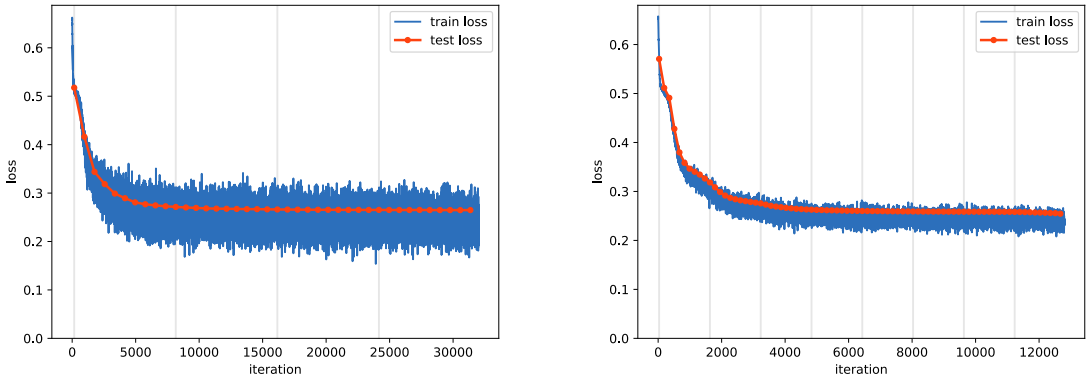


(a) Batchsize 100

(b) Batchsize 500

Fig. 5.8: Different Batch Sizes with Adam, $\lambda = 0.01$ on 128-FC, tanh FC, tanh architecture

From the above results, we concluded that different layouts yield significantly different outcomes and the choice of activation function has a significant role in the results. Especially between hidden layers, the activation function is seen to determine the effectiveness of the optimization. Thus, the goal is to find the best combination of activation functions that on the one hand provide low errors and on the other, are easy to optimize.

Having gained some experience in designing a network for a simple channel, the next intuitive step has been to extend this to a more challenging scenario. We considered a channel with a single path with a random delay. A dataset with 40000 samples has been generated with a random delay for each sample and an average power of $0dB$. The simplest approach of feeding the distorted OFDM data symbols to a naively designed network did not work. From other experiences, it was considered to use the preambles specified in the standard and systematically tailor a network to get good results. An idea to design a simple LS equalization scheme in TensorFlow and test which parts of this equalizer can be replaced and learnt with a neural network with a constraint that the results obtained must be comparable to the initial LS equalizer was considered. Accordingly, for the training phase, the preambles that are specified in the IEEE 802.11p standard are used along with the data OFDM symbols. The output of the network are the estimated values of the data OFDM symbols like in the previous case.

Designing a LS equalizer in TensorFlow is not straightforward since complex numbers and operations on a complex number are not fully supported in the underlying framework. However, since the network architecture already splits the input and output into real and imaginary parts, the same can be used for the equalizer. Let $y_{d,i}$ and $y_{p,i}$ represent the $i^{th}$

distorted data and preamble subcarrier respectively. Similarly, $x_{d,i}$ and $x_{p,i}$ represent the transmitted data and preamble subcarriers respectively. Thus, at the receiver, the transmitted data subcarriers that have to be estimated are denoted as $\hat{x}_{d,i}$. The complex division of $z_1 = a + bi$ and $z_2 = c + di$ that has to be implemented at the receiver can be simplified as,

$$\frac{z_1}{z_2} = \frac{a+bi}{c+di} = \frac{a+bi}{c+di}\frac{c-di}{c-di} = \frac{ac+bd-adi+bci}{c^2+d^2} = \frac{ac+bd}{c^2+d^2} + i\frac{-ad+bc}{c^2+d^2} \tag{5.12}$$

which can be used to implement complex divisions in TensorFlow using simple operations on the real and imaginary parts. Since a multipath delay corresponds to a subcarrier specific complex multiplication, the LS equalizer can then be implemented by computing $h_i = y_{p,i}/x_{p,i}$ and subsequently the equalized data as $\hat{x}_{d,i} = x_{d,i}/h_i$. This has been implemented in TensorFlow and consistent results with good error performance was achieved on both the training and testing set. After this, a fully connected layer has been inserted to adjust the estimated channel $h_i$ before being used for equalization. The motivation here was to find out if the network would learn the identity mapping that would produce the optimal result. Unfortunately, this was not the case and an optimizer configuration with a random initialization of the fully connected layer could not be found. Different initialization schemes like in *He* and *Xavier* [7]were also tested with little success. In Figure 5.9, two optimization curves are shown that are already initialized close to the optimum. Even when a diagonal matrix with elements drawn from a standard normal distribution with mean $\mu = 1$ and standard deviation $\sigma = 1$ is provided as an initialization in Figure 5.9a, an optimum could not be found. In Figure 5.9b, the standard deviation of the normal distribution is reduced to $\sigma = 0.5$ and surprisingly a convergence is achieved. This exhibits an unexpected behavior of the optimization function which could be related to the division process. Thus, it seems hard to relate known mathematical processes with learned models.

[7]https://www.machinecurve.com/index.php/2019/09/16/he-xavier-initialization-activation-functions-choose-wisely/

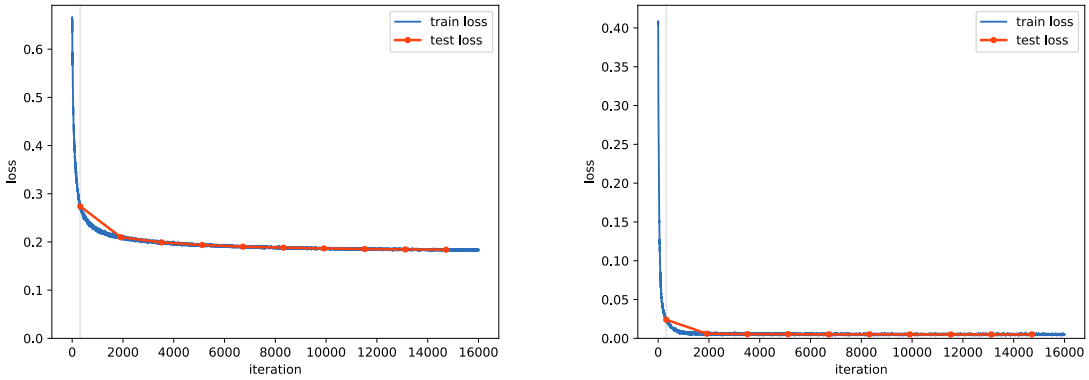


(a) $\mu = 1, \sigma = 1$ (b) $\mu = 1, \sigma = 0.5$

Fig. 5.9: Single tanh Activation Function: 128-FC, tanh — FC, linear architecture

The next idea has been to feed the OFDM preambles and data symbols to a simple network like in the direct path scenario with the expectation that the preamble will help the network give better results. The width of the first layer was increased to 256 and fed with the distorted preambles and data from the channel. This naive approach surprisingly converged to a negligible error. To ensure consistency, this experiment was extended to consider a random non-integer delay as well as multiple random non integer delays (up to 6 delay taps). The result in Figure 5.10a shows that the optimization process for a single random non-integer delay is able to converge very well towards the minimum. Even for a more challenging scenario with multiple random non-integer delays, the network is able to provide good results as seen in Figure 5.10b.

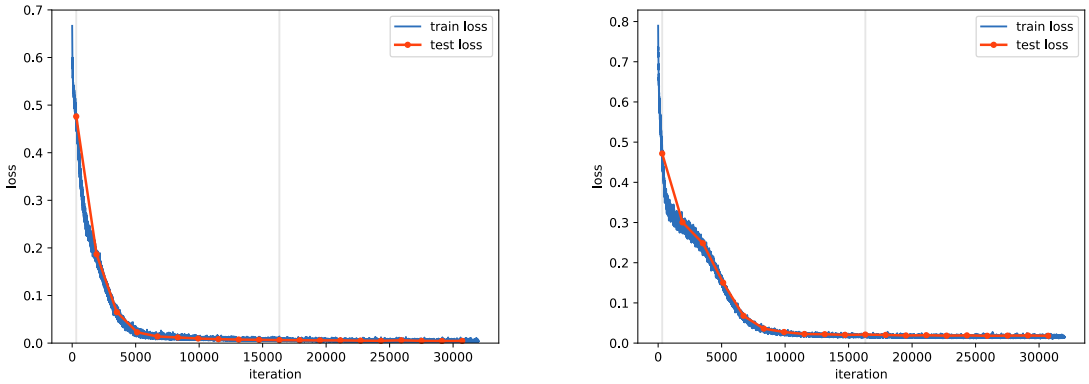


(a) single non-integer delay (b) multiple non-integer delays

Fig. 5.10: Performance on delay channels with 256-FC, RelU — FC, tanh architecture

Finally, the performance of the above network was tested with the presence of Doppler shift to investigate if the neural network is able to detect and estimate the temporal variation present in the wireless channel. For this test, we generated a larger dataset with preambles as in the previous case. A normalized Doppler shift of 10% is simulated for all the experiments. The network is trained with the preambles and the data symbols. The performance of the network for different OFDM symbols are shown in Figure 5.11. The network provides a fairly good result for the first OFDM symbol after the preamble (Figure 5.11a) whereas the performance deteriorates significantly already for the third OFDM symbol after the preamble as seen in Figure 5.11b confirming the limited ability of the network to learn the temporal variation in the wireless channel.

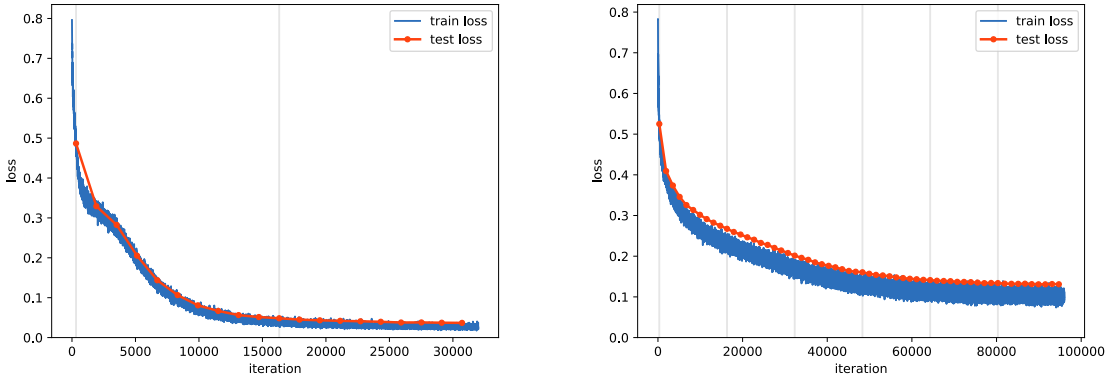


(a) single non-integer delay

(b) multiple non-integer delays

Fig. 5.11: Network performance for a doubly selective channel

The use of neural network to estimate and equalize a wireless channel has been extensively researched and many recent results can be found in literature. Nevertheless, most cases still do not provide adequate results or are computationally intensive limiting their scope. In this thesis, we focus on developing compressed sensing based estimation schemes and evaluate them against conventional methods with the motivation to provide an intuitive view on the strengths and weaknesses of the proposed approach. In the next chapter, the concept of compressed sensing and its application in channel estimation is described.

# CHAPTER 6

# COMPRESSED SENSING CHANNEL ESTIMATION

The theory of Compressed Sensing (CS) has been laid by two revolutionary papers by Candes et.al [14] and Donoho [40] in 2006. These papers attempt to design protocols for data acquisition that would acquire only the most important information about the signals or images and thus, preemptively ignoring all the data that would be eventually discarded by lossy compression algorithms. This signal representation problem has been formulated in the papers cited above and have initiated the novel paradigm of compressed sensing. A definition for compressed sensing can be found in [34] and is quoted, *"Compressed sensing is a technique where a signal that is sparse in a known transform domain can be acquired with significantly fewer samples than is usually required by the dimensions of this domain"*. Without loss of generality, this definition can be viewed from a signal recovery standpoint. Accordingly, compressed sensing can be interpreted as a technique to recover a sparse signal from a handful of non-adaptive, linear measurements by convex optimization as described in [96]. Intuitively, it can be referred as the precise recovery of a sparse vector in a high dimensional space. The theory of compressed sensing has found applications in various fields like medicine, radar, astronomy and seismology. In this thesis, we explore the possibilities of developing compressed sensing schemes to estimate a time-varying multipath channel.

## 6.1 CS Foundations

The philosophy of CS where a few samples are adequate to reconstruct a signal might seem (at the first glance), to go against one of the most sacred concepts in digital signal processing, namely the sampling theorem. For an arbitrary signal with a given maximum frequency component, the sampling theorem governs the number of samples required for a lossless signal recovery. In general, we know that the sampling theory is based on harmonic

decomposition but if the underlying samples are related differently, a coarser representation can be found. The following aspects help understand the differences between the CS theory and the sampling theorem [34].

**Signal Type:** The CS theory provides a framework that is used to measure vectors in a finite-dimensional space, while classical sampling deals with time-continuous signals with an infinite length [34].

**Sampling Mechanism:** According to the sampling theorem, the sampling mechanism involves measuring the signal at specific equidistant points in time. In contrast, CS schemes acquire measurements that are in the form of inner products of the signal and so-called test or basis functions that are part of the dictionary. The design of the dictionary plays a important role in the effectiveness of CS schemes.

**Signal Recovery:** According to the Nyquist-Shannon framework, signal recovery is simply realized using *sinc* interpolation. This is a linear process that is intuitive to understand and computationally cheap to implement. On the other hand, signal recovery in CS is achieved using non-linear methods [34].

CS theory also deals with the problem of *sparse recovery*. Sparsity is an important precondition that must be fulfilled in order to use CS schemes. This sparsity consideration is fulfilled in wireless channels wherein, most of the signal energy can be found in a handful of delay taps as explained in Chapter 3. Moreover, channel models that emulate the characteristics of the wireless channel also specify a handful of delay taps with appropriate delay spreads as seen in Section 3.5. Exploiting this sparsity, CS algorithms have produced interesting results for channel estimation and equalization and are described in Section 6.2.

The theory of compressed sensing can be intuitively adapted to the problem of estimating wireless channels. The system model derived in Section 5.1 gives us the sender-receiver relation as $\mathbf{y} = \mathbf{RHTs} + \mathbf{z}$ where, $\mathbf{s}$ and $\mathbf{y}$ are transmitted and received OFDM symbols in the frequency domain, $\mathbf{H}$ is the channel transfer matrix and $\mathbf{T}$, $\mathbf{R}$ denote the modulation and demodulation matrices respectively. If the channel transfer matrix $\mathbf{H}$ is sparse [141] i.e. $||\mathbf{H}||_0 := \neq \{k,l : H_{k,l} \neq 0\}$ is very small, then according to [15, 34, 96, 100], there exists an orthonormal basis that can represent this sparse signal. Note that $\|(\cdot)\|_0$ denotes the $l_0$ norm and gives the number of non-zero elements in a vector/matrix. Let $\phi$ represents the orthonormal basis that contains all the delays that an arbitrary channel can produce. The problem that CS algorithms need to solve is represented in Equation (6.1).

$$\mathbf{H} = \phi \hat{\mathbf{c}} \tag{6.1}$$

here $\hat{\mathbf{c}}$ represents the indices and the corresponding coefficients of the delay taps that superimpose at the receiver. In addition to this, the CS theory also defines a measurement matrix that determines what parts of the signal are relevant for signal recovery. This is straightforward in our case since, at the receiver, the pilots specified in the standard are intended to be used for the purpose of channel estimation. The underlying idea behind using CS based schemes in channel estimation is that a sparse wireless channel can be reconstructed at the receiver by recovery algorithms using a handful of precise measurements. However, it should also be noted that until now, we have only spoken about the multipath delays and, in a doubly selective channel the CS algorithm has to be extended to estimate both the delay taps and the corresponding Doppler shifts.

Recovery algorithms are broadly classified into $l_1$ minimization, greedy algorithms, and combinatorial schemes. $l_1$ minimization approaches are powerful techniques for computing sparse representations of signals but are complex. Greedy algorithms rely on iterative approximation of the signal coefficients and the corresponding support. This is achieved either by iteratively identifying the support of the signal until a convergence criterion is met, or by obtaining an improved estimate of the sparse signal at each iteration that attempts to account for the mismatch to the measured data [34]. Some of the greedy approaches can in fact be shown to have performance guarantees similar to $l_1$ minimization schemes. A simple and well known greedy approach is the Basic Matching Pursuit (BMP) algorithm and a slightly improved version known as the Orthogonal Matching Pursuit (OMP) algorithm described in [107]. The BMP algorithm is modified in this thesis to estimate the wireless channel (refer to Section 6.3). Finally, combinatorial approaches that stem from theoretical computer science, could also be applicable to sparse signal recovery as explained in [34, 96]. It is also interesting to note that some of these methods precedes CS literature and have found applications in diverse fields like geophysics, statistics, astronomy and communication. In this thesis, we deal with greedy approaches to estimate the channel due to their simplicity and effectiveness.

## 6.2 Survey of CS Schemes for Channel Estimation

Compressed sensing algorithms that are suitable to reconstruct the channel matrix have been widely researched. In [100], a compressed sensing scheme is introduced for the estimation underwater acoustic channels that also exhibit fast fading channels. The authors propose the Matching Pursuit (MP) algorithm, a compressed sensing scheme to estimate the channel.

However, a vital pre-requisite of the MP algorithm namely the dictionary, is not investigated in the paper. In [141], a joint estimation of delay and Doppler shift is proposed. The authors also investigate leakage effects that may appear when a joint estimation of delay-Doppler is performed. They propose a sparsity-enhancing basis expansion and a method for optimizing the basis by leveraging prior statistical information about the channel. These improvements attempt to exploit the sparsity in both the delay and Doppler search. A joint estimation of delay and Doppler shift can be complicated and will result in algorithms with a high computational demand. A similar paper from the same authors is found in [142]. A sparsity adaptive MP algorithm for compressed sensing has been proposed in [37]. The novelty in this paper is that the channel reconstruction is theoretically guaranteed without prior knowledge about the sparsity of the underlying wireless channel. However, an optimal stopping criteria which is an essential part of the adaptive aspect of the algorithm is not provided rather, the algorithm stops when no improvement is seen for two subsequent iterations. Moreover, a step size must be chosen in prior that could result in the algorithm being slow or provide a sub optimal result. Most of the literature cited above do not apply the algorithms to specific wireless standards which makes a direct evaluation/comparison very difficult. Nevertheless, it is interesting to note the development of the compressed sensing techniques in the research community.

A channel estimation scheme using the MP algorithm has been developed for the ISDB-T standard in [104]. The paper models the physical effects of the channel and how these can be leveraged to perform estimation. Unfortunately, the mechanism to estimate the delays and the Doppler shift is unclear. Moreover, the delay estimates are not updated for every frame. While this might be acceptable in a simulation setup, the delays in a real channel can change with time and result in poor performance in this case. The resulting error performance although promising, are not adequate enough to be used in practical systems. Another example of a CS based channel estimation scheme for Layer Modulated Time Domain Synchronous-OFDM (LM-TDS-OFDM) systems for the estimation of severely frequency selective channel is proposed in [102]. Another CS based scheme for ICI cancellation is proposed for OFDM systems in [105]. This paper explicitly states that the channel can be estimated in the time and the frequency domain by proving an orthogonality in the search domains. In essence, the authors propose to estimate the delays in the frequency domain and the Doppler shift in the time domain. A similar approach has also been proposed in [42]. The underlying idea makes intuitive sense and is described in detail in Section 6.3. However, the Doppler search in time domain is compromised by the extremely slow phase progression that makes it impossible to design a dictionary that is able to accurately estimate the Doppler shift. Moreover, the authors in [105] also assume that an ideal dictionary is already present

in both the time and the frequency domains. In [103], a mobile radio OFDM system with pre-equalization is proposed. This paper deals with direct feedback mobile radio OFDM systems. The idea is to extract the pilots from the feedback signal (sent from the receiver) at the transmitter to generate the channel information and pre-equalize (or pre-distort) the signal before transmission. Although a nice idea, modern wireless systems do not allow for a feedback mechanism in the standard that would make this possible. An iterative method for ICI cancellation using CS algorithms is proposed in [106]. The authors propose an approach wherein, an initial estimate of the channel using the conventional LS scheme is computed after which the ICI components are estimated using a CS scheme. The estimated ICI components are then subtracted from the received signal. This is done iteratively and the resulting signal should in theory be free of ICI. This scheme is shown to work relatively well but it raises questions when a rich multipath channel is simulated. Not surprisingly, the results in this paper only consider a two-path fast fading channel. This approach is also very similar to the idea presented in [105]. An improved channel estimation scheme has been proposed for ISDB-T systems in [119, 120]. These papers propose an oversampling Modified Orthogonal Matching Pursuit (MOMP) based channel estimation in a fractional delay TU6 channel. However, this paper does not deal with a doubly selective channel. A hardware implementation of the proposed scheme is also described in [56]. A relatively recent paper proposes a sparse channel estimation for time-varying systems along with a tracking method using a polynomial basis expansion model. The authors propose a three step estimation where, in the first step a modified OMP algorithms is used to estimate the delay taps. In the second step, the delay taps are tracked iteratively using another modified OMP algorithm and in the third step, the tap gains are estimated using a polynomial basis expansion model. The results given in this paper only show the Bit Error Rate (BER) values after a successive data interference suppression scheme is applied. This makes it difficult to independently evaluate the effectiveness of the proposed CS scheme. The authors also evaluate the proposed algorithm with a simple 128 subcarrier OFDM signal with a high pilot density (25%). Moreover, the channel model used to simulate the doubly selective channel is not described. Nevertheless, we notice that CS based schemes to estimate the wireless channel is widely studied in literature. In the next section, the classical matching pursuit algorithm is explained.

## 6.3 Classical Matching Pursuit Algorithms

Matching pursuit schemes belong to a family of greedy CS recovery algorithms that uses a set of bases to represent a signal. It also involves finding the precise coefficients for the

chosen set of basis functions. Intuitively, the ability of a basis to represent a sparse signal accurately depends on the how closely the properties of the signal match the properties of the basis [85]. As an example, smooth signals that are continuous can be sparsely represented by a Fourier basis, while impulses can not be sparsely represented in this basis. A smooth signal with confined discontinuities can be sparsely represented by a wavelet basis. On the other hand, the wavelet basis is not suited to represent a signal whose Fourier correspondence has a narrow high frequency support as described in [34, 85]. Moreover, when the effects of the wireless channel on the transmitted signal are considered, a single basis might not be adequate to reconstruct the signal at the receiver. To alleviate this problem, matching pursuit algorithms enable us to build a so-called *dictionary* that is a combination of basis functions. Accordingly, the columns of the dictionary are basis function vectors that represent all the different time and frequency effects of the wireless channel. At the receiver, a MP algorithm recovers the channel and reconstructs it by using a small subset of basis vectors in the dictionary. Thus, a sparse reconstruction of the wireless channel is achieved at the receiver.

As pointed out in [34], compressed sensing builds on the foundation that sparse signals can be represented using a handful of non-zero coefficients in an appropriate basis. A linear combination of these basis vectors along with the corresponding non-zero weighting coefficients, enables signal reconstruction from a few measurements. This perspective makes the theory of compressed sensing more intuitive [14].

The MP algorithm greedily computes the best linear approximation of a signal in a complete dictionary. Compared to other CS based recovery algorithms, the MP algorithm is proven to be relatively more efficient although remaining analytically less tractable as discussed in [100]. An important prerequisite of MP algorithms is an appropriate dictionary that models all the channel perturbations with the use of basis functions. The dictionary consists of the preambles and pilots of the underlying standard that are distorted by the different channel perturbations. Once the dictionary has been generated, the received preambles or pilots are compared with the atoms of the dictionary to provide the best matching atom at every iteration. The delay and Doppler shift of the corresponding atoms of the dictionary are considered to be the distortions that are introduced by the wireless channel. Note that, atoms are just the columns of the dictionary and represent the preambles or pilots of the underlying standard that have been corrupted by the channel.

### 6.3.1 Dictionary Generation

The dictionary is a vital prerequisite for MP algorithms and is one of the decisive factors that affects the performance of channel estimation. To understand the technique behind generating the dictionary, consider a wireless channel that has an arbitrary upper bound on the multipath delay and Doppler shift denoted by $\tau_{max}$ and $f_{d_{max}}$ respectively[1]. An integer value representing the maximum multipath delay $\tau_{max}$ can be formulated as $K = \tau_{max}/\Delta_\tau$, where $\Delta_\tau$ is the smallest delay resolution in the estimated channel at the receiver. Similarly, an integer value that represents the maximum Doppler shift in the channel $f_{d_{max}}$ is represented as $L = 2 \cdot f_{d_{max}}/\Delta_{f_d}$, with $\Delta_{f_d}$ being the smallest Doppler shift resolution measured in Hz. Thus, the integers $K$ and $L$ represent the total number of delay and Doppler bins that have to be searched at the receiver. Choosing a small (or a fine) resolution for the delay and Doppler search will result in a more accurate estimate of the channel while making the search slow. On the other hand, choosing a large (or a coarse) resolution for the searches could yield in a slightly inaccurate channel estimate but would speed up the search process. In this thesis, the search resolution is adapted according to the application and the corresponding wireless standard being evaluated. For instance, in applications that allow large multipath delays (few 100 $\mu s$) like in DVB-T2, the search resolution is relatively coarser compared to applications that allow smaller multipath delays (few $\mu s$) like the IEEE 802.11p standard.

With $K$ and $L$ being the maximum delay and Doppler bins respectively, the dictionary denoted by $D$ in its simplest from will contain a total of $(K \cdot L)$ vectors. Each of these vectors have the dimension of the preambles or pilots that are used for channel estimation. Considering the IEEE 802.11p standard where the long preamble is used for estimation, each element of the dictionary is a complex vector with a length equal to the FFT size. Thus, each element of the dictionary can be denoted as $\mathbf{d}_{k,l} \in \mathbb{C}^{N\times 1}$ where $k \in 0 \ldots K-1$ and $l \in 0 \ldots L-1$. The vector $\mathbf{d}_{k,l}$ denotes the dictionary atom corresponding to the $k^{th}$ delay and $l^{th}$ Doppler shift bin. The atoms of the dictionary can be viewed as the transmitted preambles $I_p$ that are distorted by the channel transfer matrix [22] as seen in Equation (6.2).

$$\begin{aligned} \mathbf{d}_{k,l} &= \mathbf{H}_f \mathbf{I}_p \\ \mathbf{d}_{k,l} &= \left( \sum_{k=0}^{K-1} \sum_{l=0}^{L-1} \mathbf{U}_{k,l} \mathbf{C}_l \lambda_k \right) \mathbf{I}_p \end{aligned} \tag{6.2}$$

[1] The upper bounds depend on the application and the respective wireless standard

The channel transfer matrix $\mathbf{H}_f$ in the frequency domain is split into its respective components as described in Section 3.4. The matrix $\mathbf{U}_{k,l}$ are the complex coefficients that signify the attenuations experienced by the signal along different propagation paths. $\mathbf{C}_l$ denotes a circular Doppler shift matrix in the frequency domain and $\lambda_k$ is the diagonal delay matrix in the frequency domain. A potential problem using greedy algorithms is that when the size of the dictionary is large (due to a fine search resolution or large search domains), searching through all the elements of a large dictionary to find the best matching atom in every iteration is impractical. To alleviate this problem, the structure of the preambles along with adaptive search techniques can be used to reduce the computational effort as seen in [41]. Now, most literature that deal with CS for channel estimation either assume that a suitable dictionary is already present or do not provide details of the same. This section gives a generic insight into the construction of the dictionary. However, in practical implementations, due to the large search domains, the size of the resulting dictionary is huge and prohibits practical implementation. To address this problem, novel approaches to construct the dictionary and optimize the computational effort of channel estimation in general are also developed in this thesis and are discussed in Section 6.4

### 6.3.2 Basic Matching Pursuit

Once the complete dictionary has been generated, it is given as an input to the BMP algorithm which is an iterative scheme that estimates the dominant delay taps and the associated tap coefficients. In every iteration, the BMP algorithm selects a column of the dictionary that best correlates with the residual from the previous iteration [100]. It has been shown in Chapter 3 that a multipath delay corresponds to a frequency-dependent phase shift and is characterized by a diagonal matrix in the frequency domain. In a similar manner, a Doppler shift corresponds to a time-dependent phase shift and is characterized by a diagonal matrix in the time domain. Thus, it is intuitive to search for the multipath delays in the frequency domain and the Doppler shift in the time domain [42]. The BMP algorithm is listed in Algorithm 1.

The input to the BMP algorithm is the received preambles or pilots denoted as $\mathbf{y}$ and the stopping criteria. The dictionary is generated in the initialization step, where the atoms of the dictionary represent different combinations of delays and Doppler. The algorithm begins with setting the residual error $\mathbf{r}_0$ as the received preamble in Equation (6.3). The next step is to compute the rank-one projection of the received preamble onto all the atoms of the dictionary $\mathbf{D}$ as given in Equation (6.4). To simplify the algorithm, $j$ is considered to be the linear index for the atoms of the dictionary. $(\cdot)^H$ refers to a Hermitian transpose or conjugate transpose of a matrix/vector. In Equation (6.5), the rank-one projections are

maximized to provide the dictionary atom that best matched the received preamble or pilots. This dictionary atom is denoted by the linear index $s_1$. Note that $|(\cdot)|$ denotes the magnitude of a complex number and $\|(\cdot)\|_2$ denotes the $l_2$ norm of a vector.

**Algorithm 1:** Basic Matching Pursuit Algorithm

**Input:** Dictionary $\mathbf{D}$, received signal $\mathbf{y}$, stopping criterion

*Initialization*

$$\mathbf{r}_0 = \mathbf{y} \tag{6.3}$$

$$b_{0,j} = \mathbf{d}_j^H \mathbf{r}_0, \qquad \text{for } j = 1 \cdots KL \tag{6.4}$$

$$s_1 = \underset{j=1\cdots KL}{\arg\max} \frac{|b_{0,j}|^2}{\|\mathbf{d}_j\|_2} \tag{6.5}$$

$$\mathbf{i}_1 = \{s_1\} \tag{6.6}$$

$$\hat{c}_1 = \frac{b_{0,s1}}{\|\mathbf{d}_{s_1}\|_2^2} \tag{6.7}$$

$$b_{1,j} = b_{0,j} - \hat{c}_1 \mathbf{d}_j^H \mathbf{d}_{s_1}, \qquad \text{for } j = 1 \cdots KL, j \notin \mathbf{i}_1 \tag{6.8}$$

*the $p^{th}$ iteration, $p > 1$*

$$s_p = \underset{j=1\cdots KL, j\notin \mathbf{i}_{p-1}}{\arg\max} \frac{|b_{p-1,j}|^2}{\|\mathbf{d}_j\|_2} \tag{6.9}$$

$$\mathbf{i}_p = \{\mathbf{i}_{p-1}, s_p\} \tag{6.10}$$

$$\hat{c}_p = \frac{b_{p-1,s_p}}{\|\mathbf{d}_{s_p}\|_2^2} \tag{6.11}$$

$$b_{p,j} = b_{p-1,j} - \hat{c}_p \mathbf{d}_j^H \mathbf{d}_{s_p}, \qquad \text{for } j = 1 \cdots KL, j \notin \mathbf{i}_p \tag{6.12}$$

**Output:** Delays, Doppler shift and their corresponding complex weighting factors

Equation (6.6) stores the index of the chosen dictionary atom for the first iteration and will be used in a subsequent step of the BMP algorithm. This vector also stores the indices of dictionary atoms that are chosen in subsequent iterations. Once the dictionary atom is found, the next step is to compute the complex weighting factor (denoted by $\hat{c}$) associated with the corresponding atom. This complex coefficient quantifies the correlation between the residual vector and the chosen atom of the dictionary. Once the complex coefficient $\hat{c}$ is computed, the rank-one projections calculated in Equation (6.4) are updated to remove the contribution of chosen atom as in Equation (6.8). This is done so that other dominant channel effects can be easily found in the subsequent iterations. If required, the $\hat{c}$ can also be used to update the residual vector [100].

In the following iterations of the BMP algorithm, the updated rank-one projections $b_{p-1,j}$ are used to calculate the next maximum while ignoring the atoms that were found in previous iterations as seen in Equation (6.9). Equations (6.10) to (6.12) update the vector of chosen indices $\mathbf{i_p}$, calculate the complex coefficient of the chosen atom and update the rank-one projections respectively. Thus, for each iteration, the BMP algorithm provides a delay Doppler pair along with the respective complex coefficient that can be used to reconstruct the channel. Finally, the algorithm stops when a stopping criteria is fulfilled. The stopping criterion is mostly composed of an upper limit on the number of iterations and an error threshold for the residual error vector. The residual error vector can be obtained by subtracting all the contributions of the chosen atoms from the received vector as seen in Equation (6.13). Note that the residual error vector has been initialized in Equation (6.3) of the BMP algorithm.

$$\mathbf{r}_p = \mathbf{r}_{p-1} - \hat{c}_p \mathbf{d}_{s_p} \tag{6.13}$$

The outcome of the BMP algorithm is a set of dictionary atoms and the corresponding complex coefficients that is used to reconstruct an estimate of the wireless channel. This is then used by channel equalization schemes to compensate the effects of the channel. The BMP algorithm conducts a search through all the atoms of the dictionary and thus, for each iteration, the computational complexity is proportional to the size of the received vector being processed. Thus, the complexity of the BMP algorithm as a whole is $\mathbb{O}(KLqN)$, where $K$ and $L$ are the total number of delay and Doppler bins respectively, $q$ is the number of iterations and $N$ is the size of the received preamble/pilot vector. A more thorough analysis of the computational complexity is provided in Section 6.7.

### 6.3.3 Orthogonal Matching Pursuit

The BMP algorithm listed in Algorithm 1 assumes that the atoms of the dictionary are orthogonal to each other. This orthogonality ensures that the estimated complex coefficients $\hat{c}_p$ are accurate. Once a precise value of $\hat{c}_p$ is computed, updating the rank-one projections in Equations (6.8) and (6.12) is also deemed to be correct. However, if the atoms of the dictionary are not orthogonal to each other, the complex coefficients and the subsequent revision of the rank-one projections are not accurate and will result in an false residual error. To alleviate this problem in the BMP algorithm, the OMP algorithm was proposed in [100].

A significant change in the OMP algorithm is the calculation of the complex coefficients. The equation to compute these complex coefficients denoted as $\hat{c}_{p,omp}$ and is given in Equation (6.14) [100].

$$\begin{aligned} \hat{c}_{p,omp} &= \underset{\mathbf{x},\mathbf{y}\in\mathbb{C}^N}{\arg\min} \|\mathbf{y} - \mathbf{D}_{s,p}\mathbf{x}\|_2^2 \\ &= \left[\mathbf{D}_{s,p}^H \mathbf{D}_{s,p}\right]^{-1} \mathbf{D}_{s,p}^H \mathbf{y} \end{aligned} \tag{6.14}$$

Note that, $\mathbf{D}_{s,p} := [\mathbf{d}_{s_1}, \mathbf{d}_{s_2}, \ldots, \mathbf{d}_{s_p}]$ is a matrix that contains those atoms that are chosen by the OMP algorithm till the $p^{th}$ iteration and $(\cdot)^{-1}$ represents matrix inversion. Equation (6.14) formulates the LS minimization on the chosen dictionary atoms. In effect, the complex coefficients $\hat{c}$ computed in the OMP algorithm provide a better estimate of the coefficients when the underlying atoms of the dictionary are not orthogonal to each other [100].

Regardless of the MP scheme chosen, the underlying principle adopted by classical matching pursuit algorithms is the same wherein, the multipath delays are searched in frequency domain and the Doppler shift is searched in the time domain [41, 42]. An illustration of classical MP algorithms in the context of a generic OFDM receiver is shown in Figure 6.1. The channel estimation block has been expanded to show the inner mechanism of the classical MP schemes. The input to the channel estimation block are the preambles or the pilots specified in the underlying wireless standard. The first step in the channel estimation process is to search for the delays. The MP based search algorithm uses the preambles/pilots and the atoms that are generated by the delay-Doppler dictionary generator and outputs the delay tap that best matched the characteristics of the wireless channel. The delay search is done in the frequency domain as already mentioned. Once the delay tap is found, the algorithm proceeds with the Doppler search in the time domain. For this, the

corresponding atoms of the dictionary are transformed back into the time domain using the $IFFT$ block. The received preambles/pilots are also transformed into the time domain. The MP based Doppler search algorithm searches for the best Doppler estimate for the given delay parameters. The search algorithm is identical to the delay search but it takes place in the time domain. Once the Doppler shift is estimated, the residual vectors are computed and the stopping criterion are checked. The algorithms iterates with the delay-Doppler search until the stopping criteria is fulfilled. Once the stopping criteria is met, the estimated delay and Doppler shift parameters are used to construct the channel transfer matrix $\mathbf{H}_f$ that will be leveraged by channel equalization schemes. Ideally, the channel equalizer is able to compensate the effects of the channel and provide the necessary BER performance at the receiver.

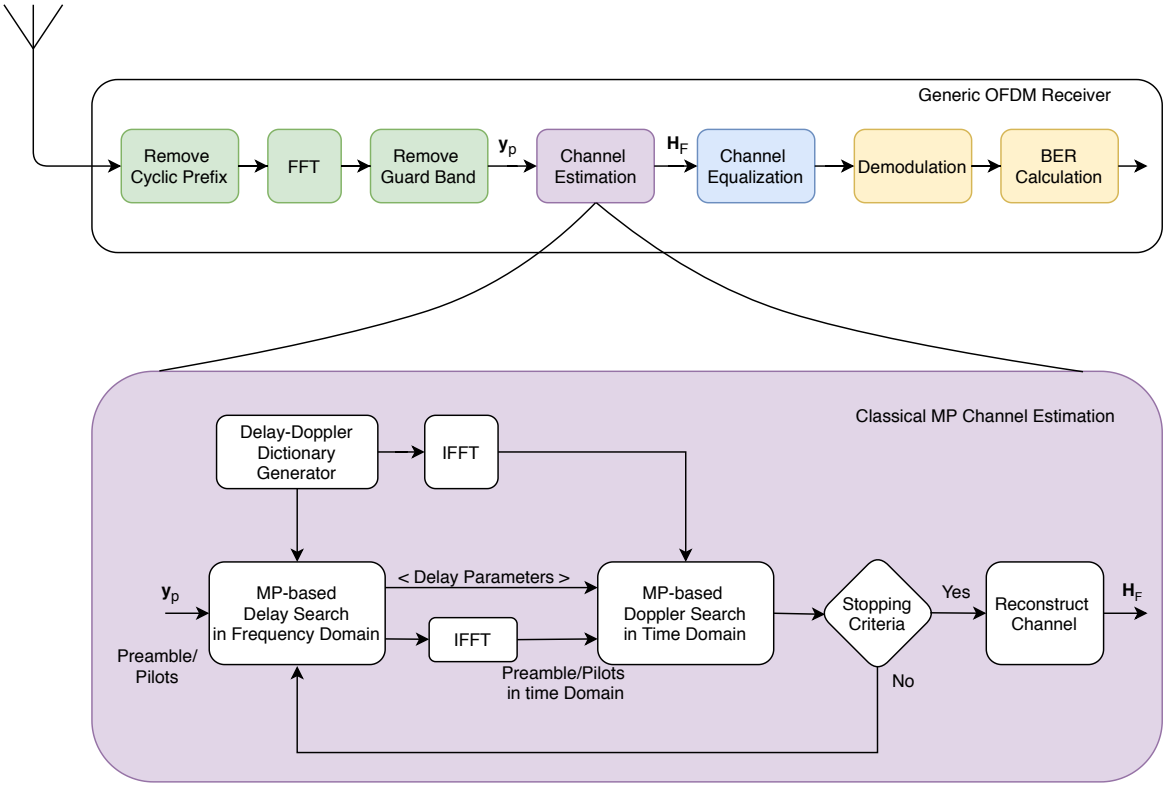


Fig. 6.1: Classical MP based Channel Estimation

The classical MP channel estimation schemes are significantly affected by two major flaws that affect the accuracy of the estimated channel and are described below.

**The Delay Search Metric** shown in Equations (6.3) and (6.4) of Algorithm 1 uses both the amplitude and the phase of the received preamble to compute the rank-one projections. These are maximized to find the corresponding delay tap. However, we know from

Section 3.3, that a multipath delay corresponds to a frequency-dependent phase shift in the frequency domain (time shift property of the Fourier transform). Therefore, using both the amplitude and the phase variation to search for the delays will lead to an inaccurate or sometime a completely wrong estimate of the delay taps [21]. To alleviate this problem, a novel delay search metric is proposed in Section 6.4.

**Doppler Search in the Time Domain:** Performing the Doppler search in the time domain is intuitive due to the frequency shift property of the Fourier transform. This property states that, "a shift in frequency corresponds to a time-dependent phase shift in the time domain". Thus, the classical MP algorithms treat the delay and Doppler shift in a mathematically identical manner. However, there is an inherent asymmetry in these searches from a systems perspective that affects the accuracy of the estimated channel and exhibit inadequate results. Consider a Doppler shift $f_d$ that is introduced in the channel due to the relative mobility between communicating devices. According to the frequency shift property of the Fourier transform, the Doppler shift correspondence can be formulated as $\mathbf{y}(f \pm f_d) \circ\!\!-\!\!\bullet\, \mathbf{Y}(f) \cdot exp(\mp j2\pi f_d t_s)$. The extremely smooth and slow progression of the phase due to the sampling interval $t_s$ makes it nearly impossible to generate dictionary atoms that are able to differentiate these extremely small differences in phase progression. Even a large deviation of Doppler shift $f_d$, will result in a relatively small difference in phase progression. As a result, the estimated channel matrix is neither robust nor accurate and when used for equalization will result in a poor BER performance at the receiver [16].

Due to these flaws in the classical MP schemes, the accuracy of the channel estimate in highly mobile scenarios is not sufficient to overcome the effects of the channel. In order to improve the estimation of the Doppler shift, we explored the possibilities of time-domain pilots in Section 6.3.4 and proposed a novel and robust estimation mechanism in Section 6.4.

### 6.3.4 Time-Domain Pilots

Modern OFDM based wireless communication systems specify pilots (and preambles) in the frequency domain since most of the analysis at the receiver is done post the FFT block in the frequency domain. However, in scenarios of mobility the resulting doubly selective channel introduces selectivity in both the time as well as the frequency domain. Moreover, since classical MP algorithms estimate the Doppler shift in the time domain, it is worthwhile to investigate the impact of time-domain pilots on the channel estimate. The introduction of time pilots must be done systematically. Modifying the time domain signal at the transmitter

naively is not the solution as this would modify the regulated frequency mask of the transmitted OFDM signal. Thus, the task is to design the OFDM signal in the frequency domain such that, a transformation to the time domain (using IFFT) will result in time-domain pilots at the desired locations. In addition to this, it must be ensured that the number of additional carriers to be sacrificed in the frequency domain to enable time pilots should be kept to a minimum and the computational effort should also be realizable.

In [17], we have developed a technique that generates pilot patterns in the time domain by modifying a subset of the subcarriers in the frequency domain and without significantly modifying the transmitter structure. The scope of this proposed technique is to design time-domain pilots for standards that do not have a contiguous pilot pattern in the frequency domain like the DVB-T2 standard. In such cases, the time-domain pilots can aid in estimating the doubly selective channel by providing an additional dimension in which the channel can be measured. A scheme to produce time-domain pilots is introduced for convolutional multiplexed multicarrier systems in [155]. However, the use of complementary codes to generate the pilots in the time domain is not suitable for implementation in DVB–T2. Another example that can be found in literature is a time domain pilot averaging scheme proposed in [166]. The authors propose a scheme that uses the frequency-domain pilots and interpolate it so that the attenuation for every subcarrier of the OFDM symbol is computed. The authors then average this information over subsequent OFDM symbols so that an inherent averaging over time can be achieved. This scheme is shown to perform slightly better than conventional schemes for an AWGN channel and a very slow fading channel. However, even for very small amounts of Doppler shift (maximum relative speed of 50 kmph), the performance of this scheme deteriorates and is very similar to the conventional LS estimator. As far as we know, generating time-domain pilots by modifying the subcarriers in the frequency domain is a novel technique. It provides a reference signal in the time domain that could be used by any estimation and equalization scheme [17].

The underlying idea to generating time-domain pilots is to modify a carrier subset in the frequency domain in a way that generates a periodic pilot pattern in the time domain. This requires the forming of a well-conditioned equation system [17]. Considering the Hermitian transpose of the FFT matrix denoted as $\mathbf{F}^H \in \mathbb{C}^{N\times N}$, the symbol vector of the frequency-domain $\mathbf{x}_f \in \mathbb{C}^{N\times 1}$ is related to the time domain signal $\mathbf{x}_t \in \mathbb{C}^{N\times 1}$ via the Fourier transform as

$$\mathbf{x}_t = \mathbf{F}^H \mathbf{x}_f \tag{6.15}$$

The symbol vector in the frequency domain $\mathbf{x}_f$ is composed of data as well as the specified pilot subcarriers. Let the valid indices of the subcarriers in an OFDM symbol be denoted by the set $\mathbb{P}$, the specified indices (or locations) of the frequency-domain pilots be denoted by the set $\mathbb{P}_{fPil}$, and the indices of the data subcarriers is given by the set $\mathbb{P}_{data}$. In order to generate time-domain pilots, we want to compute the values of a set of subcarriers in the frequency domain denoted as $\mathbb{P}_{sc} \subset \mathbb{P}_{data}$ that takes the data and the pilot subcarriers into account such that, a pilot pattern is present in the time domain after the IFFT transformation at the transmitter. These sets are related as $\mathbb{P} = \mathbb{P}_{fPil} \cup \mathbb{P}_{data}; \mathbb{P}_{sc} \subset \mathbb{P}_{data}$ and $\mathbb{P}_{data} = \mathbb{P}'_{data} \cup \mathbb{P}_{sc}$. Note that, $\mathbb{P}'_{data}$ represent the effective indices remaining for data transmission. Finally, if $\mathbb{P}_{tPil}$ denote indices of the pilots in the time domain, the equation system that has to be solved to generate these time-domain pilots is given in Equation (6.16). Note that, the dimensions of the respective matrices are written as a subscript for convenience.

$$\mathbf{F}^{H}_{(\mathbb{P}_{tPil} \times \mathbb{P}_{sc})} \mathbf{A}_{(\mathbb{P}_{sc} \times 1)} = \mathbf{b}_{(\mathbb{P}_{tPil} \times 1)} \tag{6.16}$$

Here, the coefficient matrix $\mathbf{F}^{H}_{(\mathbb{P}_{tPil} \times \mathbb{P}_{sc})}$ is a subset of the DFT matrix and consists $\mathbb{P}_{tPil}$ rows and $\mathbb{P}_{sc}$ columns. $\mathbf{A}_{(\mathbb{P}_{sc} \times 1)}$ is a column vector that contains the unknown variables and $\mathbf{b}_{(\mathbb{P}_{tPil} \times 1)}$ is a column vector containing the constants from the equation system. The column vector $\mathbf{b}$ is generated by subtracting the contributions of the data subcarriers $(\mathbb{P}_{data})$ and the pilots $(\mathbb{P}_{fPil})$ from the required values of the time-domain pilots [17]. The equation system is then solved by a suitable technique like the QR[2] or the LU[3] decomposition method [140] to provide the column vector $\mathbf{A}_{(\mathbb{P}_{sc} \times 1)}$. The OFDM symbol is then recomposed in the frequency domain with the pilots $\mathbb{P}_{fPil}$, data subcarriers $\mathbb{P}'_{data}$ and the solution of the equation system $\mathbb{P}_{sc}$. Converting this OFDM symbol to the time domain will result in periodic pilots at the locations given by the set $\mathbb{P}_{tPil}$.

A linear system of equations is solvable if the coefficient matrix $\mathbf{F}$ in Equation (6.16) is full rank. This can be ensured by appropriately choosing the subcarrier set $\mathbb{P}_{sc}$ that has to be modified to generate the required time-domain pilots. If the cardinality of the set $\mathbb{P}_{sc}$ denoted as $\mathbf{card}(\mathbb{P}_{sc})$ is less than $\mathbf{card}(\mathbb{P}_{tPil})$, the system of equations is under determined and a solution is not available. If the cardinalities of the two sets are equal, a solution is available but in most cases, it can add a very large power on the transmitted OFDM signal making it unfeasible for practical implementation. However, if $\mathbf{card}(\mathbb{P}_{sc}) > \mathbf{card}(\mathbb{P}_{tPil})$ the solution obtained is realizable at the cost of marginally over-determining the equation system [17].

[2] decomposition of matrix $A$ into a product of an orthogonal matrix $Q$ and an upper triangular matrix $R$ [150]
[3] decomposition of a matrix into a lower and an upper triangular matrix [135]

To implement the time-domain pilots, we chose the DVB-T2 standard and use the Common Simulation Platform (CSP) for development. The specifications of this standard has been described concisely in Section 4.2 and the CSP will be introduced in Section 9.3. The modified block diagram of the DVB-T2 transmitter is shown in Figure 6.2. The pilot insertion block in the transmitter chain has been developed to achieve pilots in the time-domain. The necessary data to formulate the equation system is available in this block. Note that the time pilots only appear after the IFFT block.

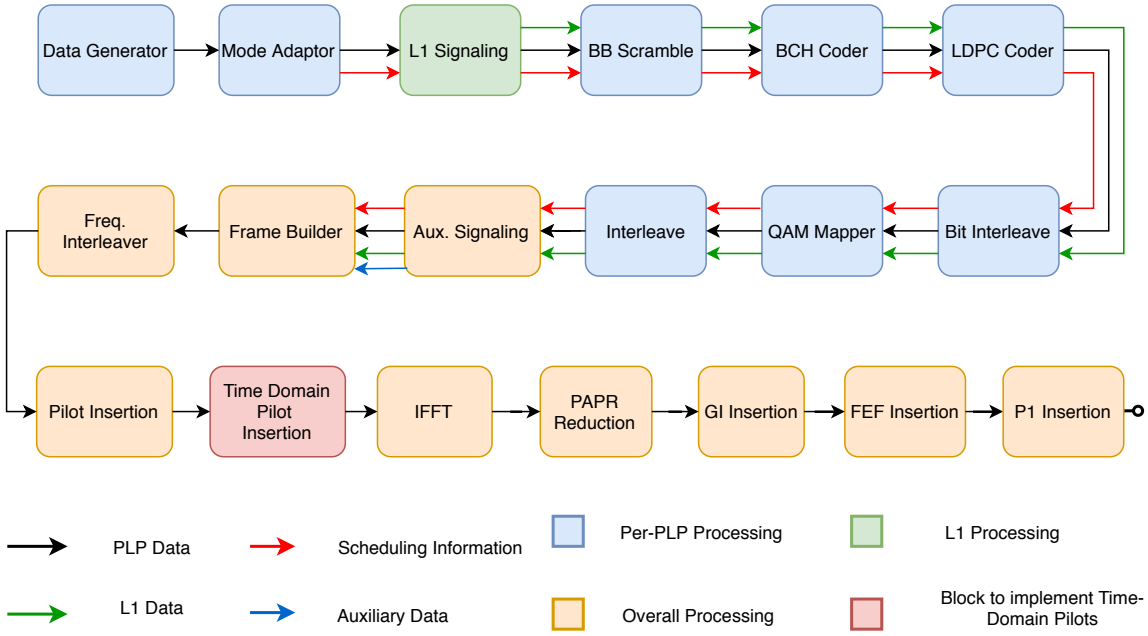


Fig. 6.2: Modified DVB-T2 Transmitter that Implements Time-Domain Pilots

The blocks of the transmitter chains remain unaltered as a small set of the processed subcarriers are modified before the IFFT block. The time domain pilot insertion block carries all the added complexity to generate the time-domain pilots. The receiver chain remains completely untouched, and the only information needed at the receiver is the location of the time-domain pilots. The receiver can leverage these pilots to measure the time selectivity of the wireless channel.

Evaluation is done with random data for different physical layer frames operating in the 8$k$ mode with a guard interval fraction of 0.25 and the PP1 pilot pattern. However, the proposed scheme is also applicable to all other modes available in the DVB-T2 standard. The result is the presence of time-domain pilots that have the required values at the desired locations in the time domain. Figure 6.3 shows an example of a simple time-domain pilot

pattern that is extracted from the OFDM signal in the time domain. Here, the equation system is configured such that the time-domain pilots have a value of 2 and are spaced $11.922\mu s$ apart in the time domain. The total number of time-domain pilots in this case is 75. The number of subcarriers in the frequency domain that were required to generate time-domain pilots in this example have been $\mathbf{card}(\mathbb{P}_{sc}) = 667$. Of course, the equation system can be designed and solved by more advanced techniques such that fewer data subcarriers have to be sacrificed. Nevertheless, the goal has been to show that it is possible to generate time-domain pilots by modifying a subset of carriers in the frequency domain that keeps that spectrum mask unaffected and keeps most of the specified transmitter chain (see Figure 6.2) unchanged.

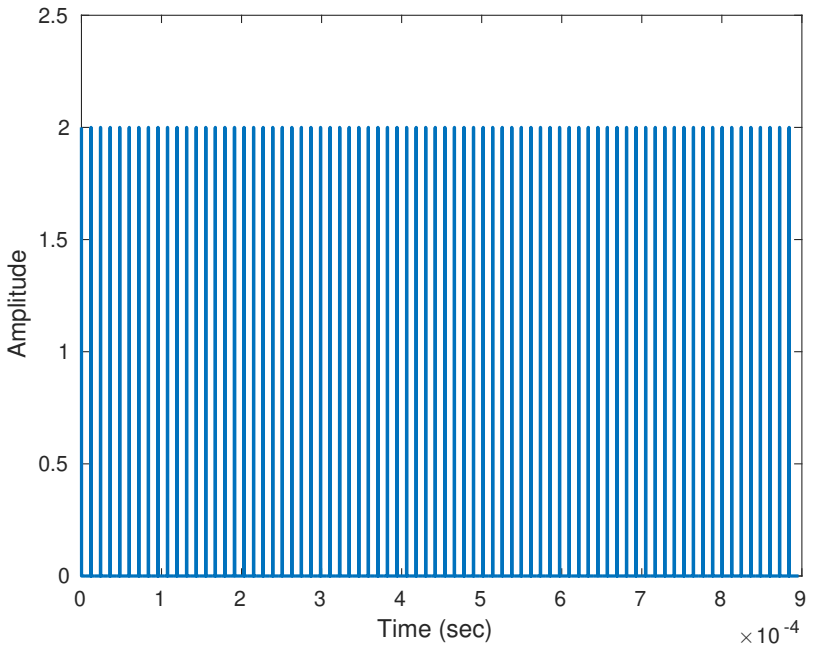


Fig. 6.3: Time-domain pilots in an OFDM signal

The computational burden of this algorithm predominantly is related to finding a solution of the equation system. Although the QR decomposition with column pivoting technique, which is used in this thesis has a cubic complexity, only a few hundred unknowns (667 in the example above) are used to solve the equation system. Moreover, the time-domain pilots have to be designed at the transmitter and they need not be done for every OFDM symbol in the frame [17]. In addition to this, techniques to find the optimal set of unknowns such that a smaller equation system needs to solved and fast algorithms for solving linear equations can be explored to reduce complexity as pointed out in [17].

Unfortunately, although the presence of time-domain pilots are helpful in improving the accuracy of the channel estimate, it has not been adequate enough to provide an improvement in error performance at the receiver. This is because the inherent problem with the extremely slow phase progression corresponding to a Doppler shift still exits and it is difficult to develop an efficient (and effective) search metric for CS based techniques to estimate the Doppler shift in the time domain. However, the time-domain pilots can significantly help other algorithms that rely on measurements in the time domain to estimate the channel.

To summarize, classical matching pursuit schemes estimate the delays and Doppler shift in the frequency and the time domain respectively. Even though this approach is intuitive, the search metrics to estimate the delays and the Doppler shift behave very differently. As a result, a very large change in mobility conditions (and correspondingly the Doppler shift), results in a small change in the time-domain. This makes it difficult to design a Doppler search algorithm using the classical MP schemes even with the presence of time-domain pilots. Thus, after several experiments and trials, a novel algorithm based on the MP scheme has been conceptualized to estimate a doubly selective channel and is described in the following section.

## 6.4 Rake Matching Pursuit

The Rake Matching Pursuit Algorithm (RMP) has been developed in this thesis to overcome the limitations of classical MP schemes like the BMP and the OMP algorithm in the estimation of a doubly selective channel. It forms the basis of this thesis and proposes various changes that contribute towards the robustness of the algorithm and help reduce the computational complexity at the same time. The two primary sources of distortions introduced by the wireless channel stem from delays and Doppler shift. The improvements to the delay and the Doppler shift search are described in this section.

### Delay Search with RMP

The delay search should ideally estimate a set of delays along with their corresponding complex weighting factors or tap coefficients accurately. In the context of the MP algorithm, this corresponds to a high degree of correlation between the ideal set of dictionary columns (or the ideal set of delays) and the received preamble or pilots. Accordingly, it is imperative that the dictionary should be designed to emulate the distortions of the channel. We know that a multipath delay corresponds to a frequency-dependant phase shift in the frequency domain

as described in Section 3.2. Keeping this in mind, the classical MP algorithms uses the entire complex received preamble/pilot and considers both the amplitude and the phase variations while searching for the delays. Such a delay search metric can result in an imprecise and sometimes a completely wrong estimate of delays. The main cause of this is the amplitude variations that skews the rank-one projections and can have a direct influence on the estimated delay. As a result, an imprecise estimate of the channel leads to poor equalization performance. Moreover, considering both the amplitude and the phase variations while designing the dictionary would would not be computationally efficient and increase the storage requirement at the receiver [21].

To alleviate this problem, a novel and intuitive approach proposed in this thesis has been to modify the delay search metric such that it considers only the frequency-dependent phase variations of received preambles/pilots. This can be easily implemented by simply normalizing the magnitude of the received preamble/pilot vector $\mathbf{y}$ as shown in Equation (6.17) and then using it in the delay search.

$$\mathbf{r}_0 = \frac{\mathbf{y}}{|\mathbf{y}|} \tag{6.17}$$

Normalizing the received preambles removes the amplitude variations that are detrimental in the delay search algorithm. Thus, a more robust correlation to the atoms of the dictionary can be achieved and a robust estimate of the multipath delays is ensured [21]. The Rake Matching Pursuit (RMP) algorithm employs this robust delay search metric while searching for the multipath delays.

The first part of the proposed RMP algorithm involves estimating the multipath delays and Algorithm 2 lists the different steps involved in the delay search. The use of the modified delay search metric can be immediately seen in Equation (6.18) where the residual error $\mathbf{r}_0$ is initialized to the normalized received preamble or pilots. The received signal is then projected to every column of the dictionary in Equation (6.19). By normalizing the magnitudes, it is implicitly ensures that the rank-one projections are free from all magnitude variations. The rank-one projections are then maximized in Equation (6.20). In Equation (6.22), the complex weighting factor corresponding to the chosen delay is computed. In the next step, the rank-one projections are updated in Equation (6.23) by subtracting the contributions of the chosen dictionary atom. The algorithm iterates until a stopping criteria is reached or the maximum number of iterations are completed. The outcome is a set of delays along with the

corresponding complex weighting factors.

**Algorithm 2:** Rake Matching Pursuit Algorithm - Delay Search

**Input:** Dictionary $\mathbf{D}$, received signal $\mathbf{y}$, stopping criterion

*Initialization*

$$\mathbf{r}_0 = \frac{\mathbf{y}}{|\mathbf{y}|} \tag{6.18}$$

$$b_{0,j} = \mathbf{d}_j^H \mathbf{r}_0, \qquad \text{for } j = 1 \cdots K \tag{6.19}$$

$$s_1 = \underset{j=1\cdots K}{\arg\max} \frac{|b_{0,j}|^2}{\|\mathbf{d}_j\|_2} \tag{6.20}$$

$$\mathbf{i}_1 = \{s_1\} \tag{6.21}$$

$$\hat{c}_1 = \frac{b_{0,s_1}}{\|\mathbf{d}_{s_1}\|_2^2} \tag{6.22}$$

$$b_{1,j} = b_{0,j} - \hat{c}_1 \mathbf{d}_j^H \mathbf{d}_{s_1}, \qquad \text{for } j = 1 \cdots K, j \notin \mathbf{i}_1 \tag{6.23}$$

*the $p^{th}$ iteration, $p > 1$*

$$s_p = \underset{j=1\cdots K, j\notin \mathbf{i}_{p-1}}{\arg\max} \frac{|b_{p-1,j}|^2}{\|\mathbf{d}_j\|_2} \tag{6.24}$$

$$\mathbf{i}_p = \{\mathbf{i}_{p-1}, s_p\} \tag{6.25}$$

$$\hat{c}_p = \frac{b_{p-1,s_p}}{\|\mathbf{d}_{s_p}\|_2^2} \tag{6.26}$$

$$b_{p,j} = b_{p-1,j} - \hat{c}_p \mathbf{d}_j^H \mathbf{d}_{s_p}, \qquad \text{for } j = 1 \cdots K, j \notin \mathbf{i}_p \tag{6.27}$$

**Output:** Delays and their corresponding complex weighting factors

At a first glance, the delay search in Algorithm 2 looks deceptively similar to the classical MP scheme shown in Algorithm 1. But the use of a modified search metric (Equation (6.18)) along with the fact that the delay search algorithm, as the name suggests, only searches for the multipath delays in Algorithm 2 while the classical MP algorithm jointly estimates the delays and the Doppler shift. This becomes evident by comparing Equations (6.4) and (6.19). Once the delays are estimated, the next part of the RMP algorithm is the estimation of the Doppler shift.

## Doppler Search with RMP

The Doppler search mechanism developed for the RMP algorithm is significantly different to the classical MP algorithms that estimates the Doppler shift in the time domain due to the fact that a Doppler shift is a time-dependent phase shift. However, as explained in Section 6.3, this approach has a few flaws that results in a wrong estimate of the Doppler shift component.

A novel idea to estimate the Doppler shift in the channel has been conceived and developed in this thesis. The underlying idea has been triggered by Figure 6.4 that shows a model of a time-variant channel model. This figure shows an input signal denoted by $x(t)$ being delayed by different delay taps $\tau_k$. Each of these delay taps also have a complex weighting factor denoted by $h(\tau_k, t)$. The most important observation to be made here is that the complex weighting factors or the complex coefficients of the respective delay taps are not constant, but a function of time. This temporal variation of the weighting factors is caused by the Doppler shift in scenarios of high mobility. The extent of this temporal progression depends on the mobility. In stationary conditions, the weighting factors remain constant; while in highly mobile scenarios, a significant variation of the weighting factors in a physical layer frame is observed. We also note that the delay taps themselves are relatively stable and only the complex weighting factors need to be adapted. Consequently, the ingredients required to precisely parameterize the doubly selective channel are i. the delay taps, ii. the initial estimate of the corresponding weighting factors and, iii. the temporal variation of these weighting factors.

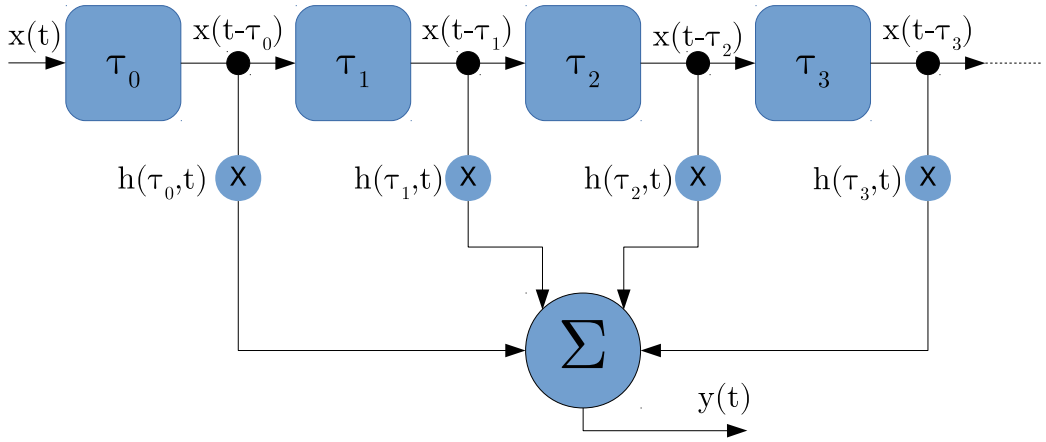


Fig. 6.4: Time-Variant Channel Model [91]

From the perspective of the receiver, this observation implies that, once the delays along with the initial complex weighting factors have been estimated using the proposed RMP delay search algorithm, the temporal progression of the complex weighting factors should be estimated. This implies that the weighting factors for each delay tap is updated for every OFDM symbol in a physical layer frame. Note that, since we are updating the complex weighting factors for every delay tap individually, an inherent separation between the delay and the Doppler search is achieved. Thus, at the receiver, tracking the weighting factors of the delay taps implicitly estimates the Doppler shift in the channel. The reasons behind naming the proposed scheme as the Rake Matching Pursuit algorithm are due to the structure of the time-variant channel in Figure 6.4 and the fact that we estimate the Doppler shift parallelly for the delay taps. The inherent Doppler shift estimation scheme has been listed in Algorithm 3.

The input to the RMP Doppler estimation algorithm are the delay taps along with the initial estimates of the complex weighting factors, the dictionary atom corresponding to the estimated delay taps and the received pilots. In the first step, the vector of received pilots $\mathbf{y}_p \in \mathbb{C}^{1\times N_p}$ is initialized as the residual error vector $r_0$ as seen in Equation (6.28). Note that, $N_p$ is the number of specified pilots in the data OFDM symbols. These pilots are used to track the temporal variation of the weighting factors. For the next step in Equation (6.29), the

total number of delay taps that have been found in the delay search are assumed to be $q_{taps}$.

**Algorithm 3:** Rake Matching Pursuit Algorithm - Doppler Search

**Input:** Estimated delay taps and respective dictionary atoms $\mathbf{D}' = [\mathbf{d}_1, \ldots, \mathbf{d}_q]$, received pilots $\mathbf{y_p}$

*Initialization*

$$\mathbf{r}_0 = \mathbf{y}_p \tag{6.28}$$

$$b_{0,j} = \mathbf{d}_j^H \mathbf{r}_0, \qquad \text{for } j = 1 \cdots q_{taps} \tag{6.29}$$

$$\mathbf{i}_1 = \{1\} \tag{6.30}$$

$$\hat{c}_{1,r_p} = \frac{b_{0,1}}{\|\mathbf{d}_1\|_2^2} \tag{6.31}$$

$$b_{1,j} = b_{0,j} - \hat{c}_{1,r_p} \mathbf{d}_j^H \mathbf{d}_1, \qquad \text{for } j = 1 \cdots q_{taps}, j \notin \mathbf{i}_1 \tag{6.32}$$

*the $p^{th}$ iteration, $p > 1$ and $p \leq q_{taps}$*

$$\mathbf{i}_p = \{\mathbf{i}_{p-1}, p\} \tag{6.33}$$

$$\hat{c}_{p,r_p} = \frac{b_{p-1,p}}{\|\mathbf{d}_p\|_2^2} \tag{6.34}$$

$$b_{p,j} = b_{p-1,j} - \hat{c}_{p,r_p} \mathbf{d}_j^H \mathbf{d}_p, \qquad \text{for } j = 1 \cdots q_{taps}, j \notin \mathbf{i}_p \tag{6.35}$$

**Output:** Updated complex weighting factors for the given OFDM symbol

The delay vectors in the frequency domain corresponding to these delay taps are denoted as $\mathbf{d}_1 = exp(j2\pi\mathbf{f}\tau_1), \mathbf{d}_2 = exp(j2\pi\mathbf{f}\tau_2), \ldots, \mathbf{d}_q = exp(j2\pi\mathbf{f}\tau_q)$. These vectors make up the dictionary and are used to track the Doppler shift. These vectors can be written as $\mathbf{D}' = [\mathbf{d}_1, \mathbf{d}_2, \ldots, \mathbf{d}_q]; \mathbf{D}' \in \mathbb{C}^{N_p \times q_{taps}}$. The rank-one projections are computed for the delay taps and stored in $b_{0,j}$ as seen in Equation (6.29). It is also important to note that, the normal-

ization of the initial vector is not done since we want to track both the magnitude and the phase of the complex weighting factors $\hat{c}$. Once the rank-one projections are computed, the complex weighting factors for the first delay tap is computed in Equation (6.31). Next, the rank-one projections of the other delay taps are updated in Equation (6.32). In the subsequent iterations, the previously updated rank-one projection is used to find the weighting factors of the next delay tap as in Equation (6.34) followed by updating the rank-one projections in Equation (6.35). The algorithm stops when an updated value of the complex weighting factor has been computed for all the $q_{taps}$ delay taps. The Doppler search of the RMP algorithm is conducted for all the OFDM data symbols in the physical layer frame. Effectively, all the ingredients to precisely model the doubly selective channel have been estimated and can be used for equalization [21].

It is important to note that the maximization step is not necessary in the Doppler search since the dominant delay taps have already been found in the RMP delay search algorithm and are also sorted according to their strengths. Another interesting remark about the proposed RMP algorithm is its behavior in a stationary environment (no Doppler shift). In such a scenario, the Doppler tracking scheme will compute the same (or very similar) values of the complex weighting factors for all the OFDM data symbols. This ensures that the proposed scheme gives an optimal result not only in scenarios of high mobility but also in stationary channel conditions. The results in Chapter 10 will confirm this behavior.

A block diagram showing the RMP based channel estimation at the OFDM receiver is given in Figure 6.5. Compared to the classical MP scheme (in Figure 6.1), the most important difference can be seen. Once the delays have been estimated robustly using the improved delay metric, the channel tracking block tracks the temporal variations of the weighting factors using the data pilots. The updated delay parameters are then used to reconstruct the channel and used by the equalizer to compensate the effects of the wireless channel.

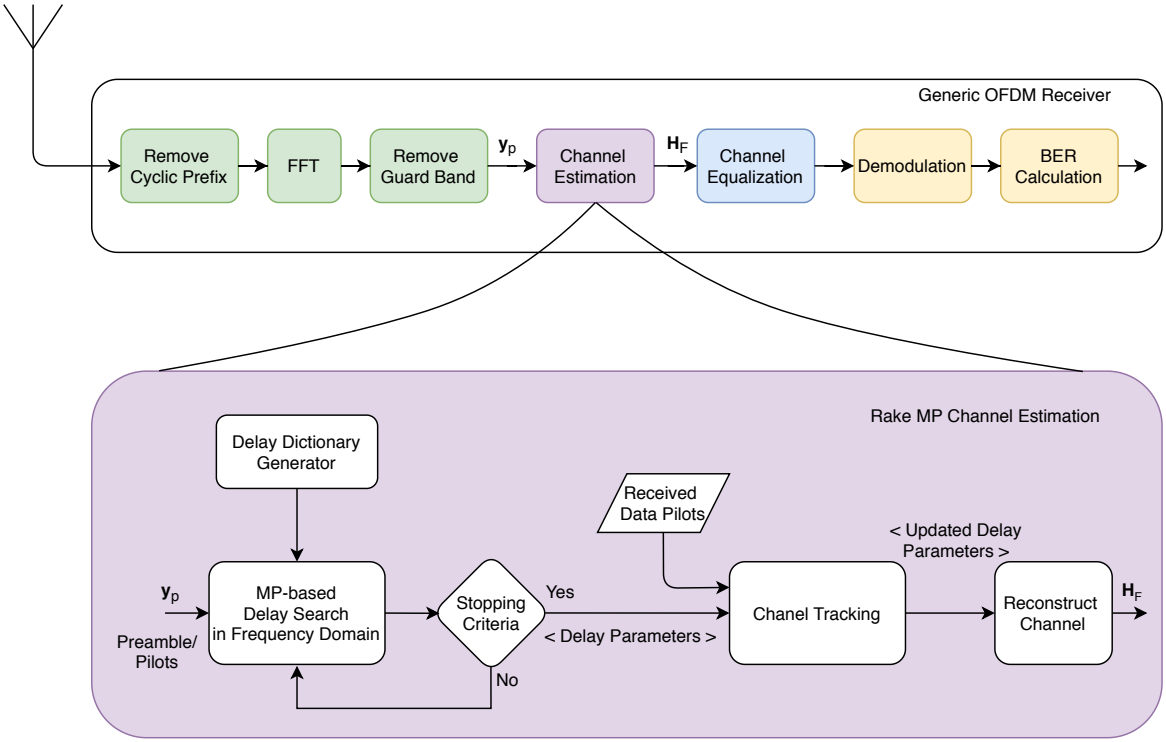


Fig. 6.5: Rake MP based Channel Estimation

The complexity of the proposed RMP algorithm is composed of $\mathbb{O}(KqN)$ for the delay search and $\mathbb{O}(qN_p)$ for the Doppler search. Comparing this to the classical MP algorithms that have a complexity of $\mathbb{O}(KLqN_p)$ where, $K$ and $L$ correspond to the maximum number of delay and Doppler bins, $q$ is the number of iterations and $N_p$ is the size of the received preamble/pilot vector, a significant complexity reduction has already been achieved by the RMP algorithm. A more thorough analysis of the computational complexity is provided in Section 6.7.

The proposed RMP algorithm has been developed to estimate the doubly selective channel at an acceptable complexity. This has been achieved by a novel metric for the delay search that is unaffected by the amplitude variations caused in the channel. We have also exploited the fact that a Doppler shift results in a temporal variation of weighting factors to develop a precise, robust and efficient scheme to estimate the Doppler shift in the channel. The RMP Doppler estimation scheme tracks these weighting factors for every delay tap and for every OFDM symbol in the physical layer frame and thereby implicitly estimate the Doppler shift in the channel. The proposed scheme are also designed to work robustly in stationary channel conditions. The computational complexity involved has been significantly reduced when compared to the classical schemes [21]. A further reduction in complexity by optimizing

the delay search has been described in Section 6.5 and a novel cognitive framework that cleverly senses the channel and switches to an appropriate channel estimation scheme has been introduced in Chapter 7.

## 6.5 Gradient Rake Matching Pursuit

Computation complexity is a crucial factor that needs to be addressed especially when algorithms are to be implemented on consumer hardware. The Gradient Rake Matching Pursuit (GRMP) algorithms is a modified version of the RMP algorithm that drastically reduces the complexity involved in estimating the channel.

During the development and evaluation of RMP algorithm, an important aspect of the RMP algorithm was found. It showed that the RMP algorithm is immune to errors even when a wrong delay tap is found during the delay search. This is mainly due to the tracking mechanism to estimate the Doppler shift wherein, there is a very high probability that for a wrongly estimated delay tap, the weighting coefficients have a negligible magnitude. Accordingly, when the channel model is reconstructed, the contribution from the wrong delay tap is also negligible (because it is multiplied by the weighting factor whose magnitude is nearly zero) and the resulting channel is robust to the wrongly estimated delay tap. This feature has been exploited to make gains in complexity and is used in the GRMP algorithm [20].

The underlying idea of the GRMP algorithm is to compute a rough estimate of the delays along with the respective complex weighting factors in a single iteration or pass. Due to the improved modified metric for delay search presented in Section 6.4, the rank-one projections computed during the delay search provide a clear maxima at the locations of the delay taps. Accordingly, a gradient method can be applied to extract the location of these peaks that correspond to the delays introduced in the channel. Since a gradient method is used to locate the peaks, this algorithm is called Gradient Rake Matching Pursuit algorithm [20]. Once the delays are estimated, the Doppler estimation scheme (discussed in Section 6.4 ) that is robust against an imprecise estimate of delay taps is used to track the temporal variations in the channel. The different steps of the GRMP algorithm have been listed in Algorithm 4.

The input to the GRMP algorithm is the dictionary and the received pilots/preambles. In Equation (6.36), a magnitude normalization of the received pilots/preambles is done and is initialized as the error vector $r_0$. The rank-one projections are computed in Equation (6.37)

and normalized in Equation (6.38).

**Algorithm 4:** Gradient Rake Matching Pursuit Algorithm

**Input:** Dictionary **D**, received signal **y**

*Initialization*

$$\mathbf{r}_0 = \frac{\mathbf{y}}{|\mathbf{y}|} \tag{6.36}$$

$$b_{0,j} = \mathbf{d}_j^H \mathbf{r}_0, \qquad \text{for } j = 1 \cdots K \tag{6.37}$$

$$s_{0,j} = \frac{|b_{0,j}|^2}{\|\mathbf{d}_j\|_2}, \qquad \text{for } j = 1 \cdots K \tag{6.38}$$

$$m_{0,j} = \nabla \mathbf{s}_0, \qquad \boldsymbol{s}_0 = [s_{0,j}] \forall (j = 1 \cdots K) \tag{6.39}$$

**for** $j \in \{1, 2, \cdots, K\}$ **do**
  **if** $m_{0,j-1} \leq m_{0,j} \geq m_{0,j+1}$ **then**

$$\boldsymbol{i}_0 = \{\boldsymbol{i}_0, j\} \tag{6.40}$$

$$\hat{\mathbf{c}}_{i_0} = [\mathbf{D}_{i_0}^H \boldsymbol{D}_{i_0}]^{-1} \mathbf{D}_{i_0}^H \boldsymbol{y} \tag{6.41}$$

**Output:** Delays and their corresponding complex weighting factors

In the next step, a first order derivative is computed in Equation (6.39). This is then followed by finding the most dominant taps by using a very simple peak finding mechanism shown in Equation (6.40). The peaks are stored in a vector **i** and correspond to the delay taps. The complex weighting factors associated with the delays are computed in Equation (6.41). Note that, the GRMP algorithm bypasses the iterative $l_1$-minimization process in the delay search. The outcome of the GRMP algorithm is a set of delays and the corresponding weighting factors. Once a rough estimate of the delays are computed, the Doppler search is done for every OFDM in the physical layer frame. A block diagram that described the GRMP algorithm is shown in Figure 6.6. A significant change when compared to the RMP algorithm (Figure 6.5) is the single-pass delay search and the absence of a stopping criteria.

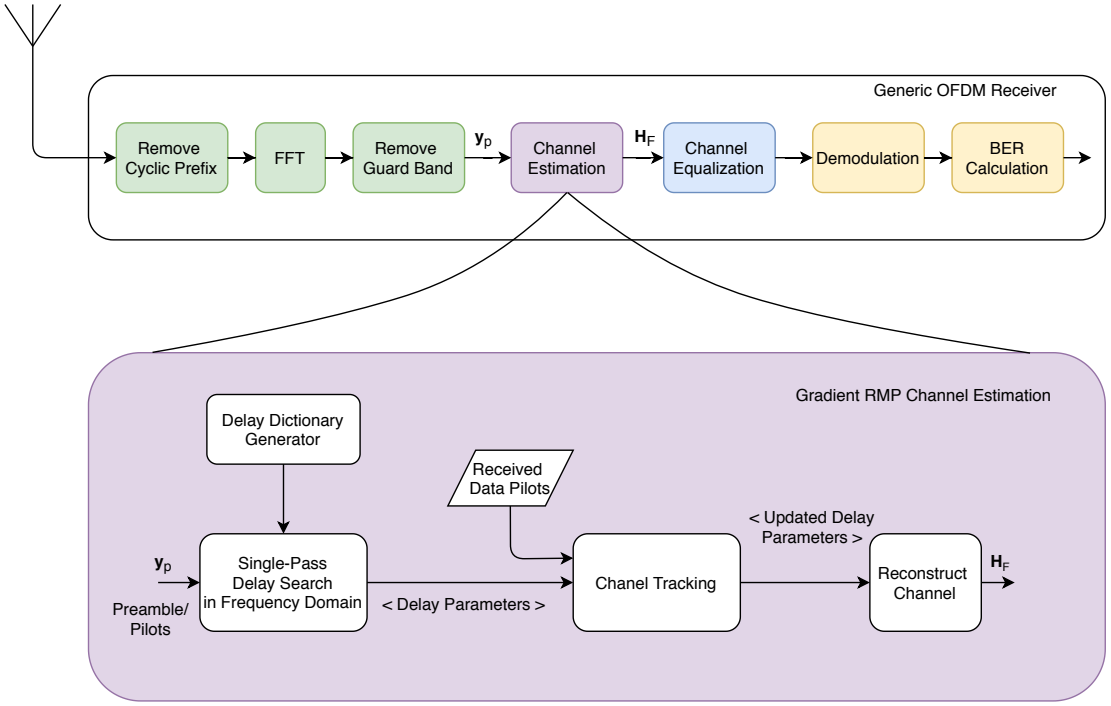


Fig. 6.6: Gradient RMP based Channel Estimation

Circumventing the iterative process in the GRMP algorithm significantly reduces the complexity but has a few disadvantages. In the iterative delay search process of the RMP algorithm, the contribution of each found delay on all the other delays (or rank-one projections) is subtracted before the next iteration. Thus, even when the estimated delay is not ideally accurate, the RMP algorithm is able to achieve results that are similar to $l_1$-minimization as shown in [14, 34, 96]. However, in the GRMP algorithm the estimated delay taps are required to precisely represent the multipath effects of the channel in order to obtain good error performance. This observation is also confirmed consistently for different channel conditions in the results in Chapter 10.

The absence of the iterative delay search in the GRMP is evident in Algorithm 4 and has significantly reduced the computational complexity to $\mathbb{O}(KN)$ when compared to the delay search of the RMP algorithm that has a complexity of $\mathbb{O}(qKN)$, where $K$ is the total number of delay bins and $N$ the size of the received preamble/pilot vector. The complexity is reduced by a factor of $q$, which is number of iterations in the RMP algorithm. In addition to the gains made with respect to the complexity in the GRMP algorithm, the computationally intensive process of generating the dictionary has also been optimized and is described in the next section.

## 6.6 Optimizing Dictionary Generation

The dictionary is a prerequisite of the MP based channel estimation algorithms and generating it is a computationally intensive process. The classical mechanism of generating a dictionary involves computing a phase progression corresponding to each of the delay or Doppler bin to be searched during channel estimation. Additionally, storing these complex vectors of the dictionary atoms requires a significant amount of storage. Moreover, since the dictionary is a pre-requisite for compressed sensing, it is worthwhile to optimize the computation and storage associated with it.

In order to build towards an intuitive mechanism to generate the dictionary, let us consider the classical approach first. It has been established that a multipath delay can be represented by a frequency-dependent phase shift in the frequency domain. Accordingly, the classical approach of generating the dictionary atom $\mathbf{d}_k$ for a delay $\tau_k$ can be written as shown in Equation (6.42).

$$\mathbf{d}_k = \mathbf{I}_p \circ exp(-j2\pi f \tau_k) \tag{6.42}$$

here, $\mathbf{I}_p \in \mathbb{C}^{N\times 1}$ refer to the specified preamble or pilots, $N$ is the size of the FFT and $\circ$ just denotes an element wise operation. Note that, the exponential function in Equation (6.42) and the dictionary atoms generated are periodic. Thus, the question was asked if this periodicity can be exploited to make gains in complexity.

Since the dictionary atoms are computed from the complex exponential function, the idea has been to store a single high resolution representation of this vector that contains all the values required to generate any arbitrary dictionary atom. From an implementation standpoint, pointer arithmetic can be used to pick the required complex values and generate the required delay vector. Since this high resolution vector is used to generate the rest of the dictionary atoms, we call this vector as a mother wavelet [20]. The mother wavelet is represented as $\mathbf{d}_{mw,\Omega} = exp(-j\Omega_m)$. When the search resolution for the delays is $\Delta_\tau$ and the sampling interval is $T_s$, the $\Omega_m$ is an array consisting of values from $-\pi$ and $\pi$ in steps of $\frac{2\pi\Delta_\tau}{NT_s}$ as seen in Equation (6.43).

$$\Omega_m = -\pi + \frac{n \cdot 2\pi\Delta_\tau}{NT_s}, \qquad n = [0, 1, \ldots, \frac{NT_s}{\Delta_\tau}] \tag{6.43}$$

Now that the mother wavelet is generated, pointer arithmetic is used to generate the indices that extracts the respective complex values and generate the delay vector for a given

delay $\tau_k$. Since the OFDM symbols are centered in the complex band according to the specifications of the underlying standard, the subcarriers will consist of positive and negative frequencies. This is nothing but a 180° phase shift in the underlying mother wavelet. Thus, if we consider the complex exponential function $exp(-j\Omega_m)$ on the complex plane, it is analogous to moving along the unit circle in the clockwise direction for negative frequencies and moving in the counter clockwise direction for positive frequencies. Thus, for each of the delay bin $\tau_k$, two sets of indices are required to construct the corresponding dictionary atom. The indices of the OFDM subcarriers with the positive frequencies are denoted as $\alpha_{\tau_{ccw}} \in \mathbb{Z}^{\frac{N}{2}\times 1}$ (ccw just means counter clockwise), where $\mathbb{Z}$ represents integer numbers. These indices are computed according to Equation (6.44).

$$\alpha_{\tau_{ccw}} = \frac{NT_s}{2\Delta_\tau} + \Psi_i \cdot \frac{\tau_k}{\Delta_\tau} \tag{6.44}$$

where, $\Psi_i = [0, 1, \ldots, \frac{N}{2}]$. In a similar manner, the indices of the negative OFDM subcarriers represented as $\alpha_{\tau_{cw}} \in \mathbb{Z}^{\frac{N}{2}\times 1}$ (cw means clockwise) and are computed as in Equation (6.45).

$$\alpha_{\tau_{cw}} = \frac{NT_s}{2\Delta_\tau} - 1 - \left(\frac{N}{2} \cdot \frac{\tau_k}{\Delta_\tau} - 1\right) + \Psi_i \cdot \frac{\tau_k}{\Delta_\tau} \tag{6.45}$$

Equations (6.44) and (6.45) can be simplified to form a single set of indices and is given in Equation (6.46), where, $\alpha_{\tau_k} \in \mathbb{Z}^{N\times 1}$, $\lambda_{i,\Omega} = [-\frac{N}{2}, \ldots, (\frac{N}{2} - 1)]$ and *mod* denotes the modulo operation that enables repetition of the integer indices within the bounds of the mother wavelet [20].

$$\alpha_{\tau_k} = \left(\frac{NT_s}{2\Delta_\tau} + \lambda_{i,\Omega} \cdot \frac{\tau_k}{\Delta_\tau}\right) mod \left(\frac{NT_s}{\Delta_\tau}\right) \tag{6.46}$$

Equation (6.46) gives a simple mechanism to generate the indices for a given delay $\tau_k$. The delay vector of the dictionary atom is then simply extracted from the mother wavelet $\mathbf{d}_{mw,\Omega}$ using the index set $\alpha_{\tau_k}$ as seen in Equation (6.47).

$$\mathbf{d}_{p,\tau_k} = \mathbf{I}_p \circ \mathbf{d}_{mw,\Omega}(\alpha_{\tau_k}) \tag{6.47}$$

For a given multipath delay $\tau_k$, the dictionary atom generated using the wavelet procedure in Equation (6.47) is identical to the atom generated by the classical method shown in Equation (6.42) when the value of $\frac{NT_s}{2\Delta_\tau}$ is chosen to be an integer. If the required search resolution for the delays $\Delta_\tau$ is chosen such that $\frac{NT_s}{2\Delta_\tau}$ is not an integer, the two dictionary atoms can have an error of $\frac{\pi\Delta_\tau}{NT_s}$ for a given delay $\tau_k$. The number of elements in the mother wavelet for a given delay resolution $\Delta_\tau$ is constant and is equal to $\left(\frac{NT_s}{\Delta_\tau} + 1\right)$. In contrast, the size of the

dictionary using the classical approach is proportional to the number of the delay bins $K$ [20].

It is also important to note that although Equation (6.46) looks complicated, it consists of only integer operations and can be computed efficiently. The complexity of the proposed scheme is reduced to $\mathbb{O}(K)$ since the indexing function (in Equation (6.46)) is invoked $K$ times, where $K$ is the number of delay bins to be searched. Note that, the mother wavelet is already precomputed and stored at the receiver. The proposed 'in place' mechanism of generating the dictionary has significant gains in computational complexity and memory requirements. It can also be used in any of the compressed sensing based schemes that require a dictionary and to also generate the Doppler dictionary for the conventional MP algorithms.

Finally, we compare the sizes of the dictionaries for the CS based channel estimation schemes proposed in this thesis in order to evaluate and emphasize the effectiveness of the proposed optimizations to generate the dictionary. Let us assume, the IEEE 802.11p standard for evaluation. The most relevant specifications of this standard are listed in Table 6.1

Table 6.1: Specifications of the IEEE 802.11p Standard

| Parameters | Value |
|---|---|
| FFT Size ($N$) | 64 |
| Bandwidth ($B$) | $10MHz$ |
| Sub-carrier spacing ($B/N$) | $0.15625MHz$ |
| FFT period ($T_d$) | $6.4\mu sec$ |
| Guard Interval ($T_{GI}$) | $1.6\mu sec$ |
| Total Symbol duration ($T_{sym} = T_d + T_{GI}$) | $8\mu sec$ |
| Sampling Interval ($T_s$) | $100nsec$ |

Let the longest multipath delay $\tau_{max}$ be equal to the duration of the guard interval $T_{GI}$ and the desired search resolution for the delays be $\Delta_\tau = 1nsec$. Thus, the total number of delay bins to be search is computed as $K = T_{GI}/\Delta_\tau \implies 1.6\mu sec/1nsec = 1600$.

Now, considering the RMP scheme that uses a dictionary to search for the delays, the conventional scheme of dictionary generation (see Section 6.3.1) computes $K \times N \implies$

$1600 \times 64 = 102,400$ elements during the delay search. If these elements are stored as a double data type[4] that requires 8 bytes for every element, the total size of the delay dictionary is $8 \times 102,400 = 819.24KB$ on memory. Using the proposed wavelet based scheme to generate the dictionary, the number of elements is reduced to $\left(\frac{NT_s}{\Delta_\tau} + 1\right) \implies \frac{64 \times 10^{-7} sec}{1 nSec} + 1 = 6401$. Subsequently, using a double data type, the storage requirement is computed as $8 \times 6401 = 51.208KB$ which is significantly smaller than the conventional method. It is also important to note that, for a give delay search resolution, the size of the dictionary remains constant and can be precomputed and stored at the receiver.

The size of the dictionary remains identical for the GRMP algorithm but, it must be noted that the dictionary atoms are generated only once in this case.

## 6.7 Complexity Analysis

Computational complexity is a measure of computation resources required to run a given algorithm. It provides a metric to evaluate the efficiency of algorithms [35]. Computational complexity plays an important role in the development of channel estimation algorithms since in most cases, these have to be deployed on battery operated consumer grade hardware.

Literature describes two main aspects to quantify complexity. Time complexity is a function that measures the amount of time an algorithm needs to execute and is typically represented with respect to the size of the input to the said algorithm [136]. The other aspect is the space complexity, that quantifies the amount of working storage an algorithm requires [136]. Both of these complexities can be asymptotically expressed in terms of the Big-O notation. This notation is used in computer science to classify different algorithms based on how the space and run time requirements increase with the size of the input [113]. In this thesis, the Big-O notation has been used extensively to describe the run time complexity of the different CS based channel estimation schemes. Although this representation provides a tool to compare different algorithms, it does not provide any information regarding the absolute computational resources required by the underlying algorithm. Thus, in this section we measure the complexity of the proposed channel estimation algorithms in terms of the number of real valued multiplication/division and addition/subtraction required to estimate the channel for a received OFDM frame specified according to the IEEE 802.11p standard. Table 6.2 shows the number of real values operations required for the corresponding complex valued operations.

[4] constructed according to IEEE standard 754

Table 6.2: Number of Real Valued Operations required for a Complex Valued Operation

| Complex Operator | # Real Multiplication/-Divisions | # Real Additions/Subtractions |
|---|---|---|
| Addition | - | 2 |
| Subtraction | - | 2 |
| Multiplication | 4 | 2 |
| Division | 8 | 3 |

Considering the IEEE 802.11p standard, the number of active subcarriers in the long preamble is $N_{pre} = 52$ and the number of data pilots in an OFDM data symbol is $N_p = 4$. In order to compute the exact number of operations, we have to assume the search resolutions. Let the delay search resolution be $\Delta_\tau = 10nsec$ that gives the total number of delay bins to be searched as $K = \tau_{max}/\Delta_\tau \implies 1.6\mu sec/1nsec = 160$. For the BMP algorithm, the Doppler search is performed in the time domain and a Doppler search resolution should also be assumed in this case. Let the Doppler search resolution be $\Delta_{f_d} = 100Hz$ and the maximum Doppler shift in the channel be $f_{d_{max}} = 15625Hz$. This gives us the number of Doppler bins to be search as $L = \lceil 2 \cdot f_{d_{max}}/\Delta_{f_d} \rceil \implies \lceil 2 \cdot 15625Hz/100Hz \rceil = 313$. Finally, the total number of real valued operations for the LS, BMP, RMP and the GRMP algorithm is tabulated in Table 6.3. A detailed description for calculating the number of real valued operations for the RMP algorithm can be found in Appendix A.

The large differences in the computational requirements of different algorithms are evident from Table 6.3. To begin with, the conventional LS channel estimator that uses the two preambles of the IEEE 802.11p standard to compute the channel estimate requires very few real multiplications and additions. The presence of block pilots (the long preamble) in this standard simplifies the computation significantly. However, it must be noted that, for standards that specify comb type pilots (like DVB-T2 and LTE-V) the need for interpolation to get the complete channel transfer function increases the number of computations.

Table 6.3: Computational Complexity of Channel Estimation Algorithms

| Complex Operator | # Real Multiplication/Divisions | # Real Additions/Subtractions |
|---|---|---|
| LS | $52 \cdot 10 = 520$ | $52 \cdot 11 = 572$ |
| BMP | $52 \cdot 5,784,248 = 300,780,896$ | $52 \cdot 2,950,967 = 153,450,284$ |
| RMP - Delay Search | $52 \cdot 12,176 = 633,152$ | $52 \cdot 7,046 = 366,392$ |
| RMP - Doppler Search | $4 \cdot 216 = 864$ | $4 \cdot 174 = 696$ |
| GRMP - Delay Search | $52 \cdot 1970 = 102,440$ | $52 \cdot 1,144 = 59,488$ |
| GRMP - Doppler Search | $4 \cdot 256 = 1,024$ | $4 \cdot 192 = 768$ |

Next, the BMP algorithm that searches for the Delays in the frequency and the Doppler shift in the time domain results in an enormous number of computations even for the moderate search resolutions that we have chosen. This confirms the drawbacks of classical CS based schemes to estimate the wireless channel from a computational standpoint as well. A stark contrast can be seen in the proposed RMP and the GRMP algorithm. Considering the RMP algorithm, the number of real computations required are lesser by a factor of roughly 230 when compared to the conventional BMP algorithm. Thus, the RMP algorithm is not only able to precisely estimate the wireless channel but also do so with a significantly smaller computational effort. The proposed Doppler search mechanism of the RMP algorithm is also optimized with respect to the number of computations required. Moreover, it only uses the data pilots (generally fewer in number) to track the Doppler shift. Finally, the proposed GRMP algorithm achieves a further improvement in complexity by conducting the delay search in a single iteration. Thus, the number of computations required is reduced by a factor of roughly 6 when compared to the RMP algorithm.

Vehicular environments typically pose a heterogeneous channel conditions with varying degrees of mobility. In Chapter 7, we propose a cognitive framework to sense the channel and choose the best parameters for estimation. This enables the receiver to use a simple LS scheme in stationary channel conditions and only use the powerful RMP algorithm in highly mobile scenarios. Such a solution will optimize complexity while ensuring the best channel estimate regardless of channel conditions.

# CHAPTER 7

# COGNITIVE FRAMEWORK

Fidelity in wireless communication systems under high mobility has become an important requirement for current as well as future communication systems. In scenarios of high mobility, the wireless channel exhibits selectivity in both the time and frequency domains. The estimation of the resulting doubly selective channel is a non trivial task [34].

In a typical highly mobile application scenario, the degree of mobility varies drastically with time. Consider for example a V2X application (vehicles are communicating with each other and roadside infrastructure) wherein, the speed of the vehicles are varying continuously. One one extreme, a highly mobile environment is experienced on the highways when vehicles are traveling at high speeds while, on the other extreme, a near stationary environment is present at a traffic light or when the vehicle is parked. Thus, vehicular environments pose a heterogeneous wireless channel with varying degrees of mobility [18, 19]. An ideal channel estimation scheme should provide an accurate estimate of the channel with a complexity that is appropriate for a given channel condition.

Novel schemes like the RMP algorithm are able to estimate doubly selective channels in a robust, precise and computationally efficient manner (see Section 6.4). However, in low mobility or stationary conditions, although the RMP algorithm is robust, the associated computational complexity is unnecessary and thus not efficient. Although many improvements that significantly reduce the complexity have been proposed in this thesis, it is relatively more complex compared to conventional schemes like the LS channel estimator. Thus, in scenarios of low mobility, the use of conventional schemes is more appropriate to estimate the channel. Moreover, for battery driven end devices, the right choice of an estimation scheme can significantly improve battery life. This line of thought has led to a hybrid channel estimation scheme based on a cognitive framework that optimizes the estimation scheme

according to channel conditions. The resulting estimation scheme is thus closer to an ideal estimation scheme and gives an accurate estimation of the channel in all channel conditions while adapting the complexity to be optimal for the channel being estimated.

## 7.1 Framework

The role of the cognitive framework is to sense the condition of the channel reliably and use this information to tune the parameters of the estimation algorithm such that the best error performance at an optimal computational complexity is ensured at the receiver. Thus, the goal has been to develop a framework that can detect the different channel conditions, without explicitly estimating them, and with a marginal increase of computational complexity is able to facilitate switching between different channel estimation mechanisms to provide good error performance at the receiver consistently [19]. This has led us to identify two aspects that need to be evaluated while developing the cognitive framework. The first aspect is the performance in terms of BER at the receiver. It is important that the cognitive framework is able to robustly choose the right estimation parameters that would result in good error performance. The second aspect is the complexity. The complexity of the chosen channel estimation scheme and the added complexity of the cognitive framework must be taken into account.

The proposed cognitive framework is depicted in Figure 7.1 that shows the relevant parts of the receiver chain along with the cognitive framework. It is seen that the cognitive framework collects data from different positions in the receiver chain. The data collected before the channel estimation block is termed as detection metrics and the data collected after the channel estimation is called feedback metrics. The *Detection Metrics* block receives measurements from the received signal at predefined positions, processes the same and gives the parameters for channel estimation to the decision metrics block. In a similar manner, the *Feedback Metrics* block receives the channel estimate along with the received signal and computes if the chosen channel estimation parameters are optimal. This information is also relayed to the decision metrics block. Finally, the *Decision Metrics* block processes the information from the detection and well as the feedback metrics and provides the parameter set to the *Channel Estimation* block in the receiver. The outcome of the decision metrics block is classified into *Intra-Frame Cognition* and *Inter-Frame Cognition*. The former deals with controlling the performance and complexity within the physical layer frame, while the latter selects channel estimation parameters for the entire physical layer frame. Thus,

depending on the requirements the cognitive framework can be configured to adapt the granularity of cognition.

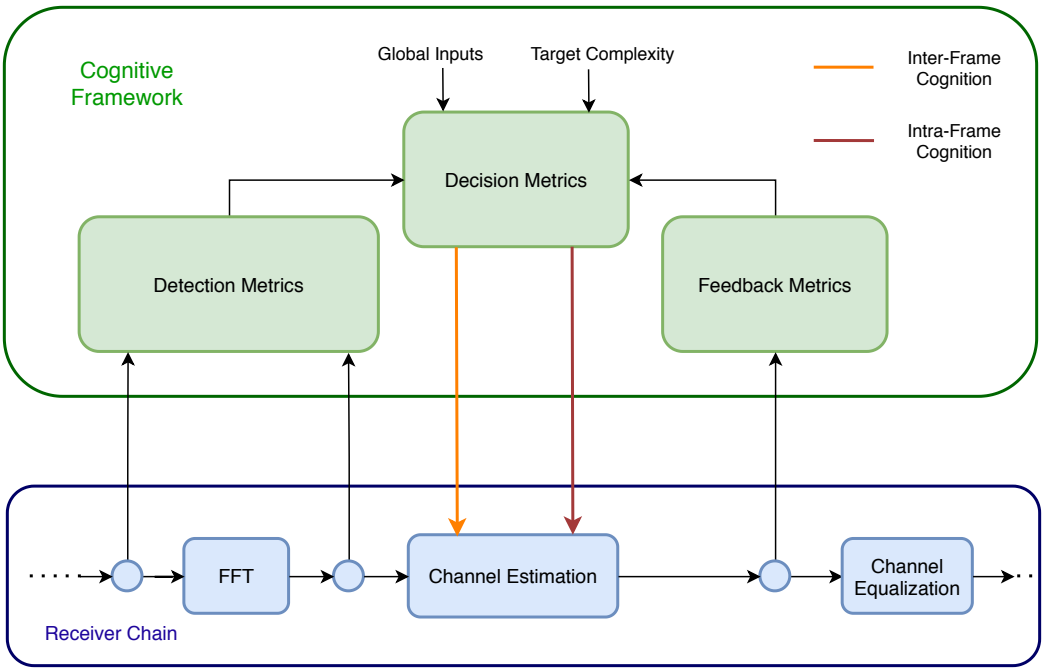


Fig. 7.1: Cognitive Framework Architecture

## 7.2 Technique based on Correlation

The detection metric block extracts the preambles/pilots from the received OFDM signal and infers the amount of Doppler spread in the channel by the use of different metrics [19]. A correlation metric provides a measure of the Doppler spread in vehicular environments. In this case, the correlation coefficient approximates the temporal variation or the Doppler spread in the channel [12]. However, computing the correlation in every physical frame or for the pilots in every OFDM symbol significantly increases the complexity and beats the purpose of the cognitive framework. Thus, a simple measure of similarity called the Tanimoto Coefficient (TC) that is commonly used in the field of chemistry has been used to detect the temporal variation of the channel [139]. The TC can be computed between two complex vectors $\mathbf{a} \in \mathbb{C}^{N\times 1}$ and $\mathbf{b} \in \mathbb{C}^{N\times 1}$ according to Equation (7.1).

$$TC(\mathbf{a},\mathbf{b}) = \frac{\Re(\mathbf{a}^H \cdot \mathbf{b})}{\|\mathbf{a}\|_2^2 + \|\mathbf{b}\|_2^2 - \Re(\mathbf{a}^H \cdot \mathbf{b})} \tag{7.1}$$

here, $\Re$ represents the real part of the complex number. The TC has a value of 1, when the two complex vectors are perfectly correlated, and on the other extreme, when the two complex vectors are uncorrelated to each other, the value of the TC is 0. Intuitively, the idea of the detection metrics is to acquire the preambles or pilots at different location of the physical layer frame and compute the TC between them to infer the degree of temporal variation in the channel. A low value of the TC indicates that the two preambles/pilots differ from each other because of Doppler shift (or the temporal variation), while a value closer to 1 points more towards a stationary channel. The following metrics are adopted in the cognitive framework to aid in cognition.

**Inter-Frame Preamble TC** is the averaged TC between the preambles of consecutive physical layer frames and works well for moderate Doppler shifts.

**Inter-Frame Chan TC** quantifies the similarity between the channel transfer function $\mathbf{H}_f$ of consecutive physical layer frames.

**Intra-Frame Preamble TC** is computed for the two received preambles or pilots of a physical layer frame and works well under high mobility due to the extreme temporal variation introduced in the channel.

$\hat{c}$ **variance** is an important metric and quantifies the temporal variation in the complex weighting factors $\hat{c}$ (calculated in the RMP algorithm for each delay tap) in a given frame.

These metrics are implemented in the detection and feedback metrics block in the cognitive framework architecture. The information from these metrics are then forwarded to the decision metrics block wherein, a priority scheme is implemented based on the confidence of each input metric. This priority scheme is illustrated as a decision flowchart in Figure 7.2.

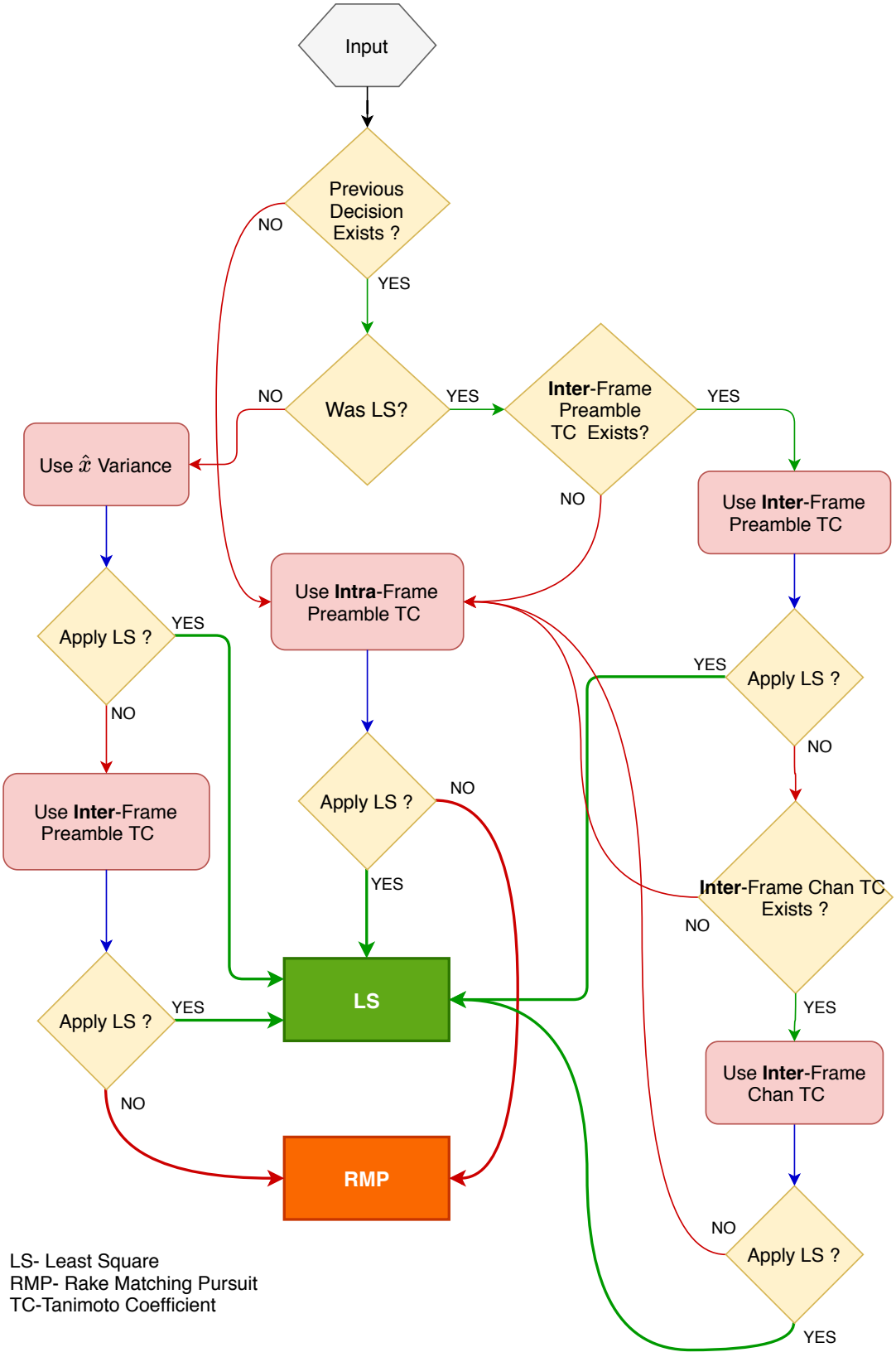


Fig. 7.2: Decision Metric Flowchart

The decision flowchart mainly has two branches. One branch deals with high mobility and uses the RMP algorithm for channel estimation while the other branch is concerned with low mobility schemes like the LS algorithm. The input metrics along with the decision scheme decide if the system continues with the previously used channel estimation scheme or switch to another scheme. However, there is an exception for the first frame wherein, only the detection metric *Intra-Frame Preamble TC* is used to choose between channel estimation methods. This is due to the fact that for the first frame, the other metrics are not yet available. For the second frame onward, a previous decision already exists and based on the other metrics a decision of the channel estimation scheme is chosen. The proposed decision scheme is developed to favor the low complex LS scheme and switch to the more complicated RMP algorithm only when necessary [19]. This is evident from the decision flowchart in Figure 7.2 where, four paths lead to the LS scheme and two paths lead to the RMP algorithm. The various metrics that have been developed are robust enough to ensure good error performance as well. The estimated channel parameters are used to compute the channel transfer function which is used to construct a one-tap equalizer to compensate the effects of the underlying channel. This cognitive framework has been implemented and evaluated for the IEEE 802.11p standard but can be easily adapted to other wireless standards. Also, the cognitive framework is flexible to work with other combinations of channel estimation schemes [19].

The thresholds for the TC used in the cognitive framework are dependent on the SNR and sometimes susceptible to errors. To find an optimal threshold curve, multiple simulations were performed under different SNR levels and Doppler spreads. The data collected showed that the TC followed an exponential curve for different SNR levels. We also observed that the values approach 0 with increasing Doppler shift in the channel. Using the data collected, a least squares fit with an exponential function gave us the best threshold value for a given SNR (refer Appendix B ). The equation to compute the threshold based on the SNR is shown in Equation (7.2).

$$\gamma_{TC} = -0.9 \cdot exp(-0.14 \cdot SNR_{dB}) + 1 \tag{7.2}$$

The threshold for the $\hat{c}$ metric is more robust to noise. The $\hat{c}$ values for the different paths over multiple SNR values and a varying Doppler shift were collected from several simulation runs. The data showed that the variation in the complex $\hat{c}$ values was less than 0.11 in both the real and imaginary parts for low Doppler shifts. Considering $\hat{c}_{t_0}$ and $\hat{c}_{t_S}$ to

be the tap coefficients for the first and last OFDM data symbol in the physical layer frame, the $\hat{c}$ variance metric can be calculated according to Equation (7.3).

$$\begin{aligned} \hat{\mathbf{c}}_{\sigma^2,\Re} &= |\Re(\hat{\mathbf{c}}_{t_S}) - \Re(\hat{\mathbf{c}}_{t_0})| \\ \hat{\mathbf{c}}_{\sigma^2,\Im} &= |\Im(\hat{\mathbf{c}}_{t_S}) - \Im(\hat{\mathbf{c}}_{t_0})| \end{aligned} \tag{7.3}$$

The final part of the puzzle is the calculation of the SNR. We propose to use the preambles/pilots in the frequency domain to calculate the SNR [19]. The power in the received signal is computed in Equation (7.4) where, $\mathbf{y}_{nz}$ represents the non-zero subcarriers and $N_{nz}$ is the number of non-zero subcarriers in an OFDM symbol.

$$P_{signal} = \frac{1}{N_{nz}}\Big(\sum |\mathbf{y}_{nz}|^2\Big) \tag{7.4}$$

The noise power can be computed from the subcarriers that are specified to have a value of 0. If $\mathbf{y}_z$ represents the zero subcarriers and $N_z$ denotes the number of zero subcarriers, the noise power in the receiver signal can be computed as Equation (7.5)

$$P_{noise} = \frac{1}{N_z}\Big(\sum |\mathbf{y}_z|^2\Big) \tag{7.5}$$

Finally the SNR is computed by dividing the signal power by the noise power as shown in Equation (7.6)

$$SNR_{dB} = 10 \cdot log_{10}\Big(\frac{P_{signal} - P_{noise}}{P_{noise}}\Big) \tag{7.6}$$

The gains in complexity by using the cognitive framework can be easily inferred. Consider the IEEE 802.11p standard. The LS scheme computes the channel estimate for the two preamble and has a complexity of $\mathbb{O}(2N)$ where, $N$ is the FFT size. The delay search RMP algorithm estimates the channel taps using a preamble and has a complexity of $\mathbb{O}(qKN)$ where, $q$ is the number of iterations and $K$ is the total number of delay bins. Additionally the Doppler search of the RMP algorithm, tracks the tap coefficients for the data OFDM symbols and has a complexity of $\mathbb{O}(qN_p)$ where, $N_p$ is the number of pilots in a data OFDM symbol. Thus the total complexity associated with the RMP algorithm for the complete physical layer frame is $\mathbb{O}(qKN + SqN_p)$ where, S denotes the total number of data OFDM symbols in the frame. The cognitive framework also adds some complexity to the overall channel estimation. The two TC are calculated with a complexity of $\mathbb{O}(N)$ each and the averaged TC has a complexity of $\mathbb{O}(2N)$. The $\hat{c}$ values are computed with a complexity of $\mathbb{O}(q)$ when the RMP

algorithm is chosen. In total, the cognitive framework has a complexity of $\mathbb{O}(4N+1)$ for the entire physical layer frame. This marginal increase in complexity enables the channel estimation process to be optimized with respect to the complexity and performance at the receiver and thus, in heterogeneous channel conditions exhibits a significantly lower complexity when compared to using the RMP algorithm as the only channel estimation scheme [23].

## 7.3 Technique based on Variance to Mean Ratio

In addition to the TC based metric for cognition, other metrics that reliably quantify channel variations are also investigated [23]. The Variance to Mean Ratio (VMR) is a normalized measure of dispersion and has been found to be a good candidate to quantify the channel variations. As its name suggests, the VMR is the ratio of the variance $\sigma^2$ to the mean $\mu$ and is given in Equation (7.7).

$$VMR = \frac{\sigma^2}{\mu} \tag{7.7}$$

The VMR is computed for the pilot subcarriers of the OFDM data symbols in the physical layer frame. To reduce the effect of noise, the VMR is calculated as an average between a set of pilot subcarriers in the received frame. A single threshold is then used to switch between the LS scheme and the RMP algorithm. Like with the TC based cognitive framework, a VMR value of 0 indicates that the data is not dispersed (stationary environment), a value between 0 and 1 means that the data is under-dispersed, and a value larger than 1 implies that the data is over-dispersed (high mobility environment) [32]. Thus, a threshold value between 0 and 1 can be used to switch between channel estimation schemes and plays an important role in favoring a channel estimation scheme. At the beginning of the physical layer frame, the default value of the threshold is set to be 1, then an estimate of the noise power is calculated from the received pilots and the threshold is dynamically tuned inversely proportional to the noise estimate. Thus, even in low SNR scenarios, a reliable mechanism to choose the optimal channel estimation scheme is ensured. The VMR based cognitive framework has been found to perform well for the LTE standard despite the sparse pilot patterns as seen in the results in Section 10.2.

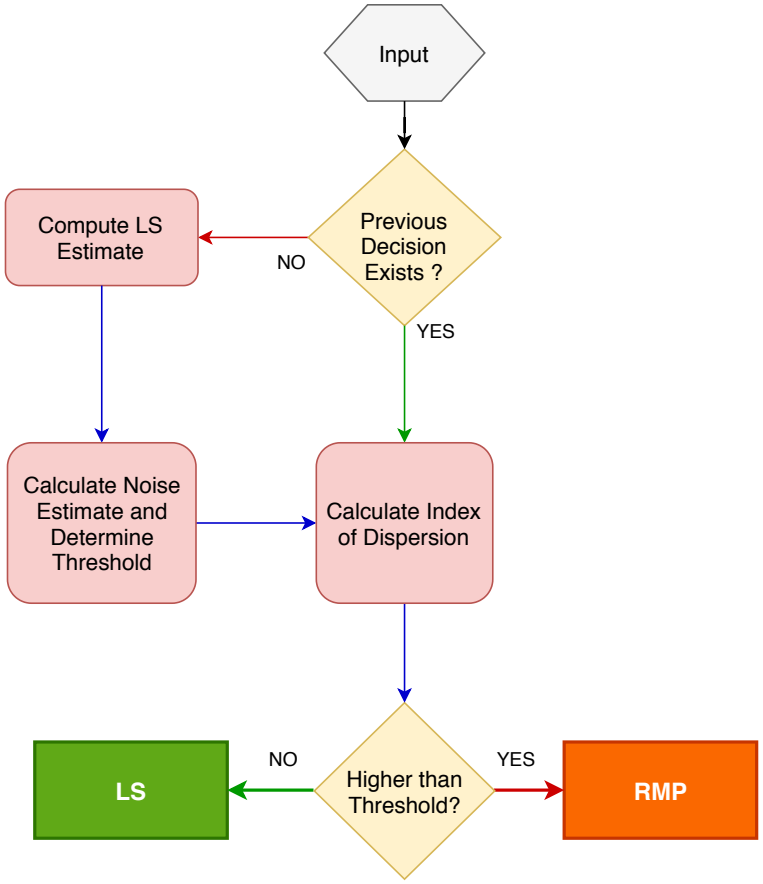


Fig. 7.3: Decision Flowchart based on VMR

The decision flowchart of theVMR based cognitive framework is shown in Figure 7.3. In the beginning of the physical layer frame, a previous estimate of the channel is not available. In this case, a simple LS estimate is computed for the pilots locations after which the noise is estimated using the received pilot subcarriers. The threshold is adjusted based on the noise level. If the noise power is high, the threshold is lowered such that a more powerful channel estimation scheme is chosen. This slightly conservative approach helps in ensuring better error performance at the receiver. Once the threshold is set, the VMR metric quantifies the channel variations and if its value is greater than the threshold, the channel is considered to vary temporally and the RMP algorithm is used for channel estimation. On the other hand, if the value of the computed VMR is below the threshold, the LS scheme is adequate to estimate the channel. For the subsequent physical layer frames, a previous decision on the channel estimate already exists. In this case, the VMR metric is computed for the current frame and after thresholding, a suitable channel estimation scheme is chosen.

For the LTE standard, the cognitive framework is configured to adjust the estimation parameters for every subframe thus achieving intra-frame cognition [23, 137]. This ensures that for any given subframe, the most optimal channel estimation scheme is employed. After the channel estimate is computed for the entire frame, a simple one-tap equalizer is used to compensate the effects of the wireless channel at the receiver. The different equalization schemes are discussed in the next chapter.

# CHAPTER 8

# EQUALIZATION

The task of a channel equalizer is to compensate for the distortions introduced by the wireless channel by leveraging some kind of knowledge about it. Channel equalizers can be classified into two broad categories based on the extent of channel knowledge they are assumed to have. Coherent channel equalizers use an estimate of the channel (computed by a channel estimation scheme) to perform equalization. The second category are the so called non-coherent equalizers that assume certain statistical properties of the wireless channel to perform equalization [123]. In this thesis, we consider coherent channel equalizers that leverage the channel estimate generated by the schemes discussed in Chapter 6 to compensate the effects of the channel at the receiver.

## 8.1 One-Tap Equalizer

The one-tap equalizer is a simple and computationally efficient technique that is ideally suited for frequency selective or time-invariant channels. The OFDM based wireless systems that we consider in this thesis perform equalization in the frequency domain. Thus, information about the delays and the corresponding weighting factors are contained in the estimated channel response $\mathbf{h} \in \mathbb{C}^{N\times 1}$, where $N$ is the FFT size or the number of subcarriers in the underlying OFDM symbol. If $\mathbf{y}_i \in \mathbb{C}^{N\times 1}$ denotes the $i^{th}$ received symbol in the frequency domain, the corresponding equalized data $\hat{\mathbf{x}}_i \in \mathbb{C}^{N\times 1}$ is a simple element-wise division given as,

$$\hat{\mathbf{x}}_i = \frac{\mathbf{y}_i}{\mathbf{h}} \tag{8.1}$$

A conventional coherent equalization scheme combines the LS scheme (discussed in Section 5.2) to provide an estimate of the channel and the one-tap equalizer to compensate

the effects of the channel at the receiver. This equalization scheme is well suited for time-invariant channels. The associated complexity is linear and thus ideally suited for practical implementation on consumer grade equipment [75]. In this thesis, we use this equalization scheme (LS estimation and one-tap equalization) as a baseline to evaluate the effectiveness of the proposed channel estimation and equalization schemes.

However, in scenarios of high mobility, the temporal variation or the time selectivity introduced by the channel severely affects the performance of the LS estimator along with the one-tap equalizer. The LS channel estimate computed either using the preambles in the beginning of the frame or the pilots in the data OFDM symbols is not able to model the rapid temporal variation in the channel [123]. Thus, a strong degradation in error performance can been seen in scenarios of high mobility (see results in Chapter 10).

Nevertheless, in thesis we propose to use the one-tap equalizer in combination with the proposed channel estimation schemes like the RMP and the GRMP algorithm. These schemes (discussed in Section 6.4) robustly estimate the delay taps and track the corresponding complex weighting factors for each of the OFDM data symbols in the physical layer frame. Thus, an accurate estimate of the channel response can be computed for every OFDM symbol by linearly combining the multipath delays along with the updated complex weighting factors. This has enabled us to use the one-tap equalizer to compensate the effects of the doubly selective channel. If the channel response of the $i^{th}$ data OFDM symbol is represented by $\mathbf{h}_i \in \mathbb{C}^{N\times 1}$, the equalized data can be computed as given below.

$$\hat{\mathbf{x}}_i = \frac{\mathbf{y}_i}{\mathbf{h}_i} \tag{8.2}$$

Here, we can see that each received OFDM data symbol $\mathbf{y}_i$ is equalized using an updated version of the channel response $\mathbf{h}_i$. Thus, another advantage of the CS based channel estimation techniques developed in this thesis is its ability to be combined with simple and computationally efficient equalization schemes to compensate the effects of the channel at the receiver. On the other hand, most of the CS based estimation techniques in literature rely on more complicated equalization techniques [41] as discussed in the following section.

## 8.2 Linear Minimum Mean Square Equalizer

The Linear Minimum Mean Square Error (LMMSE) equalizer performs equalization by minimizing the error between the transmitted and received signals. It is generally used when

the channel estimation scheme (like classical MP or BEM) produces a channel response matrix $\mathbf{H} \in \mathbb{C}^{N \times N}$ at the receiver. In such cases, the LMMSE equalizer performs better than the one-tap equalizer, but at the expense of higher computational complexity [73]. In the context of channel estimation and equalization, the underlying idea is to use the mean square error between the transmitted and received OFDM symbols as the cost function to be minimized [74] and is given by Equation (8.3). Minimizing the cost function suppresses the interfering effects introduces by the doubly selective channel.

$$MMSE = \underset{\mathbf{y} \in \mathbb{C}^{N \times 1}}{\arg\min} \|\mathbf{x} - \mathbf{G}\mathbf{y}\|_2^2 \tag{8.3}$$

In the above equation, the equalization matrix is assumed to be known. The linear solution (also known as the linear least squares regression solution) is given in Equation (8.4), where $\mathbf{y}$ denotes the received symbols and $\hat{\mathbf{x}}$ denotes the equalized symbols at the receiver. The MMSE solution is derived in Appendix C.

$$\hat{\mathbf{x}} = (\mathbf{G}^H \mathbf{G})^{-1} \mathbf{G}^H \mathbf{y} \tag{8.4}$$

Now, we can incorporate the channel matrix $\mathbf{H} \in \mathbb{C}^{N \times N}$ provided by the channel estimation scheme by modifying Equation (8.4) as shown below,

$$\hat{\mathbf{x}} = (\mathbf{H}^H \mathbf{H} + \sigma_n^2 \mathbf{I}_N)^{-1} \mathbf{H}^H \mathbf{y} \tag{8.5}$$

In this thesis, we use the LMMSE equalizer in combination with the classical MP estimation scheme to compensate the effects of the channel. At the receiver, OFDM data symbols $\mathbf{y}$ are equalized by leveraging the estimated channel information as seen in Equation (8.5). The LMMSE equalizer involves a matrix inversion in its solution which results in a computational complexity ranging from $\mathbb{O}(N)^2$ to $\mathbb{O}(N)^3$ [121].

In this part of the thesis, we have looked into the problem of overcoming the effects of a doubly selective or a time-varying multipath channel on OFDM based wireless communication systems. Novel channel estimation schemes that robustly and precisely estimate the underlying channel are proposed. These schemes are also analyzed from a computational complexity standpoint. Moreover, we are able to combine the proposed schemes with simple equalization techniques and obtain promising results as will be shown in Chapter 10. The following part of this thesis will introduce the simulation platforms along with the various results that bring out the merits of the proposed channel estimation schemes.

# Part III

# Climax

The doer alone learneth

*Friedrich Nietzsche*

# CHAPTER 9

# SIMULATION PLATFORMS

In order to highlight the merits of the proposed compressed sensing based channel estimation schemes, evaluation is performed for different OFDM wireless systems. Simulation platforms play an important role in the systematic evaluation of the schemes proposed in this thesis. This chapter provides a comprehensive description of the simulation platforms implemented as part of this thesis.

## 9.1 Broadband Systems - IEEE 802.11p

To evaluate the effectiveness of the channel estimation and equalization schemes in this thesis, standard compliant physical layer frames have to be corrupted by a time-variant multi-path channel to emulate scenarios of high mobility in typical V2X scenarios. A simulation platform that is standard-compliant and has the capability to simulate the wireless channel is the essential ingredient to evaluate the various channel estimation and equalization schemes.

The IEEE 802.11p standard specifies wireless access in vehicular environments. It envisions a WLAN-like environment between vehicles and roadside infrastructure aimed at increasing the safety of road users. This made the IEEE 802.11p standard very popular when it was being conceptualized around the year 2008 and also when it was finally specified in 2011. Thus, many examples of simulation platforms can be found in literature.

As part of the master thesis [22], we evaluated the effectiveness of GNU radio as a simulation platform to design and develop channel estimation and equalization schemes for different wireless standards. GNU Radio[1] is an open source software development tool kit that provides signal processing blocks to implement Software Defined Radio (SDR). An SDR

[1] www.gnuradio.org

is a radio communication system architecture that implements signal processing components that have been traditionally implemented in hardware, as software modules that can be run on a PC [6]. A transceiver implementation of the IEEE 802.11p standard in GNURadio can be found in [11], that has been extended as part of two Master theses to include channel estimation and equalization schemes in [22] and [138]. The main challenge encountered while implementing in GNURadio is the constant evolution of channel models and even the underlying base implementation of the standard. Thus, we decided to use Matlab as a simulation platform to implement and evaluate the proposed channel estimation schemes in this thesis.

It is also promising to note that plenty of examples can be found in literature that use Matlab to design and develop channel estimation schemes. A simulation platform in Matlab is found in [9] where, the performance of the IEEE 802.11p standard is evaluated. Another example is [57] where the physical layer specification has been implemented on an Field-Programmable Gate Array (FPGA) to evaluate its performance. Similar attempts that implement and evaluate the standard are seen in [108]. Although these examples advocate Matlab as a viable tool to implement the standard, none of these provide the simulation platform, or are in a form that allows for a systematic incorporation of channel estimation and equalization schemes. Thus, we decided to develop a standard compliant simulation platform adhering to best known programming standards and make it available to the research community. The IEEE 802.11p simulation platform is available to download from [24]. Figure 9.1 shows the structure of the transceiver that the simulation platform implements.

At the transmitter, custom data bits of a fixed size are generated according to the specifications of the user. The *MAC Header* block then organizes the data into the MAC frame according to the framing rules in the standard. The MAC frames are then modulated using one of the specified modulation schemes. In the next step, the signaling field is generated using the information from the configuration like the code rate and the length of the data symbols in the payload. In the next block, the data pilots are added to the data OFDM symbols according to the specifications described in Section 4.3.

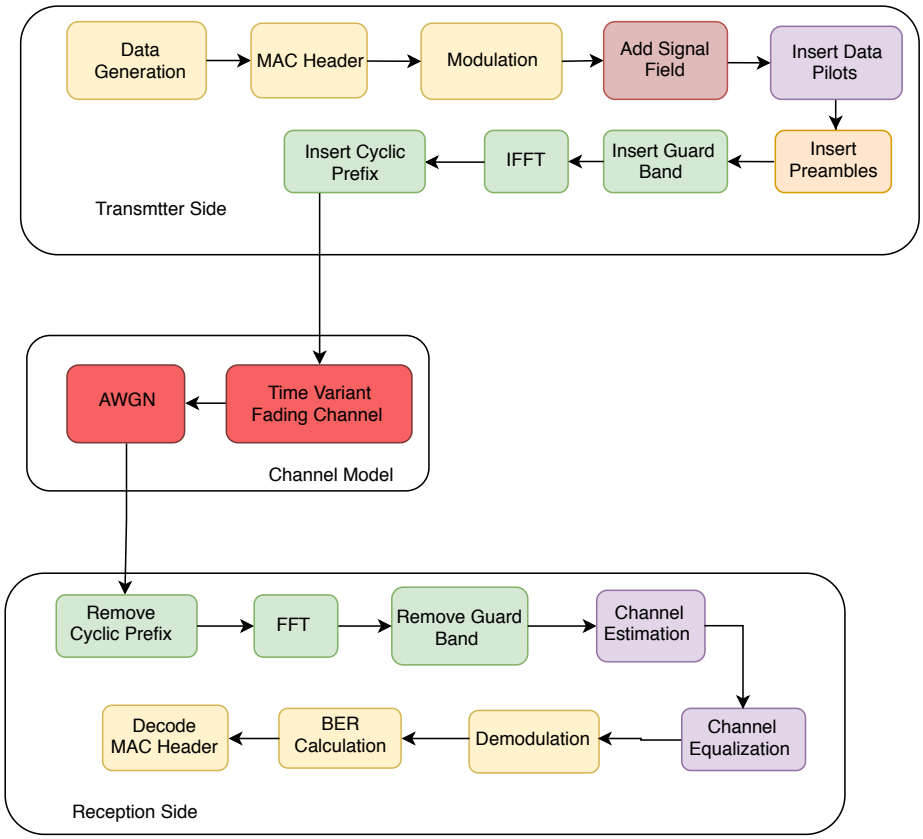


Fig. 9.1: IEEE 802.11p Transceiver

The preambles are then inserted in the *Insert Preambles* block followed by the guard band insertion. At this point, the frequency grid is complete and an IFFT produces a time domain OFDM signal. The final step in the transmitter is the insertion of the cyclic prefix after which the physical layer frame is assembled and is transmitted through the wireless channel.

The doubly selective wireless channel is simulated using the Rayleigh fading channel object from Matlab that models Rayleigh and Rician fading channels to distort the transmitted IEEE 802.11p physical layer frames [91]. Channel effects like multipath scattering due to the echoes, time dispersion and Doppler shifts arising from mobility are simulated by the channel model. The Rayleigh channel fading object consists of discrete fading taps each with a delay and a corresponding power gain. Additionally, on each delay tap a random Doppler shift is simulated. The Doppler spectra includes restricted Jake's, flat, asymmetrical Jake's, and Gaussian as described in [109]. Conventional channel models are thoroughly described in Section 3.5 and are also used in this thesis for the evaluation of the proposed schemes.

At the receiver, synchronization is performed on the distorted signal using the short preambles and performing a double autocorrelation to detect the start of the physical layer frame as explained in [112, 158]. In the next block, the cyclic prefix is stripped from the OFDM signal and a FFT is performed. The received signal is now in the frequency domain. In the next block, the guard band is removed. The *Channel Estimation* block is one of the most important blocks in the receiver. In this block, the preambles and data pilots are extracted and given to the selected channel estimation scheme. The channel estimate along with the data OFDM symbols are forwarded to the *Channel Equalization* block where the effects of the channel are compensated. After equalization, the data OFDM symbols are demodulated and the BER is computed to provide insights into the effectiveness of the channel estimation and equalization schemes. Finally, the MAC header is decoded and the information can be passed on to the higher layers.

## 9.2 Cellular Systems - LTE

The standard compliant LTE simulation platform [92] implements the downlink, uplink, and the recently specified LTE-V mode. The simulation platform is implemented using Matlab and is composed of modular blocks that can be formed into a transceiver chain able to be configured with different parameters. Another noteworthy feature of the simulation platform is the ability to extend the functionality in lieu with upcoming 3GPP releases as well as, added features that implement the physical layer with a finer granularity. The simulation platform is depicted in Figure 9.2 that shows the transmitter, receiver, and the wireless channel composed of modular signal processing blocks.

In the transmitter, the *Generate Data* block produces random bits with a random seed. The size of the data vector generated is determined by the bandwidth (that determines the number of OFDM subcarriers), the modulation scheme that indicates the number of bits modulated on each data subcarrier and lastly, the number of subframes that compose an LTE physical layer frame. It is assumed in this chapter that the transmission mode with a bandwidth of 1.4 MHz is used. Accordingly, this mode uses a 128 point FFT of which $N_{ds} = 72$ subcarriers are assigned for data and the remaining subcarriers form the guard band. It is also assumed that the extended cyclic prefix mode is used such that each subframe contains 12 OFDM symbols and an LTE frame is made up of 10 subframes.

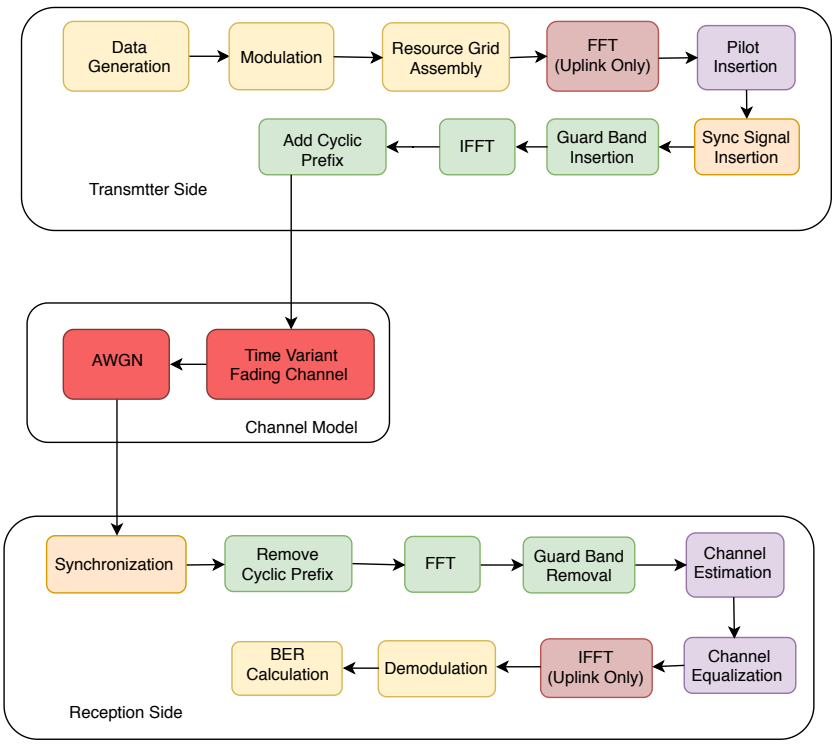


Fig. 9.2: Block Diagram of Simulation Platform

Once the data is generated, the *Modulation* block performs one of the specified modulation schemes. The modulation scheme can be selected in a configuration file that is global to the simulation platform. The next step in the transmitter is the *Resource Grid Assembly* block that generates a raster of the LTE frame as a $N_{ds} \times M$ matrix, where $N_{ds}$ is the number of data subcarriers and $M$ is the number of OFDM symbols in a given LTE frame. For the chosen configuration, the LTE frame is made up of $M = 120$ OFDM symbols (10 subframes with 12 OFDM symbols each). Accordingly, the *Resource Grid Assembly* blocks assigns the modulated symbols to the appropriate OFDM data subcarriers (also known as resource elements). In the Figure 9.3, an example of the LTE resource block is shown where in the arrangement of the data symbols (colored in yellow) in a LTE frame is clearly seen. The blue resource elements in this figure are just placeholders for pilots, synchronization signals and control information that will be inserted in subsequent blocks of the transmitter chain.

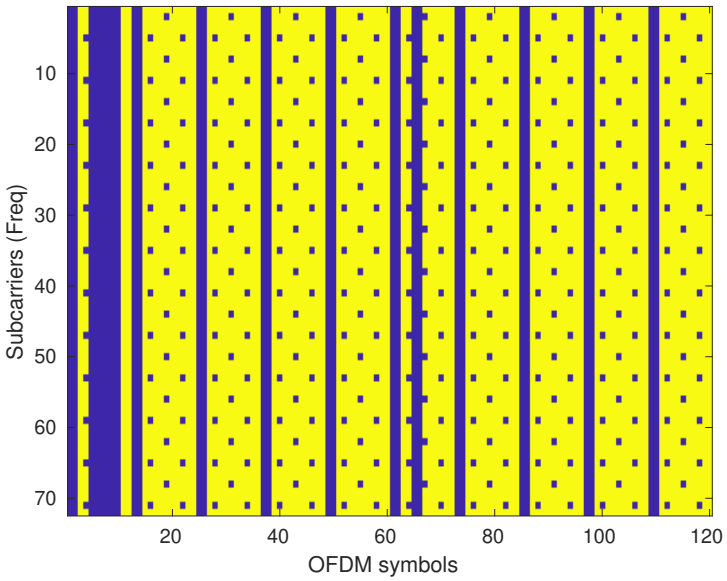


Fig. 9.3: LTE Resource Grid (data in yellow)

The next block in the transmitter is applicable only for Uplink and V2X transmissions. The *FFT* block generates SC-FDM symbols as explained in Section 5.3. The next block in the transmitter chain is *Pilot Insertion*, where the pilot/reference symbols are inserted at the corresponding resource elements. These pilots play a vital role in channel estimation and compensation at the receiver. LTE specifies different pilot patterns for the uplink, downlink and V2X transmissions to enable an optimal trade-off between overhead and the accuracy of the channel estimation techniques. In Figure 9.4, the pilot arrangement in the different transmission modes are illustrated. Note that here, the pilots are colored in yellow.

Once the pilots are inserted, the next step in the transmitter is to add the synchronization signals at the specified locations. The synchronization signals help in estimating the time offset introduced at the receiver. The LTE standard does not specify synchronization signals in the uplink and V2X modes as the presence of block pilots enable synchronization. The synchronization signal for the downlink mode is shown in Figure 9.5.

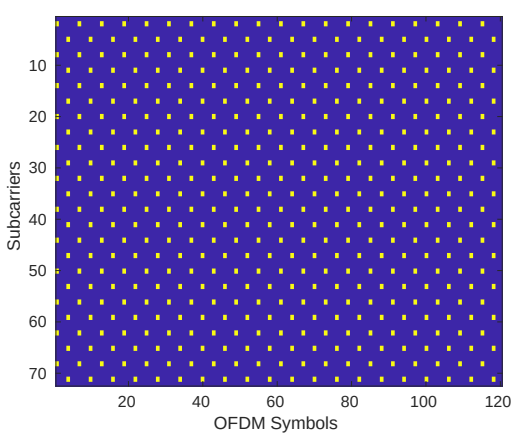


(a) Downlink Pilot Pattern (pilots in yellow)

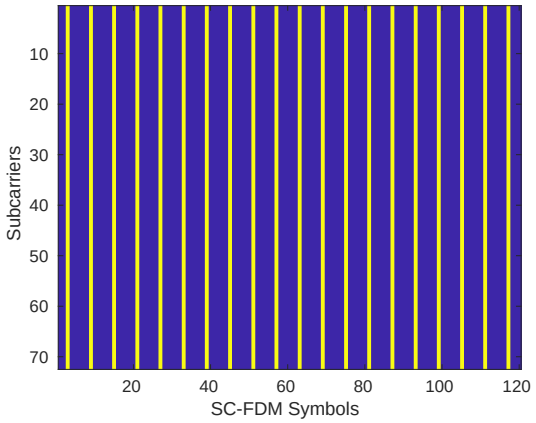


(b) Uplink Pilot Pattern (pilots in yellow)

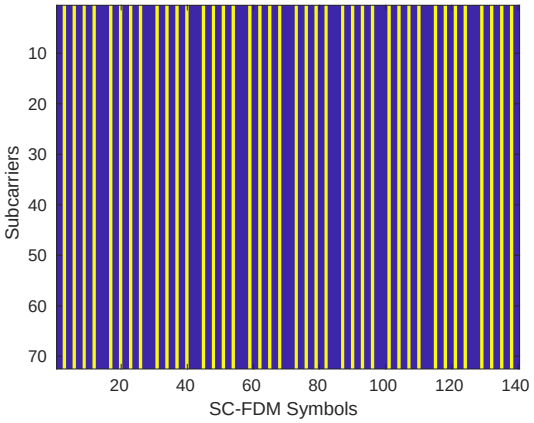


(c) V2X Pilot Pattern (pilots in yellow)

Fig. 9.4: Pilot Patterns in LTE

In the next step, the guard band is added that extends the size of the resource grid to $(N_{ds}+N_{gb})\times M$, where $N_{gb}$ is the number of subcarriers used in the guard band. An IFFT is then applied to each column of the resource grid that transforms the data into the time domain. The final block of the transmitter in the simulation platform is the *Add Cyclic Prefix* block where a cyclic prefix is added to the beginning of each OFDM symbol in the time domain. Assuming that $N_{cp}$ is the size of cyclic prefix, the time domain grid is a matrix with the dimensions, $(N_{ds}+N_{gb}+N_{cp})\times M$. This matrix is then reshaped into a vector that sequentially transmits the data. In the simulation platform, this data is transferred to the channel model block. A spectrogram shown in Figure 9.6 highlights several aspects of the transmitted wave-

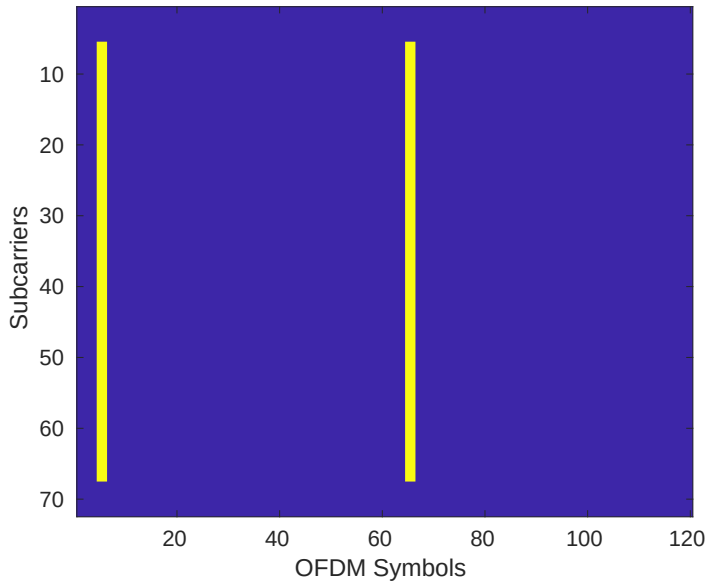


Fig. 9.5: Synchronization Signals for Downlink Transmission

form including the guard band on the edges each OFDM symbol in the frequency domain.

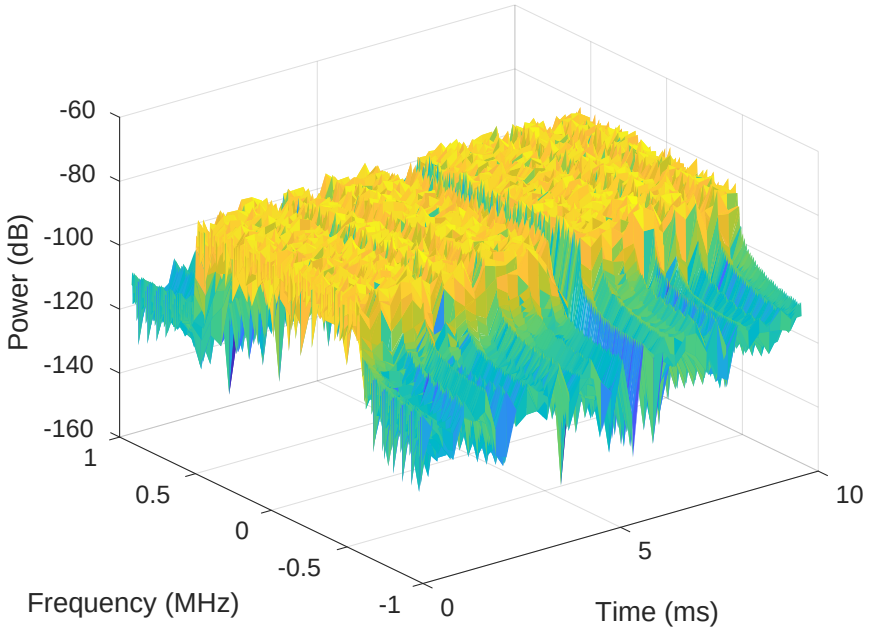


Fig. 9.6: Spectrogram of Transmitted Waveform

The channel part of the transceiver chain is composed of two blocks. The *Time Variant Fading Channel* block utilizes the multipath fading channel model from the LTE system toolbox in Matlab [39]. This channel model implemented by Mathworks follows the guidelines from the 3GPP specifications and other channel sounding experiments to simulate a doubly selective channel model that can be configured to the typical usage scenarios of LTE systems [39]. The fading channel model specifies three different delay profiles, Extended Pedestrian A mode (EPA), Extended Vehicular A (EVA), and the Extended Typical Urban (ETU) profile that represent delay profiles with an increasing delay spread. An overview of these profiles is given in Table 9.1.

The fading channel model in Matlab also allows for custom delay profiles. A maximum Doppler shift can then be configured for each of the delay profiles. Finally, AWGN noise is added to the signal based on the SNR simulated and the resulting signal is then sent to the receiver chain.

| Tap Delay (*ns*) | Relative Power (*dB*) |
|---|---|
| 0 | 0.0 |
| 30 | -1.0 |
| 70 | -2.0 |
| 90 | -3.0 |
| 110 | -8.0 |
| 190 | -17.2 |
| 410 | -20.8 |

(a) EPA Delay Profile

| Tap Delay (*ns*) | Relative Power (*dB*) |
|---|---|
| 0 | 0.0 |
| 30 | -1.5 |
| 150 | -1.4 |
| 310 | -3.6 |
| 370 | -0.6 |
| 710 | -9.1 |
| 1090 | -7.0 |
| 1730 | -12.0 |
| 2510 | -16.9 |

(b) EVA Delay Profile

| Tap Delay (*ns*) | Relative Power (*dB*) |
|---|---|
| 0 | -1.0 |
| 50 | -1.0 |
| 200 | 0.0 |
| 230 | 0.0 |
| 500 | 0.0 |
| 1600 | -3.0 |
| 2300 | -5.0 |
| 5000 | -7.0 |

(c) ETU Delay Profile

Table 9.1: Delay Profiles in Matlab Fading Channel

The receiver chain can be regarded to have an inverse order of the transmitter that can be observed in Figure 9.2. The first step in the receiver is to synchronize the received signal by calculating timing offsets using the synchronization signals in the beginning of the received

signal. The process of synchronization is very similar to other wireless standards wherein, the received signal is correlated with the specified synchronization signal from which the temporal offset can be estimated and compensated [5]. In the next block, the received signal is reshaped in to an LTE resource grid in the time domain and the cyclic prefix is removed. The data is then transformed into the frequency domain by performing an FFT. This produces the frequency domain resource grid that is a matrix with dimensions, $(N_{ds} + N_{gb}) \times M$. Once the guard band is removed, the data resource grid with the dimensions $N_{ds} \times M$ is obtained and passed on to the *Channel Estimation* block. The *Channel Equalization* block leverages the channel information to compensate the effects of the channel.

For the LTE standard, the following channel estimation and equalization schemes have been implemented in the simulation platform:

- Least squares (LS) channel estimator with frequency interpolation coupled to a one-tap equalizer .
- LS with pilot averaging and interpolation in both the frequency and time domains. Equalization is done by the LMMSE technique using the Matlab LTE system toolbox.
- Rake Matching Pursuit (RMP) channel estimation with a one-tap equalizer.
- Gradient Rake Matching Pursuit (GRMP) channel estimation with a one-tap equalizer.
- Variance to Mean Ratio (VMR) based cognitive channel estimation that switches between LS and RMP based on channel conditions(described in Section 7.3). A one-tap equalization is employed in this case as well.

The process of channel estimation and equalization is clearly illustrated in Figure 9.7. For this figure, the LTE fading channel is used with the EVA delay profile and a normalized Doppler shift of 1% is simulated. Even for such a relatively small Doppler shift, the effects of the wireless channel on the received signal is clearly visible. Also, it is interesting to note that the wireless channel model has introduced a selectivity in both the time and the frequency domain. In order to highlight the role of channel estimation, an ideal channel estimator is used to generate the channel estimate seen in the figure. An LMMSE channel equalizer then uses this ideal estimate of the channel and is able to perfectly compensate the effects of the channel as seen in this figure.

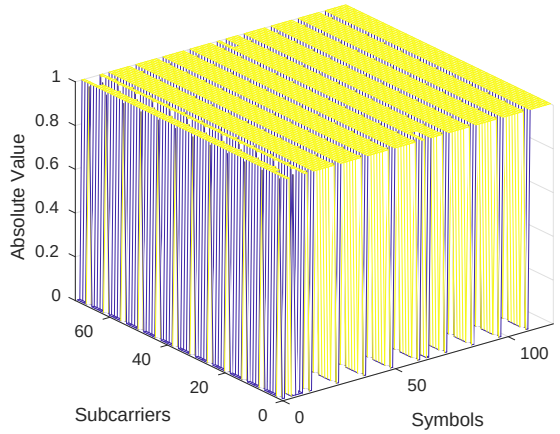


(a) Transmitted Grid

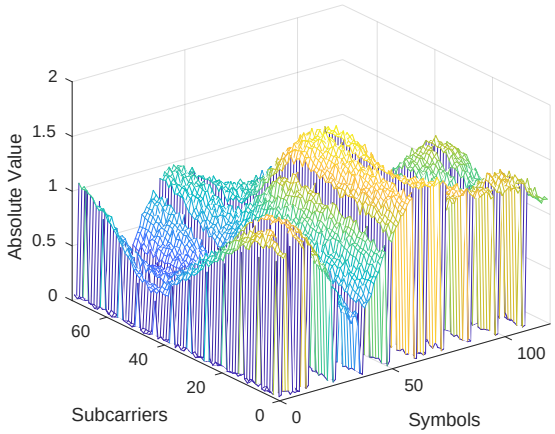


(b) Received Grid

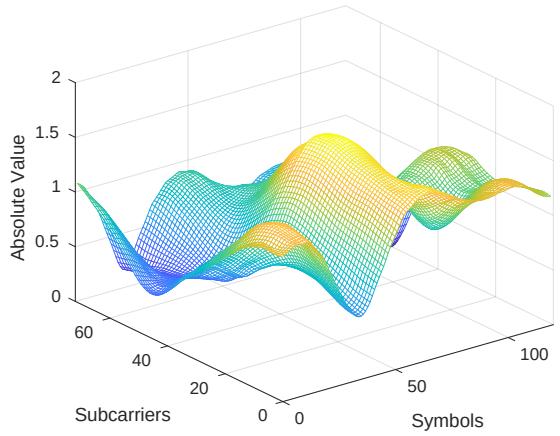


(c) Channel Estimate

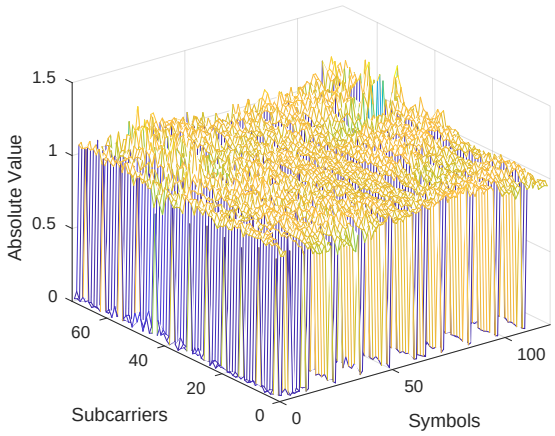


(d) Equalized Grid

Fig. 9.7: Channel Estimation and Equalization Process

For uplink transmissions, an IFFT is applied to de-spread the OFDM symbols. The next step is to perform demodulation on the equalized OFDM symbols using the appropriate scheme. The *BER Calculation* block evaluates the effectiveness of the channel estimation and equalization schemes by computing the error rates in the receiver.

## 9.3 Broadcast Systems - DVB-T2

Evaluation for the DVB-T2 standard is done using the Common Simulation Platform (CSP[2]). The CSP has been originally conceived and developed by members of the DVB consortium with BBC R&D and Panasonic as some of the major contributors [70]. The simulation platform is a standard compliant software end-to-end transceiver chain implemented in Matlab [45, 89]. The simulation platform has a modular architecture that provides the flexibility to setup a custom transceiver chain and enables a seamless development of novel channel estimation and equalization algorithms. The software architecture and the implementation principles employed in the CSP has also inspired the development of simulation platforms for other wireless standards. Figure 9.8 shows the transmitter chain in the simulation platform.

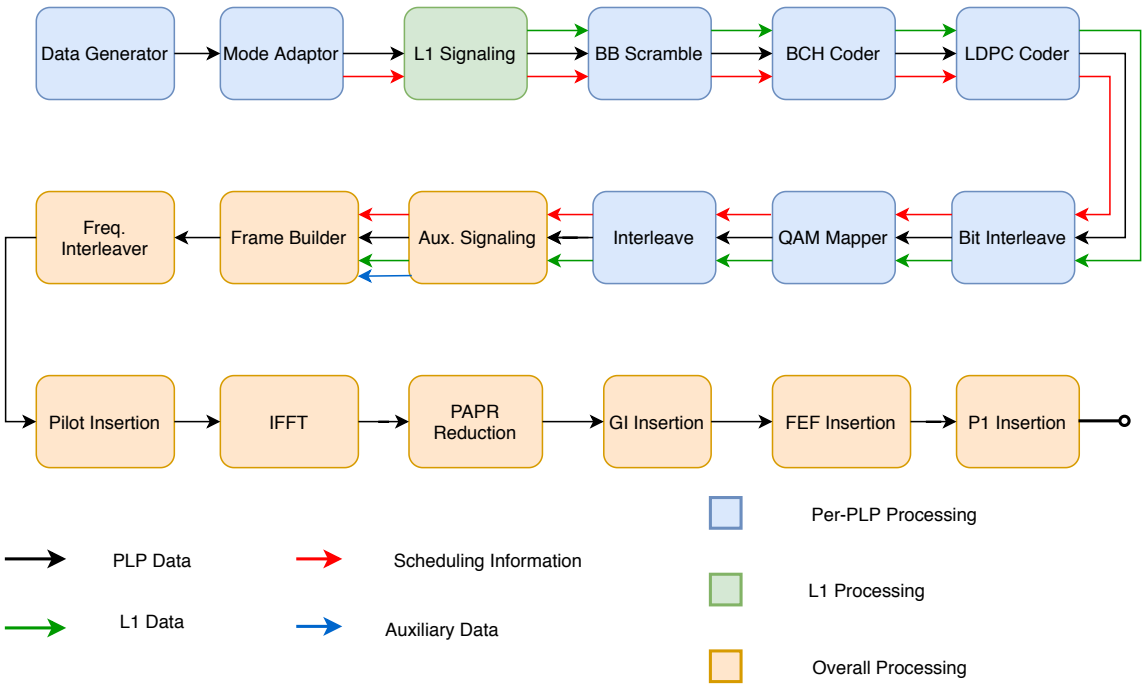


Fig. 9.8: Block Diagram of DVB-T2 Transmitter in Common Simulation Platform

**Input Data:** The *Data Generator* module generates the input data for the system. It can be configured to produce either random, Moving Picture Experts Group (MPEG) transport stream data or reads the data from a file. For the evaluations in this thesis, this module is configured to produce random data with a configurable seed. The amount of data to be produced can be configured depending on the requirements. Next, the *Mode*

[2]Available with an open source license (MIT) at: https://sourceforge.net/projects/dvb-t2-csp/

*Adaptor* block allocates the bits to baseband frames depending on the configured data rate. DVB-T2 allows multiple data streams and the mode adaptor modules uses the data rate to slice the data stream to produce data fields that make up the baseband frames. Additionally, it also provides the scheduling information.

**L1 Signaling** basically implements the entire L1 signaling. This includes arranging the various bit fields for the pre- and post- signaling, coding, and modulation as described in Section 4.2.

**Bit Interleaved Coding and Modulation (BICM) Modules** include the *BBScrambler*, *BCH Coder*, *LDPC Coder*, *Bit Interleaver*, *QAM Mapper*, and the *Interleaver* that performs time- and cell- interleaving. The CSP provides only a couple of concrete implementations of this block and other modes can be implemented if necessary. In the next step, the *Aux. Signalling* block will generate the transmitter signature in the auxiliary stream that is sent in a dedicated data container to the next block.

**Frame Builder** does the function of mapping the L1, scheduling, auxiliary, and PLP data into the specified frame structure. It also generates the dummy cells where necessary.

**OFDM Generation** modules perform frequency interleaving, pilot and reserved tone insertion. The *Pilot Insertion* modules modulates specified cells within an OFDM frame with the suitable pilots. The simulation platform supports all the types of pilots that are specified in the standard and include scattered, continual, edge, P2, and frame closing pilots. At this stage, the physical layer frame is transformed into the time domain by the *IFFT* block. The *PAPR reduction* block currently implements the tone reservation scheme for PAPR optimization. If enabled, the FEF frames are generated and inserted in the DVB-T2 super frame by the *FEF Insertion* block.

**P1 Insertion** is the last module of the transmitter. It generates the P1 symbol that is vital at the receiver for the initial signal scan and the detection of the DVB-T2 signal. The resulting DVB-T2 signal is then sent to the channel model.

The various blocks can be enabled/disabled by modifying the configuration file and a suitable transceiver chain can be assembled in a straightforward manner. It should be noted that changes in the transmitter must be mirrored at the receiver to ensure a working transceiver chain.

The wireless channel is modeled by the Rayleigh fading channel object in Matlab. It emulates the effects of multipath propagation and mobility in the frequency and the time domain respectively. The DVB-T2 implementation guidelines recommends the TU-6 profile that reproduces terrestrial propagation in an urban setting. The TU-6 mobile channel model is made up of 6 paths that exhibit a wide delay dispersion. The profile parameters recommended for the evaluation are given in Table 9.2 [47].

Table 9.2: TU 6 - Channel Model for DVB-T2

| Tap Num. | Delay ($\mu$s) | Power (dB) | Doppler Spectrum |
|---|---|---|---|
| 1 | 0.0 | $-3$ | classic |
| 2 | 0.2 | 0 | classic |
| 3 | 0.5 | $-2$ | classic |
| 4 | 1.6 | $-6$ | classic |
| 5 | 2.3 | $-8$ | classic |
| 6 | 5.0 | $-10$ | classic |

A maximum normalized Doppler shift with the Jake's spectrum is also configured for the evaluation. Next, AWGN noise is added based on the simulated SNR and the resulting signal is then sent to the receiver chain. Figure 9.9 portrays the DVB-T2 receiver signal chain that is mostly the reverse implementation of the transmitter chain.The receiver implemented in the CSP assumes perfect synchronization and does not perform signal detection.

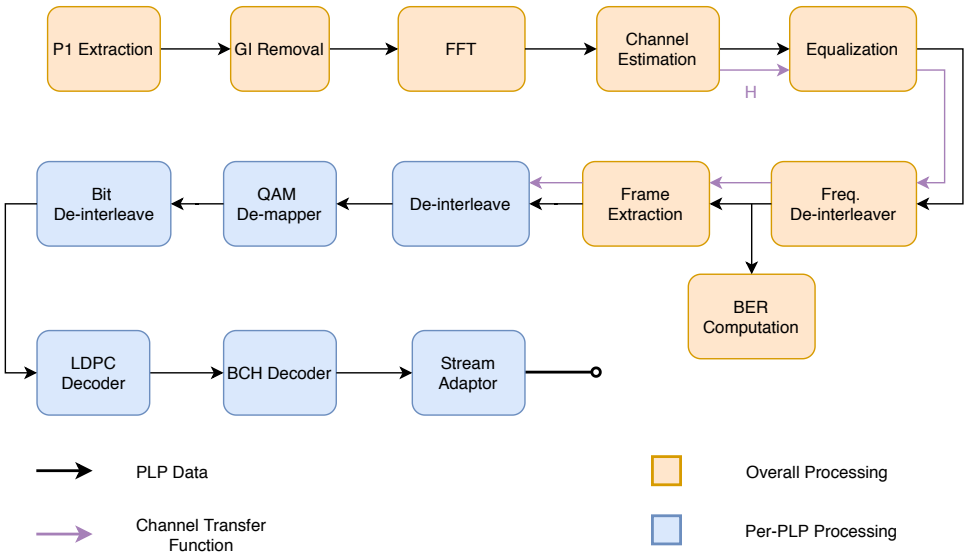


Fig. 9.9: Block Diagram of DVB-T2 Receiver in Common Simulation Platform

**Signal Extraction:** The *P1 Extraction* block in the CSP is implemented to remove and discard the P1 preambles. This block also removes the FEF frames. In order to simplify the receiver implementation, the CSP gets the basic transmission parameters from the simulation configuration files and does not decode the P1 and the FEF frames. The *GI Removal* block simply removes the cyclic prefix.

**Frequency Domain Processing:** In the next step, the *FFT* block transforms the active symbols to the frequency domain thus, providing an array of OFDM symbols that are processed in the rest of the receiver chain. The native *Channel Estimation* and *Equalization* block in the CSP performs an ideal channel estimation and assumes perfect channel state information for equalization. These two blocks have been completely reimplemented in this thesis to perform the proposed estimation and equalization schemes. Tests have also been conducted to ensure that the newly implemented blocks does not disrupt the functionality of the receiver chain. A transparent selection of the various channel estimation and equalization scheme (including the native schemes) is ensured in the simulation configuration files. After equalization, the BER is computed to transparently evaluate the effectiveness channel estimation and equalization schemes without any intervention from FEC schemes. This differs from the native implementation wherein, the BER is computed after the FEC decoding to evaluate the receiver chain in its entirety. Next, frequency deinterleaving is performed and the *Frame Extraction* block extracts the active cells and feeds it to the subsequent modules.

**Demodulation:** After time and cell deinterleaving, log-likelihood ratios are computed for each bit and an appropriate demodulation is performed.

**Decoding:** The CSP implements a few concrete examples for decoding. For the LDPC decoding, the communication toolbox in Matlab is used while for the BCH decoding, the transmitted BCH codeword is assumed to be known and a correction is done if the number of errors is below the threshold. Although slightly restrictive, it did not affect the development of channel estimation and equalization schemes in this thesis since, the BER used for evaluation are computed before the FEC decoding is performed.

The DVB-T2 is a widely accepted and fairly complex terrestrial broadcasting standard that is widely adopted across the world. The CSP provides an excellent platform for the research community to evaluate the standard and is used in this thesis to develop channel estimation and equaization schemes.

# CHAPTER 10

# RESULTS

Having established the theory and contributions towards enabling high mobility in OFDM based wireless systems, this chapter describes the results of these schemes for different channel conditions. The proposed channel estimation techniques have been evaluated for broadband, cellular and broadcast wireless standards to reinforce the merits of the underlying schemes. Simulation runs are conducted with channel models that have been specifically developed for doubly selective wireless channels and that are widely accepted in the research community.

## 10.1 IEEE 802.11p

The characteristics and challenges of a doubly selective channel at the receiver have been discussed in Chapter 5. In order to understand the models that emulate this channel and evaluate its effects on the transmitted signal, a wireless standard with an uncomplicated physical layer parameterization is sought. The relative simplicity of the IEEE 802.11p standard and the straightforward physical layer specifications provide an excellent platform to study the characteristics of the wireless channel and develop channel estimation and equalization schemes. Thus, it has been the first OFDM based wireless standard that was used to develop the various channel estimation and equalization techniques that are described in this thesis. In this section, the channel estimation schemes are evaluated for the IEEE 802.11p standard and a few interesting intermediate results are discussed that advocate the effectiveness of Compressed Sensing (CS) based channels estimation and equalization schemes.

A time variant multipath channel exhibits selectivity in both the time and the frequency domain. While an OFDM signal is robust to frequency selectivity, it is susceptible to time

selectivity. A common practice to overcome the effects of time selectivity on the underlying OFDM signal is to ensure that the coherence time of the channel is greater than the physical layer packet duration [4, 10]. This would ensure that a simple preamble based LS channel estimation scheme would provide an adequate equalization of the channel. However, the physical layer parameterization of the IEEE 802.11p standard makes it relatively more sensitive to Doppler shifts and results in smaller coherence times as explained in Chapter 3. In the following set of results, the channel transfer function obtained from the various channel estimation schemes are compared to the PCSI for different Doppler shifts. The PCSI has been obtained from configuring the Rayleigh fading object that allows to save the tap coefficients.

To stimulate an intuitive feeling for the doubly selective channel that is modeled by the Rayleigh fading object in Matlab, the magnitude of the PCSI is shown in Figure 10.1 for two different scenarios. The red curves correspond to a channel that is characterized by multipath alone and as such depicts 0% normalized Doppler shift. The blue curves on the other hand, portray a channel with high mobility and is simulated with a 10% normalized Doppler shift. The figure shows the OFDM symbols in one IEEE 802.11p physical layer frame. However, due to space constraints, the short training symbols and the OFDM symbol with the signaling information are omitted and only one of the two long training symbols (denoted as a preamble) is depicted in the figure. On the X-axis, the OFDM symbols in the physical layer frame are shown and separated by vertical lines and for each of these OFDM symbols the magnitude of the Channel Transfer Function (CTF) is plotted. The CTF is denoted as $h_f \in \mathbb{C}^{N\times 1}$ for an FFT size of $N$. Thus, this figure is able to adequately show the temporal variation of the CTF for different channel scenarios. Accordingly, the red curve for 0% normalized Doppler shift shows a stationary CTF throughout the physical layer frame while the blue curve that simulates a 10% normalized Doppler shift, unambiguously shows the extreme temporal variation of the CTF and the challenges involved in terms of overcoming the effects of such a channel. Note that, a very high SNR (0 dB Noise) is simulated in Figure 10.1.

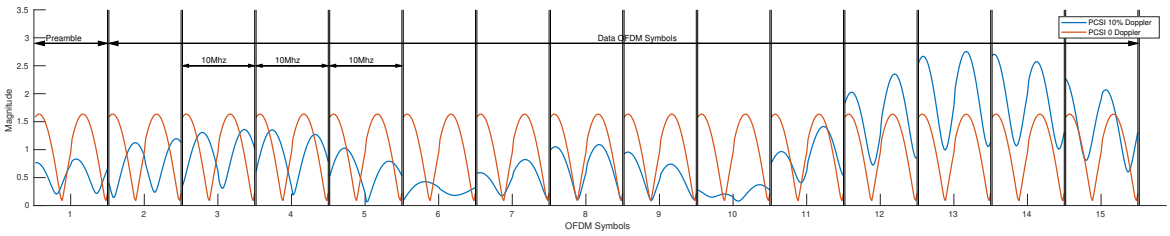


Fig. 10.1: Comparing PCSI for different Mobility Conditions

Figure 10.2 compares the estimated CTF's from different techniques in a pure multipath environment with a very high SNR . An important criteria adopted for the development of channel estimation and equalization techniques is a robust and deterministic behavior that is agnostic to the degree of mobility present in the underlying channel. The figure compares the CTF estimated from the LS, Classical MP as well as the proposed Rake MP to the PCSI. Unsurprisingly, the LS estimation provides an excellent estimate of the stationary channel. It is also evident that both the Classical MP as well as the Rake MP provide a CTF that is close to the PCSI. A closer comparison of the CTF for a few selected OFDM symbols is shown in Figure 10.3.

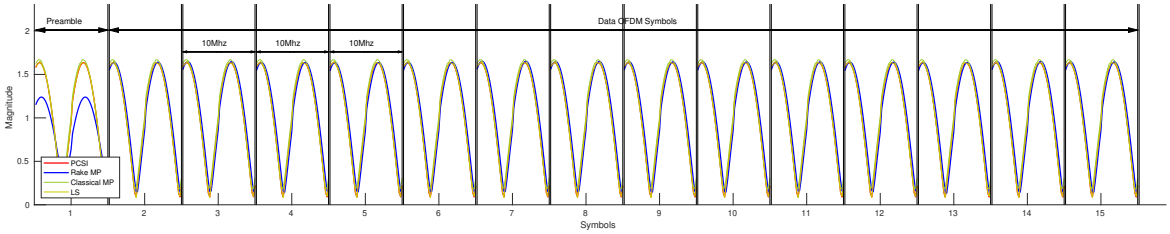


Fig. 10.2: Comparing CTF for 0% Doppler Shift

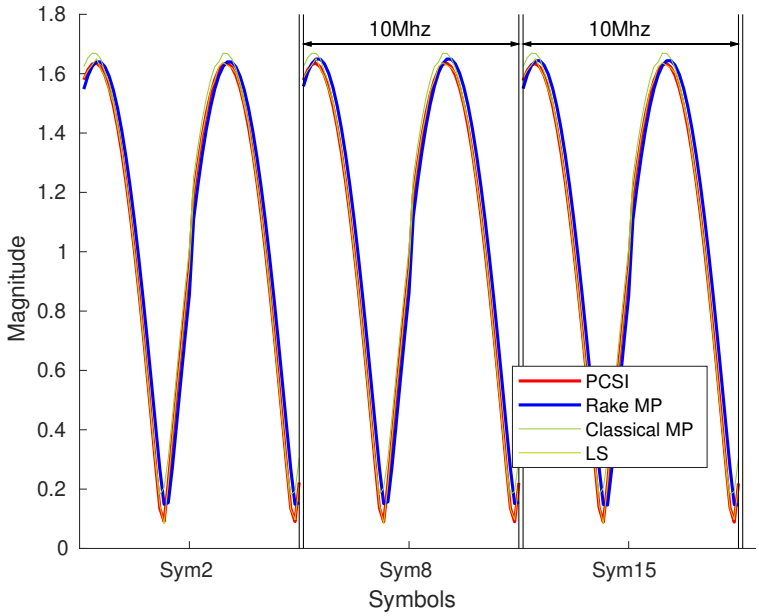


Fig. 10.3: Closer Comparison of CTF for Selected Symbols with 0% Doppler Shift

Along similar lines, Figure 10.4 considers a highly mobile channel and compares the estimated CTF's of the various techniques to the PCSI. A normalized Doppler shift of 10%

is simulated in this case. It is evident that the CTF estimated from the proposed RMP comes the closest to the PCSI and is an indicator of better BER performance that will be discussed shortly. The classical MP estimation techniques is not able to precisely estimate the multipath delays and Doppler shift due to reasons already highlighted in Section 6.3. The LS channel estimate is also ill suited for doubly selective channels. It is interesting to observe that the RMP algorithm provides a slightly wrong estimate for the first OFDM symbol (i.e the preamble ). This is simply due to the use of the proposed delay metric that normalizes the magnitude of the received pilots/preambles in order to ensure a robust estimation of the delay taps as discussed in Section 6.4. Moreover, for the preambles only the delays are estimated while the Doppler tracking only starts from the symbol that contains useful data for the receiver. A closer look of the CTF for selected symbols of the physical layer frame is shown in Figure 10.5

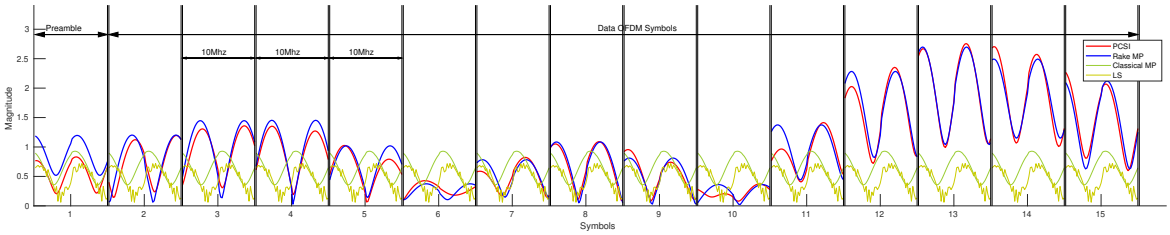


Fig. 10.4: Comparing CTF for 10% Doppler Shift

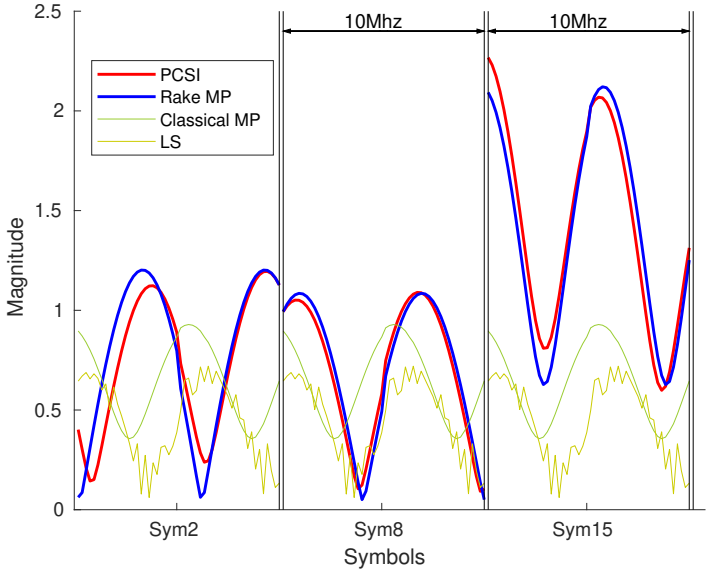


Fig. 10.5: Closer Comparison of CTF for Selected Symbols with 10% Doppler Shift

A surface plot of the CTF magnitude and phase are depicted in Figures 10.6 and 10.7 respectively for a channel with 10% normalized Doppler shift. The surface plot is interesting because it shows both the frequency as well as the temporal variation of the wireless channel along with the estimated CTF of the different channel estimation techniques. Although a bit crowded, it is clear to see that the channel estimate from the RMP algorithm is in tandem with the PCSI even in regions of high channel variations. The LS and the classical MP is again confirmed to perform poorly in scenarios of high mobility.

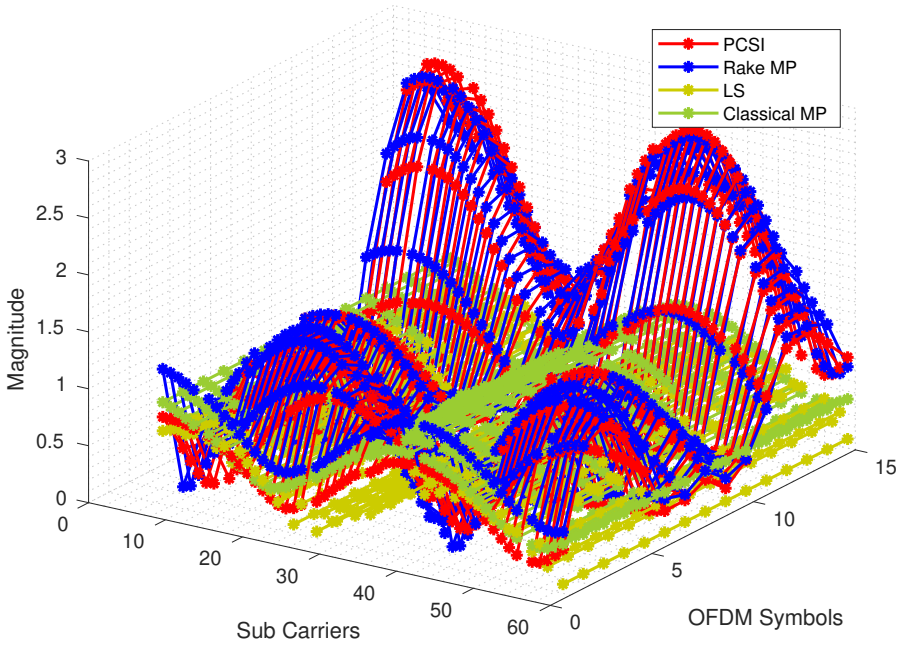


Fig. 10.6: Surface Plot of CTF Magnitude with10% Doppler Shift

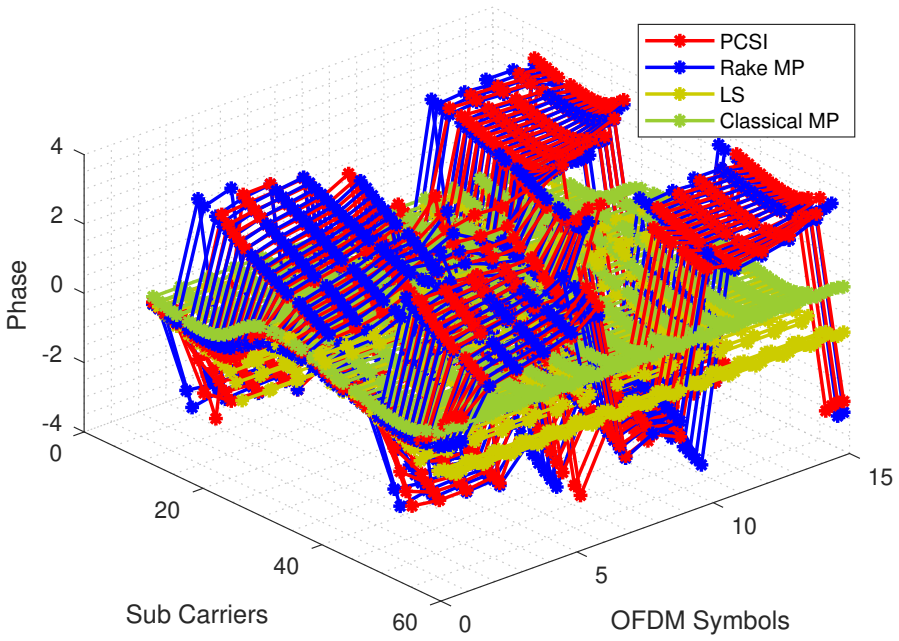


Fig. 10.7: Surface Plot of CTF Phase with10% Doppler Shift

Now that the estimated channels have been evaluated, the next set of results explores the error performance of these schemes. The evaluation consists of SNR vs. Bit Error Rate (BER) curves for the different channel estimation and equalization schemes under different channel conditions. In order to facilitate a better understanding of the results and maintaining cohesiveness, results for the different schemes are introduced progressively. The simulation platform, the channel model configuration and the computation of the BER curves are already introduced in Section 9.1. In short, physical layer frames generated from a random set of bits and conforming to the IEEE 802.11p standard are generated by the transmitter. The doubly selective channel object is configured to emulate different mobility scenarios. The transmitted frames are corrupted by this channel after which noise (AWGN) is added. At the receiver, channel estimation and equalization is performed using the received preambles and pilots. The equalized data is then compared to the transmitted template and the number of errors are used to generate the SNR vs. BER curves.

The first set of results evaluate the BER performance of the RMP algorithm in relation to the LS and the classical MP channel estimation techniques. The results are consolidated in Figure 10.8 for different Doppler shifts. The IEEE 802.11p standard specifies a convo-

lutional encoder as FEC mechanism that can tolerate a BER of around 8%[1] with a code rate of 0.5. Thus, if the error rate is below this threshold a significant number of physical layer frames are passed on to the higher layers. In Figure 10.8a, a purely frequency selective channel is simulated. As expected, the LS scheme performs optimally in such a channel. It is also evident that both the RMP as well as the classical MP perform well and are almost identical to the optimal LS channel estimation scheme. The slightly better performance with the classical MP approach can be attributed to the dual equalization in as well the frequency as the time domain. However, this slight gain in performance comes at a significant increase in computational complexity. Thus, in a purely frequency selective channel, the LS scheme has to be the optimal choice with regards to performance and complexity.

In Figure 10.8b, a small Doppler shift is simulated to already show the deterioration of the LS and classical MP schemes. At higher SNR's, the merits of the proposed RMP channel estimation scheme is evident from the lower error rates. The normalized delay search metric is able to robustly estimate the delay taps and the implicit Doppler shift estimation technique is able to adequately track the temporal variations in the channel (described in Section 6.4), thus providing better results.

In Figures 10.8c and 10.8d, a moderate Doppler shift of 1000 Hz and 5000 Hz is simulated. In both the cases, a clear benefit in performance is seen with the RMP scheme. It is also evident that in some cases, the classical MP has a higher error rate than the LS scheme indicating that something went wrong in the delay and/or the Doppler search.

A high Doppler shift of 10000Hz and 15000 Hz is simulated in Figures 10.8e and 10.8f. This corresponds to a normalized Doppler shift of roughly 6% and 10% respectively. In such extreme mobility conditions, the error rate achieved by the RMP algorithm increases but it is significantly better than the competing schemes and lower than the FEC bit error rate threshold of 8%.

[1] from simulations

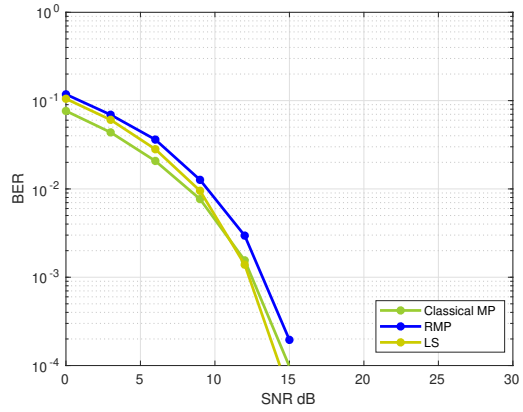


(a) Pure Multipath

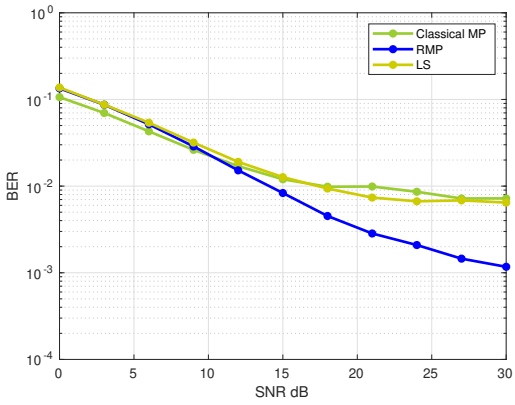


(b) Doppler Shift: 500 Hz

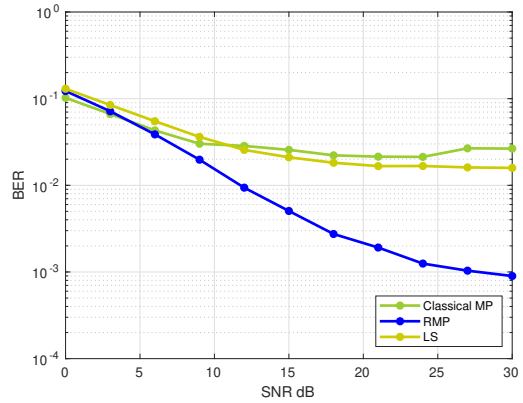


(c) Doppler Shift: 1000 Hz

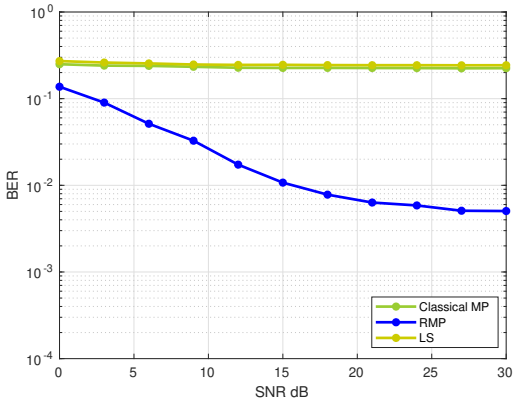


(d) Doppler Shift: 5000 Hz

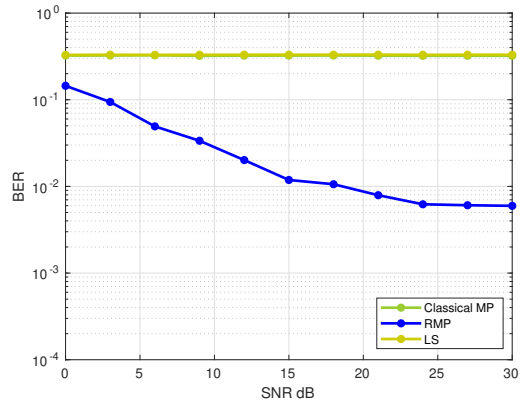


(e) Doppler Shift: 10000 Hz

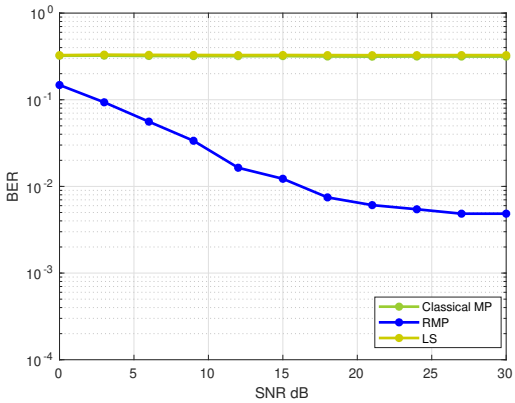


(f) Doppler Shift: 15000 Hz

Fig. 10.8: Evaluation of RMP

The RMP algorithm has been shown to perform well not only in highly mobile environments but also in stationary scenarios. However, the computational complexity involved does not justify the use of RMP especially in stationary environments. To address this issue and reduce the overall complexity, the GRMP algorithm has been developed. The underlying idea in GRMP has been to optimize the delay search by replacing the iterative estimation with a single step delay estimation as explain in Section 6.5. This has resulted in a complexity reduction by a factor of $q$, which is the number of iterations in the delay search of the RMP algorithm (Section 6.4). The advantage of the iterative delay estimation procedure is that, the contributions of the estimated delays are considered in the subsequent iterations leading to a precise estimate of the delay taps. Estimating all the delays in a single run is expected to provide a coarse estimate of the delays and consequently have an impact on the results. Apart from this, it must be noted that the Doppler shift estimation that tracks the temporal variation of the channel remain unchanged in GRMP.

The GRMP algorithm is compared with the LS and RMP channel estimation schemes in Figure 10.9. From the outset, it is evident that the omission of an iterative search for the delays results in a imprecise channel estimate and thus, a relatively worse error performance with respect to the RMP algorithm. A pure multipath channel is simulated in Figure 10.9a and all the three schemes perform equally well. In the absence of Doppler shift, the modified delay search technique adopted in the GRMP algorithm is able to estimate the delay taps accurately.

A Doppler shift of 500 Hz and 1000 Hz is simulated in Figures 10.9b and 10.9c respectively. In both cases, a deterioration of performance is evident with the LS scheme while the performance of the GRMP although worse than the RMP estimation, is significantly better than the LS channel estimation. The disadvantage of the modified delay search in GRMP that is only able to provide a coarse estimate of the delay is beginning to become visible in the results.

A moderate Doppler shift of 5000 Hz is simulated in Figure 10.9d and the gap in performance between the GRMP and the RMP has gotten bigger. On the other hand, the LS estimation is shown to be ineffective under such channel conditions.

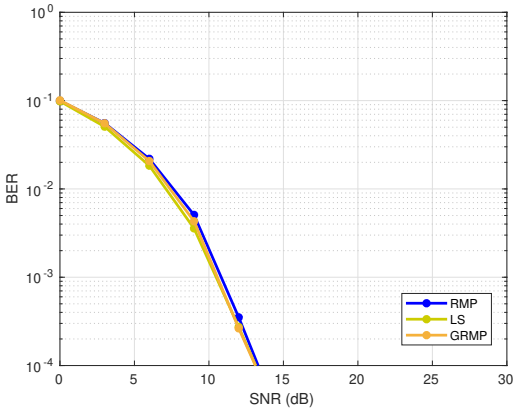


(a) Pure Multipath

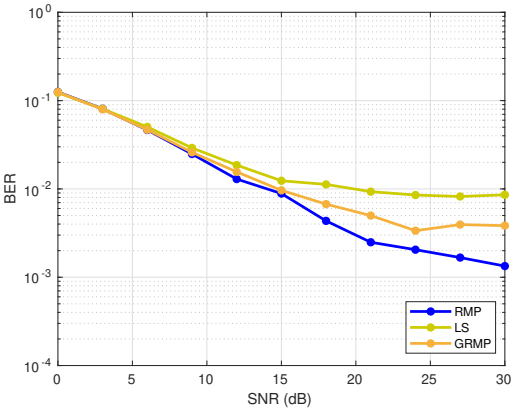


(b) Doppler Shift: 500 Hz

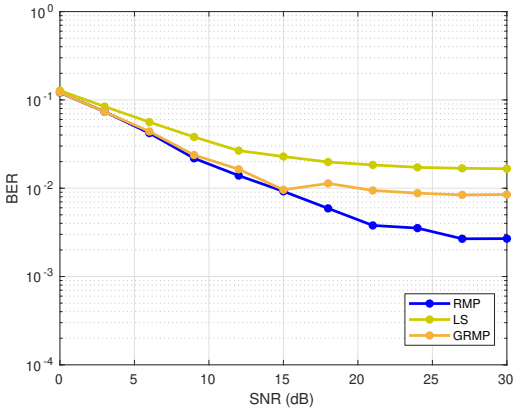


(c) Doppler Shift: 1000 Hz

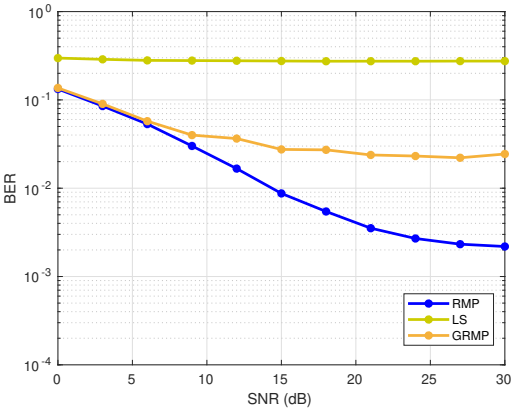


(d) Doppler Shift: 5000 Hz

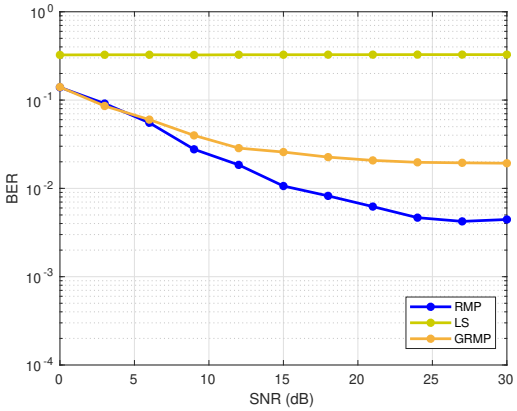


(e) Doppler Shift: 10000 Hz

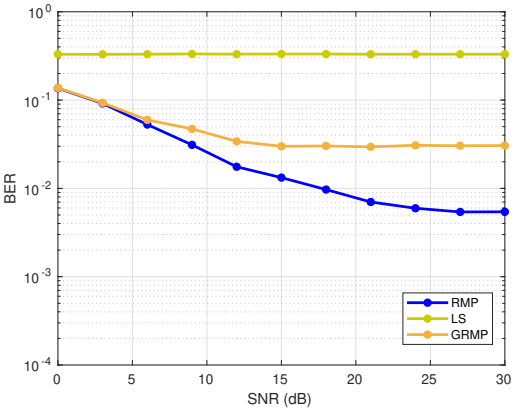


(f) Doppler Shift: 15000 Hz

Fig. 10.9: Evaluation of GRMP

A high Doppler shift of 10000 Hz and 15000 Hz has been simulated in Figures 10.9e and 10.9f respectively. The LS estimation remains to be ineffective when the Doppler shift increases. The performance gap between GRMP and RMP remains to be consistent even at higher Doppler shifts. The GRMP algorithm, by virtue of a simpler delay search mechanism is able to perform satisfactorily with a lower computational complexity compared to the RMP scheme. If the performance is acceptable, the reduction in complexity paves the way for practical realizations. It is also promising to note the general consistency of the RMP and the LS schemes between simulation runs as seen in Figures 10.8 and 10.9.

Although the GRMP scheme significantly reduced the complexity, the performance in different channel conditions is not optimal (Figure 10.9). Moreover, compared to the LS the computational complexity is still high in pure multipath and low mobility environments. Thus, there has been a clear stimulus for a more pragmatic solution wherein different channel estimation schemes are employed depending on the channel condition. Such a solution would as well provide the best error performance as optimize the computational complexity. In pure multipath environments, the different estimation schemes perform equally. But, the computational complexity associated with the RMP and GRMP algorithms cannot be justified. Thus, in low mobility scenarios, the LS scheme is the ideal choice for channel estimation. On the other hand, in scenarios of high mobility or in doubly selective channels, the RMP algorithm significantly outperforms the conventional channel estimation techniques and becomes the ideal choice.

The cognitive framework proposed in Chapter 7 provides such an ideal scheme for channel estimation. The framework includes a mechanism that can sense the temporal variation in the channel and appropriately employ a channel estimation scheme. Accordingly, the cognitive framework chooses the LS scheme for estimation in pure multipath channels while in scenarios of high mobility, the RMP algorithm is chosen for channel estimation. Thus, in heterogeneous channel conditions, the cognitive framework chooses an estimation scheme with an appropriate computational complexity and one that provides the best performance. Moreover, the cognitive framework is systematically developed to be modular and in principle allows for different channel estimation schemes to be combined as required.

The cognitive framework is evaluated for BER performance in Figure 10.10 and for robustness in Table 10.1 (for low SNR's) and Table 10.2 (for high SNR's). These tables consolidate the instances where each of the channel estimation schemes are chosen and expresses them as a percentage for different Doppler shifts and different SNR. The proposed cognition

metric works reliably in extreme channel conditions like pure multipath and high Doppler shift. However, in low to moderate mobility conditions and in the presence of noise, the cognitive framework must be evaluated closely. Thus, in Figure 10.10 only low and moderate Doppler shifts are simulated. The *ideal* cognition curves seen in the figures are generated in the simulation by simultaneously performing both the RMP and LS estimation for the entire physical layer frame. The BER is computed and the scheme that provided fewer errors was chosen to be the ideal channel estimation scheme under the given circumstances. This forms the ground truth against which the cognitive framework is evaluated. It must be noted that this ground truth is only available in a simulation setup wherein the ideal channel estimation can be decided in hindsight. For the sake of completeness the RMP and the LS schemes that are part of the developed cognitive framework are also shown in the figures.

In Figure 10.10a, a pure multipath channel is simulated where both LS and the RMP algorithms perform equally as expected. More significantly, the cognitive framework is able to detect the stationary channel and switch on the LS scheme. This is also seen in Tables 10.1 and 10.2, for a Doppler shift of 0 Hz, the LS scheme is chosen in most cases (shown as a percentage). However, in low SNR scenarios the correlation based cognition metric is sensitive towards noise and makes a wrong decision on the channel estimation scheme to be chosen. However, since for low mobility, both the schemes perform equally well, the error performance of the cognitive framework is not affected as seen in Figure 10.10a.

For a low Doppler shift of 200 Hz in Figure 10.10b, the cognitive framework is still expected to favor the LS estimation scheme. This seems to be the case where the SNR is high and the correlation based cognition metric makes the right choice. However, for lower SNR's there are instances where the cognition metric could make a wrong decision and chooses the RMP algorithm 100% of the time. These instances of failure strengthen the indication that the cognition metric used is sensitive to noise. Nevertheless, the performance of the cognitive frame with respect to BER is still good.

As the Doppler shift is increased to 400 Hz in Figure 10.10c a clear choice of estimation scheme becomes unclear. These are fringe cases, where it is difficult to adapt the thresholds to make the right choice. The performance of both the RMP and the LS schemes remain to be similar. Tables 10.1 and 10.2 provide further insights into the cognitive framework. In addition to showing the distribution of the two schemes, it again shows a few cases of failure in low SNR's.

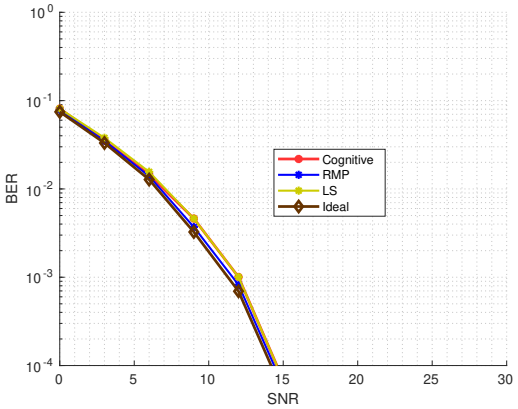


(a) Pure Multipath

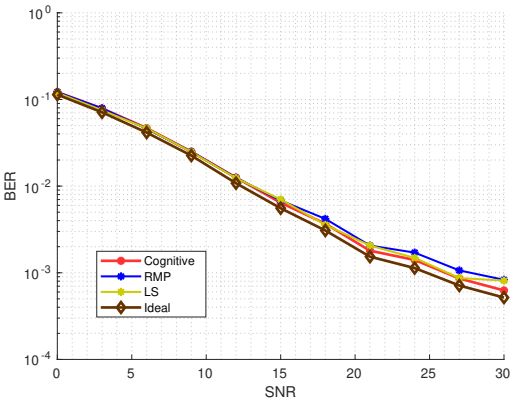


(b) Doppler Shift: 200 Hz

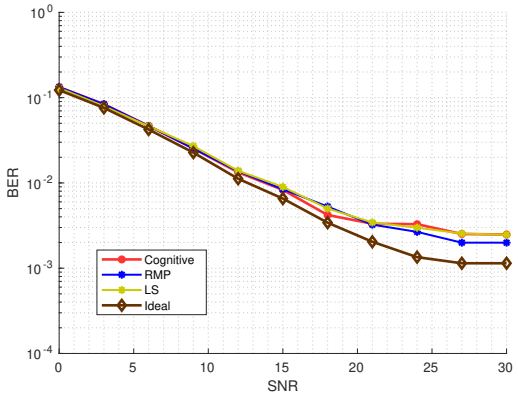


(c) Doppler Shift: 400 Hz

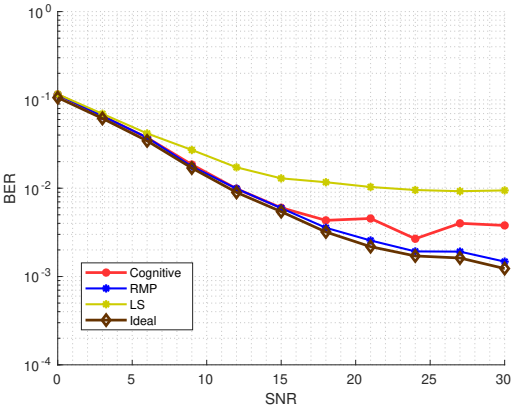


(d) Doppler Shift: 800 Hz

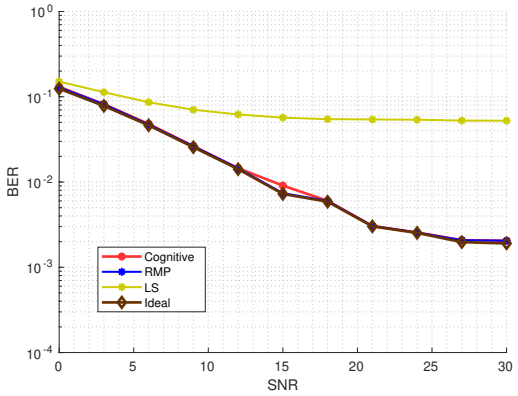


(e) Doppler Shift: 1600 Hz

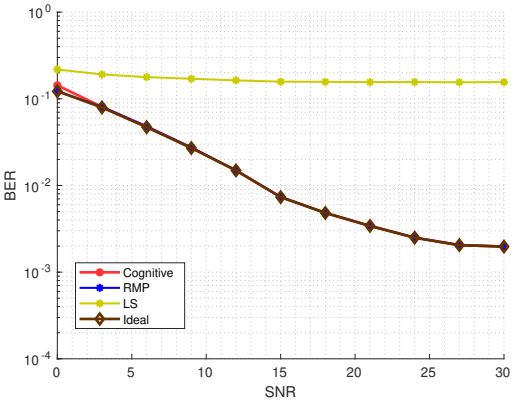


(f) Doppler Shift: 3200 Hz

Fig. 10.10: Evaluation of the Cognitive Framework

A Doppler shift of 800 Hz is simulated in Figure 10.10d. This amount of Doppler shift is sufficient to exhibit a degradation in performance with the LS scheme, thus justifying the use of RMP for channel estimation.

Table 10.1: Insights into Cognitive Framework (low SNR)

| Doppler (Hz) | Chosen Scheme | SNR (dB) | | | | | |
|---|---|---|---|---|---|---|---|
| | | 0 | 3 | 6 | 9 | 12 | 15 |
| 0 | LS | 100% | 26% | 56% | 100% | 100% | 100% |
| | RMP | 0% | 74% | 44% | 0% | 0% | 0% |
| 200 | LS | 43% | 0% | 28% | 0% | 54% | 70% |
| | RMP | 57% | 100% | 72% | 100% | 46% | 30% |
| 400 | LS | 6% | 0% | 5% | 14% | 46% | 45% |
| | RMP | 94% | 100% | 95% | 86% | 54% | 55% |
| 800 | LS | 15% | 0% | 0% | 0% | 0% | 2% |
| | RMP | 85% | 100% | 100% | 100% | 100% | 98% |
| 1600 | LS | 8% | 0% | 1% | 0% | 0% | 4% |
| | RMP | 92% | 100% | 99% | 100% | 100% | 96% |
| 3200 | LS | 17% | 0% | 0% | 0% | 0% | 0% |
| | RMP | 83% | 100% | 100% | 100% | 100% | 100% |

In Figures 10.10e and 10.10f, a moderate Doppler shift of 1500 Hz and 3000 Hz is simulated. In these cases, it is promising to see that the cognitive framework almost exclusively chooses the RMP algorithm (Tables 10.1 and 10.2). This amount of Doppler shift is enough for the cognition metrics to unambiguously detect a doubly selective channel and choose the right channel estimation scheme. As the Doppler shift in the channel increases beyond 3200 Hz, the cognitive framework continues to work reliably and choose the right channel estimation algorithm. This results in a channel estimation scheme that is reliable, lies below the FEC bit error rate threshold and is optimized with respect to the required computational complexity.

Table 10.2: Insights into Cognitive Framework (high SNR)

| Doppler (Hz) | Chosen Scheme | SNR (dB) | | | | |
|---|---|---|---|---|---|---|
| | | 18 | 21 | 24 | 27 | 30 |
| 0 | LS | 100% | 100% | 100% | 100% | 100% |
| | RMP | 0% | 0% | 0% | 0% | 0% |
| 200 | LS | 88% | 92% | 94% | 95% | 96% |
| | RMP | 12% | 8% | 6% | 5% | 4% |
| 400 | LS | 73% | 80% | 78% | 92% | 88% |
| | RMP | 27% | 20% | 22% | 8% | 12% |
| 800 | LS | 0% | 4% | 13% | 13% | 10% |
| | RMP | 100% | 96% | 87% | 87% | 90% |
| 1600 | LS | 0% | 0% | 0% | 0% | 0% |
| | RMP | 100% | 100% | 100% | 100% | 100% |
| 3200 | LS | 0% | 0% | 0% | 0% | 0% |
| | RMP | 100% | 100% | 100% | 100% | 100% |

The goal of the cognitive framework has been to combine multiple channel estimation techniques and employ them depending on the channel conditions. To achieve this, it uses a computationally inexpensive correlation based metric to sense the channel. This metric is shown to work adequately in most of the channel conditions but exhibits some weaknesses in a few fringe cases where, for the given amount of Doppler shift a clear choice between competing estimation schemes is not available. Even in these cases, the error rate remains to be below the FEC threshold. Moreover, the broader perspective confirms the advantages of the cognitive framework that allows the adaptation of channel estimation according to channel conditions. The results show that the cognitive framework is fairly close to the ideal case and has achieved this with a metric that is very simple to calculate.

The results discussed in this chapter confirms the strengths of the proposed RMP, GRMP as well as the cognitive framework in the estimation and equalization of a doubly selective channel for the IEEE 802.11p standard.

## 10.2 LTE

The evaluation for the LTE standard primarily consists of SNR vs. BER curves for the different channel estimation and equalization schemes under different channel conditions. The EVA delay profile has been specified for scenarios with mobility (like V2X applications) and is thus chosen for simulations in this section. To evaluate the effectiveness of the channel estimation schemes, different normalized Doppler shifts have been simulated as shown in Table 10.3. A normalized Doppler shift is a percentage of the subcarrier spacing and serves as a uniform metric that quantifies the amount of Doppler shift agnostic to the specifications of the underlying wireless standard. The Doppler shifts and the corresponding relative velocities are also shown in Table 10.3 for the LTE-V mode that is proposed to work in the 5.9 GHz unlicensed band as mandated in [49].

Table 10.3: Simulated Doppler Shift and the Corresponding Velocity

| Normalized Doppler Shift (%) | Maximum Doppler Shift ($Hz$) | Velocity ($km/h$) |
|---|---|---|
| 1 | 150 | 27 |
| 2 | 300 | 55 |
| 3 | 450 | 82 |
| 4 | 600 | 110 |
| 5 | 750 | 137 |
| 6 | 900 | 165 |
| 7 | 1050 | 192 |
| 8 | 1200 | 220 |
| 9 | 1350 | 247 |
| 10 | 1500 | 275 |

Accordingly, evaluations are carried out for the LTE downlink, LTE uplink and the LTE-V specifications where the effectiveness of channel estimation schemes and the impact of the different physical layer waveforms and pilot patterns are investigated.

The LTE downlink specifies a sparse comb pilot-type pattern in the physical layer that is used by channel estimation and equalization schemes. For the LTE standard, the LS, MMSE, RMP, GRMP and the hybrid channel estimation scheme based on RMP and LS are evaluated in the following figures. LTE specifies an Adaptive Modulation and Coding

(AMC) mechanism to adjust coding parameters based on feedback and meet a stipulated block error rate [50]. Simulation in [114] have show that the AMC has a BER threshold of around 10%. In Figure 10.11 a normalized Doppler shift of 0% is simulated.

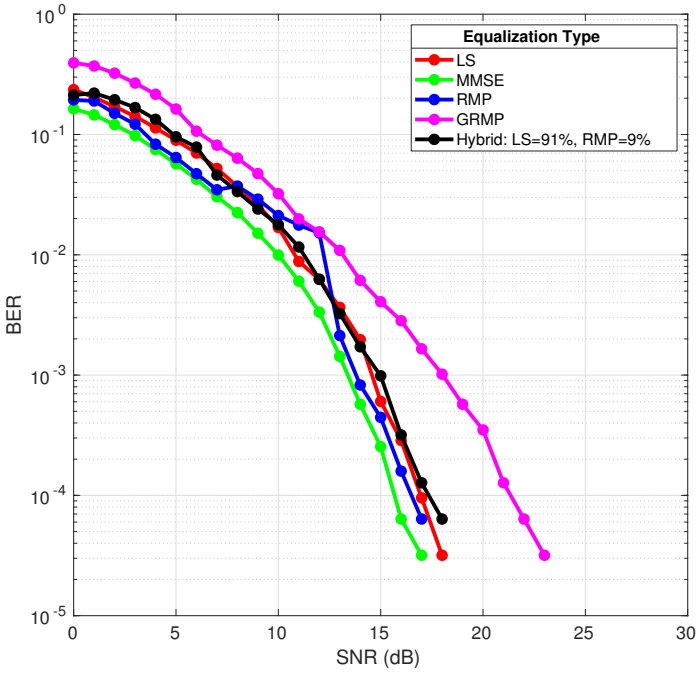


Fig. 10.11: LTE Downlink with 0% Normalized Doppler Shift

In such a pure frequency selective channel, classical schemes like LS are known to perform well. The MMSE channel estimation and equalization scheme from the LTE toolbox in Matlab performs the best in stationary channel conditions. The LTE channel estimation routines developed by Mathworks are based on LS with several post processing steps that include averaging, noise reduction, interpolation and optimization of channel estimates in the time and frequency domain as described in [38]. Not surprisingly, these channel estimation schemes provide very good results as is evident in the figure. The RMP channel estimation scheme that is conceptualized and developed for doubly selective channels performs similar to the LS scheme. This is an important result because it again indicates that even in a purely frequency selective channel, the delay taps are identified accurately and are tracked appropriately through out the physical layer frame. This result endorses the RMP channel estimation algorithm to work adequately even in purely frequency selective channels. However, a slight fluctuation of the RMP results between the SNR range of 5 and $12dB$ can be observed in Figure 10.11. This can be attributed to the very sparse comb type pilot pattern in the LTE downlink specification where either a wrong delay tap has been estimated or a delay tap is wrongly tracked through the physical layer frame causing a poor error

performance. The GRMP channel estimation scheme that reduced the computational effort significantly relative to the RMP algorithm pays a price in terms of error rate performance. In GRMP, all the delay taps are computed from just one iteration and thus provide only a coarse estimate of the delays in the best case. This techniques suffers even in stationary and low mobility conditions as the coarse delay estimate does not benefit from tracking when the coherence time is high. Lastly, the hybrid channel estimation scheme exhibits a similar performance to the LS and RMP schemes. It is seen from the figure that the detection metrics have appropriately chosen the LS scheme for channel estimation for most of the simulation run. Next, a Doppler shift of 5% corresponding to scenarios in towns where a moderate relative velocity between end stations is simulated in Figure 10.12.

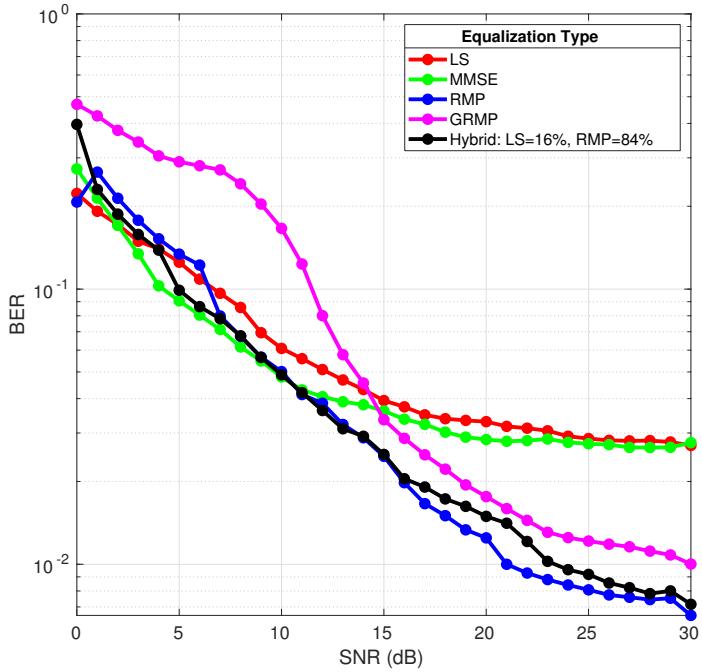


Fig. 10.12: LTE Downlink with 5% Normalized Doppler Shift

The conventional schemes like the LS and even the MMSE scheme from Matlab start to perform poorly. The proposed RMP and GRMP estimation schemes perform significantly better than conventional schemes especially when the SNR is high. In low SNR conditions, both CS based estimation scheme exhibit deterioration in performance. For the RMP scheme, this is attributed to the incorrect tracking of delay tap coefficients over time due to the presence of noise while for the GRMP scheme, this gap in performance is mainly due to the coarse estimate of the delay taps that is not enough to adequately compensate the channel. In order to alleviate this problem, a higher number of pilots are required in the downlink to be robust against noise. The channel detection metrics in the hybrid scheme also have to finely

adapt the thresholds to make the right choice of estimation schemes. Thus, for moderate Doppler shifts, the proposed channel estimation schemes outperform conventional schemes but do suffer when the SNR is low mainly due to the scarcity of pilots.

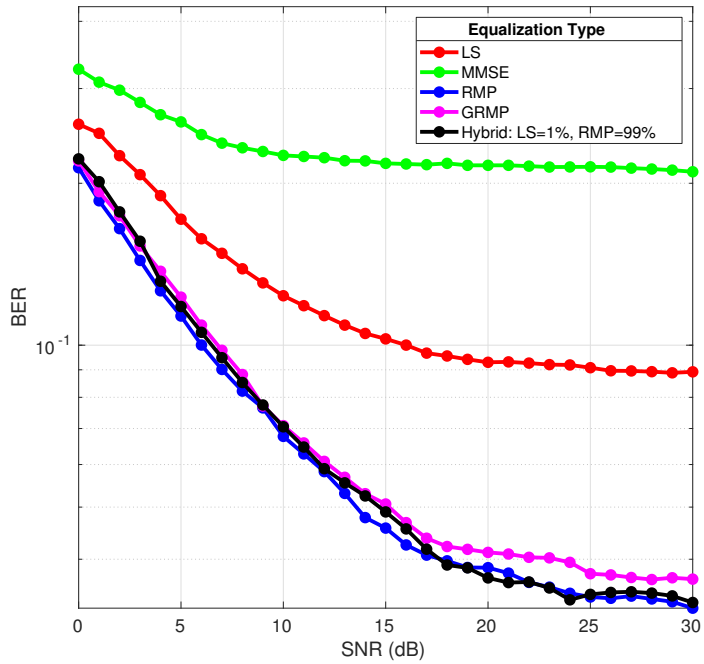


Fig. 10.13: LTE Downlink with 10% Normalized Doppler Shift

A high Doppler shift of 10% is simulated in Figure 10.13. It is immediately evident that the LS channel estimation scheme performs poorly in a doubly selective channel. It is also seen that the MMSE based channel compensation scheme perform worse than the conventional LS scheme. This can possibly be caused due to aggregation of inter-domain interpolation errors. On the other hand, the compressed sensing based channel estimation schemes like the RMP, GRMP and the hybrid estimator perform significantly better. Moreover, the error performance of the proposed schemes lie significantly below the FEC error threshold of 10% for moderate to high SNR scenarios. Nevertheless, we observe that the scarcity of pilots has an impact on channel estimation (and consequently error performance) at the receiver. It is also important to note that the GRMP estimator is able to exhibit a comparable performance due to the ability to track the clear temporal variation of the delay tap coefficients at a significantly reduced computational effort. The detection metrics of the hybrid scheme as well have clearly identified the RMP as the appropriate scheme for channel estimation under doubly selective channels.

Next, the LTE uplink mode is evaluated. As already discussed in Sections 4.1 and 9.2, the uplink mode uses SC-FDM waveform in the physical layer to optimize the PAPR in battery operated mobile devices. However, it must be noted that the block type of pilots specified for the uplink configuration are added in the transmitter after the DFT spreading and consequently at the receiver, the channel estimation is performed before de-spreading. The presence of a block pilot pattern in itself should provide a reliable estimate of the channel. Nevertheless, the presence of a single pilot symbol in a LTE uplink slot limits the performance as soon as the channel begins to exhibit temporal variations in the presence of mobility. The performance of the channel estimation schemes in a pure frequency selective channel is seen in Figure 10.14.

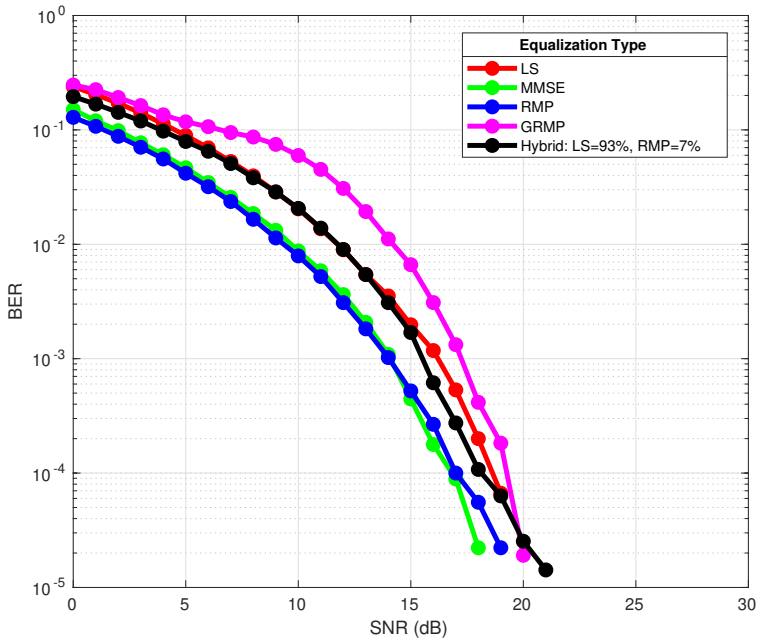


Fig. 10.14: LTE Uplink with 0% Normalized Doppler Shift

The LS and MMSE schemes show similar performance to the downlink configuration. In fact, the presence of a block pilot structure in a stationary channel makes the curves slightly better than that of the downlink configuration. The RMP scheme exhibits similar performance to the LS scheme which again strengthens the fact that it is suitable in stationary channel conditions. The detection metrics of the hybrid scheme are again able to detect that the channel is stationary and has chosen the LS scheme most of the time to perform channel estimation. The GRMP scheme for channel estimation has also performed well in the uplink mainly due

to the presence of block pilots which enable a more accurate estimate of the delay taps.

Figure 10.15 evaluates performance for a moderate normalized Doppler shift of 5%. The RMP and the hybrid schemes perform better than the conventional schemes like the LS. A noticeable fluctuation in the performance is seen in the hybrid channel estimation which is caused due to the same reasons discussed in the downlink results. The MMSE scheme is still able to adequately estimate and equalize the channel and is also helped by the block pilot structure in the uplink. The GRMP scheme begins to suffer from the temporal variation of the channel and as a result of wrongly detected delay taps being tracked over the physical layer frame, the error performance is affected.

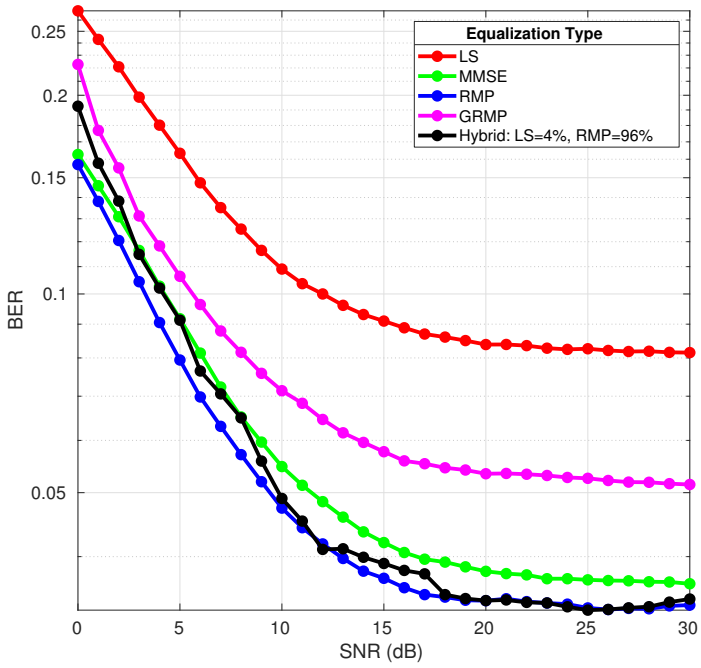


Fig. 10.15: LTE Uplink with 5% Normalized Doppler Shift

The performance of channel estimation schemes begin to significantly deteriorate for normalized Doppler shifts higher than 5%. Channel coherence times for such channels are smaller than $666.67\mu S$ (for 5% Doppler shift the coherence time $T_c = 666.67\mu S$) and thus the channel produces temporal variations within a physical layer frame of $1ms$. Moreover, the single pilot symbol in a RB is not sufficient to track the temporal variation of the channel accurately within a physical layer frame. This is improved in in LTE-V by the introduction of additional pilots symbols in every RB.

The LTE-V standard recently specified as part of Release-14 enables V2X capabilities and is intended to be adapted in 5G. The physical layer differences compared to the LTE uplink and downlink are discussed in Section 4.1. Twice as many block pilots compared to the uplink mode are specified in LTE-V. The higher density of pilots should in principle improve the capabilities of channel estimation schemes and correspondingly result in better performance. Figure 10.16 evaluates the performance for the LTE-V mode. The GRMP scheme performs slightly worse in stationary conditions compared to the other techniques like in the uplink and downlink modes.

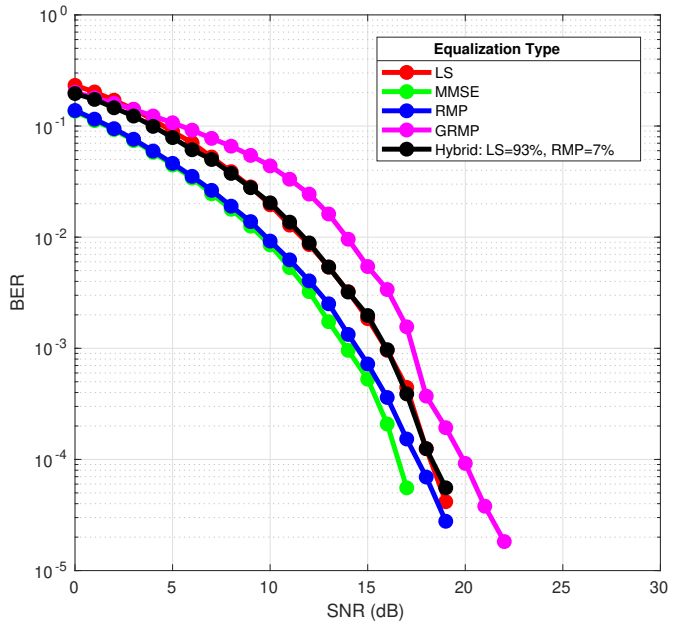


Fig. 10.16: LTE V2X with 0% Normalized Doppler Shift

Conventional schemes like the LS and MMSE show similar performance as in the uplink. The presence of additional pilot symbols improve the performance slightly. The RMP scheme is also able to leverage the additional pilot symbols to match the performance of the MMSE estimation scheme. The detection metrics of the the hybrid estimator has appropriately detected a stationary channel and has chosen the LS scheme for estimation over the entire simulation run.

A 5% normalized Doppler shift is simulated in Figure 10.17 and it is clearly evident again that the conventional schemes like the LS and MMSE start to struggle. On the other hand, the proposed RMP and the hybrid schemes have performed better due to the additional pilot symbols. The GRMP channel estimate performs poorly which might be due to an incorrect

estimation of delay taps.

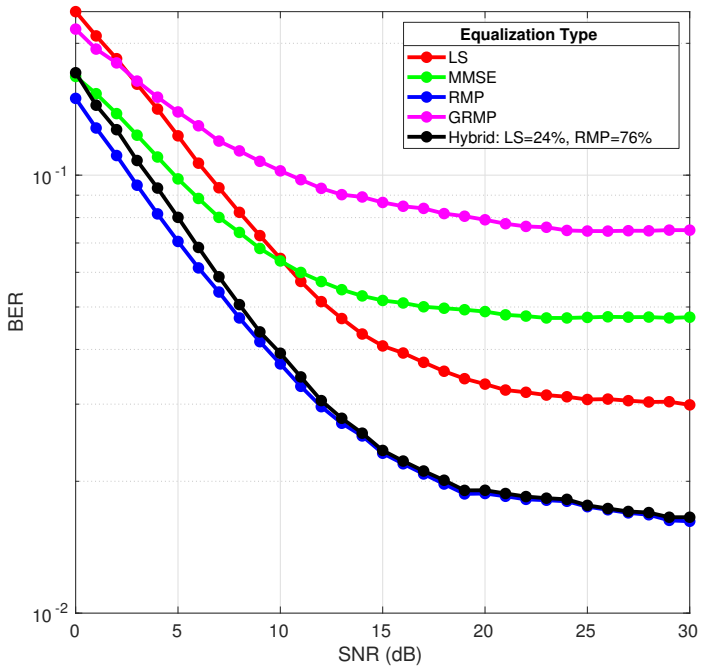


Fig. 10.17: LTE V2X with 5% Normalized Doppler Shift

Finally, a high normalized Doppler shift of 10% is simulated in Figure 10.18. Conventional schemes are not suitable in such channel conditions and performs very poorly. However, the proposed RMP channel estimator does well to provide a good estimate of the doubly selective channel and compensate its effects. However, the use of SC-FDM proves detrimental to the performance of the channel estimation schemes in general because the de-spreading in the receiver performed by means of IDFT spreads the errors in equalization over the entire OFDM symbol on which the BER is computed. If the number of such errors are high, which is possible when the channel is highly selective, the net error over the OFDM symbol is increased that results in slightly worse BER performance. Despite this, the RMP is the only scheme that clearly lies below the FEC threshold of 10% when the SNR is greater than 8 dB.

It should be noted that the detection metrics for the hybrid scheme have not been tweaked for the different modes and channel conditions. Moreover for LTE, an inter-frame cognition is implemented wherein for each subframe, the channel estimation scheme is adapted to optimize the computational effort proportional to the channel conditions.

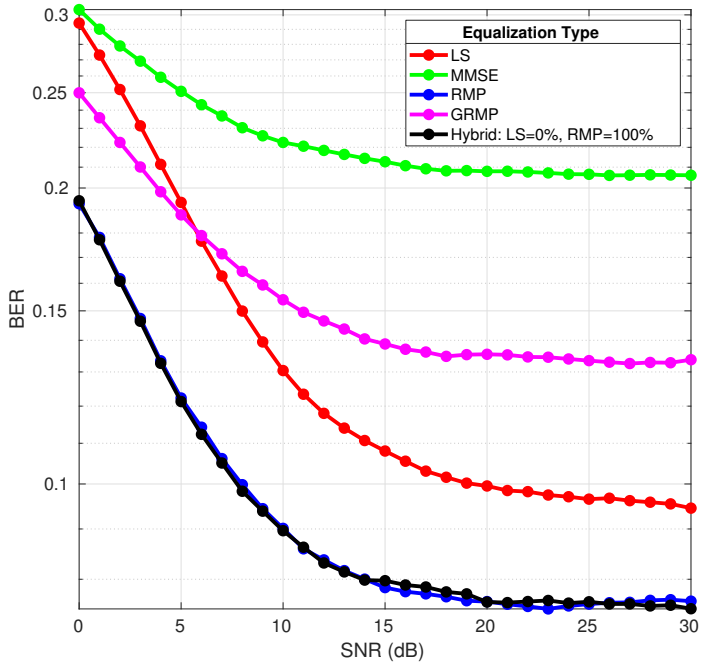


Fig. 10.18: LTE V2X with 10% Normalized Doppler Shift

To summarize, the proposed channel estimation and equalization schemes have proven to work better than conventional methods under varying channel conditions for the different modes in LTE. The physical layer specifications for these modes have had an effect on the performance of channel estimation. Generally, the use of block pilots or adequate number of comb pilots along with the use of OFDM would offer the best compromise as seen in the results for the other wireless standards in this chapter. Not surprisingly, 5G proposes to use OFDM in both the uplink and downlink [33].

## 10.3 DVB-T2

The final set of evaluations are conducted for the DVB-T2 terrestrial broadcasting standard to confirm the versatility of the proposed compressed sensing based channel estimation schemes under heterogeneous channel conditions and for fundamentally different wireless standards. The simulation parameters for applications involving mobility are recommended by the implementation guidelines [47] and is shown in Table 10.4. The conservative choice of the guard interval inherently makes the system robust to the effects of multipath propagation. The PP1 pilot pattern also provides an adequate density of pilots that are necessary to accurately estimate the doubly selective wireless channel.

Table 10.4: Simulation Parameters for DVB-T2 Evaluation

| Parameter | Value |
|---|---|
| FFT Size | 8192 |
| Num. Data Subcarriers | 6817 |
| Modulation | 16-QAM |
| Pilot Pattern | PP1 |
| Symbol Duration | $896\,\mu s$ |
| Guard Interval Fraction | $1/4$ |
| Bandwidth | $8\,MHz$ |
| Subcarrier Spacing | $1116\,Hz$ |
| Sampling Interval | $109.375\,ns$ |

The DVB-T2 transceiver chain is configured to the parameters in Table 10.4. The channel model is also configured using a TU-6 delay profile with a Doppler shift as described in Section 9.3. At the receiver, the BER is computed after channel estimation and equalization is performed (and before FEC decoding) to get a transparent measure to evaluate the performance of the channel estimation schemes. Similar to the results in previous sections, evaluation consists for SNR vs. BER curves for different amounts of mobility. Figure 10.19 shows the results for a stationary channel. In a purely frequency selective channel, the conventional LS scheme along with a simple one-tap equalizer is able to precisely estimate the channel and compensate its effects resulting in excellent BER performance. The compressed sensing based RMP channel estimation scheme has been developed primarily for time-varying multipath or doubly selective channels. Nevertheless, it is also evaluated for a purely frequency selective channel to show the versatility of the proposed scheme. The RMP

algorithm is able to accurately detect the delay taps of the channel and correctly track the absence of temporal variation in the frequency selective channel. The equalizer leverages this channel estimate and compensates the effects of the channel at the receiver. Figure 10.19 clearly shows that the performance of the RMP algorithm is very close to the conventional LS scheme. The FEC threshold is also plotted in the evaluations. It quantifies the amount of error that the FEC mechanisms can tolerate. Error coding in the simulation platform is configured as a concatenation of LDPC and BCH codes with the most robust mode (code rate of $1/2$). The error threshold for this concatenation is computed to be $12\%$ which means that errors below this threshold are corrected by the coding mechanisms [41]. The results thus show that a minimum SNR of $10\,dB$ is required at the receiver to be able to decode and forward the data to the subsequent blocks in the receiver chain.

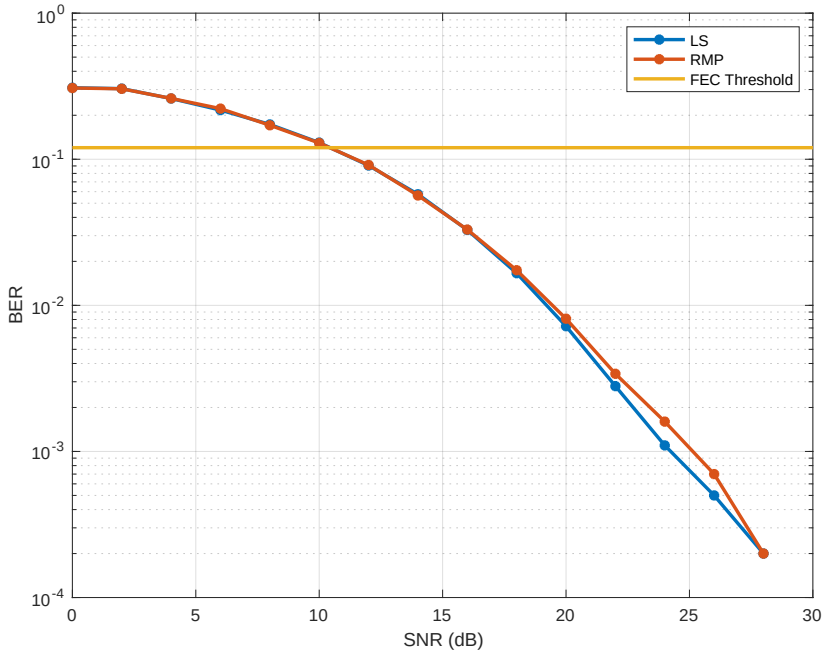


Fig. 10.19: Evaluation for 0% Doppler shift

In Figure 10.20 , a normalized Doppler shift of $1\%$ is simulated. This corresponds to a Doppler shift of $11\,Hz$ for the simulation parameters given in Table 10.4. Considering channel 32 with a centre frequency of 562 MHz, this Doppler shift corresponds to a relative velocity of roughly 20 Kmph. Channel 32 is also used in Saarland to transmit the *Das Erste* channel[2]. The results show that the LS estimation scheme is affected by the temporal variation of the channel and performs poorly even when the SNR is high. The RMP algorithm

[2]the flagship television channel of the public broadcasters association in Germany (www.ard.de/)

is again able to accurately estimate the delay taps and track the temporal variation of the channel across the DVB-T2 frame. This also results in better performance compared to the conventional LS scheme as seen in Figure 10.20. Although both the schemes have a similar performance at the FEC threshold, the better performance by the RMP scheme at higher SNR's is significant.

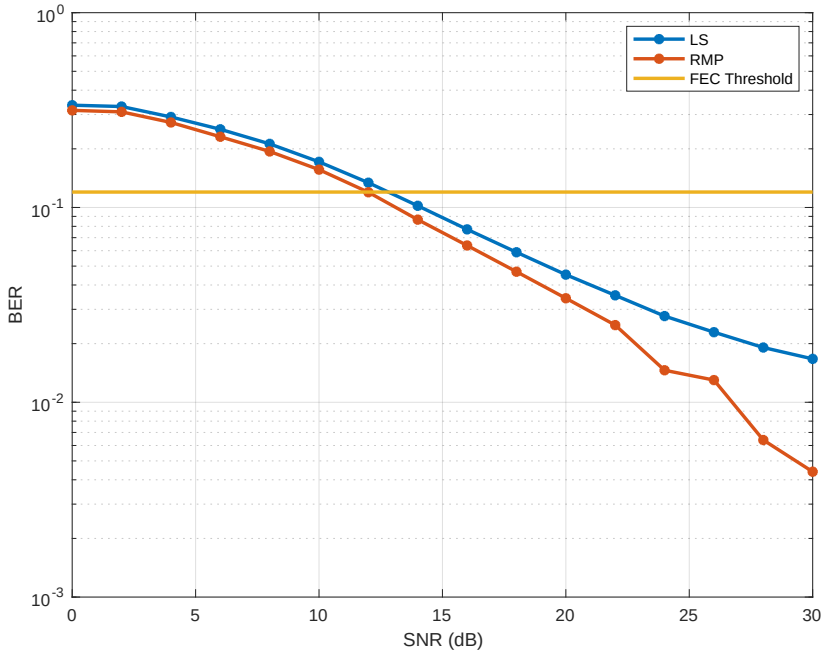


Fig. 10.20: Evaluation for 1% Doppler shift

A normalized Doppler shift of 5% is simulated in Figure 10.21. This corresponds to a Doppler shift of 50 Hz for the chosen simulation parameters. For the channel 32 transmitting at 562 MHz this translates to a relative velocity of around 92 Kmph that is indicative of typical motorway driving. The higher Doppler shift deteriorates the overall performance of the channel estimation and equalization schemes. However, it is seen that the RMP algorithm clearly out performs the conventional LS schemes at higher SNR. At lower SNR's, the performance of both the schemes converge which is also consistent with the observations from the other standards discussed in this chapter. The figure also shows that a minimum SNR of 14 dB is required to stay below the FEC threshold when the RMP scheme is chosen for channel estimation.

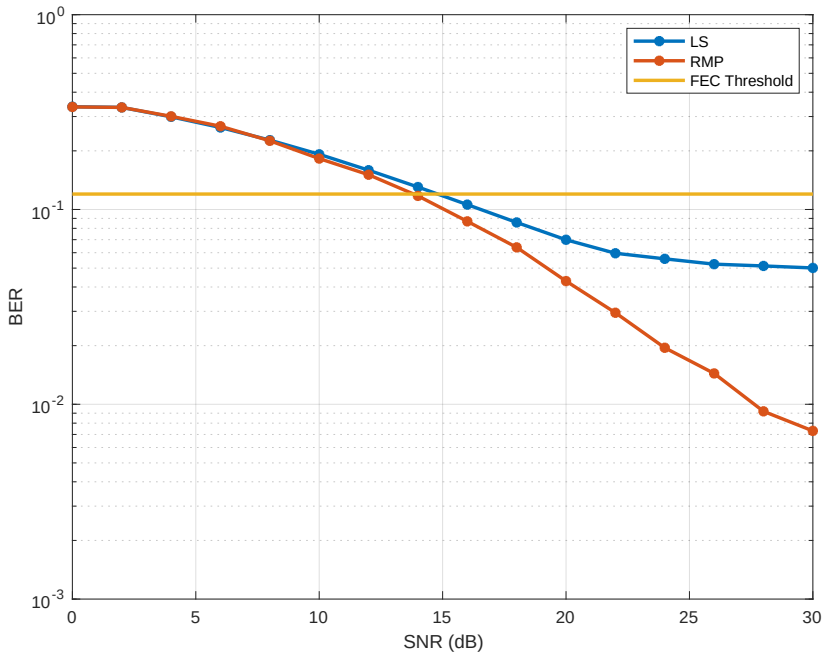


Fig. 10.21: Evaluation for 5% Doppler shift

As the simulated Doppler shift increases, the performance of the channel estimation and compensation schemes deteriorates proportionally. However, the use of coded OFDM in DVB-T2 that specifies a concatenated error coding mechanism in the physical layer is able cope with significant number of errors in the most robust mode as seen from the FEC threshold shown in the results above. The compressed sensing based RMP algorithm for channel estimation is shown to perform significantly better than the conventional LS estimator.

In this part of the thesis, we have rigorously evaluated the proposed schemes for channel estimation and equalization. In addition to the clear improvement in error performance, we have shown that these scheme are versatile and can be deployed in fundamentally different wireless schemes serving different purposes. While we know that the performance of the proposed schemes are influenced by the underlying specification, the schemes have out performed conventional channel estimation schemes. Thus, we conclude that the proposed RMP scheme and its variants perform adequately in heterogeneous channel conditions and is a significant step towards bringing high mobility in OFDM based wireless communication systems.

# CHAPTER 11

# CONCLUSION

In this thesis, we have systematically investigated the effects of high mobility in OFDM based wireless communication systems. The doubly selective or the time varying multipath channel is derived and the effect it has on an OFDM signal is explained and visualized. A thorough survey of conventional and state-of-art schemes showed that a robust, computationally efficient and standard compliant scheme for the estimation of such channels is still being investigated in literature. We observe that current system design either circumvents this issue by limiting the maximum relative velocity or proposes to solve this problem with a complexity that is prohibitive for practical implementation on consumer grade hardware.

Channel estimation based on Compressed Sensing (CS) allows us to exploit the inherent sparsity of the wireless channel and is investigated in this thesis. We have conceptualized and developed a CS based scheme called Rake Matching Pursuit (RMP) algorithm to robustly estimate the doubly selective channel. The proposed delay search metric and the Doppler tracking mechanism are shown to be robust as well as computationally efficient. We have also developed the Gradient Rake Matching Pursuit (GRMP) algorithm that further optimizes the complexity with a small trade-off in error performance at the receiver. In addition to this, we have developed a cognitive framework with a goal of optimizing the process of channel estimation in heterogeneous channel conditions. The cognitive framework is able to sense the mobility in the channel and appropriately parameterize the estimation process. Thus, in low mobility conditions the simple Least Squares (LS) estimation scheme is used while in high mobility scenarios, a more sophisticated estimation algorithm is chosen. In addition to this, we have also optimized the process of generating the dictionary which is a prerequisite for CS based channel estimation. The storage and computational requirement associated with generating the dictionary is reduced significantly.

We have also extensively evaluated the proposed channel estimation schemes. Simulation platforms for current cellular (LTE, LTE-V), broadcast (DVB-T2) and broadband (IEEE 802.11p) technologies have been implemented in Matlab. To simulate doubly selective channels in this thesis, we use channel models that are either part of the specifications or are widely accepted in literature. We have shown that the proposed schemes exhibit good performance for these wireless systems despite the significant differences in physical layer specifications. The associated computational requirements are also analyzed and show that the proposed schemes are relatively more efficient when compared to conventional CS based estimation schemes.

We have also proposed a mechanism to systematically generate time domain pilots without significantly modifying the specified transmitter chain. Although the channel estimation schemes proposed in this thesis do not require time domain pilots, they can be leveraged by conventional estimation schemes and provide valuable measurements in the time domain for the estimation of doubly selective channels.

Thus, the work of this thesis has resulted in novel channel estimation and equalization schemes that perform consistently better than conventional schemes in varying channel conditions and also for different wireless standards. It has also led to eight publications at renowned conferences. The simulation platforms developed as part of this thesis are also made available as open source software to further promote the development of channel estimation schemes and contribute towards enabling high mobility in OFDM based wireless communication systems.

# REFERENCES


[1] 3GPP. *Initial Cellular V2X standard completed*. 2016. URL: http://www.3gpp.org/news-events/3gpp-news/1798-v2x_r14.

[2] Abdeldime Abdelgader and Lenan Wu. "The Physical Layer of the IEEE 802.11 p WAVE Communication Standard: The Specifications and Challenges". In: vol. 2. Oct. 2014.

[3] M. Abramowitz and I.A. Stegun. *Handbook of Mathematical Functions: With Formulas, Graphs, and Mathematical Tables*. Applied mathematics series. Dover Publications, 1965. ISBN: 9780486612720. URL: https://books.google.de/books?id=MtU8uP7XMvoC.

[4] G. Acosta-Marum and M. A. Ingram. "Six time- and frequency- selective empirical channel models for vehicular wireless LANs". In: *IEEE Vehicular Technology Magazine* 2.4 (Dec. 2007), pp. 4–11. ISSN: 1556-6080.

[5] Sassan Ahmadi. "Chapter 9 - Downlink Physical Layer Functions". In: *LTE-Advanced*. Ed. by Sassan Ahmadi. Academic Press, 2014, pp. 399 –720. ISBN: 978-0-12-405162-1. DOI: https://doi.org/10.1016/B978-0-12-405162-1.00009-5. URL: http://www.sciencedirect.com/science/article/pii/B9780124051621000095.

[6] R. Akeela and B. Dezfouli. "Software-defined Radios: Architecture, State-of-the-art, and Challenges". In: *Computer Communications* 128 (Mar. 2018), pp. 106–125. ISSN: 0140-3664. DOI: https://doi.org/10.1016/j.comcom.2018.07.012.

[7] J. Akhtman and L. Hanzo. "Decision Directed Channel Estimation Aided OFDM Employing Sample-Spaced and Fractionally-Spaced CIR Estimators". In: *IEEE Transactions on Wireless Communications* 6.4 (2007), pp. 1171–1175.

[8] M. Bellanger. "Physical layer for future broadband radio systems". In: *2010 IEEE Radio and Wireless Symposium (RWS)*. 2010, pp. 436–439. DOI: 10.1109/RWS.2010.5434093.

[9] Katrin Bilstrup, Elisabeth Uhlemann, Erik Ström, and Urban Bilstrup. "Evaluation of the IEEE 802.11p MAC Method for Vehicle-to-Vehicle Communication". In: Oct. 2008, pp. 1 –5. DOI: 10.1109/VETECF.2008.446.

[10] Bastian Bloessl, Mario Gerla, and Falko Dressler. "IEEE802.11P in Fast Fading Scenarios: From Traces to Comparative Studies of Receive Algorithms". In: *Proceedings of the First ACM International Workshop on Smart, Autonomous, and Connected Vehicular Systems and Services*. CarSys '16. New York, NY, USA: ACM, 2016, pp. 1–5. ISBN: 978-1-4503-4250-6. DOI: 10.1145/2980100.2980104. URL: http://doi.acm.org/10.1145/2980100.2980104.

[11] Bastian Bloessl, Michele Segata, Christoph Sommer, and Falko Dressler. "Towards an Open Source IEEE 802.11p Stack: A Full SDR-based Transceiver in GNURadio". In: *5th IEEE Vehicular Networking Conference (VNC 2013)*. Boston, MA: IEEE, Dec. 2013, pp. 143–149. DOI: 10.1109/VNC.2013.6737601.

[12] A. Borhani and M. Pätzold. "Correlation and Spectral Properties of Vehicle-to-Vehicle Channels in the Presence of Moving Scatterers". In: *IEEE Transactions on Vehicular Technology* 62.9 (2013), pp. 4228–4239.

[13] Kavita Burse, R.N. Yadav, and S.C. Shrivastava. "Channel Equalization Using Neural Networks: A Review". In: *Systems, Man, and Cybernetics, Part C: Applications and Reviews, IEEE Transactions on* 40 (June 2010), pp. 352 –357. DOI: 10.1109/TSMCC.2009.2038279.

[14] E. J. Candes and M. B. Wakin. "An Introduction To Compressive Sampling". In: *IEEE Signal Processing Magazine* 25.2 (2008), pp. 21–30.

[15] Peter G. Casazza and Gitta Kutyniok. *Finite Frames: Theory and Applications*. Birkhäuser Basel, 2012. ISBN: 0817683720.

[16] K. Chelli and T. Herfet. "Doppler shift compensation in Vehicular Communication Systems". In: *2016 2nd IEEE International Conference on Computer and Communications (ICCC)*. 2016, pp. 2188–2192. DOI: 10.1109/CompComm.2016.7925088.

[17] K. Chelli and T. Herfet. "Time-domain pilots in DVB-T2". In: *2017 IEEE International Symposium on Broadband Multimedia Systems and Broadcasting (BMSB)*. 2017, pp. 1–4. DOI: 10.1109/BMSB.2017.7986165.

[18] K. Chelli and T. Herfet. "Estimating Doubly-Selective Channels in DVB-T2". In: *2018 IEEE International Symposium on Broadband Multimedia Systems and Broadcasting (BMSB)*. 2018, pp. 1–5. DOI: 10.1109/BMSB.2018.8436760.

[19] K. Chelli, P. Sirsi, and T. Herfet. “Cognitive Framework for the Estimation of Doubly Selective Channels”. In: *2017 IEEE 86th Vehicular Technology Conference (VTC-Fall)*. 2017, pp. 1–5. DOI: 10.1109/VTCFall.2017.8287926.

[20] K. Chelli, P. Sirsi, and T. Herfet. “Complexity reduction for consumer device compressed sensing channel estimation”. In: *2017 IEEE 7th International Conference on Consumer Electronics - Berlin (ICCE-Berlin)*. 2017, pp. 189–194. DOI: 10.1109/ICCE-Berlin.2017.8210625.

[21] K. Chelli, P. Sirsi, and T. Herfet. “Sparse doubly-selective channels: Estimating path parameters unambiguously”. In: *2017 European Conference on Networks and Communications (EuCNC)*. 2017, pp. 1–5. DOI: 10.1109/EuCNC.2017.7980687.

[22] Kelvin Chelli. “Doppler Shift Compensation in Vehicular Communication Systems”. MA thesis. Universität des Saarlandes, 2015.

[23] Kelvin Chelli, Ramzi Theodory, and Thorsten Herfet. “Compressed Sensing Channel Estimation for LTE-V”. In: *2nd International Conference on 5G for Ubiquitous Connectivity*. Ed. by Baoliu Ye, Weihua Zhuang, and Song Guo. Cham: Springer International Publishing, 2020, pp. 13–24. ISBN: 978-3-030-22316-8.

[24] Kelvin Chelli, Praharsha Sirsi, Ramzi Theodory, and Thorsten Herfet. *IEEE 802.11p Simulation Platform*. (2017) [Online]. Available: http://www.nt.uni-saarland.de/. Accessed on: Mar.28, 2017.

[25] S. Chen and Y. Yang. “Low-Complexity MMSE-SIC Equalizer Employing $\mathbf{LDL}^H$ Factorization for OFDM Systems Over Time-Varying Channels”. In: *IEEE Transactions on Vehicular Technology* 59.8 (2010), pp. 4128–4131.

[26] X. Cheng, D. Liu, Z. Zhu, W. Shi, and Y. Li. “A ResNet-DNN based Channel Estimation and Equalization Scheme in FBMC/OQAM Systems”. In: *2018 10th International Conference on Wireless Communications and Signal Processing (WCSP)*. 2018, pp. 1–5.

[27] Richard Chernock, Jerry C. Whitaker, and Yiyan Wu. “ATSC 3.0—The Next Step in the Evolution of Digital Television”. In: *IEEE Transactions on Broadcasting* 63.1 (2017), pp. 166–169. DOI: 10.1109/TBC.2017.2652018.

[28] L. Cimini. “Analysis and Simulation of a Digital Mobile Channel Using Orthogonal Frequency Division Multiplexing”. In: *IEEE Transactions on Communications* 33.7 (1985), pp. 665–675.

[29] H. A. Cirpan and M. K. Tsatsanis. “Maximum likelihood blind channel estimation in the presence of Doppler shifts”. In: *IEEE Transactions on Signal Processing* 47.6 (1999), pp. 1559–1569.

[30] IEEE Computer Society. LAN/MAN Standards Committee, Institute of Electrical, and Electronics Engineers. *IEEE Standard for Information Technology: part 11, wireless LAN medium access control (MAC) and physical layer (PHY) specifications*. IEEE std. IEEE, 2007. ISBN: 9780738156552. URL: https://books.google.de/books?id=KYQ1ywEACAAJ.

[31] Altera Corporation. *1536-Point FFT for 3GPP Long Term Evolution*. Oct. 2007. URL: https://www.intel.com/content/dam/www/programmable/us/en/pdfs/literature/an/an480.pdf.

[32] David Cox and P. Lewis. *The statistical analysis of series of events / by D. R. Cox and P. A. W. Lewis*. Jan. 1966. DOI: 10.1007/978-94-011-7801-3.

[33] E. Dahlman, S. Parkvall, and J. Skold. *5G NR: The Next Generation Wireless Access Technology*. Elsevier Science, 2018. ISBN: 9780128143230. URL: https://books.google.de/books?id=lcSLswEACAAJ.

[34] Mark A Davenport, Marco F Duarte, YC Eldar, and G Kutyniok. “Introduction to compressed sensing”. In: *Compressed Sensing: Theory and Applications*. Cambridge University Press, 2011.

[35] Walter Dean. “Computational Complexity Theory”. In: *The Stanford Encyclopedia of Philosophy*. Ed. by Edward N. Zalta. Winter 2016. Metaphysics Research Lab, Stanford University, 2016.

[36] Ling Deng, Zhonghui Chen, and Yisheng Zhao. “Basis expansion model for channel estimation in LTE-R communication system”. In: *Digital Communications and Networks* 2.2 (2016), pp. 92 –96. ISSN: 2352-8648. DOI: https://doi.org/10.1016/j.dcan.2016.04.001. URL: http://www.sciencedirect.com/science/article/pii/S2352864816300128.

[37] T. T. Do, L. Gan, N. Nguyen, and T. D. Tran. “Sparsity adaptive matching pursuit algorithm for practical compressed sensing”. In: *2008 42nd Asilomar Conference on Signals, Systems and Computers*. 2008, pp. 581–587.

[38] Matlab LTE System Toolbox Documentation. *Channel Estimation*. URL: https://de.mathworks.com/help/lte/ug/channel-estimation.html.

[39] Matlab LTE System Toolbox Documentation. *Propagation Channel Models*. URL: https://www.mathworks.com/help/lte/ug/propagation-channel-models.html.

[40] D. L. Donoho. “Compressed sensing”. In: *IEEE Transactions on Information Theory* 52.4 (2006), pp. 1289–1306.

[41] N. Eldarov, G. Tan, and T. Herfet. “Delay-Doppler search for matching pursuit algorithms in time-variant channels”. In: *2015 IEEE International Symposium on Broadband Multimedia Systems and Broadcasting*. 2015, pp. 1–5. DOI: 10.1109/BMSB.2015.7177226.

[42] N. Eldarov, G. Tan, and T. Herfet. “High mobility in OFDM systems based on FFT”. In: *2015 IEEE International Conference on Consumer Electronics (ICCE)*. 2015, pp. 414–415.

[43] European Telecommunications Standards Institute (ETSI). “Base Station (BS) radio transmission and reception”. In: ETSI TS 36.104 (2008), pp. 1–95.

[44] European Telecommunications Standards Institute (ETSI). “LTE; Evolved Universal Terrestrial Radio Access (E-UTRA); Long Term Evolution (LTE) physical layer:General Description”. In: ETSI TS 136 201 (2009), pp. 1–15.

[45] European Telecommunications Standards Institute (ETSI). “Digital Video Broadcasting (DVB);Frame structure channel coding and modulation for a second generation digital terrestrial television broadcasting system (DVB-T2)”. In: ETSI EN 302 755 (2010), pp. 1–177.

[46] European Telecommunications Standards Institute (ETSI). “Digital cellular telecommunications system (Phase 2+): Radio transmission and reception”. In: ETSI TS 145 005 (2011), pp. 1–95.

[47] European Telecommunications Standards Institute (ETSI). “Digital Video Broadcasting (DVB); Implementation guidelines for a second generation digital terrestrial television broadcasting system (DVB-T2)”. In: ETSI TS 102 831 (2012), pp. 1–244.

[48] European Telecommunications Standards Institute (ETSI). “LTE; Evolved Universal Terrestrial Radio Access (E-UTRA) and Evolved Universal Terrestrial Radio Access Network (E-UTRAN); Overall description;Stage 2 ”. In: ETSI TS 136 300 (2016), pp. 1–15.

[49] European Telecommunications Standards Institute (ETSI). “LTE; Evolved Universal Terrestrial Radio Access (E-UTRA); User Equipment (UE) radio transmission and reception ”. In: ETSI TS 136 101 (2017), pp. 1–1371.

[50] European Telecommunications Standards Institute (ETSI). “LTE:Evolved Universal Terrestrial Radio Access (E-UTRA); Multiplexing and channel coding”. In: 3GPP TS 36.212 (2017), pp. 10–149.

[51] European Telecommunications Standards Institute (ETSI). “5G: Study on Scenarios and Requirements for Next Generation Access Technologies”. In: ETSI TR 38.913 version 14.2.0 Release 14 (2018), pp. 14–15.

[52] European Telecommunications Standards Institute (ETSI). “5G: Study on channel model for frequencies from 0.5 to 100 GHz”. In: ETSI TR 138 901 (2018), pp. 1–95.

[53] M. Failli and Commission of the European Communities. *Digital Land Mobile Radio Communications. COST 207*. Information technologies and sciences. EC, 1989. URL: https://books.google.de/books?id=1DF4oAEACAAJ.

[54] B. Farhang-Boroujeny. “OFDM Versus Filter Bank Multicarrier”. In: *IEEE Signal Processing Magazine* 28.3 (2011), pp. 92–112. DOI: 10.1109/MSP.2011.940267.

[55] Philip Feinsilver. “Circulants, inversion of circulants, and some related matrix algebras”. In: *Linear Algebra and its Applications* 56 (1984), pp. 29–43. ISSN: 0024-3795. DOI: https://doi.org/10.1016/0024-3795(84)90111-3. URL: https://www.sciencedirect.com/science/article/pii/0024379584901113.

[56] Rian Ferdian, Yafei Hou, and Minoru Okada. “A Low-Complexity Hardware Implementation of Compressed Sensing-Based Channel Estimation for ISDB-T System”. In: *IEEE Transactions on Broadcasting* 63.1 (2017), pp. 92–102. DOI: 10.1109/TBC.2016.2617286.

[57] J. A. Fernandez, K. Borries, L. Cheng, B. V. K. Vijaya Kumar, D. D. Stancil, and F. Bai. “Performance of the 802.11p Physical Layer in Vehicle-to-Vehicle Environments”. In: *IEEE Transactions on Vehicular Technology* 61.1 (Jan. 2012), pp. 3–14. ISSN: 0018-9545. DOI: 10.1109/TVT.2011.2164428.

[58] G. Fettweis, M. Krondorf, and S. Bittner. “GFDM - Generalized Frequency Division Multiplexing”. In: *VTC Spring 2009 - IEEE 69th Vehicular Technology Conference*. 2009, pp. 1–4. DOI: 10.1109/VETECS.2009.5073571.

[59] Eduardo Garro, Jordi Joan Gimenez, Sung Ik Park, and David Gomez-Barquero. “Scattered Pilot Performance and Optimization for ATSC 3.0”. In: *IEEE Transactions on Broadcasting* 63.1 (2017), pp. 282–292. DOI: 10.1109/TBC.2016.2630304.

[60] Matthew Gast. *802.11N: A Survival Guide*. O’Reilly Media, Inc., 2012. ISBN: 1449312047, 9781449312046.

[61] Geert Leus, Zijian Tang and Paolo Banelli. *Chapter 4 - Estimation of Time-Varying Channels - a Block approach. In Franz Hlawatsch and Gerald Matz, editors, Wireless Communication Over Rapidly Time-Varying Channels*. Academic Press, Oxford, 2011.

[62] Gerald Matz and Franz Hlawatsch. *Chapter 1 - Fundamentals of Time-Varying Communication Channels - a Block approach. In Franz Hlawatsch and Gerald Matz, editors, Wireless Communication Over Rapidly Time-Varying Channels*. Academic Press, Oxford, 2011.

[63] Robin Gerzaguet et al. "The 5G candidate waveform race: a comparison of complexity and performance". In: *EURASIP Journal on Wireless Communications and Networking* 2017.1 (2017), p. 13. DOI: 10.1186/s13638-016-0792-0. URL: https://doi.org/10.1186/s13638-016-0792-0.

[64] Zahid Ghadialy. *OFDM and SC-FDMA*. 2009. URL: http://blog.3g4g.co.uk/2009/02/ofdm-and-sc-fdma.html.

[65] G. B. Giannakis and C. Tepedelenlioglu. "Basis expansion models and diversity techniques for blind identification and equalization of time-varying channels". In: *Proceedings of the IEEE* 86.10 (1998), pp. 1969–1986.

[66] Jordi Joan Gimenez, Jose Luis Carcel, Manuel Fuentes, Eduardo Garro, Simon Elliott, David Vargas, Christian Menzel, and David Gomez-Barquero. "5G New Radio for Terrestrial Broadcast: A Forward-Looking Approach for NR-MBMS". In: *IEEE Transactions on Broadcasting* 65.2 (2019), pp. 356–368. DOI: 10.1109/TBC.2019.2912117.

[67] Ian Goodfellow, Yoshua Bengio, and Aaron Courville. *Deep Learning*. http://www.deeplearningbook.org. MIT Press, 2016.

[68] David Gottlieb and Chi-Wang Shu. "On the Gibbs Phenomenon and Its Resolution". In: *SIAM Rev.* 39.4 (Dec. 1997), 644–668. ISSN: 0036-1445. DOI: 10.1137/S0036144596301390. URL: https://doi.org/10.1137/S0036144596301390.

[69] M. Guillaud and D. T. M. Slock. "Channel modeling and associated inter-carrier interference equalization for OFDM systems with high Doppler spread". In: *2003 IEEE International Conference on Acoustics, Speech, and Signal Processing, 2003. Proceedings. (ICASSP '03).* Vol. 4. 2003, pp. IV–237.

[70] Oliver Haffenden. *DVB-T2: The Common Simulation Platform. BBC Research White Paper WHP 196*, Available at: http://www.bbc.co.uk/rd/publications/whitepaper196. 2012.

[71] Haiying Zhu, L. Bouchard, and L. Boucher. "Performance of OFDM based wireless LAN system under Doppler over Rayleigh fading". In: *International Conference on Communication Technology Proceedings, 2003. ICCT 2003.* Vol. 2. 2003, 1234–1237 vol.2.

[72] Harmoko Habibi Roni, Shyue-Win Wei, Yih-Haw Jan, Tung-Chou Chen, and Jyh-Horng Wen. "Low complexity qSIC equalizer for OFDM system". In: *2009 IEEE 13th International Symposium on Consumer Electronics*. 2009, pp. 434–438.

[73] Simon Haykin. *Adaptive filter theory*. 4th. Upper Saddle River, NJ: Prentice Hall, 2002.

[74] Simon Haykin and Michael Moher. *Modern Wireless Communication*. USA: Prentice-Hall, Inc., 2004. ISBN: 0130224723.

[75] Robert Heath. *Introduction to Wireless Digital Communication: A Signal Processing Perspective*. Jan. 2017. ISBN: 978-0134431796.

[76] Thorsten Herfet. *Audio/Visual Communication and Networks*. Germany: Telecommunications Lab, Uni Saarland, 2019.

[77] Thorsten Herfet. *Digital Transmission & Signal Processing*. Germany: Telecommunications Lab, Uni Saarland, 2019.

[78] R. Hicheri, M. Paetzold, and N. Youssef. "On the statistical properties of the capacity of sparse multipath fading channels". In: *2014 International Conference on Advanced Technologies for Communications (ATC 2014)*. 2014, pp. 338–343. DOI: 10.1109/ATC.2014.7043408.

[79] Elad Hoffer, Itay Hubara, and Daniel Soudry. *Train longer, generalize better: closing the generalization gap in large batch training of neural networks*. 2017. arXiv: 1705.08741 [stat.ML].

[80] Andreas Hoglund, Xingqin Lin, Olof Liberg, Ali Behravan, Emre Yavuz, Martin Zee, Yutao Sui, Tuomas Tirronen, Antti Ratilainen, and David Eriksson. "Overview of 3GPP Release 14 Enhanced NB-IoT". In: *IEEE Network* 31 (Nov. 2017), pp. 16–22. DOI: 10.1109/MNET.2017.1700082.

[81] R. Hopkins. "Digital terrestrial HDTV for North America: the Grand Alliance HDTV system". In: *IEEE Transactions on Consumer Electronics* 40.3 (1994), pp. 185–198. ISSN: 1558-4127. DOI: 10.1109/30.320795.

[82] T. Hrycak, S. Das, G. Matz, and H. G. Feichtinger. "Low Complexity Equalization for Doubly Selective Channels Modeled by a Basis Expansion". In: *IEEE Transactions on Signal Processing* 58.11 (2010), pp. 5706–5719. ISSN: 1053-587X. DOI: 10.1109/TSP.2010.2063426.

[83] T. Hrycak, S. Das, G. Matz, and H. G. Feichtinger. "Practical Estimation of Rapidly Varying Channels for OFDM Systems". In: *IEEE Transactions on Communications* 59.11 (2011), pp. 3040–3048. ISSN: 0090-6778. DOI: 10.1109/TCOMM.2011.082111.110075.

[84] Huawei. *5G: New Air Interface and Radio Access Virtualization*. http://www.huawei.com/minisite/has2015/img/5g_radio_whitepaper.pdf. Accessed on: Feb.8, 2017. 2015, [Online].

[85] Zakria Hussain and John S. Shawe-taylor. "Theory of matching pursuit". In: *Advances in Neural Information Processing Systems 21*. Ed. by D. Koller, D. Schuurmans, Y. Bengio, and L. Bottou. Curran Associates, Inc., 2009, pp. 721–728. URL: http://papers.nips.cc/paper/3612-theory-of-matching-pursuit.pdf.

[86] "IEEE Standard for Information technology, Amendment 6: Wireless Access in Vehicular Environments". In: *IEEE Standard 802.11p* (2010), pp. 1–35.

[87] Nazar Idrees, Werner Haselmayr, David Schellander, and Andreas Springer. "Time Variant Channel Estimation using a Modified Complex Exponential Basis Expansion Model in LTE-OFDM Systems". In: Oct. 2010, pp. 603 –607. DOI: 10.1109/PIMRC.2010.5671762.

[88] Telesystem Innovations Inc. *LTE in a Nutshell: The Physical Layer*. 2010. URL: https://home.zhaw.ch/kunr/NTM1/literatur/LTE%20in%20a%20Nutshell%20-%20Physical%20Layer.pdf.

[89] European Telecommunications Standards Institute. "ETSI EN 302 755 v1.4.1 Digital Video Broadcasting (DVB); Frame structure channel coding and modulation for a second generation digital terrestrial television broadcasting system (DVB-T2)". In: (2015).

[90] European Telecommunications Standards Institute. " ETSI EN 302 663 V1.3.0 Intelligent Transport Systems (ITS); ITS-G5 Access layer specification for Intelligent Transport Systems operating in the 5 GHz frequency band". In: (May 2019).

[91] Michel C. Jeruchim, Philip Balaban, and K. Sam Shanmugan, eds. *Simulation of Communication Systems: Modeling, Methodology and Techniques*. 2nd. Norwell, MA, USA: Kluwer Academic Publishers, 2000. ISBN: 0306462672.

[92] Ramzi Theodory Kelvin Chelli Praharsha Sirsi and Thorsten Herfet. *IEEE802.11p Simulation Platofrm*. https://git.nt.uni-saarland.de/HiMo/SimTool_LTE. Accessed on: Jan.8, 2020. 2018, [Online].

[93] Johanna Ketonen, Markku Juntti, Jari Ylioinas, and Joseph R. Cavallaro. "Decision-Directed Channel Estimation Implementation for Spectral Efficiency Improvement in Mobile MIMO-OFDM". In: *Journal of Signal Processing Systems* 79.3 (2015), pp. 233–245. DOI: 10.1007/s11265-013-0833-4. URL: https://doi.org/10.1007/s11265-013-0833-4.

[94] William R. Kirkland and D. P. Taylor. "Neural Network Channel Equalization". In: *Neural Networks in Telecommunications*. Ed. by Ben Yuhas and Nirwan Ansari. Boston, MA: Springer US, 1994, pp. 143–171. ISBN: 978-1-4615-2734-3. DOI: 10.1007/978-1-4615-2734-3_8. URL: https://doi.org/10.1007/978-1-4615-2734-3_8.

[95] J. Kreber. "Estimating Heterogeneous Channel Conditions in Vehicular networks using Deep Learning and Basis Expansion Models. (Advisor: Kelvin Chelli)". MA thesis. Universität des Saarlandes, 2019.

[96] Gitta Kutyniok. "Theory and applications of compressed sensing". In: *GAMM-Mitteilungen* 36.1 (2013), pp. 79–101. ISSN: 1522-2608. DOI: 10.1002/gamm.201310005. URL: http://dx.doi.org/10.1002/gamm.201310005.

[97] Houda Labiod, Afifi Hossam, and Costantino De Santis. *Wi-Fi, Bluetooth, Zigbee and WiMax*. Berlin, Heidelberg: Springer-Verlag, 2007. ISBN: 1402053967.

[98] Seok-Jun Lee, Manish Goel, Yuming Zhu, Jing-Fei Ren, and Yang Sun. "Forward error correction decoding for WiMAX and 3GPP LTE modems". In: Nov. 2008, pp. 1143 –1147. DOI: 10.1109/ACSSC.2008.5074593.

[99] G. Leus. "On the estimation of rapidly time-varying channels". In: *2004 12th European Signal Processing Conference*. 2004, pp. 2227–2230.

[100] Weichang Li and James C Preisig. "Estimation of rapidly time-varying sparse channels". In: *IEEE Journal of Oceanic Engineering* 32.4 (2007), pp. 927–939.

[101] Yunxin (Jeff) Li. "An Overview of the DSRC/WAVE Technology". In: *Quality, Reliability, Security and Robustness in Heterogeneous Networks*. Ed. by Xi Zhang and Daji Qiao. Berlin, Heidelberg: Springer Berlin Heidelberg, 2012, pp. 544–558. ISBN: 978-3-642-29222-4.

[102] Jingjing Liu, Chao Zhang, and Changyong Pan. "Priori-Information Hold Subspace Pursuit: A Compressive Sensing-Based Channel Estimation for Layer Modulated TDS-OFDM". In: *IEEE Transactions on Broadcasting* 64.1 (2018), pp. 119–127. DOI: 10.1109/TBC.2017.2704432.

[103] Z. Ma, T. Sato, and M. Okada. “Compressed sensing based low-complexity moible radio OFDM systems with pre-equalization”. In: *2012 International Symposium on Intelligent Signal Processing and Communications Systems*. 2012, pp. 515–520. DOI: 10.1109/ISPACS.2012.6473544.

[104] Z. Ma, H. Liu, T. Higashino, M. Okada, and H. Furudate. “Low-complexity channel estimation for ISDB-T over doubly-selective fading channels”. In: *2013 International Symposium on Intelligent Signal Processing and Communication Systems*. 2013, pp. 114–118. DOI: 10.1109/ISPACS.2013.6704531.

[105] Ziji Ma, T. Sato, and M. Okada. “Compressed sensing based ICI cancellation method for OFDM systems”. In: *2012 IEEE International Conference on Consumer Electronics (ICCE)*. 2012, pp. 624–625. DOI: 10.1109/ICCE.2012.6162004.

[106] Ziji Ma, T. Sato, M. Okada, and H. Furudate. “ICI cancellation method for OFDM systems using compressed sensing based channel estimation”. In: *2011 International Symposium on Intelligent Signal Processing and Communications Systems (ISPACS)*. 2011, pp. 1–5. DOI: 10.1109/ISPACS.2011.6146095.

[107] S. G. Mallat and Zhifeng Zhang. “Matching pursuits with time-frequency dictionaries”. In: *IEEE Transactions on Signal Processing* 41.12 (1993), pp. 3397–3415.

[108] Mathworks. *802.11p Packet Error Rate Simulation for a Vehicular Channel*. URL: https://www.mathworks.com/help/wlan/examples/802-11p-packet-error-rate-simulation-for-a-vehicular-channel.html.

[109] Mathworks. *Fading Channels*. URL: https://www.mathworks.com/help/comm/ug/fading-channels.html.

[110] Mikel Mendicute, Iker Sobron, Lorena Martinez, and Pello Ochandiano. “DVB-T2: New Signal Processing Algorithms for a Challenging Digital Video Broadcasting Standard”. In: Feb. 2010. ISBN: 978-953-7619-70-1. DOI: 10.5772/8033.

[111] N. Michailow, M. Matthé, I. S. Gaspar, A. N. Caldevilla, L. L. Mendes, A. Festag, and G. Fettweis. “Generalized Frequency Division Multiplexing for 5th Generation Cellular Networks”. In: *IEEE Transactions on Communications* 62.9 (2014), pp. 3045–3061. DOI: 10.1109/TCOMM.2014.2345566.

[112] A. N. Mody and G. L. Stuber. “Synchronization for MIMO OFDM systems”. In: *GLOBECOM’01. IEEE Global Telecommunications Conference (Cat. No.01CH37270)*. Vol. 1. 2001, 509–513 vol.1. DOI: 10.1109/GLOCOM.2001.965169.

[113] Austin Mohr. “Quantum computing in complexity theory and theory of computation”. In: *Carbondale, IL* (2014).

[114] H. Mousavi, Iraj S. Amiri, M.A. Mostafavi, and C.Y. Choon. "LTE physical layer: Performance analysis and evaluation". In: *Applied Computing and Informatics* 15.1 (2019), pp. 34–44. ISSN: 2210-8327. DOI: https://doi.org/10.1016/j.aci.2017.09.008. URL: https://www.sciencedirect.com/science/article/pii/S2210832717301990.

[115] R. Nissel and M. Rupp. "Doubly-selective MMSE channel estimation and ICI mitigation for OFDM systems". In: *2015 IEEE International Conference on Communications (ICC)*. 2015, pp. 4692–4697.

[116] A.V. Oppenheim, A.S. Willsky, and S.H. Nawab. *Signals & Systems*. Prentice-Hall signal processing series. Prentice-Hall International, 1997. ISBN: 9780136511755. URL: https://books.google.de/books?id=O9ZHSAAACAAJ.

[117] O. O. Oyerinde and S. H. Mneney. "Decision Directed Channel Estimation for OFDM Systems Employing Fast Data Projection Method Algorithm". In: *2009 IEEE International Conference on Communications*. 2009, pp. 1–5.

[118] T. O'Shea and J. Hoydis. "An Introduction to Deep Learning for the Physical Layer". In: *IEEE Transactions on Cognitive Communications and Networking* 3.4 (2017), pp. 563–575.

[119] R. Paderna, T. Higashino, and M. Okada. "Improved channel estimation for ISDB-T using Modified Orthogonal Matching Pursuit over fractional delay TU6 channel". In: *Signal and Information Processing Association Annual Summit and Conference (APSIPA), 2014 Asia-Pacific*. 2014, pp. 1–5.

[120] Ryan Paderna, Duong Quang Thang, Yafei Hou, Takeshi Higashino, and Minoru Okada. "Low-Complexity Compressed Sensing-Based Channel Estimation With Virtual Oversampling for Digital Terrestrial Television Broadcasting". In: *IEEE Transactions on Broadcasting* 63.1 (2017), pp. 82–91. DOI: 10.1109/TBC.2016.2606938.

[121] J. Park, Y. Whang, and K. S. Kim. "Low Complexity MMSE-SIC Equalizer Employing Time-Domain Recursion for OFDM Systems". In: *IEEE Signal Processing Letters* 15 (2008), pp. 633–636. DOI: 10.1109/LSP.2008.2003991.

[122] J.T.J. Penttinen. *The LTE-Advanced Deployment Handbook: The Planning Guidelines for the Fourth Generation Networks*. Wiley, 2016. ISBN: 9781118484807. URL: https://books.google.de/books?id=H67QCgAAQBAJ.

[123] Philip Schniter, Sung-Jun Hwang, Sibasish Das and Arun P. Kannu. *Chapter 6 - Equalization of Time-Varying Channels. In Franz Hlawatsch and Gerald Matz, editors, Wireless Communication Over Rapidly Time-Varying Channels*. Academic Press, Oxford, 2011.

[124] ITU Recommendation. "ITU-R M. 1225-0". In: *Guidelines for evaluation of radio transmission technologies for IMT-2000* (2000).

[125] Ulrich Reimers, ed. *DVB: The Family of International Standards for Digital Video Broadcasting*. 2nd. Berlin, Germany: Springer-Verlag Berlin Heidelberg, 2004. ISBN: 978-3-642-07807-1.

[126] T. Richardson. "Error Floors of LDPC Codes". In: *41st Annual Conference on Communication, Control and Computing*. 2003, pp. 1426–1435.

[127] A. A. Rontogiannis, A. Marava, K. Berberidis, and J. Palicot. "Semi-blind estimation of multipath channel parameters via a separable least squares approach". In: *2002 14th International Conference on Digital Signal Processing Proceedings. DSP 2002 (Cat. No.02TH8628)*. Vol. 1. 2002, 49–52 vol.1.

[128] Sebastian Ruder. *An overview of gradient descent optimization algorithms*. 2016. arXiv: 1609.04747 [cs.LG].

[129] H. Choi S. Kim H. Oh. "The Physical Layer of the IEEE 802.11p WAVE Communication Standard: The Specifications and Challenges". In: *Proceedings of the World conference on Systems, Cybernetics and Informatics, (WCECS 2014), San Francisco, USA, October 2014*. SF, USA: Springer, 2014.

[130] Prasan Sahoo, Ming-Jer Chiang, and Shih-Lin Wu. "SVANET: A Smart Vehicular Ad Hoc Network for Efficient Data Transmission with Wireless Sensors". In: *Sensors (Basel, Switzerland)* 14 (Dec. 2014), pp. 22230–60. DOI: 10.3390/s141222230.

[131] H. Sari, G. Karam, and I. Jeanclaude. "Transmission techniques for digital terrestrial TV broadcasting". In: *IEEE Communications Magazine* 33.2 (1995), pp. 100–109. DOI: 10.1109/35.350382.

[132] Jürgen Schmidhuber. "Deep learning in neural networks: An overview". In: *Neural Networks* 61 (2015), 85–117. ISSN: 0893-6080. DOI: 10.1016/j.neunet.2014.09.003. URL: http://dx.doi.org/10.1016/j.neunet.2014.09.003.

[133] T. M. Schmidl and D. C. Cox. "Robust frequency and timing synchronization for OFDM". In: *IEEE Transactions on Communications* 45.12 (1997), pp. 1613–1621. ISSN: 0090-6778. DOI: 10.1109/26.650240.

[134] P. Schniter. “Low-complexity equalization of OFDM in doubly selective channels”. In: *IEEE Transactions on Signal Processing* 52.4 (2004), pp. 1002–1011.

[135] A. Schwarzenberg-Czerny. “On Matrix Factorization and Efficient Least Squares Solution.” In: 110.7 (1995), p. 405.

[136] M. Sipser. *Introduction to the Theory of Computation*. Cengage Learning, 2012. ISBN: 9781133187790. URL: https://books.google.de/books?id=-RuDtQAACAAJ.

[137] P. Sirsi, K. Chelli, and T. Herfet. “Tap coefficient based cognitive framework for estimating a dynamic channel”. In: *2017 International Conference on Circuits, Controls, and Communications (CCUBE)*. 2017, pp. 31–36. DOI: 10.1109/CCUBE.2017.8394173.

[138] Praharsha Sirsi. “Cognitive Framework for Channel Equalization in Vehicular Communication Systems”. MA thesis. Universität des Saarlandes, May 2017.

[139] O Steve, Neil Swainston, Julia Handl, Douglas B Kell, et al. “A ‘rule of 0.5’ for the metabolite-likeness of approved pharmaceutical drugs”. In: *Metabolomics* 11.2 (2015), pp. 323–339.

[140] Gilbert Strang. *Introduction to Linear Algebra*. 5th ed. Wellesley MA 02482: Wellesley-Cambridge Press, May 2016. ISBN: 978-09802327-7-6.

[141] G. Taubock, F. Hlawatsch, D. Eiwen, and H. Rauhut. “Compressive Estimation of Doubly Selective Channels in Multicarrier Systems: Leakage Effects and Sparsity-Enhancing Processing”. In: *IEEE Journal of Selected Topics in Signal Processing* 4.2 (2010), pp. 255–271. ISSN: 1932-4553. DOI: 10.1109/JSTSP.2010.2042410.

[142] Georg Tauböck, Franz Hlawatsch, and Holger Rauhut. “Compressive estimation of doubly selective channels: exploiting channel sparsity to improve spectral efficiency in multicarrier transmissions”. In: *ArXiv* abs/0903.2774 (2009).

[143] Agilent Technologies and Moray Rumney. *LTE and the Evolution to 4G Wireless: Design and Measurement Challenges*. 2nd. Wiley Publishing, 2013. ISBN: 1119962579.

[144] Keysight Technologies. *802.11 OFDM Overview*. 2019. URL: http://rfmw.em.keysight.com/wireless/helpfiles/89600b/webhelp/subsystems/wlan-ofdm/Content/ofdm_80211-overview.htm.

[145] Keysight Technologies. *LTE Physical Layer Overview*. 2019. URL: http://rfmw.em.keysight.com/wireless/helpfiles/89600B/WebHelp/Subsystems/lte/content/lte_overview.htm.

[146] Techplayon. *LTE TDD Special Subframe and Its significance for Cell Size*. 2017. URL: http://www.techplayon.com/lte-tdd-special-subframe-and-its-significance-for-cell-size/.

[147] T. A. Thomas and F. W. Vook. "Multi-user frequency-domain channel identification, interference suppression, and equalization for time-varying broadband wireless communications". In: *Proceedings of the 2000 IEEE Sensor Array and Multichannel Signal Processing Workshop. SAM 2000 (Cat. No.00EX410)*. 2000, pp. 444–448.

[148] S. Tomasin, A. Gorokhov, Haibing Yang, and J. . Linnartz. "Iterative interference cancellation and channel estimation for mobile OFDM". In: *IEEE Transactions on Wireless Communications* 4.1 (2005), pp. 238–245.

[149] German Federal Ministry of Transport and Digital Infrastructure. *Intelligent transport systems in the field of road transport*. 2015. URL: https://www.bmvi.de/EN/Topics/Digital-Matters/Intelligent-Transport-Systems/intelligent-transport-systems.html.

[150] L.N. Trefethen and D. Bau. *Numerical Linear Algebra*. Other Titles in Applied Mathematics. Society for Industrial and Applied Mathematics, 1997. ISBN: 9780898719574. URL: https://books.google.de/books?id=JaPtxOytY7kC.

[151] Michail K. Tsatsanis and Georgios B. Giannakis. "Modelling and equalization of rapidly fading channels". In: *International Journal of Adaptive Control and Signal Processing* 10.2-3 (1996), pp. 159–176. DOI: 10.1002/(SICI)1099-1115(199603)10:2/3<159::AID-ACS346>3.0.CO;2-M. eprint: https://onlinelibrary.wiley.com/doi/pdf/10.1002/. URL: https://onlinelibrary.wiley.com/doi/abs/10.1002/.

[152] M. Uehara, M. Takada, and T. Kuroda. "Transmission scheme for the terrestrial ISDB system". In: *IEEE Transactions on Consumer Electronics* 45.1 (1999), pp. 101–106. ISSN: 1558-4127. DOI: 10.1109/30.754424.

[153] L. Vangelista, N. Benvenuto, S. Tomasin, C. Nokes, J. Stott, A. Filippi, M. Vlot, V. Mignone, and A. Morello. "Key technologies for next-generation terrestrial digital television standard DVB-T2". In: *IEEE Communications Magazine* 47.10 (2009), pp. 146–153. ISSN: 0163-6804. DOI: 10.1109/MCOM.2009.5273822.

[154] T. Wang, Azhar Hussain, Yue Cao, and Sangirov Gulomjon. "An Improved Channel Estimation Technique for IEEE 802.11p Standard in Vehicular Communications". In: *Sensors (Basel, Switzerland)* 19 (2019).

[155] Y. Wang, J. Zhou, L. Fang, and D. Li. "Analysis of a novel time domain pilot scheme in convolutional multiplexed multicarrier systems". In: *International Symposium on Personal, Indoor and Mobile Radio Communications*. 2012, pp. 2007–2113. DOI: 10.1109/PIMRC.2012.6362702.

[156] Hong Wen, Pin-Han Ho, and Guang Gong. "A Novel Framework for Message Authentication in Vehicular Communication Networks". In: Nov. 2009, pp. 1–6. DOI: 10.1109/GLOCOM.2009.5425519.

[157] Karen Wheeless and Federal Communications Commission. *A Short History of Radio A Short History of Radio With an Inside Focus on Mobile Radio*. https://transition.fcc.gov/omd/history/radio/documents/short_history.pdf. [Online; accessed 23-Feb-2021]. 2003.

[158] P. Xiao, C. Cowan, T. Ratnarajah, and A. Fagan. "Time synchronization algorithms for IEEE 802.11 OFDM systems". In: *IET International Communication Conference on Wireless Mobile and Computing (CCWMC 2009)*. 2009, pp. 287–290.

[159] Xiaoli Ma and G. B. Giannakis. "Maximum-diversity transmissions over doubly selective wireless channels". In: *IEEE Transactions on Information Theory* 49.7 (2003), pp. 1832–1840.

[160] G.Hirtz Y.El Hajj Shehadeh S.Baumgartner. "Low Complexity Intercarrier Interference Reduction for High Mobility Wireless Systems". In: *Proceedings of International Conference on Consumer Electronics (ICCE), 2015, Las Vegas*. IEEE, 2015, pp. 672–675.

[161] H. Ye, G. Y. Li, and B. Juang. "Power of Deep Learning for Channel Estimation and Signal Detection in OFDM Systems". In: *IEEE Wireless Communications Letters* 7.1 (2018), pp. 114–117.

[162] Yoon-Kyeong Kim, Jang-Mi Oh, Yoo-Ho Shin, and Cheol Mun. "Time and frequency domain channel estimation scheme for IEEE 802.11p". In: *17th International IEEE Conference on Intelligent Transportation Systems (ITSC)*. 2014, pp. 1085–1090. DOI: 10.1109/ITSC.2014.6957832.

[163] E. Zafarani, M. J. Omidi, F. Heydaryan, and S. Mahmoodi. "Oversampled Legendre basis expansion model for doubly-selective channels". In: *2011 19th Iranian Conference on Electrical Engineering*. 2011, pp. 1–1.

[164] T. Zemen and C. F. Mecklenbrauker. "Time-variant channel estimation using discrete prolate spheroidal sequences". In: *IEEE Transactions on Signal Processing* 53.9 (2005), pp. 3597–3607.

[165] T. Zemen, C. F. Mecklenbräuker, and R. R. Müller. “Time Variant Channel Equalization for MC-CDMA via Fourier Basis Functions”. In: *Multi-Carrier Spread-Spectrum*. Ed. by Khaled Fazel and Stefan Kaiser. Dordrecht: Springer Netherlands, 2004, pp. 451–458. ISBN: 978-94-017-0502-8.

[166] S. Zettas, S. Kasampalis, P. Lazaridis, Z. D. Zaharis, and J. Cosmas. “Channel estimation for OFDM systems based on a time domain pilot averaging scheme”. In: *2013 16th International Symposium on Wireless Personal Multimedia Communications (WPMC)*. 2013, pp. 1–6.

[167] Youwei Zhang, Ian L. Tan, Carl Chun, Ken Laberteaux, and Ahmad Bahai. “A Differential OFDM Approach to Coherence Time Mitigation in DSRC”. In: *Proceedings of the Fifth ACM International Workshop on VehiculAr Inter-NETworking*. VANET ’08. San Francisco, California, USA: ACM, 2008, pp. 1–6. ISBN: 978-1-60558-191-0. DOI: 10.1145/1410043.1410045. URL: http://doi.acm.org/10.1145/1410043.1410045.

[168] Zhongyuan Zhao, Mehmet C. Vuran, Fujuan Guo, and Stephen Scott. *Deep-Waveform: A Learned OFDM Receiver Based on Deep Complex Convolutional Networks*. 2018. arXiv: 1810.07181 [eess.SP].

[169] Zijun Zhao, Xiang Cheng, Miaowen Wen, Bingli Jiao, and Cheng-Xiang Wang. “Channel Estimation Schemes for IEEE 802.11p Standard”. In: *IEEE Intell. Transport. Syst. Mag.* 5.4 (2013), pp. 38–49. URL: http://dblp.uni-trier.de/db/journals/itsm/itsm5.html#ZhaoCWJW13.

# APPENDIX A

## A.1 Complexity Calculation

In this appendix, we show the calculation of the number of real multiplications/divisions and additions/subtractions for the RMP algorithm. As in Section 6.7, we consider the IEEE 802.11p standard and provide a concrete example of calculating the number of mathematical operations. The notations used in the calculations and their corresponding values are listed in the table below.

Table A.1: Notations used

| Notation | Description |
|---|---|
| $N = 64$ | FFT size |
| $K_d = 48$ | # of data subcarriers |
| $K_p = 4$ | # of pilot subcarriers |
| $K_{on} = 52$ | # of active subcarriers in long preamble |

In order to compute the exact number of operations, we have to assume the search resolutions. Let the delay search resolution be $\Delta_\tau = 10nsec$ that gives the total number of delay bins to be searched as $K = \tau_{max}/\Delta_\tau \implies 1.6\mu sec/1nsec = 160$. The delay search of the RMP

algorithm is listed in Algorithm 5 along with the number of complex operations for each step.

**Algorithm 5:** Rake Matching Pursuit Algorithm - Delay Search

$$\mathbf{r}_0 = \frac{\mathbf{y}}{|\mathbf{y}|} \qquad \{\div : K_{on}\} \tag{A.1}$$

$$b_{0,j} = \mathbf{d}_j^H \mathbf{r}_0, \qquad \text{for } j = 1 \cdots K \qquad \{\times : K \cdot K_{on}\} \tag{A.2}$$

$$s_1 = \underset{j=1\cdots K}{\arg\max} \frac{|b_{0,j}|^2}{\|\mathbf{d}_j\|_2} \qquad \{\div : K \cdot K_{on}\} \tag{A.3}$$

$$\mathbf{i}_1 = \{s_1\} \tag{A.4}$$

$$\hat{c}_1 = \frac{b_{0,s_1}}{\|\mathbf{d}_{s_1}\|_2^2} \qquad \{\div : K_{on}\} \tag{A.5}$$

$$b_{1,j} = b_{0,j} - \hat{c}_1 \mathbf{d}_j^H \mathbf{d}_{s_1}, \qquad \text{for } j = 1 \cdots K, j \notin \mathbf{i}_1 \qquad \{\times : K \cdot K_{on};\ + : K \cdot K_{on}\} \tag{A.6}$$

*the $p^{th}$ iteration, $p > 1$*

$$s_p = \underset{j=1\cdots K, j \notin \mathbf{i}_{p-1}}{\arg\max} \frac{|b_{p-1,j}|^2}{\|\mathbf{d}_j\|_2} \qquad \{\div : (K-1) \cdot K_{on}\} \tag{A.7}$$

$$\mathbf{i}_p = \{\mathbf{i}_{p-1}, s_p\} \tag{A.8}$$

$$\hat{c}_p = \frac{b_{p-1,s_p}}{\|\mathbf{d}_{s_p}\|_2^2} \qquad \{\div : K_{on}\} \tag{A.9}$$

$$b_{p,j} = b_{p-1,j} - \hat{c}_p \mathbf{d}_j^H \mathbf{d}_{s_p}, \qquad \text{for } j = 1 \cdots K, j \notin \mathbf{i}_p \qquad \{\times : K \cdot K_{on};\ + : K \cdot K_{on}\} \tag{A.10}$$

The total number of complex operations for the delay search of the RMP algorithm are calculated from Algorithm 5 and consolidated in Equation (A.11). Note that Equation (A.7) to Equation (A.10) are computed $p-1$ times, where $p$ is the total number of iterations. First,

the total number of complex operations are calculated and then the number of real valued operations are inferred.

$$\begin{aligned} \text{Complex Divisions} &= (2+K)\cdot K_{on} + (p-1)\cdot K\cdot K_{on} && \Rightarrow 2K_{on} + p\cdot K\cdot K_{on} \\ \text{Complex Multiplications} &= 2K\cdot K_{on} + (p-1)\cdot K\cdot K_{on} && \Rightarrow (p+1)\cdot K\cdot K_{on} \\ \text{Complex Additions} &= K\cdot K_{on} + (p-1)\cdot K\cdot K_{on} && \Rightarrow p\cdot K\cdot K_{on} \end{aligned} \tag{A.11}$$

**Algorithm 6:** Rake Matching Pursuit Algorithm - Doppler Search

$$\mathbf{r}_0 = \mathbf{y}_p \tag{A.12}$$

$$b_{0,j} = \mathbf{d}_j^H \mathbf{r}_0, \qquad \text{for } j = 1\cdots q_{taps} \qquad \{\times : q_{taps}\cdot K_p\} \tag{A.13}$$

$$\mathbf{i}_1 = \{1\} \tag{A.14}$$

$$\hat{c}_{1,r_p} = \frac{b_{0,1}}{\|\mathbf{d}_1\|_2^2} \qquad \{\div : K_p\} \tag{A.15}$$

$$b_{1,j} = b_{0,j} - \hat{c}_{1,r_p}\mathbf{d}_j^H\mathbf{d}_1, \qquad \text{for } j = 1\cdots q_{taps}, j \notin \mathbf{i}_1 \qquad \{\times : q_{taps}\cdot K_p;\ +: q_{taps}\cdot K_p\} \tag{A.16}$$

*the $p^{th}$ iteration, $p > 1$ and $p \leq q_{taps}$*

$$\mathbf{i}_p = \{\mathbf{i}_{p-1}, p\} \tag{A.17}$$

$$\hat{c}_{p,r_p} = \frac{b_{p-1,p}}{\|\mathbf{d}_p\|_2^2} \qquad \{\div : K_p\} \tag{A.18}$$

$$b_{p,j} = b_{p-1,j} - \hat{c}_{p,r_p}\mathbf{d}_j^H\mathbf{d}_p, \qquad \text{for } j = 1\cdots q_{taps}, j \notin \mathbf{i}_p \qquad \{\times : q_{taps}\cdot K_p;\ +: q_{taps}\cdot K_p\} \tag{A.19}$$

In a similar manner, the number of complex operations are computed for the Doppler search of the RMP algorithm. Algorithm 6 lists the Doppler search technique along with the number of complex operations for each step. Here, $q_{taps}$ is the total number of delay taps found in the delay search algorithm. The total number of complex operations for the Doppler search of the RMP algorithm are calculated from Algorithm 6 and consolidated in Equation (A.20). Note that Equations (A.18) and (A.19) are computed $(q_{taps}-1)$ times.

$$\begin{aligned}
\text{Complex Divisions} &= K_p + (q_{taps}-1)\cdot K_p && \Rightarrow q_{taps}\cdot K_p \\
\text{Complex Multip.} &= 2q_{taps}\cdot K_p + (q_{taps}-1)\cdot q_{taps}\cdot K_p && \Rightarrow (q_{taps}^2 + q_{taps})\cdot K_p \\
\text{Complex Additions} &= q_{taps}\cdot K_p + (q_{taps}-1)\cdot q_{taps}\cdot K_p && \Rightarrow q_{taps}^2\cdot K_p
\end{aligned} \tag{A.20}$$

Combining the complex operations from both the searches, we will get the total number of complex operations. Let us assume that the total number of iterations for the delay search is $p = q_{taps} = 6$ and considering the specifications of the underlying standard i.e $K_{on} = 52$, $K_p = 4$ and the maximum number of delay bins $K = 160$, the complex operations can be simplified as in Equation (A.21).

$$\begin{aligned}
\text{Complex Divisions} &= 2K_{on} + p\cdot K\cdot K_{on} + q_{taps}\cdot K_p && = 50,048 \\
\text{Complex Multiplications} &= (p+1)\cdot K\cdot K_{on} + (q_{taps}^2 + q_{taps})\cdot K_p && = 58,408 \\
\text{Complex Additions} &= p\cdot K\cdot K_{on} + q_{taps}^2\cdot K_p && = 50,064
\end{aligned} \tag{A.21}$$

Finally, the number of real operations can be computed. Table A.2 shows the number of real operations required for different complex operators and Table A.3 shows the real operations that the RMP algorithm requires. In the same manner, the number of real operations can be calculated for the BMP and the GRMP and the LS algorithms.

Table A.2: Number of Real Valued Operations required for a Complex Valued Operation

| Complex Operator ↓ | # Real Multiplication/-Divisions | # Real Additions/Subtractions |
|---|---|---|
| Division | 8 | 3 |
| Multiplication | 4 | 2 |
| Addition | | 2 |
| Subtraction | - | 2 |

Table A.3: Total number of Real Operations for RMP

| Complex Operator | # Real Multiplication/-Divisions | # Real Additions/Subtractions |
|---|---|---|
| Division | $50,048 * 8 = 400,384$ | $50,048 * 3 = 150,144$ |
| Multiplication | $58,408 * 4 = 233,632$ | $58,408 * 2 = 116,816$ |
| Addition | - | $50,064 * 2 = 100,128$ |
| **Total** $\Rightarrow$ | $634,016$ | $367,088$ |

# APPENDIX B

## B.1 Least Squares Fit for Tanimoto Coefficient

Listing B.1: Tanimoto Coefficient Threshold Computation

```
figure ();
xdata = [0:3:30];
ydata = tanimoto_coef;
fun = @(x, xdata ) ( -0.9)* exp(x (1) * xdata ) + 1;
x0 = [0.14];
x = lsqcurvefit (fun ,x0 ,xdata , ydata );
times = linspace ( xdata (1) ,xdata ( end ));
plot (xdata ,ydata ,'ko',times , fun (x, times ),'b-');
legend ('Data','Matched exponential')
title ('Data and Matched Curve')
```

# APPENDIX C

## C.1 Linear Least Squares Solution

The minimum mean square error, also called as linear least squares error is given as

$$MMSE = \underset{y}{arg\,min} \|\boldsymbol{x} - \boldsymbol{G}\boldsymbol{y}\|_2^2$$

The objective function can be written as

$$O_{LLSR}(\boldsymbol{y}) = \|\boldsymbol{x} - \boldsymbol{G}\boldsymbol{y}\|_2^2$$

Taking the derivative with respect to $\boldsymbol{y}$,

$$\nabla_{\boldsymbol{y}}(O_{LLSR}) = -2\boldsymbol{G}^H(\boldsymbol{x} - \boldsymbol{G}\boldsymbol{y})$$

The necessary condition for an extrema of $O_{LLSR}$ is:

$$\begin{aligned}
&-2\boldsymbol{G}^H(\boldsymbol{x} - \boldsymbol{G}\boldsymbol{y}) = 0 \\
&\implies \boldsymbol{G}^H(\boldsymbol{x} - \boldsymbol{G}\boldsymbol{y}) = 0 \\
&\boldsymbol{G}^H\boldsymbol{x} - \boldsymbol{G}^H\boldsymbol{G}\boldsymbol{y} = 0 \\
&\boldsymbol{G}^H\boldsymbol{x} = \boldsymbol{G}^H\boldsymbol{G}\boldsymbol{y} \\
&\boldsymbol{G}^H\boldsymbol{x} = \left(\boldsymbol{G}^H\boldsymbol{G}\right)\boldsymbol{y} \\
&\implies \boldsymbol{y} = \left(\boldsymbol{G}^H\boldsymbol{G}\right)^{-1}\boldsymbol{G}^H\boldsymbol{x}
\end{aligned}$$